



Interactions polymère/silice : de la structure locale au renforcement mécanique d'hydrogels hybrides

Séverine Rose

► To cite this version:

Séverine Rose. Interactions polymère/silice : de la structure locale au renforcement mécanique d'hydrogels hybrides. Matériaux. Université Pierre et Marie Curie - Paris VI, 2013. Français. NNT : . pastel-00843578

HAL Id: pastel-00843578

<https://pastel.hal.science/pastel-00843578>

Submitted on 11 Jul 2013

HAL is a multi-disciplinary open access archive for the deposit and dissemination of scientific research documents, whether they are published or not. The documents may come from teaching and research institutions in France or abroad, or from public or private research centers.

L'archive ouverte pluridisciplinaire **HAL**, est destinée au dépôt et à la diffusion de documents scientifiques de niveau recherche, publiés ou non, émanant des établissements d'enseignement et de recherche français ou étrangers, des laboratoires publics ou privés.

THESE DE DOCTORAT DE
L'UNIVERSITE PIERRE ET MARIE CURIE

Spécialité

Chimie et Physico-Chimie des Polymères
(ED 397, Physique et Chimie des Matériaux)

Présentée par

Mlle Séverine ROSE

Pour obtenir le grade de

DOCTEUR DE L'UNIVERSITE PIERRE ET MARIE CURIE

Sujet de la thèse :

**Interactions polymère/silice :
de la structure locale au renforcement
mécanique d'hydrogels hybrides**

Soutenue le 14 juin 2013 devant le jury composé de :

M. Guy Schlatter	Rapporteur
M. Loïc Vanel	Rapporteur
M. Thibaud Coradin	Examineur
M. Bruno Grassl	Examineur
M. Jean-François Tassin	Président du jury
M. Ludwik Leibler	Invité
M. Dominique Hourdet	Directeur de thèse - Invité
Mme. Alba Marcellan	Encadrante de thèse
M. Tetsuharu Narita	Encadrant de thèse

Remerciements

Je souhaite tout d'abord remercier Christian Frétigny, directeur du Laboratoire PPMD-SIMM de l'ESPCI ParisTech, de m'avoir accueillie et fourni tous les éléments nécessaires pour effectuer ma thèse.

Je tiens à remercier sincèrement mes trois encadrants de thèse, Dominique, Alba et Tetsu. Merci pour la confiance, la pédagogie et la disponibilité dont vous avez fait preuve lors de nos discussions scientifiques. Cette expérience m'a permis de beaucoup apprendre de vos différences et de votre complémentarité. Grâce à vous, mon séjour au PPMD a été ponctué par de nombreuses conférences aussi bien en France, à Cargèse, Lorient, Lyon, Strasbourg, qu'à l'étranger : Goslar en Allemagne, Katmandou au Népal et Grenade en Espagne. Je suis très reconnaissante de la confiance que vous m'avez témoignée en me laissant participer à ces multiples conférences, parfois couronnées de distinctions.

Je remercie chaleureusement les membres de mon jury pour l'intérêt qu'ils ont témoigné à l'égard de mon travail. Merci en particulier à Guy Schlatter et Loïc Vanel d'avoir accepté de rapporter ce manuscrit et merci à Jean-François Tassin qui a présidé ce jury. Je remercie également Thibaud Coradin et Bruno Grassl d'avoir enrichi la discussion en apportant de nouveaux points de vue. Enfin je remercie sincèrement Ludwik Leibler de m'avoir fait l'honneur de participer à mon jury ainsi que pour sa grande participation à la compréhension de notre système, suite à nos passionnantes discussions face à l'Himalaya. Merci pour votre confiance, vos encouragements et vos gentils mots qui m'ont énormément rassurée à quelques minutes de ma soutenance.

Ce travail de thèse a été effectué au sein d'un laboratoire extrêmement dynamique, composé de personnes ayant contribué aux résultats présentés et que je souhaite remercier : Guylaine pour son expertise en rhéologie, Ludovic et David pour les montages expérimentaux sur mesure, Mohamed pour la DSC et l'ATG. Je tiens à remercier également Freddy pour ses nombreux conseils pratiques ainsi qu'Armand pour son aide précieuse en informatique. Je souhaite aussi remercier les stagiaires ayant contribué à ce travail de thèse : Alexis Fallet

pour son travail sur l'acrylamide, Valentine Pauleau pour les analyses ATG, Magali Mangeant et Sarah Mosbah pour leur étude du taux de gonflement dans différents solvants, Alexandre Dizeux pour les belles images des gels et la rhéologie et Lauriane Alison pour son aide en mécanique des gels. Merci également à Annie, Gilles, Flore et Pierre pour leur aide au quotidien, sans qui le laboratoire ne tournerait pas rond, ainsi qu'à tous les permanents qui contribuent à cette ambiance très chaleureuse dont on se sépare difficilement.

Je tiens à remercier sincèrement Fabrice Cousin, François Boué et Arnaud Hélyary du Laboratoire Léon Brillouin (CEA, Saclay) pour leur accueil chaleureux lors de mes nombreuses sessions sur Orphée pour la diffusion de neutrons aux petits angles. Merci à la bonne humeur de Fabrice qui a réussi à transformer nos week-ends, soirées et jours fériés à Saclay en d'agréables moments qui resteront gravés dans nos mémoires.

J'aimerais remercier chaleureusement Cédric Lorthioir de l'Institut de Chimie et des Matériaux Paris-Est pour les expériences de RMN du solide qui ont ouvert une nouvelle voie de compréhension de notre système.

Au cours de ma thèse, j'ai eu l'opportunité d'enseigner, dans le cadre d'une mission doctorale, au sein de l'UPMC. Je tiens à remercier les acteurs de cette formidable aventure d'enseignement. Merci en particulier à Benjamin Isare, François Stoffelbach et Damien Brégiroux pour la confiance qu'ils m'ont toujours accordée.

Je tiens à remercier également Christel Laberty-Robert pour la confiance qu'elle m'a accordée à la fin de ma thèse et pour l'opportunité que j'ai de travailler avec elle actuellement.

Merci à tous les étudiants dont j'ai croisé la route et qui contribuent à l'ambiance si agréable du PPMD, avec une pensée toute particulière pour ceux qui ont partagé le bureau H2.07 avec moi : Elodie pour son accueil chaleureux, Guillaume pour nos longues discussions, ses conseils et son accueil à San Francisco, Clémence pour sa bonne humeur, nos pauses thé et ce soutien mutuel en période de rédaction, Jennifer pour son enthousiasme et pour avoir brillamment complété la « gel girl team » ! Je remercie sincèrement ceux qui ont partagé mon

quotidien escalier H et dont l'amitié compte énormément : François et Etienne. Merci aussi à Aurélie, Basile, Benjamin, Elise, Eric, Jordan, Judith, Koichi, Marie-Charlotte, Mengxing, Natacha, Nisita, Peiluo, Toan, Xavier et Yannick, pour les pauses déjeuners si animées et agréables. Même s'il faut traverser de nombreux couloirs pour parvenir à l'escalier C, la bonne humeur qui y règne a beaucoup compté pendant ma thèse. Merci donc à Céline, Eloïse, Lucie, Sandie, Sandrine, et Solenn ainsi qu'à Eric, Gabriel, Julien, Rémi, Wei, et tous ceux avec qui j'ai partagé de très bons moments durant ces années.

Je remercie mes amis et les personnes qui ont marqué ces années de thèse. Merci notamment à Jessalyn et Mathieu pour les agréables soirées en Corse, les après-midis sportives et les discussions philosophiques. J'adresse une pensée toute particulière et de profonds remerciements à Clémentine, ma binôme exceptionnelle durant mes trois années d'école et dont le soutien quotidien pendant ma thèse a été si important... Maintenant, sa maîtrise des hydrogels hybrides contenant de la silice est au moins aussi importante que ma connaissance de la déshydratation des smectites dans les bassins sédimentaires !

J'adresse enfin mes plus sincères remerciements à mes parents et à ma petite sœur pour leur soutien sans faille et leurs encouragements tout au long de mes études. Une des plus grandes découvertes de ma thèse a été celle d'Alexandre, merci pour ton soutien au quotidien, pour ta patience pendant ma rédaction, pour ta relecture attentive, pour tout.

Abbreviations

AAm	Acrylamide
CV-SANS	Contrast Variation Small Angle Neutron Scattering
DLS	Dynamic Light Scattering
DMA	<i>N,N</i> -dimethylacrylamide
GPC	Gel Permeation Chromatography
KPS	Potassium Persulfate
LCST	Lower Critical Solution Temperature
MBA	<i>N,N'</i> -methylene-bis-acrylamide
PAAm	Poly(acrylamide)
PAMPS	Poly(2-acrylamido-2-methylpropanesulfonic acid)
PDMA	Poly(<i>N,N</i> -dimethylacrylamide)
PEG	Poly(ethylene glycol)
PNIPAm	Poly(<i>N</i> -isopropylacrilamide)
SANS	Small Angle Neutron Scattering
SAXS	Small Angle X-ray Scattering
SLS	Single Light Scattering
TEMED	<i>N,N,N',N'</i> -tetramethyl-ethylenediamine
TEOS	Tetrahydroxysilane
U-SANS	Ultra Small Angle Neutron Scattering

Symbols

E	Elastic modulus
f	Functionality
F	Force
G	Shear modulus
$I(q)$	Scattering intensity
k_B	Boltzmann constant
M	Molar mass
Q	Swelling
R	Ideal gas constant
R_h	Hydrodynamic radius
$S(q)$	Structure factor
S_{spe}	Specific surface
t	Time
T	Temperature
v_{spe}	Specific volume
V	Volume
ε	Strain
σ_N	Nominal stress
σ	Stress
ϕ	Volume fraction
λ	Wavelength
Ξ	Correlation length of static heterogeneities
ξ	Correlation length of thermodynamic heterogeneities
χ^{12}	Flory interaction parameter

Table des matières

Introduction générale.....	1
General introduction.....	7
Chapter 1: Hybrid hydrogels, a general survey.....	11
Contents	12
Introduction.....	14
1. Polymer hydrogels	15
1.1. Definitions, main characteristics and applications.....	15
1.1.1. Definitions and characteristics	15
1.1.2. Applications	16
1.2. Synthesis methods.....	18
1.3. Inhomogeneities in hydrogels	19
1.3.1. Types of inhomogeneities	20
1.3.2. Characterisation and consequences of inhomogeneities.....	21
2. Reinforcement of organic hydrogels	24
2.1. Topological networks	24
2.1.1. Structure of topological networks.....	24
2.1.2. Properties of topological networks.....	25
2.2. Double networks	27
2.2.1. Synthesis and structure of double networks.....	27
2.2.2. Properties and applications of double networks.....	28
2.3. Tetra-PEG gels	31
2.3.1. Synthesis and structure of tetra-PEG gels.....	31
2.3.2. Mechanical properties of tetra-PEG gels.....	32
3. Hybrid hydrogels	34

3.1.	Hybrid hydrogels with clay platelets	34
3.1.1.	Synthesis and structure of hybrid hydrogels with clay platelets	34
3.1.2.	Mechanical properties of hybrid hydrogels with clay platelets	36
3.2.	Hybrid hydrogels with silica nanoparticles	39
3.2.1.	General aspects on silica.....	39
3.2.2.	Covalent bonding between silica and polymers.....	42
3.2.3.	Physical interactions between silica and polymers	43
4.	Objectives of the thesis	46
	References	48

Chapter 2: Covalent networks: synthesis and structure of PDMA

hydrogels	55
Contents	56
Introduction	57
1. Material and methods.....	58
1.1. Chemicals.....	58
1.2. Synthesis of hydrogels.....	59
1.3. Titration of extractible.....	60
1.4. Mechanics: tensile test	60
1.5. Swelling behaviour	63
1.6. Small Angle Neutron Scattering	66
2. Results and discussion.....	68
2.1. Titration of extractible.....	68
2.2. Mechanical properties.....	69
2.3. Swelling properties	73
2.3.1. Swelling kinetics	73
2.3.2. Swelling equilibrium.....	76
2.4. Structure of PDMA networks	79

3. Conclusion.....	85
References	87

Chapter 3: Hybrid hydrogels: synthesis and structural investigation of hydrogels containing silica nanoparticles.....89

Contents	90
----------------	----

Introduction.....	91
-------------------	----

1. Synthesis and characterization methods.....	92
--	----

1.1. Inorganic material	92
-------------------------------	----

1.1.1. Scanning electron microscopy	92
---	----

1.1.2. Dynamic light scattering	93
---------------------------------------	----

1.1.3. Small angle neutron scattering.....	94
--	----

1.2. Synthesis of hybrid hydrogels.....	95
---	----

1.3. Titration of extractibles.....	96
-------------------------------------	----

1.4. Mechanics: tensile test	97
------------------------------------	----

1.5. Swelling behaviour	97
-------------------------------	----

1.6. Structural investigations by small angle neutron scattering.....	98
---	----

2. Characterization of hybrid PDMA hydrogels.....	100
---	-----

2.1. Titration of extractible chains and silica nanoparticles.....	100
--	-----

2.2. Structural analysis by Small Angle Neutron Scattering	102
--	-----

2.2.1. Characterization of silica dispersion	102
--	-----

2.2.2. Characterization of silica dispersion in hybrid hydrogels	108
--	-----

2.2.3. Looking for the corona	114
-------------------------------------	-----

2.3. Mechanical properties: initial elastic modulus	117
---	-----

2.4. Swelling behaviour	120
-------------------------------	-----

3. Conclusions on the structure of hybrid hydrogels.....	123
--	-----

References	125
------------------	-----

Chapter 4: From covalent networks to hybrid hydrogels: time-dependence of mechanical reinforcement, dissipation and recovery.....	127
Contents	128
Introduction and general strategy	130
1. Material and methods.....	133
1.1. Synthesis of hybrid hydrogels.....	133
1.2. Rheology	133
1.3. Large strain experiments in tensile mode – rubber elasticity	134
1.3.1. Tensile tests	136
1.3.2. Cycling	136
1.3.3. Stress relaxation.....	137
1.3.4. Fracture	137
1.4. Small angle neutron scattering under deformation	138
2. Stiffening effect of nanoparticles and time-dependence	141
2.1. Rheology: small strain linear viscoelasticity	141
2.2. Tensile behaviour	144
3. Dissipation processes.....	147
3.1. Dissipation by stress relaxation.....	147
3.1.1. Stress relaxation behaviour related to the silica content	148
3.1.2. Toward a characteristic time-identification.....	150
3.2. Dissipation upon loading-unloading cycles.....	151
3.3. Recovery processes.....	155
3.3.1. Strain recovery and effect on successive moduli.....	155
3.3.2. Cycling at large strains	159
4. Damage and fracture	161
4.1. Failure properties: effects of silica content and strain rate.....	161
4.2. Fracture properties	165

5. Small angle neutron scattering under deformation	170
5.1. Strain visualisation.....	171
5.2. Reversibility	177
6. Conclusions on the mechanical reinforcement of hybrid hydrogels: picture and simple model.....	180
References	187

Chapter 5: Tunability of the system.....191

Contents	192
-----------------------	-----

Introduction	193
---------------------------	-----

1. Tuning the PDMA matrix	194
1.1. Changing the cross-linking density	194
1.1.1. Synthesis of hybrid hydrogels.....	194
1.1.2. Swelling measurements.....	195
1.1.3. Mechanical properties.....	197
1.2. Changing the swelling state.....	204
1.2.1. Mechanical properties at swelling equilibrium	205
1.2.2. SANS under deformation.....	208
2. Changing the dispersion state of silica particles.....	211
2.1. Synthesis of hybrid hydrogels.....	211
2.2. Swelling measurements.....	213
2.3. Mechanical properties.....	214
3. Playing with the magnitude of interactions	217
3.1. Changing the monomer.....	217
3.1.1. Synthesis of hybrid hydrogels.....	218
3.1.2. Structural investigations.....	218
3.1.3. Swelling properties	220
3.1.4. Mechanical properties.....	221

3.2.	Introducing a hydrogen-bonding competitor	222
3.2.1.	Swelling behaviour in urea	223
3.2.1.	Synthesis of hybrid hydrogels with urea	224
3.2.2.	Mechanical properties.....	224
4.	Conclusion.....	227
	References	229

Chapter 6: Diluted approach: study of hybrid hydrogels by Dynamic Light Scattering.....231

Contents 232

Introduction..... 234

1.	Light scattering	235
1.1.	Presentation and principle	235
1.1.1.	Static Light Scattering	235
1.1.2.	Dynamic Light Scattering and Laser Light Scattering	236
1.2.	Single Light Scattering in gels	240
1.3.	Gelation process.....	243
1.3.1.	Gelation of polymeric hydrogels.....	243
1.3.2.	Gelation of hybrid hydrogels.....	245
1.4.	Dynamics of particles.....	245
2.	Dynamics of PAAm hybrid hydrogels studied by DLS	248
2.1.	Abstract and introduction	248
2.2.	Synthesis and characterization methods.....	251
2.2.1.	Synthesis of PAAm hybrid hydrogels.....	251
2.2.2.	Dynamic light scattering measurements	252
2.2.3.	Microrheology by diffusing-wave spectroscopy	252
2.3.	Effect of chemical cross-linking.....	253
2.4.	Effect of silica nanoparticles concentration	261

2.5.	Conclusions	267
3.	Dynamics of PDMA hybrid hydrogels studied by DLS.....	269
3.1.	Abstract and introduction.....	269
3.2.	Synthesis and characterization methods.....	272
3.2.1.	Synthesis of P(AAm-co-DMA) hybrid hydrogels	272
3.2.2.	Dynamic light scattering measurements	272
3.2.3.	Hydrogels synthesis for mechanical measurements.....	273
3.2.4.	Mechanical measurements.....	273
3.3.	Effect of DMA/silica interactions on the dynamics	273
3.4.	Conclusions	287
4.	Conclusion on the DLS studies.....	289
	References	291
	 General conclusion.....	 295
	Résumé substantiel en français.....	299
	Annexes.....	321

Introduction générale

Les hydrogels font l'objet d'applications de plus en plus nombreuses et variées dans les domaines des biotechnologies tels que l'agriculture, l'industrie agroalimentaire, la biologie et le secteur biomédical. Au quotidien, nous les retrouvons dans les lentilles de contact, les superabsorbants, la libération contrôlée de médicaments... Les hydrogels constituent des matériaux prometteurs pour de nombreuses applications biocompatibles grâce à leur haute teneur en eau, leur déformabilité et leurs propriétés facilement adaptables au milieu extérieur. En effet, de nombreux hydrogels sont composés de polymères stimulables, leurs propriétés peuvent alors être contrôlées par différents paramètres extérieurs tels que la température, le pH, les champs magnétiques et électriques. Cependant, la forte teneur en eau des hydrogels (jusqu'à plus de 90% en masse) est souvent à l'origine de leur faible résistance mécanique, en termes de module élastique et de taux de déformation. La fragilité des hydrogels limite donc le nombre d'applications envisageables.

Dans la nature, les hydrogels constituent de nombreux tissus, tant dans le monde animal que dans le monde végétal. En effet, les algues, les méduses et les concombres de mer sont trois exemples d'espèces vivantes d'hydrogels, principalement constitués d'eau. Ils présentent de bonnes propriétés élastiques ainsi qu'une grande robustesse leur permettant de survivre dans des milieux hostiles. La nature peut donc nous procurer de nombreux enseignements dont il est utile de s'inspirer pour l'élaboration de nouveaux matériaux aux propriétés nouvelles. L'étude structurale des matériaux est alors une étape cruciale pour cette compréhension. Le développement de techniques de caractérisation spécialement destinées à l'étude des hydrogels a permis de nombreuses avancées. Parmi ces techniques, nous pouvons citer les techniques de diffusion : diffusion de la lumière, diffusion des rayons-X, diffusion de neutrons... L'essor de ces techniques a donné accès à une nouvelle échelle de caractérisation : l'échelle nanoscopique. La connaissance et la compréhension des organisations nanoscopiques des tissus naturellement robustes formés d'hydrogels nous permettent désormais d'élaborer des matériaux synthétiques aux propriétés renforcées.

Dans le cas des hydrogels naturels, les méduses se distinguent par exemple par une structure poreuse à couches. D'autres structures, tout aussi complexes, ont été développées en laboratoire. De nos jours, l'élaboration d'architectures macromoléculaires bien définies est

rendue possible par une chimie sophistiquée et maîtrisée, combinant des matériaux organiques et inorganiques ainsi que des interactions chimiques et physiques. En effet, l'introduction de nanoparticules au sein de matrices polymères est connue pour améliorer les propriétés mécaniques des matériaux. De nombreuses propriétés peuvent ainsi être améliorées grâce à ce concept d'hybridation : des propriétés de conduction électrique aux propriétés antimicrobiennes en passant bien entendu par les propriétés mécaniques. L'un des exemples les plus connus est celui des élastomères chargés. Les élastomères, présentant une grande élasticité, voient leurs propriétés mécaniques fortement améliorées par la présence de particules microscopiques ou nanoscopiques telles que le noir de carbone ou la silice. Les interactions existant entre la matrice polymère et les charges solides sont le paramètre clé du renforcement mécanique. En effet, des interactions spécifiques entre ces deux composants permettent un bon état de dispersion des charges, nécessaire à l'efficacité du renforcement (qu'il soit mécanique, électrique, thermique...).

Dans le domaine des hydrogels, des stratégies d'hybridation ont aussi été développées en introduisant des particules inorganiques au sein de ces réseaux de polymères gonflés. On citera en particulier les travaux pionniers du groupe de Haraguchi au Japon qui ont développé au début des années 2000 le concept de gel nanocomposite en introduisant des nanoparticules d'argile au sein d'un réseau de poly(*N*-alkylacrylamide). Les propriétés remarquables de ces gels nanocomposites, associées aux travaux non moins spectaculaires obtenus par les groupes de Gong (réseaux organiques interpénétrés) et d'Okumura et Ito (réseaux organiques à nœuds coulissants), ont vraiment été à l'origine de la très forte activité observée aujourd'hui dans ce domaine. A la même époque, les travaux réalisés au laboratoire *Science et Ingénierie de la Matière Molle* par Laurence Petit avaient démontré la possibilité d'utiliser les propriétés d'adsorption de polymères tels que le poly(*N,N*-diméthylacrylamide) (PDMA) avec des nanoparticules de silice pour générer la formation d'assemblages hybrides réversibles. Plus récemment, l'introduction de ces mêmes interactions au sein d'une matrice de PDMA réticulé a permis de valider l'utilisation des nanoparticules de silice dans le cadre du renforcement des propriétés mécaniques des hydrogels. Ce sont ces travaux précurseurs publiés en 2010 au sein de notre équipe *Soft Polymer Network* qui ont conduit vers une étude

plus systématique des propriétés viscoélastiques des gels hybrides PDMA/silice ; étude qui fait l'objet de ce travail de thèse.

Ce manuscrit de thèse se divise en six chapitres. Le premier sera consacré à une étude bibliographique concernant le domaine des hydrogels. Il présente leurs principales caractéristiques, leurs applications actuelles ainsi que leurs limitations. A partir d'une description des inhomogénéités structurales à l'origine des propriétés limitées des hydrogels, les différentes stratégies de renforcement récemment développées seront présentées.

Le deuxième chapitre s'intéressera à la synthèse et à la caractérisation d'hydrogels organiques, du point de vue de leurs propriétés thermodynamiques, structurales et mécaniques. A partir de cette étude détaillée, nous étudierons, au Chapitre 3, l'impact de l'introduction de nanoparticules de silice sur les propriétés de ces réseaux, grâce à des techniques expérimentales parfaitement adaptées aux hydrogels.

En se concentrant sur les interactions polymère/silice, les propriétés mécaniques des hydrogels hybrides seront largement étudiées dans le Chapitre 4. Nous porterons un intérêt particulier à la caractérisation de ces réseaux sur une large gamme d'échelle de temps. Enfin, cette étude nous permettra de proposer une modélisation simple dans le but de rendre compte du caractère viscoélastique de notre système.

Le Chapitre 5 sera consacré à l'étude de l'adaptabilité de notre système hybride par la modification des paramètres clés de l'architecture du réseau. Pour cela la matrice polymère, le réseau inorganique et leurs interactions seront modifiés.

Pour finir, le Chapitre 6 sera l'occasion d'exposer une étude parallèle concernant les hydrogels hybrides en s'intéressant plus particulièrement à leur structure locale. Les méthodes de diffusion de la lumière sont particulièrement adaptées à la caractérisation précise des interactions existant entre la matrice polymère et les nanoparticules de silice. Dans un premier temps, les techniques de diffusion de la lumière seront exposées. Ensuite nous nous intéresserons à l'étude de la dynamique de réseaux hybrides composés d'un

polymère ne présentant pas d'interaction avec la silice : le polyacrylamide. Enfin, nous étudierons l'impact de l'introduction progressive d'un monomère ayant des interactions avec la silice, le *N,N*-diméthylacrylamide, sur la dynamique du système.

Enfin, les apports de cette étude seront repris en conclusion et des perspectives seront proposées.

Dans un souci de diffusion scientifique et par le caractère international des participants à ce projet, nous avons choisi de rédiger la majeure partie de ce manuscrit en anglais. Cependant, cette introduction générale, la conclusion générale ainsi qu'un résumé substantiel sont rédigés en français.

General introduction

Hydrogels are being increasingly used in many bio-applications such as agriculture and food science, biology and biomedicine. In our everyday life, we can find them in contact lenses, superabsorbants, targeted drug delivery systems... Hydrogels are promising materials for biocompatible applications, thanks to their high water contents, their soft mechanical properties and their adaptability to external environment. As a matter of fact, many hydrogels are made of responsive polymers: their properties can be tuned with several parameters such as temperature, pH, magnetic and electric fields. However, the high water content of hydrogels (up to 90 wt%) is often at the origin of poor mechanical properties in terms of elastic modulus and deformability. Their fragility limits the potential applications of hydrogels.

In nature, hydrogels are widely present in tissues, in both animal and vegetal worlds. For instance, algae, jellyfish and sea cucumbers are three kinds of “living hydrogels” mainly composed of water. They have good elastic properties and a high toughness allowing them to survive in hostile media. Learning from nature is a promising way for understanding and designing new reinforced materials. For that reason, structural investigations are essential steps; they became possible thanks to the development of experimental techniques dedicated to hydrogels study. Among these techniques, one can mention the scattering ones: light scattering, X-ray scattering, neutron scattering... The development of these techniques opened a new scale of the structural investigation: the nano-scale. From the knowledge of the nano-organization of naturally tough hydrogel tissues, synthetic materials can be designed with enhanced and responsive properties.

In the case of natural hydrogels, jellyfish present a singular layered porous structure but other elaborated morphologies have been developed. Nowadays, the elaboration of well-defined macromolecular architectures is possible thanks to a sophisticated chemistry, combining organic and inorganic materials, chemical and physical interactions. For instance, hybridation of nanoparticles with a polymer network is known to improve the mechanical properties of materials. A wide range of properties can be enhanced by this hybridation concept: from the electrical conductance to antimicrobial properties and also mechanical properties. The most classical example that we can mention is the one of charged elastomers.

Elastomers are well known for their high elasticity but their mechanical properties are significantly enhanced by the presence of solid micro or nanoparticles, such as carbon black or silica. However, the interactions existing between the organic matrix and the fillers are a key parameter for the mechanical reinforcement. As a matter of fact, specific interactions enable the good dispersion of fillers, necessary to reach the full extent of reinforcement (mechanical, electrical, thermal...).

In the case of hydrogels, similar hybridation strategies have been developed with the introduction of inorganic particles in swollen polymeric network. We can mention the pioneering work of Haraguchi in Japan who developed in 2002 the concept of nanocomposite gel by introducing clay nanoparticles into a poly(*N*-alkylacrylamide) network. The outstanding properties of nanocomposite gels, together with the smart works on organic gels developed by Gong (double networks) and Okumura and Ito (slide-ring gels), have really triggered a high research activity in this domain. In the meantime, the PhD work performed by Laurence Petit in the *Soft Matter Science and Engineering* laboratory has clearly shown the possibility to take advantage of the adsorption properties of polymers like poly(*N,N*-dimethylacrylamide) (PDMA) with silica nanoparticles to build reversible hybrid assemblies. More recently, the introduction of such nanoparticles inside a covalently cross-linked PDMA network demonstrates the efficiency of silica nanoparticles to reinforce the mechanical properties of hydrogels. These preliminary works, published in 2010 within our « *Soft Polymer Network* » group have naturally led towards a more systematic study relative to viscoelastic properties of hybrid hydrogels PDMA/silica; study that forms the core of this PhD work.

This manuscript is divided into six chapters. The first one is devoted to an overview of the hydrogel science. The main characteristics of hydrogels are discussed along with their main limitations. After a description of structural inhomogeneities at the origin of the weak properties of hydrogels, the reinforcement strategies that emerged during the last ten years will be introduced.

The second chapter deals with the synthesis and the study of chemical hydrogels, in terms of thermodynamics, structure and mechanical properties. From this characterization, the elaboration of hybrid hydrogels will be described in Chapter 3. The impact of silica nanoparticles onto the general characteristics of hydrogels will be investigated following a similar approach.

In Chapter 4, the mechanical properties of hybrid hydrogels will be addressed with a special focus on PDMA/silica interactions. After a detailed investigation of the properties at different strains and probing more deeply the time-scale effects, this study will lead to a brief modelling of our structure, taking into account the viscoelastic nature of the system.

In Chapter 5, the adaptability of the system will be considered, changing the main attributes of hybrid hydrogels: the polymer matrix, the inorganic network and their interactions. The macroscopic response of such tuning will be discussed.

Chapter 6 will be dedicated to a parallel study of hybrid hydrogels in terms of local structure. Light scattering methods are perfectly adapted for that purpose, aiming at characterizing the polymer/nanoparticles interactions. After an introduction to light scattering techniques, two aspects will be developed. First, the dynamics of hybrid hydrogels prepared with a non-adsorbing polymer (polyacrylamide) will be investigated. Then, we will study how the dynamics of the system changes when interacting monomer units (*N,N*-dimethylacrylamide) are progressively introduced into the polymer network.

Finally, the main contributions of this work will be recalled and summarized in a concluding part, along with the prospects.

Chapter 1

Hybrid hydrogels: a general survey

Contents

Contents	12
Introduction.....	14
1. Polymer hydrogels	15
1.1. Definitions, main characteristics and applications.....	15
1.1.1. Definitions and characteristics	15
1.1.2. Applications	16
1.2. Synthesis methods.....	18
1.3. Inhomogeneities in hydrogels	19
1.3.1. Types of inhomogeneities	20
1.3.2. Characterisation and consequences of inhomogeneities.....	21
2. Reinforcement of organic hydrogels	24
2.1. Topological networks	24
2.1.1. Structure of topological networks.....	24
2.1.2. Properties of topological networks.....	25
2.2. Double networks	27
2.2.1. Synthesis and structure of double networks.....	27
2.2.2. Properties and applications of double networks.....	28
2.3. Tetra-PEG gels	31
2.3.1. Synthesis and structure of tetra-PEG gels	31
2.3.2. Mechanical properties of tetra-PEG gels.....	32
3. Hybrid hydrogels	34
3.1. Hybrid hydrogels with clay platelets.....	34
3.1.1. Synthesis and structure of hybrid hydrogels with clay platelets.....	34
3.1.2. Mechanical properties of hybrid hydrogels with clay platelets	36
3.2. Hybrid hydrogels with silica nanoparticles	39
3.2.1. General aspects on silica.....	39
3.2.2. Covalent bonding between silica and polymers.....	42

3.2.3. Physical interactions between silica and polymers	43
4. Objectives of the thesis	46
References	48

Introduction

The main purpose of this work is the elaboration of a hybrid material swollen by water based on the combination of a polymeric hydrogel and inorganic nanoparticles and the study of the structure-properties relationships. Nowadays an abundant literature is available on gels topic, from natural gels to synthetic ones. The first part of this chapter will be dedicated to a literature survey about hydrogels.

As hydrogels are polymeric materials highly swollen by water, their mechanical properties are quite poor, compared to other polymeric systems. Many investigations can be reported on the reinforcement of the mechanical properties of hydrogels with the elaboration of various architectures. The second part of this chapter will describe the main reinforcement strategies, always staying in the organic world.

Several teams did not limit their research activities to the solutions proposed by organic chemistry but widened it to the inorganic field. In the past decade, hybrid hydrogels have widely drawn attention and the third part of this chapter will summarize the different strategies developed for the improvement of hydrogels' properties.

As a conclusion, the objectives of the thesis and the general approach which has been followed will be described.

1. Polymer hydrogels

1.1. Definitions, main characteristics and applications

1.1.1. Definitions and characteristics

A gel is a macromolecular three-dimensional network highly swollen by a solvent. Generally, the weight concentration of solvent is up to 90 wt%. For a structural point of view, a gel is constituted of polymer chains or colloids interconnected to each other at the macroscopic scale [1]. Thanks to the percolation, gels are soft materials behaving as soft solids, with the ability of swelling and deswelling. According to the nature of the solvent, gels are classified in three groups: hydrogels (for water), organogels (for organic solvents) and aerogels (for air) [2]. In this study, we will focus on hydrogels based on covalently cross-linked polymer chains, as schematically represented on **Figure 1**.

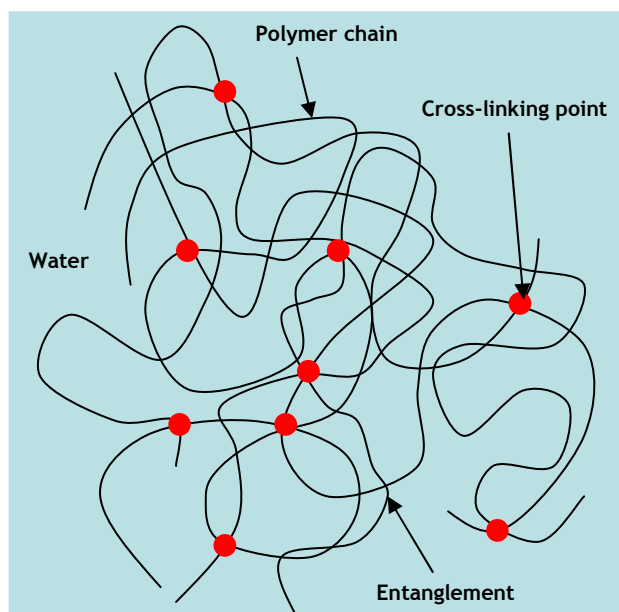


Figure 1: Schematic representation of a polymer hydrogel.

Thanks to specific interactions between the polymer chains and the solvent and thanks to many possible structures of the network, polymer hydrogels are complex materials. These two key parameters can be infinitely modified in order to obtain specific materials with defined properties. One of the most remarkable properties of hydrogels is the very low

polymer content. The cross-linking points, which can be either chemical (for covalently cross-linked gels) or physical (for self-assembled gels), are at the origin of the cohesive nature of hydrogels. In the case of covalent bonds between the different polymer chains, the cross-linking points are irreversible, if no chemical degradation is undergone. These hydrogels behave as elastic solids, with the conservation of the permanent shape under self-weight (no flowing phenomenon) and no physical modification. In the case of physically cross-linked gels, the interactions at the origin of the cross-linking points are reversible, such as Van der Waals interactions or derivatives [3]: hydrogen bonding [4], ionic [5, 6] or hydrophobic interactions [7, 8]... The different possibilities in nature of the physical interactions leading to gel formation is at the origin of a wide time-scale of the gel life-time. Other physical interactions are stiffer than the previously cited ones and the resulting hydrogels remain stable along higher time-scales. For instance, it is well known that gelatine can make gels upon cooling by the formation of triple helices in water [9, 10]. Another example of strong physical interactions on gels is the one of polyvinyl alcohol hydrogels: while polyvinyl alcohol is atactic in nature, this material is able to form crystalline domains in water, that has been widely studied [11].

1.1.2. Applications

As hydrogels are networks of hydrophilic polymers highly swollen by water, diffusion processes can occur inside the structure: water can diffuse through hydrogels. This characteristic is at the origin of many applications as hydrogels are able to absorb, store and release large amounts of water and also of aqueous solutions containing active substances. Thus, since the eighties, many applications of hydrogels have been developed in the life science area, among which can be cited contact lenses (thanks to the transparency of hydrogels) [12, 13] and superabsorbants (thanks to the high ability to swell) [14]. In the case of research on contact lenses, several solutions are proposed to enhance the comfort of users and to prevent drying out of eyes. For that purpose, gradient of cross-linking densities in the lenses cross-section has been investigated, leading to a gradient of mechanical properties with substantial differences (the surface being more cross-linked), as presented in **Figure 2**. The resulting material is characterized by a water gradient silicone hydrogel with good oxygen transmission.

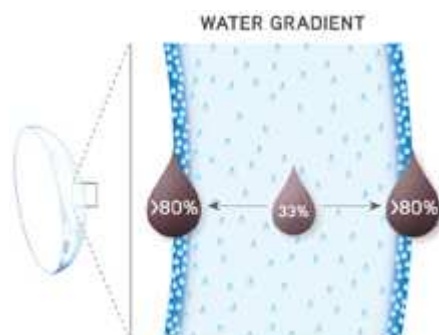


Figure 2: Representation of Alcon® technology for contact lenses with water gradient.

Recently, some new materials have been developed, based on stimuli-responsive polymer hydrogels. As a matter of fact, the high amount of water contained in hydrogels is a key parameter in responsiveness properties: modifying experimental parameters such as temperature, ionic strength and pH results in changes of the swelling properties of hydrogels and thus of mechanical properties [15]. For that reason, new applications of hydrogels appeared in the bio-area such as bio-sensors for encapsulation and drug delivery systems, where the hydrogels are used thanks to their adaptability to the environment [16-18]. An example of the use of thermosensitive polymers in drug delivery is given in **Figure 3**. From surface-specific modification of a hydrogel, a reduced-permeability layer is created at the hydrogel surface. A change in temperature produces an opening of the layer, enabling the previously loaded drug to diffuse out of the hydrogel. In this example, poly(*N*-isopropylacrylamide) (PNIPAm) can be used, for its temperature responsibility by Lower Critical Solution Temperature (LCST) mechanism [19].

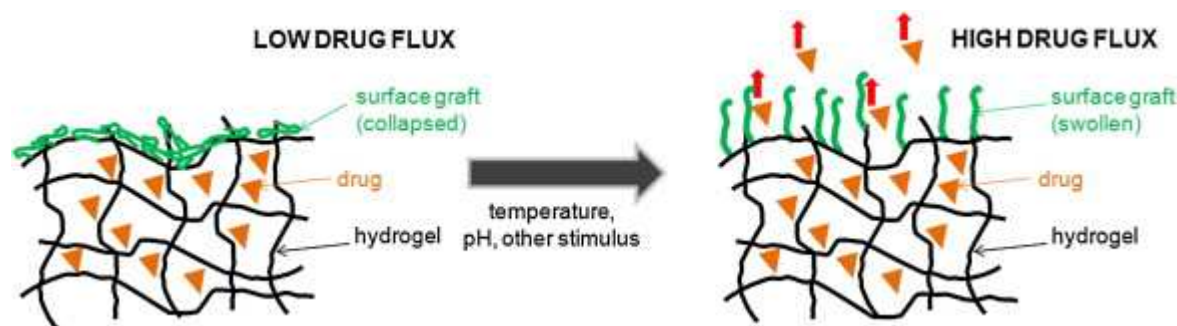


Figure 3: Schematic representation of a new hydrogel system based on a thermosensitive switch for on-off drug delivery, from [19].

Hydrogels are also used in scaffolds for tissue engineering, controlling the distribution of cells or molecular species [20-22]. In agriculture, hydrogels can also hold moisture in arid areas [23]. The number of scientific publications and applications concerning hydrogels has been increasing drastically during the last thirty years. However one main limitation remains: the poor mechanical properties of hydrogels and their durability under stimuli.

As a conclusion to this first part, hydrogels are swollen structure with a wide range of properties. The mechanical and swelling properties of gels will be influenced by the life-time of the cross-links (infinite for chemical gels and more or less temporary for physical gels) and also by structural parameters of the polymer network (such as the mesh size, the presence and type of inhomogeneities...).

1.2. Synthesis methods

The differentiation of gels depending on the medium (water, oil or air) is very common but other classifications exist. Gels can also be classified in three types, depending on their preparation methods, as illustrated in **Figure 4** [2].

From the copolymerization of monomers and cross-linkers in a solvent, a first type of three-dimensional swollen network can be obtained, using either chemical or physical cross-linkers. This first type of gel is composed of a large variety of monomers and cross-linkers, using all the classical polymerization reactions. In this first type of gel synthesis, the polymer chains and the cross-linked network are formed simultaneously. This method generally leads to heterogeneous structures, with a broad size distribution of elastic chains [24]. Co-monomers can also be polymerized, leading to numerous possibilities of architectures.

A second type of gels can be made from the cross-linking of pre-formed polymer chains in solution with cross-linker (chemical or physical). In this case, the gel formation can occur by the linkage of reactive moieties present at the chains' end or along the chains. This method is used for example in the case of gelatine gels, for which the proteins and peptide chains can be physically cross-linked (in this case no cross-linker is added, the gelation occurs thanks to the sol-gel transition of gelatine).

Then a last type of gels is obtained by the gelation of low molecular weight compounds in organic solvent [25]. Those oil gelators can be fatty acid derivatives, steroid derivatives, anthryl derivatives (radicals derived from anthracene), amino-acids, organometallic compounds... One advantage of this type of gel is the low concentration needed to reach the gelation (typically 2 wt% or less).

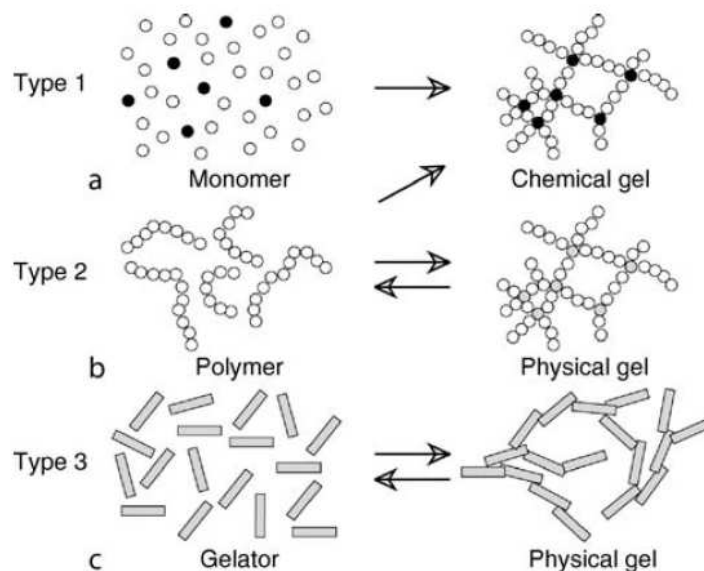


Figure 4: Shibayama's classification of gels according to the preparation method. Type 1, chemical gels: gels made by polymerization and cross-linking a mixture of monomers (open circles) and cross-linkers (solid circles). Type 2, physical gels: gels made by cross-linking polymer chains in solution (the cross-linking points are represented in grey circles). Type 3, physical gels of oil gelators: physical gels made by self aggregation of low molecular weight compounds. [2]

1.3. Inhomogeneities in hydrogels

The macroscopic behaviour of hydrogels directly depends on the architecture of the polymeric network. The presence of defects strongly influences the mechanical properties of hydrogels by weakening it. For that reason, a precise experimental characterization of the local structure of hydrogels is needed and has been deeply investigated during the last forty years. The presence of large amounts of water in hydrogels can be a serious drawback for the

characterization but new investigations techniques have been developed for that purpose. The main source of inhomogeneities in hydrogels comes from the synthesis of the networks. As a matter of fact, when the synthesis of hydrogels is conducted from monomers or polymer chains in solution in presence of cross-linkers (it corresponds to the first two cases explained in the previous part dedicated to the synthesis of hydrogels), there is no control of the incorporation of the cross-linking units: the organization of the cross-linking points is statistic along the network.

1.3.1. Types of inhomogeneities

First, in the case of gel synthesis from the copolymerization of monomers and cross-linker, the obtained networks contain inhomogeneities with concentration fluctuations [26-28]. Second, when the cross-linkers cannot be distributed all along the polymer chains but only at their ends (in the case of gel synthesis from the cross-linking of pre-formed polymer chains), the final structures are less heterogeneous than in the previous case but still remain inhomogeneous [27].

Shibayama recently proposed a new classification, schematically represented on **Figure 5**, of the three possible defects in gel structures [29]:

- A first type of defects is the one of spatial inhomogeneities, which corresponds to the non-uniform spatial distribution of cross-links along the polymeric network. Some zones are densely cross-linked while others are loosely cross-linked. When chemical cross-linkers are used, these inhomogeneities remain static, while in the case of reversible cross-linkers, these inhomogeneities can be dynamic and thus can disappear.
- A second type of defects is the one of topologic inhomogeneities, which represents the state of topology of the network such as loops, trapped entanglements and dangling chains. These defects, which appeared during the gel synthesis, are static inhomogeneities.

- A last type of defects is the one of connectivity inhomogeneities, coming from the size distribution and the spatial distribution of branched polymer clusters. This last type of inhomogeneities is dynamic.

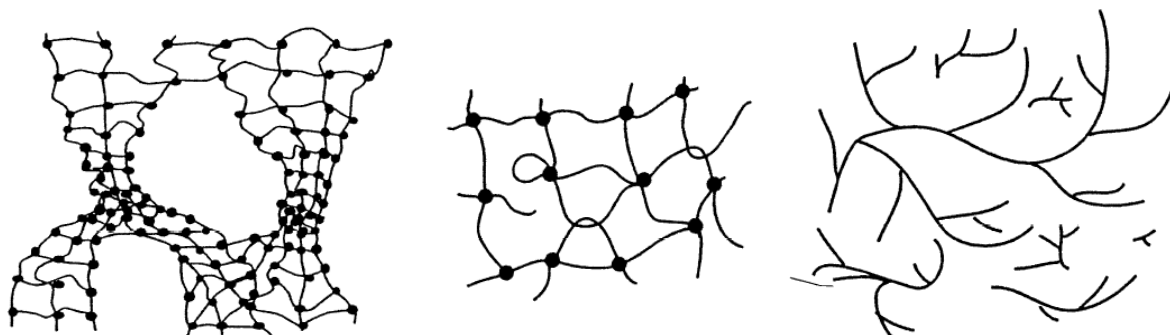


Figure 5: Shibayama's classification of inhomogeneities in gels. Left: spatial inhomogeneities. Middle: topological inhomogeneities. Right: connectivity inhomogeneities. [29]

The contrast between hydrogel heterogeneities (densely and weakly cross-linked domains) remains weak at the preparation state but can be enhanced by swelling the hydrogel: the differences of polymer concentrations within these different domains are revealed [30].

1.3.2. Characterisation and consequences of inhomogeneities

Classical ways of synthesis previously described lead to the formation of hydrogels containing inhomogeneities. Experimentally, these inhomogeneities can be expressed by abnormal behaviour under sollicitation compared to developed models and can be identified according to several methods.

Microscopic scale: diffusion properties of hydrogels

Spatial inhomogeneities are characteristic of chemically cross-linked hydrogels, resulting from the irregular incorporation of cross-linking units through the network formation. At the preparation state, physically cross-linked hydrogels can present spatial inhomogeneities which can be suppressed under certain conditions. Scattering techniques, such as Small Angle Neutron Scattering (SANS) and Light Scattering (LS), are used to evidenced these concentration fluctuation zones in hydrogels, at a scale from the dozen to the hundred of

nanometres. Indeed, a gel can be thought as a semi-dilute solution in which the polymer segments are cross-linked by chemical or physical bounds. Several theoretical models have been developed based on Lorentzian functions, such as the one of Panyukov and Rabin [2, 31] which describes a semi-dilute solution with partially inhomogeneous spatial distribution of polymer segments containing cross-links which prevents the polymer segments from free movements. These two components are represented by two correlation lengths: ξ for the polymer-polymer correlation and Ξ for the correlation length characteristic of solid-like inhomogeneities, as represented in **Figure 6**.

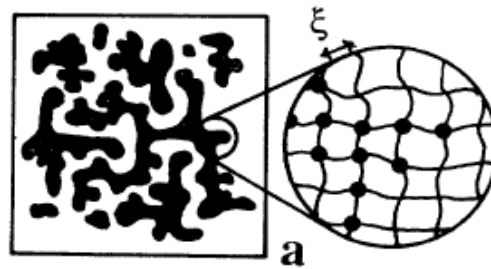


Figure 6: Schematic representation of a randomly cross-linked gel: regions of higher cross-linking density are marked in black, with a characteristic size Ξ . Chains are not shown, except in the magnified inset, from [30]. In both domains, the polymer-polymer correlation distance ξ , corresponding to the thermal blob, is unchanged.

A comparison between the theoretical and the experimental parameters can give information about the presence of inhomogeneities. The use of theoretical models such as the one mentioned here can quantify characteristic lengths, as represented in **Figure 6**.

In some cases, spatial inhomogeneities can even be detected visually by the presence of poorly transparent zones in hydrogels samples [32].

Macroscopic scale: elastic and swelling properties of hydrogels

In the 1940s, several thermodynamic and mechanical models have emerged for the description of the behaviour of ideal networks. As a matter of fact, the architecture of hydrogels is at the origin of their highly elastic properties, with an elastic modulus between 10^3 and 10^5 kPa, that have been described by the affine [33] and phantom models [34]. These

two models are based on the principles of rubber elasticity, comparing the entropy of the network in the initial unconstrained state to the one in the stresses state [35].

When immersed in a good solvent and under certain preparation conditions, a gel is able to swell up to a maximal state. The swelling properties of hydrogels have been described by Flory-Rehner's thermodynamic theory [33, 36, 37], taking into account several parameters such as the affinity of the polymer for the surrounding solvent, the initial concentrations of monomers, cross-linkers, the cross-linker functionality... These mechanical and thermodynamic models will be discussed in the next Chapters by comparison with the experimental results.

Influence of synthesis parameters on inhomogeneities

Thanks to the characterization techniques exposed here, the effect of experimental parameters on inhomogeneities of hydrogels can be evidenced. In the literature of acrylic gels, the main influencing parameters are the following (all the other parameters being constant):

- the monomer concentration: an equilibrium can be found between a diluted state, where the percolation can be unreachd, and a more concentrated state where the effective cross-linking density can decrease due to steric effects, as studied by Gundogan *et al.* [38];
- the nature of monomers: the behaviour of electrolyte polymer gels is related to their environmental medium and particularly to the presence of ionic charges, as described by Miquelard-Garnier *et al.* [39];
- the cross-linker concentration: generally, a high cross-linker concentration in the reactive medium leads to strongly inhomogeneous structures (in terms of spatial inhomogeneities), as previously represented and widely studied by Shibayama [24, 29, 40];
- the initiation system: in the case of free-radical polymerization, Okay *et al.* have shown that different morphologies can be obtained according to the nature of the initiation reaction: redox or thermal initiation [41].

2. Reinforcement of organic hydrogels

As described in the previous part, hydrogels are non ideal materials as their structures contain many types of defects. Several strategies have been developed in order to suppress or at least minimize these inhomogeneities with the aim of a reinforcement of the mechanical properties of gels. Moreover, the numerous defects of hydrogels are at the origin of poor mechanical properties. Recent studies have also been conducted in order to delay gel fracture. In this part, we will focus on three strategies recently developed on purely organic hydrogels: topological networks, double networks, and tetra-PEG gels.

2.1. Topological networks

2.1.1. Structure of topological networks

In the beginning of the twenty first century, Ito *et al.* developed a new kind of hydrogels which are designated as topological networks [42]. They are based on the concept of movable cross-links, theoretically described by Edwards twenty five years ago [43] and more recently by Rubinstein and Panyukov [44]. The main idea of this system is to introduce movable cross-links, which is totally impossible in conventional chemical hydrogels. This structure allows free movements of the cross-linking points along the polymer chains in order to equalize the tension of the polymer chains, like pulleys. This novel gel architecture is obtained from the chemical cross-linking of polyrotaxane molecules in solution, comprising poly(ethylene glycol) and α -cyclodextrin. The cross-linking of the polyrotaxane chains results from the coupling of the α -cyclodextrin rings, leading to polymer chains topologically interlocked by figure-of-eight cross-links. One particularity of these gels is the presence of bulky end groups on the polymer chains. These topological gels are also called “slide-ring gels” and their original structure is schematically represented in **Figure 7**.

A well defined architecture of such networks can be obtained, with various average numbers of α -cyclodextrin molecules per chain, by the control of complexation time, temperature and initial ratios of components, as demonstrated by Hadziioannou *et al.* [45].

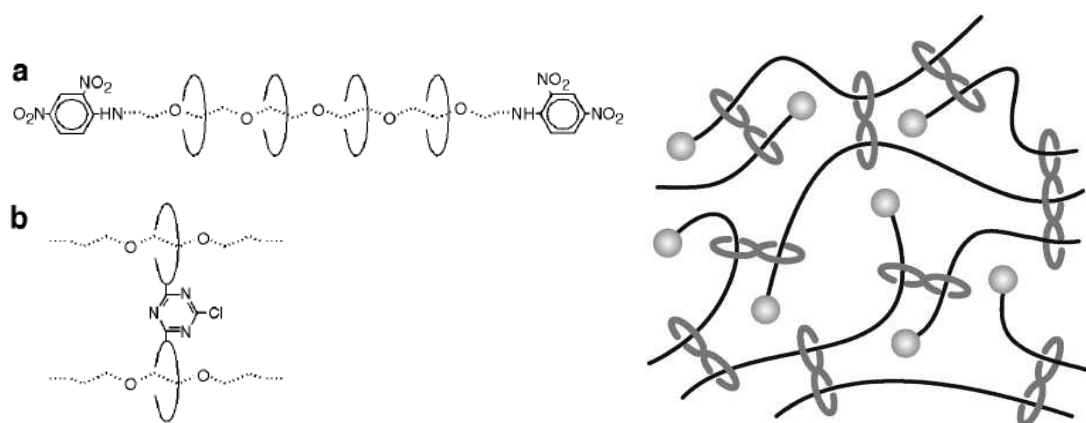


Figure 7: Left up: the polyrotaxane consisting of α -cyclodextrin and poly(ethylene glycol) and left down: the figure of eight cross-link: covalently cross-linked cyclodextrins, from [42]. Right: schematic representation of the structure of topological hydrogels, from [46].

The sliding motion of α -cyclodextrin on polyrotaxane chains has been evidenced by DLS by the appearance of a new mode in the decay-rate distribution function, between the fast one (related to cooperative diffusion) and the slow one (related to self-diffusion) [47].

By the SANS technique, an increase of the scattering intensity $I(q)$ is observed for classical gels when the cross-linking density is increased. This increase is due to frozen inhomogeneities introduced by cross-linking. However, the slide-ring gels revealed lower scattering intensity with the increase of cross-linking density [46]. This decrease has been attributed to the reduction of spatial inhomogeneities thanks to the free movement of the cross-links along the polymer chains which accommodate the imposed macroscopic strain.

2.1.2. Properties of topological networks

The original structure of slide-ring gels provides unique properties which answer the main limitations of organic hydrogels and that are summarized below.

Swelling properties of slide-ring gels

The slide-ring gels developed by Ito *et al.* behave as superabsorbent polymers as they can absorb water up to 400 times their dry weight and 1600 times the weight of the PEG contained. Interestingly, this volume changes are totally reversible, without any damage [42].

Mechanical properties of slide-ring gels

When a loading-unloading tensile cycle is applied, physical hydrogels show large hysteresis in stress-strain curves, with a J shape, like in living tissues, because of recombination of physical cross-links during deformation. On the other hand, conventional organic hydrogels do not show any hysteresis and S shape as no recombination is possible with permanent cross-links. For slide-ring gels, a different mechanical behaviour is observed: J-shaped curves (different from chemical hydrogels) with no hysteresis (different from physical hydrogels) [48]. Moreover, they can reach strains of 2000% thanks to the pulley effect represented in **Figure 8** [42].

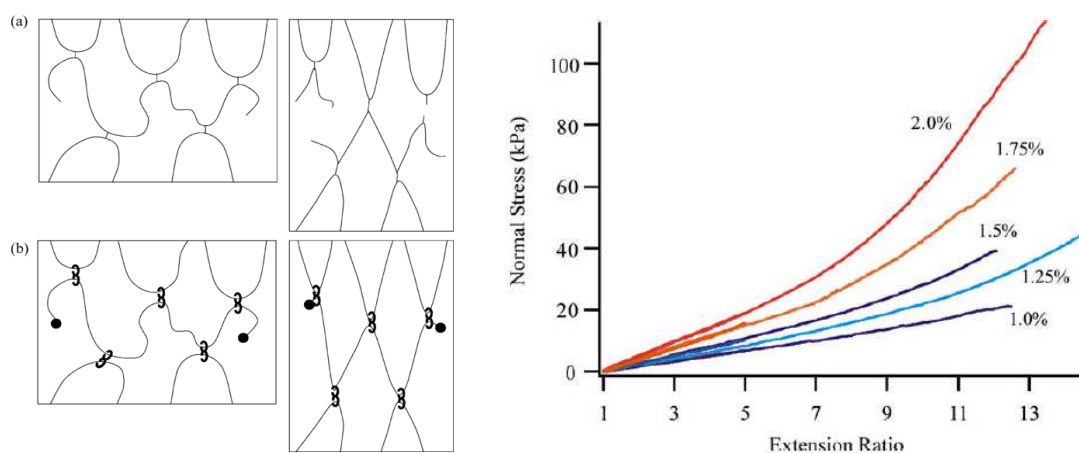


Figure 8: Left: schematic comparison of deformation in covalently cross-linked network and slide-ring gel, from [42].

Right: typical J-shaped stress-strain curves of slide-ring gels with different concentrations of cross-linker, from [49].

Recently, the mechanical behaviour of slide-ring gels has been investigated in terms of cross-linking variation and an abnormal behaviour has been pointed out, compared to conventional rubber elasticity [50]. As a matter a fact, when the cross-linking density of slide-ring gels is increased, first a normal increase of elastic modulus is observed but it is then followed by a decrease of elastic modulus. A theory of alignment entropy of cyclic molecules in addition to the conformational entropy of polymer chains has been proposed to explain this behaviour.

The viscoelastic properties of slide-ring gels have also been studied by Hadziioannou *et al.*, revealing two relaxation modes [51]. Indeed, the two evidenced viscoelastic regimes have been attributed to the molecular mechanism of the change of the mean mass distribution between the cross-linking points, thanks to the sliding motion of the α -cyclodextrin rings on the PEG chains.

Bi-dimensional small angle neutron scattering of slide-ring gels

Small angle neutron scattering experiments can be realized under deformation in order to correlate the macroscopic behaviour to the structure properties. With this technique, slide-ring gels are again different from conventional chemical hydrogels. As a matter of fact, organic hydrogels present a so-called “abnormal butterfly pattern” under deformation, due to an amplification of inhomogeneities in the stretching direction. In the case of topological gels, a “normal butterfly pattern” is observed indicating that the pulley effect suppresses the amplification of inhomogeneities thanks to the presence of movable cross-links [46].

2.2. Double networks

2.2.1. Synthesis and structure of double networks

Ten years ago, Gong *et al.* developed the concept of tough gels with double network hydrogels consisting of two interpenetrating polymer networks swollen by water [52]. The first network is made of highly cross-linked rigid polymers while the second one is a loosely, or even not, cross-linked flexible polymer network, as schematically represented in **Figure 9**. In this representation, the first neutral network of poly(acrylamide) (PAAm) is interpenetrated with a second polyelectrolyte network of poly(2-acrylamido-2-methylpropanesulfonic acid) (PAMPS) [53]. The main idea is to find an optimal combination of the first rigid and brittle polyelectrolyte network and the second flexible and ductile neutral network.

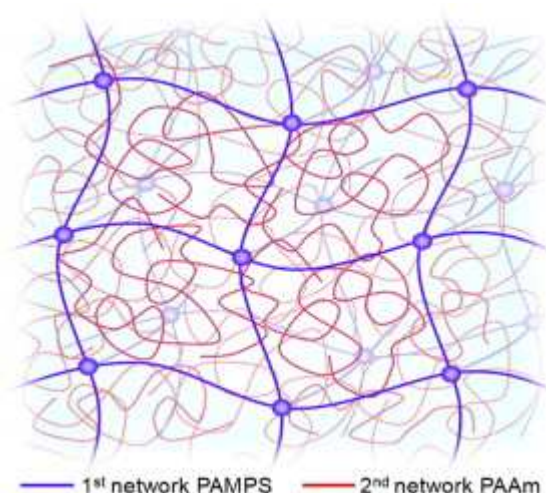


Figure 9: Schematic representation of the structure of double network hydrogels, from [53]. Note that the molar concentration of the second PAAm network is 20-30 times the one of the first PAMPS network.

Double network hydrogels are generally synthesized via a two-step sequential free-radical polymerization, starting from the synthesis of the highly cross-linked polyelectrolyte network (PAMPS), followed by the swelling of this first network by the second neutral monomer (AAm) and finishing by its polymerization with a small amount of chemical cross-linker. The double network gel is then immersed in water to reach swelling equilibrium [52].

SANS and Ultra Small Angle Neutron Scattering (U-SANS) have been used to characterize double network hydrogels. Molecular association has been evidenced, as the structures of PAMPS and PAAm networks are more homogeneous when synthesized in presence of the co-monomer than in pure water [54].

2.2.2. Properties and applications of double networks

Here we mention the main properties of double networks leading to useful applications, mainly in biomedical area.

Mechanical properties of double network hydrogels

The mechanical properties of double networks – in terms of stiffness (elastic modulus), strength and toughness - are much better than that of the individual components but optimal concentration ratios have to be found for enhancing their mechanical properties [55-58]. When the second network is loosely cross-linked (or even without chemical cross-linker), double network hydrogels exhibit high mechanical strength. As a matter of fact, when the cross-linking density of the second PAAm network is changed from 0 to 1 mol%, keeping constant the structure of the first PAMPS network, similar elastic modulus (300 kPa) are obtained but the highest fracture parameters are obtained for the uncross-linked materials [56]. Moreover, DLS analyses revealed the presence of a slow mode at low cross-linking densities of the second network, with a perfect correlation with mechanical properties at different cross-linking densities [56].

During uniaxial tensile tests, Gong's double networks show a necking phenomenon: narrowed zones appear along the samples and then grow up with elongation, as represented in **Figure 10** left. In the corresponding stress-strain curves, yielding occurs, followed by a plateau region during the neck zone propagation, [55]. This phenomenon corresponds to a break of the first PAMPS network into small clusters, because of its intrinsic fragility. These formed clusters play the role of physical cross-linking points for the long flexible PAAm chains, behaving as sliding cross-linker. This mechanism has been verified by SANS experiments under deformation [54].

In our laboratory, cyclic experiments of loading-unloading on double network hydrogels have revealed very large hysteresis. Their analysis have been used to characterize the degree of heterogeneity of different double networks: more than 80% of the network strands being very short and resulting in bond fracture at any deformation beyond 20% [59].

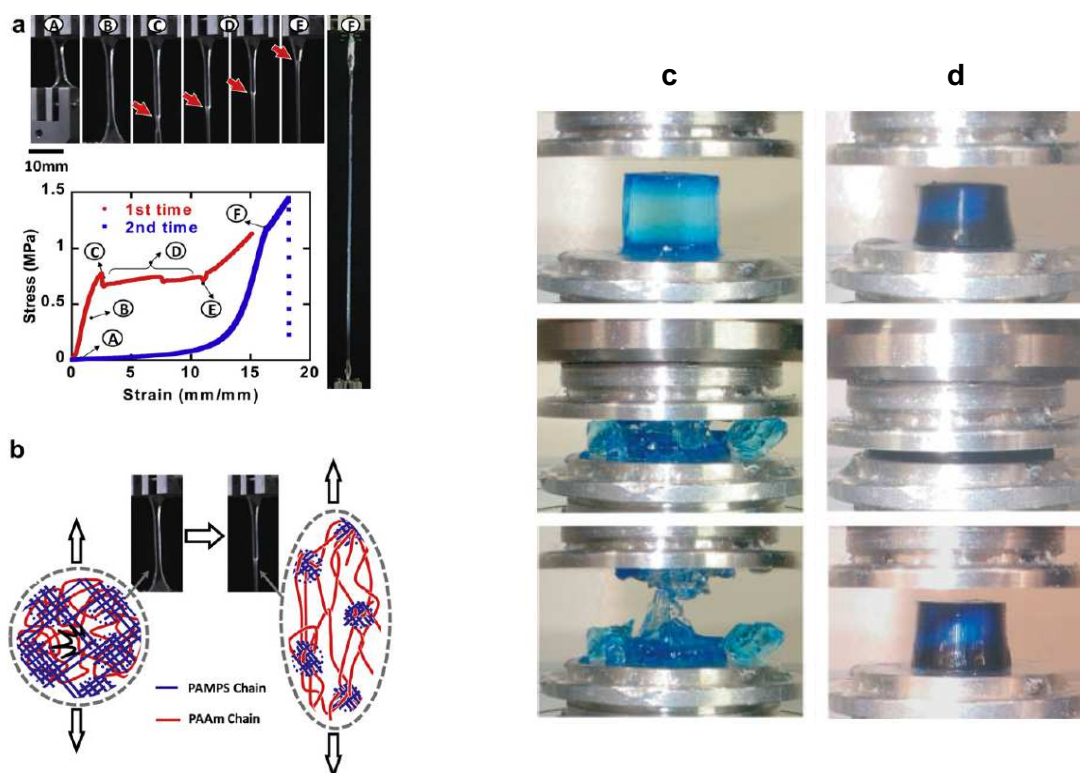


Figure 10: Left: tensile behaviour of double networks at a rate of 0.13 s^{-1} , from [55]; a: loading curves of PAMPS/PAAm double network with images demonstrating a necking process, the insert capital letters represent the correspondence between the images and the data points in the loading curves and b: illustration of the network structure before and after necking.

Right: pictures comparing mechanical behaviour of simple and double networks, from [52]; c: cross-linked PAMPS simple network and d: PAMPS/PAAm double network.

Applications of double network hydrogels

The use of soft viscoelastic polymer network to reinforce the mechanical properties of a brittle polyelectrolyte network is the success story of Gong's group. From the strong mechanical reinforcement observed, other hydrogel systems have been developed inspired by Gong's concept, leading to applications in biomaterials. Among the biocompatible hydrogels based on double networks, we can mention:

- the use of natural polymers such as bacterial cellulose together with gelatin [60],
- the combination of natural polymers and synthetic ones such as jellyfish or alginate gels and PAAm [61, 62].

The biological applications of double networks that have been well developed concern:

- substitute solution for cartilage replacement thanks to the resistance against water, the absence of detrimental effects on cartilage interface *in vivo* and the spontaneous cartilage regeneration observed for PAMPS/PDMA double network hydrogels [63-67],
- cornea reparation thanks to the transparency, the good glucose diffusion coefficient and the good tolerance of PEG/PAAc hydrogels [68].

2.3. Tetra-PEG gels

2.3.1. Synthesis and structure of tetra-PEG gels

From the previous examples of reinforced hydrogels, it is obvious that all the strategies are based on a minimisation of inhomogeneities as they are at the origin of reduced mechanical properties. We present here another strategy based on the research of ideally homogeneous network. The strategy of Sakai *et al.* aims at forming a homogeneous structure by combining two well-defined symmetrical tetrahedron-like macromonomers of the same size [69]. The particularity of these two macromonomers is that each of them has four end-linking groups reacting with each other, avoiding self-reaction as they must be connected alternately, as schematically represented in **Figure 11**. The two constitutive units are: a tetra-NHS-glutarate-terminated PEG (TNPEG) and a tetraamine-terminated PEG (TAPEG). A controlled anionic polymerization is used to obtain monodisperse macromolecules, with an important restriction of mobility of the four arms by steric repulsion. Then a simple mixing of two aqueous solutions of TNPEG and TAPEG leads to a gel formation based on the alternation of elastic blobs without any entanglements [70, 71].

SANS experiments has been conducted on tetra-PEG hydrogels, varying the length of the arms and an unusual result has been observed. As a matter of fact, polymer gels usually exhibit an upturn in scattering intensity curves in the low- q region because of inhomogeneities. Contrary to other polymer networks, tetra-PEG hydrogels do not show any upturn, confirming their “ideality” [40]. This absence of Inhomogeneity remains also at the deformed state.

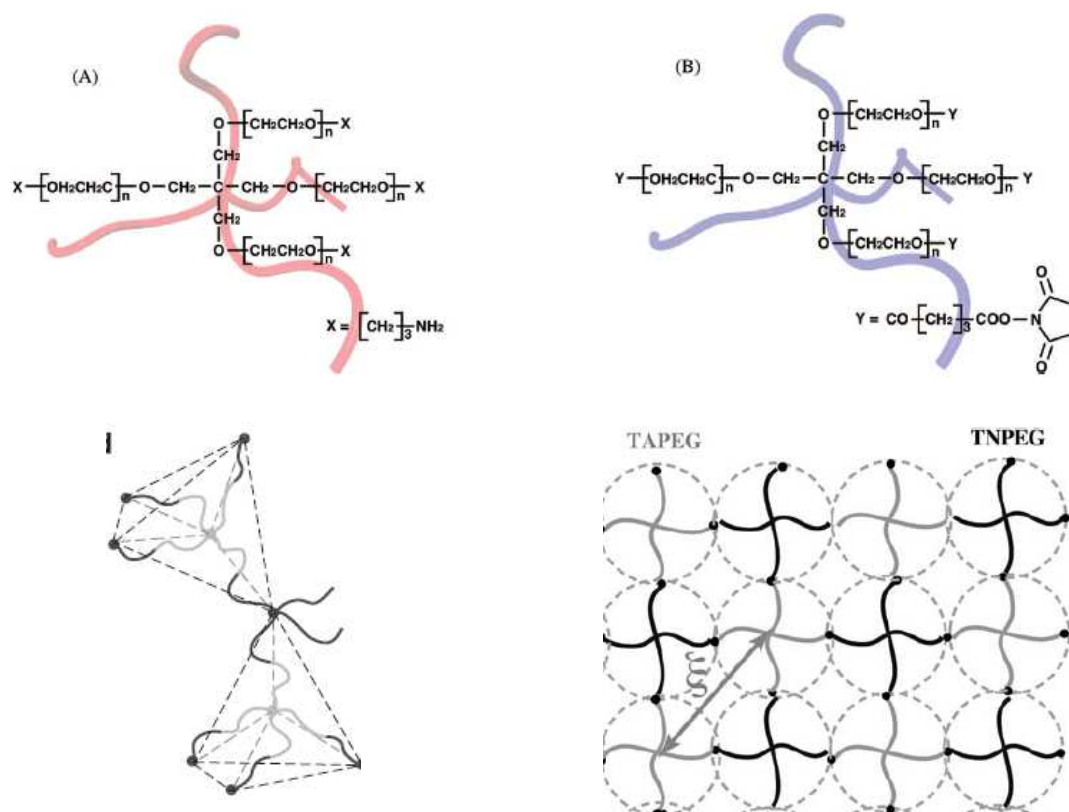


Figure 11: Up: molecular structures of TAPEG (left) and TNPEG (right), from [69]. Down: schematic illustration of the two constitutive units of tetra-PEG gels, left: two units and right: network structure, from [40].

2.3.2. Mechanical properties of tetra-PEG gels

Tensile behaviour of tetra-PEG hydrogels has been studied varying the molecular weight of the macromonomers. A threshold has been evidenced for the molecular weight of the macromonomers: below 10 kg/mol, tetra-PEG hydrogels are brittle and poorly stretchable but above this critical value, they reach high deformability and resist to high stress compared to acrylamide hydrogels having the same network concentration, as presented in **Figure 12**, [69].

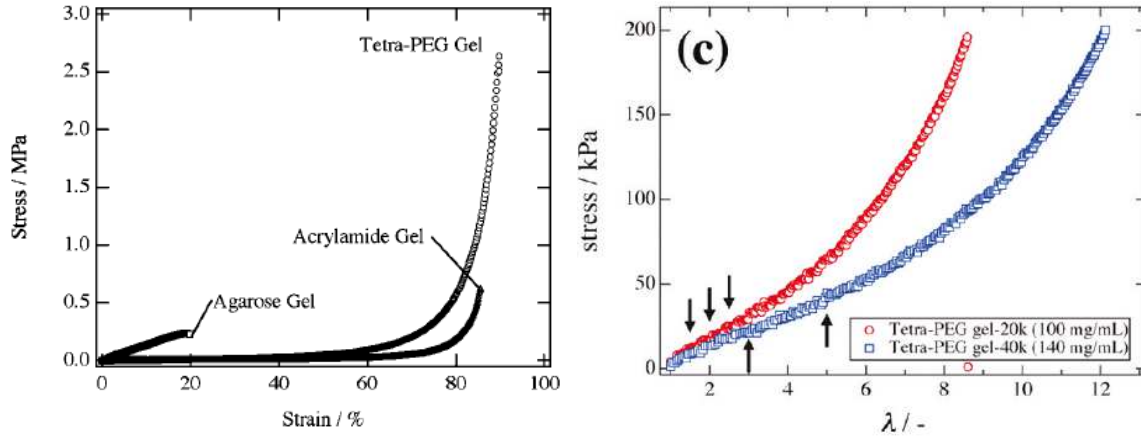


Figure 12: Left: comparison of tensile curves of agarose gel, acrylamide gel and tetra-PEG gel, at the same network concentration and in the same experimental conditions, from [69].

Right: tensile curves of tetra-PEG gels with two different molecular weight of macromonomers: 20 kg/mol (in red) and 40 kg/mol (in blue), from [72].

From the mechanical behaviour of tetra-PEG hydrogels, Sakai *et al.* evidenced a very high deformability of such “ideal” network [72]. Moreover, SANS measurements under deformation also demonstrated the absence of structural inhomogeneity which is at the origin of such mechanical behaviour (or in some cases the presence of a very low fraction of inhomogeneities) [40]. Another proof of the controlled architecture is the fracture experiments which confirmed that no entanglement was formed in such system [73].

3. Hybrid hydrogels

As discussed in the first part of this chapter, classical organic hydrogels present poor mechanical properties because of inhomogeneities and low dissipation, inducing limited applications. Research on hydrogels science has not been limited to the organic part of chemistry. As a matter of fact, the incorporation of inorganic components has been studied since the beginning of the twenty first century for the mechanical reinforcement of hydrogels. Often designated as “nanocomposite gels”, “hybrid hydrogels”, “nanohybrid hydrogels”, this novel class of materials has been introduced by Haraguchi *et al.* in Japan and is now studied in different research teams. We present here Haraguchi’s system and the other materials that ensued from it.

3.1. Hybrid hydrogels with clay platelets

3.1.1. Synthesis and structure of hybrid hydrogels with clay platelets

PNIPAm hydrogels had attracted a lot of interest because of their sensitivity to external stimuli such as temperature, solvent, pH, light... During the last decade, Haraguchi *et al.* developed a new kind of PNIPAm hydrogels with singular mechanical properties, thanks to the introduction of exfoliated clay platelets into the polymer network [74]. These gels are based on the exfoliation of clay into dispersed platelets (Laponite, 20-30 nm in diameter, 1 nm in thickness) in an aqueous solution of NIPAm followed by the polymerization of NIPAm using a redox initiation of potassium persulfate (KPS)/*N,N,N,N'*-tetramethylethylenediamine (TEMED). In the absence of chemical cross-linker, these gels are expected to be physical gels with neighbouring clay sheets connected by polymer chains: clay sheets acting as multifunctional cross-linker for the PNIPAm chains, as schematically represented in **Figure 13**.

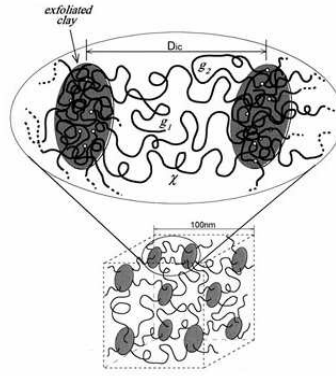


Figure 13: Schematic representation of the structure of Haraguchi 's hybrid hydrogels, from [75].

The gelation mechanism of PNIPAm/clay hybrid hydrogels and their obtained structure have been studied in details by DLS and contrast variation SANS [76]. Concerning the first technique, the formation of the hybrid network has been characterized by:

- the formation of growing clusters of nanocomposite microgels (corresponding to a depression in optical transmittance),
- followed by the gelation threshold (corresponding to an abrupt increase in the light scattering intensity).

The second technique of contrast variation SANS is based on the different scattering length densities of the three-component systems (here: PNIPAm, clay and water) and the possibility to “screen” one of the three components by suitable D₂O/H₂O ratios; this technique will be presented in details in the experimental part of Chapter 3. From this technique, Miyazaki *et al.* concluded that:

- a polymer layer surrounding the clay platelets exists, with a thickness of 1 nm,
- this fraction of polymer layer is almost constant, whatever the clay platelets concentration.

From these results, the following gelation mechanism has been proposed: the polymerization is initiated at the clay surfaces, as initiators are often concentrated near the surface of clay platelets [77]. After initiation, the free radical polymerization starts by the growing of polymer chains in the neighbourhood of clay platelets, progressively forming microgel clusters. The exfoliated clay platelets are covered by an adsorbed polymer layer. Those clusters percolate and the gel is formed (if the NIPAm initial concentration is high enough). Miyazaki's results are summarized in the schematic representation given in **Figure 14**.

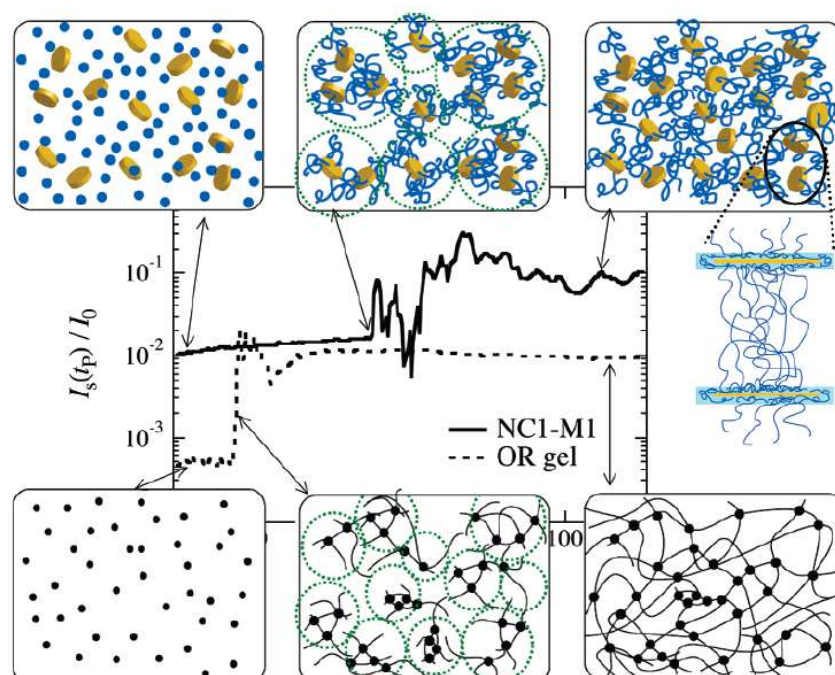


Figure 14: Schematic representation of the gelation mechanisms of PNIPAm/clay hydrogels (up) compared to the one of pure polymer hydrogel (down). Middle: normalized scattering intensity as a function of the polymerization time for both systems, from [76].

Other monomers have also been studied for the elaboration of nanocomposite hydrogels containing clay platelets, such as acrylamide (AAm) or *N,N*-dimethylacrylamide (DMA) but with different structures and less promising properties that will not be exposed here [78-80]. The use of clay platelets has also been investigated with pluronics, leading to reinforced networks [81].

3.1.2. Mechanical properties of hybrid hydrogels with clay platelets

From the novel network structure previously described, Haraguchi *et al.* obtained enhanced mechanical properties for their uncross-linked hybrid hydrogels in terms of deformation (up to strains of 1000%) and initial modulus (up to several dozens of kPa), as presented in **Figure 15**. The mechanical properties are highly dependent of synthesis conditions and concentrations of polymer and clays [74]. The high deformability, compared to organic hydrogels, can be explained by the low degree of effective physical cross-linking induced by clay platelets: a typical molecular weight of the chains between two clay platelets is about

50000 g/mol. Moreover, the effect of clay content on mechanical properties has also been studied in details.

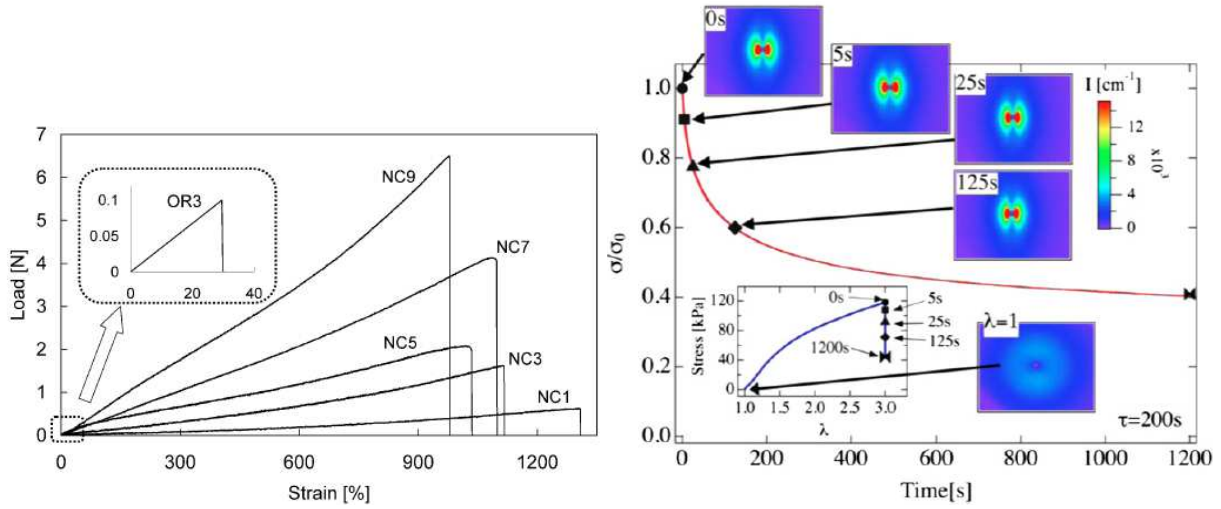


Figure 15: Left: Stress-strain curves of nanocomposite PNIPAm/clay hydrogels, varying the clay content (NC1 to NC9), compared to a corresponding organic hydrogel (OR3), from [74].

Right: Normalized stress relaxation curve at a loading strain of 200% with corresponding 2D-SAXS scattering patterns after different delays (0s, 5s, 25s and 125s), from [82].

By the non-covalent nature of the physical cross-links in Haraguchi's system, long time relaxation behaviour has been observed and coupled with Small Angle X-ray Scattering (SAXS) experiments under deformation, as presented in **Figure 15** [82]. This technique allows following the evolution of the structure as a function of time, in order to link it to mechanical experiments. From the reversible nature of the physical cross-links, good self-healing properties have been observed: contacting two cut surfaces leads to its self-healing on condition that the system is heated to at least 50°C and during up to 100 hours [83].

The presence of an organic cross-linking agent has also been characterized in terms of mechanical properties [84]. The more chemical cross-linker is introduced, the higher the elastic modulus and the lower the strain at failure. A compromise can then be found depending on the application.

Recently, Haraguchi *et al.* prepared more sophisticated nanocomposite hydrogels consisting of a tetra-PEG/clay network, combining his knowledge of nanocomposite to the ideal structure of tetra-PEG hydrogels [85]. This combination, under particular conditions such as the use of a pyrophosphate-Na buffer to ensure the dispersion of exfoliated clay platelets and the transparency of the gels, led to the structure represented on **Figure 16**. Enhanced mechanical properties were obtained compared to pure tetra-PEG systems, as shown in **Figure 16**.

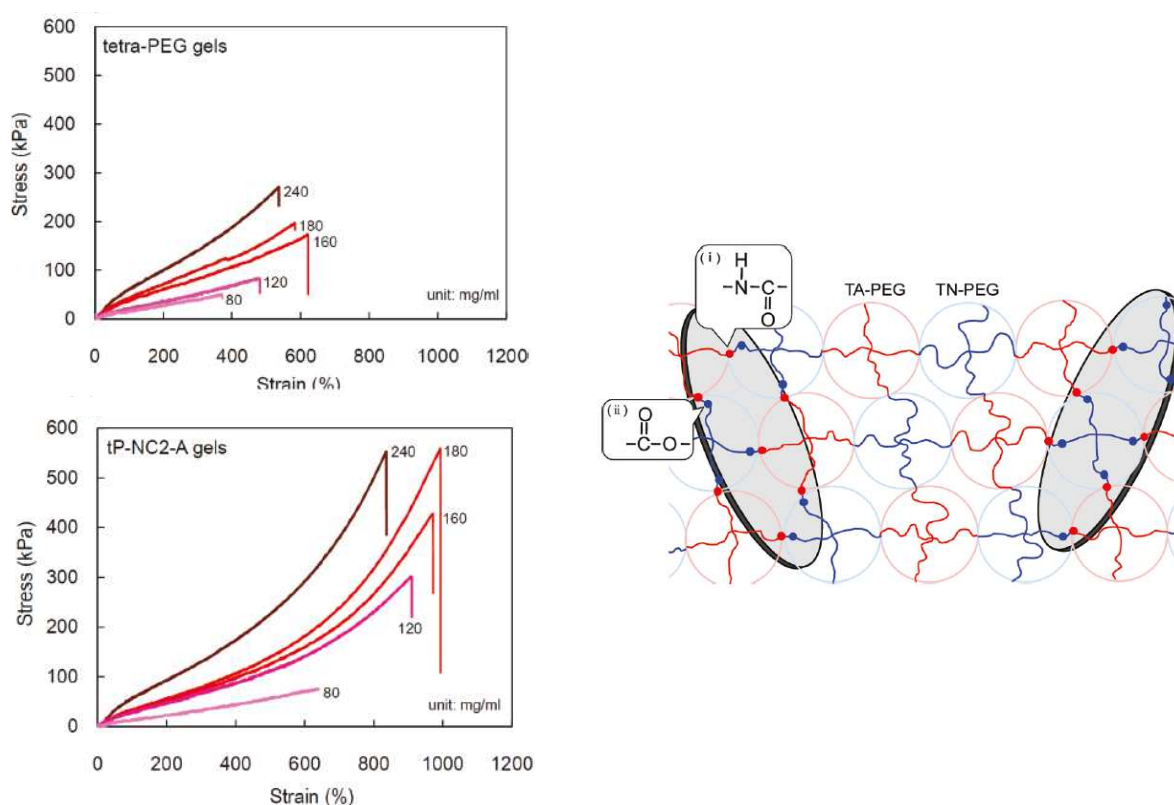


Figure 16: Left: Comparison of stress-strain curves of tetra-PEG gels without clay (up) and with clay platelets (down), at different compositions, from [85].

Right: Schematic representation of the structural model for the tetra-PEG/clay network, from [85].

Despite promising mechanical results, nanocomposite gels made of tetra-PEG and clay platelets present interesting mechanical reinforcement only for a sharp concentration range of clay. Indeed, poor mechanical properties have been obtained in other conditions where

clay platelets disturbed the formation of the tetra-PEG network, which was not ideal any more [85].

3.2. Hybrid hydrogels with silica nanoparticles

The idea of hybrid hydrogels developed by Haraguchi has been generalized to other types of inorganic particles such as silica nanoparticles. From a practical point of view, the main advantages of silica nanoparticles are the following:

- silica nanoparticles are widely commercially available with different sizes;
- aqueous colloidal suspensions are stable.

From a chemical and structural point of view, the main advantages of silica nanoparticles are the followings:

- silica nanoparticles can be spherical, preventing from any anisotropic effect (contrary to clay platelets);
- silica nanoparticles can be easily functionalized on their surface, leading to a wide range of grafting or interactions with polymers.

Nowadays, silica is a well known inorganic material, as it has been widely studied, some important characteristics will be exposed here.

3.2.1. General aspects on silica

Silica is a mineral widely used in industry and also in the academic world [86-88] and which can be synthesised following two main methods:

- One possible method consists in using tetrahydroxysilane (TEOS). This method is commonly used in research laboratories, leading to monodisperse silica suspensions with typical size of a hundred of nanometres.
- The other one is based on the precipitation of a concentrated silicates solution, depending on precise temperature and pH conditions. According to the chosen experimental parameters, different kinetics of nucleation and morphologies are obtained. This method is preferentially used in the industry thanks to the low costs of silicates, leading to nanometric particles.

General information about silica can be obtained in several books that deal with chemistry and physico-chemistry [86-88]. In our study, the silica particles used come from the precipitation of silicates. A good understanding of all the different physico-chemical mechanisms that will be involved in our system needs a characterization of the silica nanoparticles.

Surface state of silica

Amorphous silica is chemically written as SiO_2 and presents silanol groups SiOH on its surface. Those silanol groups present a pK_a value of 7.0 ± 0.2 . The iso-electric point of silica is at pH 2. For that reason, at pH higher than 2, the silica surface has a negative electrostatic potential, as represented in **Figure 17**. The pH is then at the origin of different protonation states of the silica surface. In his book, Iler referenced several studies confirming that the surface concentration of silanol groups was about 5 silanol groups per nm^2 [86]. This value, that can slightly change with the type of silica (amorphous or not), is an average value as the silanol groups are not organized in a regular distribution at the surface of amorphous silica.

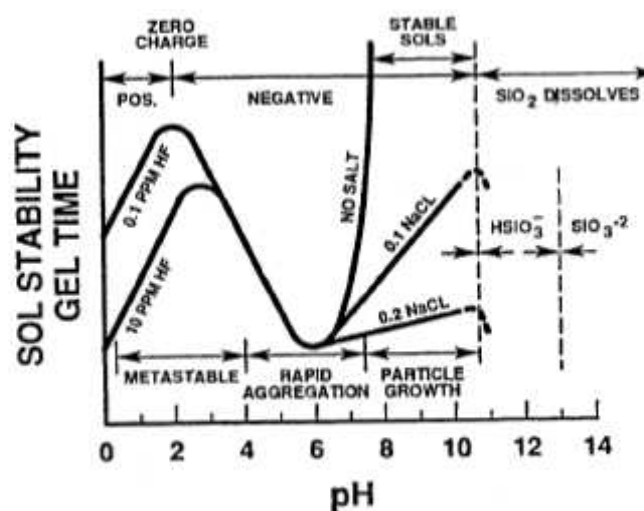


Figure 17: Effects of pH in the colloidal silica-water system, from [86].

At pH values higher than 8-9, silica starts dissolving and forms silicates that will increase the ionic strength of the medium.

As silica is a poly-acid, several pKa values are associated to the different couples depending on the protonation state of the silanol groups and of their nature. When silanol functions start to deprotonate, their typical pKa is about 6.2. It has been reported that as soon as the number of deprotonated sites increases, the pKa of the SiOH/SiO⁻ couple increases and reaches 9.2. An empirical law has been described in order to link the number of deprotonated sites to the pH [89]:

$$\log(\text{SiO}^- \text{ nm}^{-2}) = 5.2 \log(\text{pH}) - 5.35.$$

Solubility of silica in water

Several chemical reactions can occur at the surface of silica. It is well known that one can graft polymer chains onto silica surface. In water, hydrolysis and oxolation can happen. The hydrolysis of silica can start at its surface, catalyzed by hydroxide ions. One possible mechanism is presented on **Figure 18**.

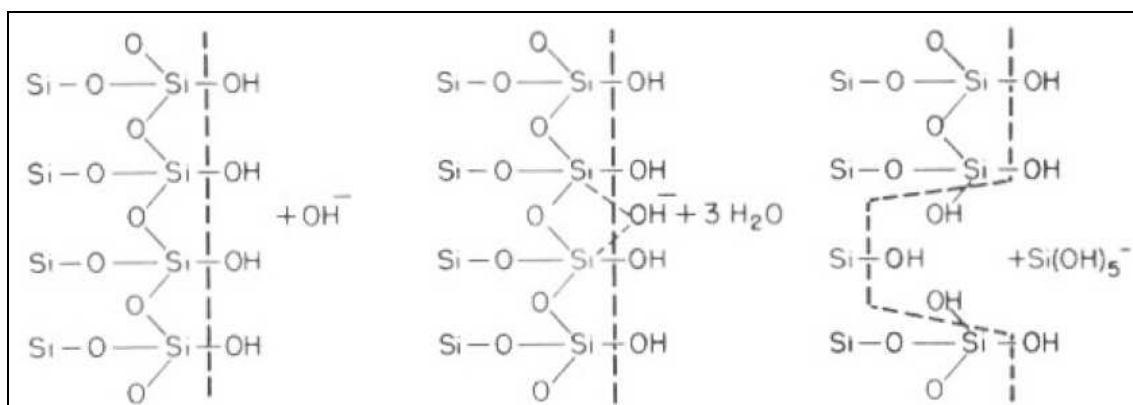


Figure 18: Schematic mechanism of silica dissolution in water in presence of hydroxide ions, from [86]. The dotted line represents the silica/water interface.

The water solubility of silica depends on various conditions, such as the pH, the temperature, the salinity, the presence of other species and the curve radius of the surface. A slow thermodynamic equilibrium between solid silica and dissolved species can be reached and has been described by Stöber [90]. Concerning the silica dissolution, he evidenced that the curve radius had no influence on it but that the important parameter was the total surface of the silica.

3.2.2. Covalent bonding between silica and polymers

Silica particles can be used as fillers in hydrogels with the formation of covalent bonds between the polymer chains and the silica particles. For instance, Takafuji *et al.* recently developed hydrogels based on polymer chains containing trimethoxysilyl groups able to react with silica surface, as presented in **Figure 19**, [91]. Hydrolysis-condensation reactions can take place between these reactive groups of the polymer and the silanol on the silica surface. As represented in **Figure 19**, hydrogen bonds can also be established between the vinylpyrrolidone groups and the SiOH groups. We are in the case of a double cross-linking as silica surface can be involved in chemical and physical cross-linking.

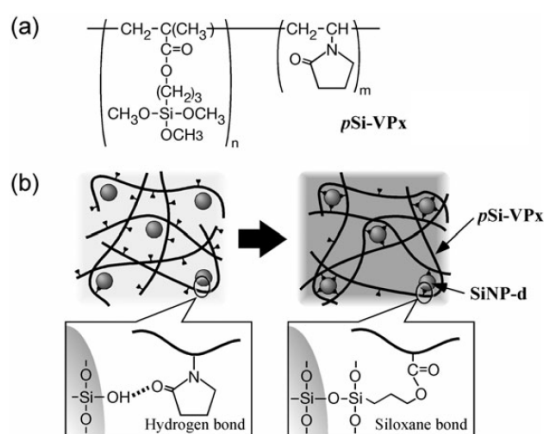


Figure 19: Up: chemical structure of water-soluble copolymer with reactive side chains. Down: schematic representation of the corresponding gelation process, from [91].

Another example of chemical cross-linking with silica can be given in the biomaterials field. Hybrid materials have been developed by Coradin *et al.* with modified silica nanoparticles and collagen: the mixing of sulfonate-grafted Stöber silica particles and collagen led to the formation of collagen shells, as represented in **Figure 20**, [92]. A strong pH effect has been demonstrated on the spatial organization of collagen at the silica surface. The elaboration of a silica nanoparticles network linked by collagen fibrils that show molecular recognition abilities could lead to useful applications in the biomedical field.

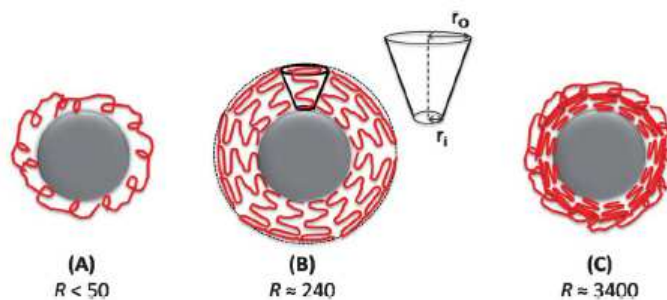


Figure 20: Schematic representation of collagen shells at the surface of silica-SiSO₃ nanoparticles, with increasing collagen concentration, from [92].

3.2.3. Physical interactions between silica and polymers

Using commercial aqueous suspensions of silica nanoparticles, Petit *et al.* succeeded in creating hybrid hydrogels based on the assembly of silica nanoparticles and some copolymers in semi diluted solution [93]. Adsorption isotherms and calorimetric studies showed that *N*-alkylacrylamide derivatives strongly interact with silica nanoparticles. By grafting the interacting oligomers (poly(*N,N*-dimethylacrylamide) and poly(*N*-isopropylacrylamide)) onto a non-adsorbing and watersoluble poly(acrylamide-co-sodium acrylate) backbone, a binding process of the adsorbing side-chains was observed. The schematic mechanism of the formation of the hybrid network is given in **Figure 21**. The use of PNIPAm side-chains led to a second level of connectivity as this polymer is able to self-assemble with temperature. In the present case, a double network was obtained in the presence of silica nanoparticles: the first one coming from the interactions between PNIPAm and silica surface and the second one coming from the temperature-dependence of the solubility of the PNIPAm side-chains, a LCST-polymer.

In the architecture developed by Petit *et al.*, the silica nanoparticles play the role of inorganic cross-linking points, leading to stable structures. However, the strong interaction between the poly(*N*-alkylacrylamide) side-chains and the silica surface leads to inhomogeneous structures, especially when the polymer concentration is increased (for concentration higher than 2 wt%).

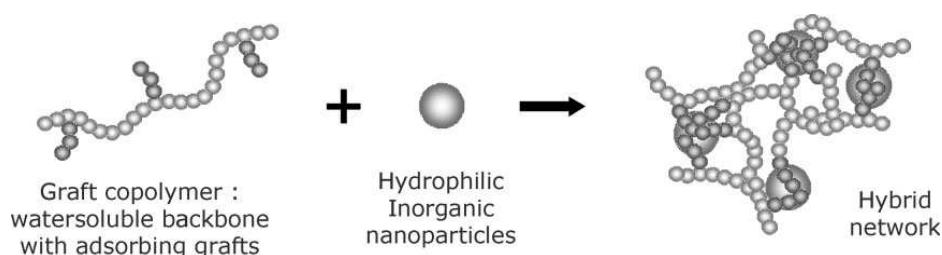


Figure 21: Schematic representation of hybrid network obtained from self-assemblies between adsorbing grafts and inorganic nanoparticles, from [93].

From this study, two different systems have been developed in our group, based on the elaboration of hybrid hydrogels. This strategy is a good mean to increase the polymer concentration compared to the previous study of associations between polymer and silica. The first system is based on the free-radical polymerization of DMA in presence of silica nanoparticles, without any chemical cross-linker [94]. This system presents enhanced mechanical properties in terms of initial modulus, strain at failure and energy dissipation, thanks to the physical cross-linking points established by PDMA onto the silica surface. As a matter of fact, these hybrid hydrogels had values of initial modulus 20 times higher than pure organic gels and strain at failure up to 1000%. However, a self-cross-linking phenomenon by transfer reactions has been evidenced for this system. A schematic representation of the obtained structure is given in **Figure 22**. The second system contains a high concentration of chemical cross-linker (*N, N'*-methylenebisacrylamide, MBA) and has been studied at the swollen state [95].

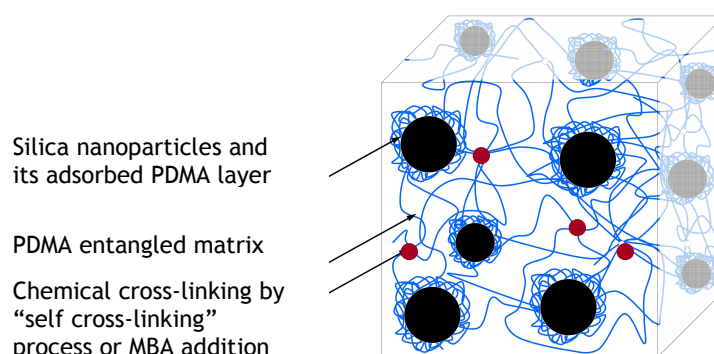


Figure 22: Schematic representation of the structure of hybrid hydrogels with silica nanoparticles covered by PDMA layer embedded into an entangled PDMA matrix, from [94].

Some hybrid hydrogels have also been developed with acrylamide as monomer, leading to no specific mechanical reinforcement [96, 97]. These results are in perfect agreement with the study of Petit *et al.* about the selective interactions of silica surface with *N*-substituted acrylamide monomer units. In this case, the silica nanoparticles act as non-interacting fillers and can be compared to filled elastomers.

4. Objectives of the thesis

As we saw in this introducing chapter, recent developments in hybrid hydrogels try to solve the main limitations of organic hydrogels, considering the intrinsic weakness of their mechanical properties. For that purpose, several strategies have been developed and we choose to focus more specifically on formulations of hybrid systems involving specific interactions between PDMA and silica. From pioneering works developed in the laboratory, it has been clearly highlighted that specific interactions taking place between PDMA chains and silica particles definitely reinforced the mechanical properties of these soft materials with a large increase of the elastic modulus. The properties of such multi-component systems can be tuned by changing several parameters such as polymer concentration, cross-linking density, swelling state, silica content... Nevertheless, while “uncross-linked” PDMA/silica hydrogels display weak retractility under deformation with residual strain, highly cross-linked systems show better reversibility under deformation but with a low deformation at break (lower than 100%). In order to compromise between these antagonistic properties (modulus and extensibility) the main part of this thesis was performed on low cross-linked networks. One of our objectives was to achieve a detailed study of hybrid hydrogels based on PDMA and silica nanoparticles, in terms of thermodynamics, structure and mechanics. These different aspects of the study require the development of experimental setups that will be detailed in this manuscript.

As the properties of hydrogels strongly depend on the swelling state (*i.e.* concentration), we will take a particular attention to separate the effects of silica and swelling on the gels' properties. For that purpose, we choose to study our system in a reference state (the preparation state), keeping the polymer/water ratio constant and varying the silica content.

The experimental part of this thesis is organized according to the following plan:

1. Chapter 2 is dedicated to the characterization of covalent polymer networks, without silica nanoparticle, using various methods to probe thermodynamics, structure and main mechanical properties as a function of cross-linking density.

2. The introduction of silica nanoparticles into the organic network is investigated in Chapter 3 with a detailed study concerning the impact of nanoparticles onto the structure/properties relationships.
3. A detailed characterization of the mechanical properties of hybrid hydrogels at different time scales will be proposed in Chapter 4.
4. From the well characterized hybrid hydrogels studied throughout the previous chapters, the adaptability of the system will be exposed in Chapter 5, changing the polymer matrix, the size of inorganic filler and the nature of the organic/inorganic interactions.
5. A study of the polymer/silica nanoparticles interactions by light scattering techniques is given in Chapter 6.

References

1. Flory, P.J., *Introductory lecture*. Faraday Discussion Chemical Society, 1974. **57**: p. 7-18.
2. Shibayama, M., *Soft Matter Characterization*. Vol. 2. 2008: Springer.
3. Rubinstein, M. and A.V. Dobrynin, *Associations Leading to Formation of Networks and Gels*. Current Opinion on Colloid and Interface Science, 1999. **4**: p. 83-87.
4. Ilmain, F., T. Tanaka, and E. Kokufuta, *Volume transition in a gel driven by hydrogen bonding*. Nature, 1991. **349**: p. 400-401.
5. Skouri, R., et al., *Swelling and elastic properties of polyelectrolyte gels*. Macromolecules, 1995. **28**(1): p. 197-210.
6. Karakasyan, C., et al., *Cold gelation of alginates induced by monovalent cations*. Biomacromolecules, 2010. **11**(11): p. 2966-2975.
7. Tuncaboylu, D.C., et al., *Tough and Self-Healing Hydrogels Formed via Hydrophobic Interactions*. Macromolecules, 2011. **44**: p. 4997-5005.
8. Miquelard-Garnier, G., C. Creton, and D. Hourdet, *Synthesis and viscoelastic properties of hydrophobically modified hydrogels*. Macromolecular Symposia, 2007. **256**: p. 189-194.
9. Joly-Duhamel, C., D. Hellio, and M. Djabourov, *All gelatin networks: 1. Biodiversity and physical chemistry*. Langmuir, 2002. **18**(19): p. 7208-7217.
10. Djabourov, M., J. Leblond, and P. Papon, *Gelation of aqueous gelatin solutions. I. Structural investigation*. J. Phys. France, 1988. **49**(2): p. 319-332.
11. Assender, H.E. and A.H. Windle, *Crystallinity in poly(vinyl alcohol). 1. An X-ray diffraction study of atactic PVOH*. Polymer, 1998. **39**(18): p. 4295-4302.
12. Peppas, N.A., *Hydrogels in Medicine and Pharmacy*. 1986: CRC Press, Boca Raton, FL.
13. Mirejovsky, D., A.S. Patel, and G. Young, *Water properties of hydrogel contact lens materials: A possible predictive model for corneal desiccation staining*. Biomaterials, 1993. **14**(14.): p. 1080-1088.
14. Buchholz, F.L. and A.T. Graham, *Modern Superabsorbent Polymer Technology*. 1997: Wiley-VCH.
15. Qiu, Y. and K. Park, *Environment-sensitive hydrogels for drug delivery*. Advanced Drug Delivery Reviews, 2001. **53**(3): p. 321-339.

16. Hoare, T.R. and D.S. Kohane, *Hydrogels in drug delivery: Progress and challenges*. Polymer, 2008. **49**(8): p. 1993-2007.
17. Oh, J.K., et al., *The development of microgels/nanogels for drug delivery applications*. Progress in Polymer Science, 2008. **33**(4): p. 448-477.
18. Qui, Y. and K. Park, *Environment -sensitive hydrogels for drug delivery*. Advanced Drug Delivery Reviews, 2001. **53**: p. 312-329.
19. Ankareddi, I. and C.S. Brazel, *Synthesis and characterization of grafted thermosensitive hydrogels for heating activated controlled release*. International Journal of Pharmaceutics, 2007. **336**(2): p. 241-247.
20. Lee, K.Y. and D.J. Mooney, *Hydrogels for tissue engineering*. Chemical Reviews, 2001. **101**(7): p. 1869-1879.
21. Balakrishnan, B. and R. Banerjee, *Biopolymer-based hydrogels for cartilage tissue engineering*. Chemical Reviews, 2011. **111**(8): p. 4453-4474.
22. Lee, K.Y. and D.J. Mooney, *Alginate: Properties and biomedical applications*. Progress in Polymer Science, 2012. **37**(1): p. 106-126.
23. Rudzinski, W.E., et al., *Hydrogels as controlled release devices in agriculture*. Designed Monomers and Polymers, 2002. **5**(1): p. 39-65.
24. Norisuye, T., et al., *Small angle neutron scattering studies on structural inhomogeneities in polymer gels: irradiation cross-linked gels vs chemically cross-linked gels*. Polymer, 2002. **43**: p. 5289-5297.
25. Terech, P. and R.G. Weiss, *Low Molecular Mass Gelators of Organic Liquids and the Properties of Their Gels*. Chemical Reviews, 1997. **97**: p. 3133-3159.
26. Shibayama, M., *Small-angle neutron scattering on polymer gels: phase behavior, inhomogeneities and deformation mechanisms*. Polymer Journal, 2011. **43**(1): p. 18-34.
27. Norisuye, T., et al., *Small angle neutron scattering studies on structural inhomogeneities in polymer gels: irradiation cross-linked gels vs chemically cross-linked gels*. Polymer, 2002. **43**(19): p. 5289-5297.
28. Candau, S., J. Bastide, and M. Delsanti, *Structural , elastic, and dynamic properties of swollen polymer networks*. Advances in Polymer Science, 1982. **44**: p. 27-71.
29. Ikkai, F. and M. Shibayama, *Inhomogeneity Control in Polymer Gels*. Journal of Polymer Science Part B - Polymer Physics, 2005. **43**(6): p. 617-628.

30. Mendes, E., et al., *Experimental evidence for inhomogeneous swelling and deformation in statistical gels*. Phys. Rev. Lett., 1991. **66**: p. 1595-1598.
31. Panyukov, S. and Y. Rabin, *Statistical physics of polymer gels*. Physics Reports, 1996. **269**: p. 1-131.
32. Shibayama, M., *Spatial inhomogeneity and dynamic fluctuations of polymer gels*. Macromolecular Chemistry and Physics, 1998. **199**: p. 1-30.
33. Flory, P.J., *Principles of Polymer chemistry*. 1943, Ithaca: Cornell University Press.
34. James, H.M. and E. Guth, *Theory of the elastic properties of rubber*. Journal of Chemical Physics, 1943. **11**: p. 455-481.
35. Obukhov, S.P., M. Rubinstein, and R.H. Colby, *Network Modulus and Superelasticity*. Macromolecules, 1994. **27**: p. 3191-3198.
36. Flory, P.J. and J. Rehner, *Statistical mechanics of cross-linked polymer networks I Rubberlike elasticity*. Journal of Chemical Physics, 1943. **11**: p. 512-520.
37. Flory, P.J. and J. Rehner, *Statistical mechanics of cross-linked polymer networks II Swelling*. Journal of Chemical Physics, 1943. **11**: p. 521-526.
38. Gundogan, N., O. Okay, and W. Oppermann, *Swelling, Elasticity and Spatial Inhomogeneity of Poly(N,N-dimethylacrylamide) Hydrogels Formed at Various Polymer Concentrations*. Macromol. Chem. Phys., 2004. **205**: p. 814-823.
39. Miquelard-Garnier, G., C. Creton, and D. Hourdet, *Strain induced clustering in polyelectrolyte hydrogels*. Soft Matter, 2008. **4**: p. 1011-1023.
40. Shibayama, M., *Small-angle neutron scattering on polymer gels: phase behavior, inhomogeneities and deformation mechanisms*. Polymer Journal, 2011. **43**: p. 18-34.
41. Orakdogan, N. and O. Okay, *Inhomogeneity in Acrylamide-based Hydrogels*. Journal of Applied Polymer Science, 2007. **103**: p. 3228-3237.
42. Okumura, Y. and K. Ito, *The Polyrotaxane Gel: A Topological Gel by Figure-of-Eight Cross-links*. Advanced Mater., 2001. **13**(7): p. 485.
43. Edwards, S.F., *The effect of entanglements in rubber elasticity*. Polymer, 1986. **27**(4): p. 483-492.
44. Rubinstein, M. and S. Panyukov, *Elasticity of Polymer Networks*. Macromolecules, 2002. **35**: p. 6670-6686.

45. Fleury, G., et al., *Synthesis and characterization of high molecular weight polyrotaxanes: Towards the control over a wide range of threaded α -cyclodextrins*. *Soft Matter*, 2005. **1**(5): p. 378-385.
46. Karino, T., M. Shibayama, and K. Ito, *Slide-ring gel: Topological gel with freely movable cross-links*. *Physica B: Condensed Matter*, 2006. **385-386**(1): p. 692-696.
47. Zhao, C., et al., *Sliding mode of cyclodextrin in polyrotaxane and slide-ring gel*. *Journal of Physics: Condensed Matter*, 2005. **17**: p. 2841-2846.
48. Ito, K., *Novel Cross-Linking Concept of Polymer Network: Synthesis, Structure, and Properties of Slide-Ring Gels with Freely Movable Junctions*. *Polymer Journal*, 2007. **39**(6): p. 489-499.
49. Ito, K., *Slide-ring materials using topological supramolecular architecture*. *Current Opinion in Solid State and Materials Science*, 2010. **14**: p. 28-34.
50. Mayumi, K., et al., *Mechanics of slide-ring gels: novel entropic elasticity of a topological network formed by ring and string*. *Soft Matter*, 2012. **8**: p. 8179-8183.
51. Fleury, G., et al., *From high molecular precursor polyrotaxanes to supramolecular sliding networks. The 'sliding gels'*. *Polymer*, 2005. **46**(19): p. 8494-8501.
52. Gong, J.P., et al., *Double-network hydrogels with extremely high mechanical strength*. *Advanced Materials*, 2003. **15**(14): p. 1155.
53. Haque, M.A., T. Kurokawa, and J.P. Gong, *Super tough double network hydrogels and their application as biomaterials*. *Polymer*, 2012. **53**: p. 1805-1822.
54. Tominaga, T., et al., *The molecular origin of enhanced toughness in double-network hydrogels: A neutron scattering study*. *Polymer*, 2007. **48**: p. 7449-7454.
55. Gong, J.P., *Why are double network hydrogels so tough?* *Soft Matter*, 2010. **6**(12): p. 2583-2590.
56. Na, Y.-H., et al., *Structural characteristics of double network gels with extremely high mechanical strength*. *Macromolecules*, 2004. **37**(14): p. 5370-5374.
57. Na, Y.-H., et al., *Necking Phenomenon of Double-Network Ge*. *Macromolecules*, 2006. **39**(14): p. 4641-4645.
58. Tanaka, Y., et al., *Determination of Fracture Energy of High Strength Double Network Hydrogels*. *Journal of Physical Chemistry B*, 2005. **109**(23): p. 11559-11562.

59. Webber, R.E., et al., *Large Strain Hysteresis and Mullins effect of tough Double-Network Hydrogels*. *Macromolecules*, 2007. **40**(8): p. 2919-2927.
60. Nakayama, A., et al., *High Mechanical Strength Double-Network Hydrogel with Bacterial Cellulose*. *Advanced Functional Materials*, 2004. **14**(11): p. 1124-1128.
61. Wang, X.Z., H.L. Wang, and H.R. Brown, *Jellyfish gel and its hybrid hydrogels with high mechanical strength*. *Soft Matter*, 2011. **7**(1): p. 211-219.
62. Sun, J.-Y., et al., *Highly stretchable and tough hydrogels*. *Nature*, 2012. **489**: p. 133-136.
63. Yasuda, K., et al., *Biomechanical Properties of High Toughness Double Network Hydrogels*. *Biomaterials*, 2005. **26**(21): p. 4468-4475.
64. Azuma, C., et al., *Biodegradation of high-toughness double network hydrogels as potential materials for artificial cartilage*. *Journal of Biomedical Materials Research. Part A.*, 2007. **81**(2): p. 373-380.
65. Tanabe, Y., et al., *Biological responses of novel high-toughness double network hydrogels in muscle and the subcutaneous tissues*. *Journal of Material Science. Materials in Medicine*, 2008. **19**(3): p. 1379-1387.
66. Yasuda, K., et al., *A Novel Double-Network hydrogel Induces Spontaneous Articular Cartilage Regeneration in vivo in a Large Osteochondral Defect*. *Macromolecular Bioscience*, 2009. **9**(4): p. 307-316.
67. Kitamura, N., et al., *Induction of Spontaneous Hyaline Cartilage Regeneration Using a Double-Network Gel: Efficacy of a Novel Therapeutic Strategy for an Articular Cartilage Defect*. *American Journal of Sports Medicine*, 2011. **39**(6): p. 1160-1169.
68. Myung, D., et al., *Glucose-permeable interpenetrating polymer network hydrogels for corneal implant applications: A pilot study*. *Current Eye Research*, 2008. **33**(1): p. 29-43.
69. Sakai, T., et al., *Design and fabrication of a high-strength hydrogel with ideally homogeneous network structure from tetrahedron-like macromonomers*. *Macromolecules*, 2008. **41**(14): p. 5379-5384.
70. Akagi, Y., et al., *Evaluation of Topological Defects in Tetra-PEG Gels*. *Macromolecules*, 2010. **43**(1): p. 488-493.
71. Sakai, T., et al., *Highly elastic and deformable hydrogel formed from tetra-arm polymers*. *Macromolecules Rapid Communication*, 2010. **31**: p. 1954-1959.

72. Matsunaga, T., et al., *SANS Studies on Tetra-PEG Gel under Uniaxial Deformation*. *Macromolecules*, 2011. **44**: p. 1203-1210.
73. Sakai, T., *Gelation mechanism and mechanical properties of Tetra-PEG gel*. *Reactive and Functional Polymers*, 2013.
74. Haraguchi, K., T. Takehisa, and S. Fan, *Effects of clay content on the properties of nanocomposite hydrogels composed of poly(N-isopropylacrylamide) and clay*. *Macromolecules*, 2002. **35**(27): p. 10162-10171.
75. Haraguchi, K., et al., *Compositional effects on mechanical properties of nanocomposite hydrogels composed of poly(N,N-dimethylacrylamide) and clay*. *Macromolecules*, 2003. **36**(15): p. 5732-5741.
76. Miyazaki, S., et al., *Gelation Mechanism of Poly(N-isopropylacrylamide)-Clay Nanocomposite Gels*. *Macromolecules*, 2007. **40**: p. 4287-4295.
77. Haraguchi, K., et al., *Mechanism of Forming Organic/Inorganic Network Structures during In-situ Free-Radical Polymerization in PNIPA-Clay Nanocomposite Hydrogels*. *Macromolecules*, 2005. **38**(8): p. 3482-3490.
78. Ren, H.-Y., M. Zhu, and K. Haraguchi, *Characteristic Swelling-Deswelling of Polymer/Clay Nanocomposite Gels*. *Macromolecules*, 2001. **44**: p. 8516-8526.
79. Haraguchi, K., K. Murata, and T. Takehisa, *Stimuli-Responsive Nanocomposite Gels and Soft Nanocomposites Consisting of Inorganic Clays and Copolymers with Different Chemical Affinities*. *Macromolecules*, 2012. **45**: p. 385-391.
80. Zhu, M.F., et al., *A novel highly resilient nanocomposite hydrogel with low hysteresis and ultrahigh elongation*. *Macromolecular Rapid Communications*, 2006. **27**(13): p. 1023-1028.
81. Wu, C.-J., et al., *Mechanically Tough Pluronic F127/Laponite Nanocomposite Hydrogels from Covalently and Physically Cross-Linked Networks*. *Macromolecules*, 2011. **44**(20): p. 8215-8224.
82. Nishida, T., et al., *Stress relaxation and hysteresis of nanocomposite gel investigated by SAXS and SANS measurement*. *Polymer*, 2012. **53**: p. 4533-4538.
83. Haraguchi, K., K. Uyama, and H. Tanimoto, *Self-healing in Nanocomposite Hydrogels*. *Macromolecular rapid communications*, 2011. **32**(16): p. 1253-8.

84. Haraguchi, K. and L.Y. Song, *Microstructures formed in co-cross-linked networks and their relationships to the optical and mechanical properties of PNIPA/clay nanocomposite gels*. *Macromolecules*, 2007. **40**: p. 5526-5536.
85. Fukasawa, M., et al., *Synthesis and Mechanical Properties of a Nanocomposite Gel Consisting of a Tetra-PEG/Clay Network*. *Macromolecules*, 2010. **43**(9): p. 4370-4378.
86. Iler, R.K., *The Chemistry of Silica*, ed. Wiley-Interscience. 1979, New York: John Wiley & Sons.
87. Brinker, C.J. and G.W. Sherer, *Sol-gel science: the physics and chemistry of sol-gel processing*. 1990, Boston: Academic Press. 908.
88. Jolivet, J.P., M. Henry, and J. Livage, *Metal oxide chemistry and synthesis*. 2000, Chichester: John Wiley & Sons.
89. Schindler, P.W., et al., *Ligand properties of surface silanol groups*. *Journal of Colloid and Interface Science*, 1976. **55**(2): p. 469-475.
90. Stöber, W., *Equilibrium Concepts in Natural Water Systems*. *Advances in Chemistry*. Vol. 67. 1967, Washington, D. C.: American Chemical Society.
91. Takafuji, M., S.-Y. Yamada, and H. Ihara, *Strategy for preparation of hybrid polymer hydrogels using silica nanoparticles as multifunctional crosslinking points*. *Chemical Communication*, 2011. **47**: p. 1024-1026.
92. Aimé, C., et al., *Controlling the nano-bio interface to build collagen-silica self-assembled networks*. *Nanoscale*, 2012. **4**: p. 7127-7135.
93. Petit, L., et al., *Responsive hybrid self-assemblies in aqueous media*. *Langmuir*, 2007. **23**(1): p. 147-158.
94. Carlsson, L., et al., *Nano-hybrid self-crosslinked PDMA/silica hydrogels*. *Soft Matter*, 2010. **6**(15): p. 3619-3631.
95. Lin, W.C., et al., *Large Strain and Fracture Properties of Poly(dimethylacrylamide)/Silica Hybrid Hydrogels*. *Macromolecules*, 2010. **43**(5): p. 2554-2563.
96. Lin, W.-C., et al., *Effect of polymer-particle interaction on the fracture toughness of silica filled hydrogels*. *Soft Matter*, 2011. **7**: p. 6578-6582.
97. Kalfus, J., N. Singh, and A.J. Lesser, *Reinforcement in nano-filled PAA hydrogels*. *Polymer*, 2012. **53**: p. 2544-2547.

Chapter 2

Covalent networks: synthesis and structure of PDMA hydrogels

Contents

Contents	56
Introduction.....	57
1. Material and methods.....	58
1.1. Chemicals	58
1.2. Synthesis of hydrogels.....	59
1.3. Titration of extractible	60
1.4. Mechanics: tensile test	60
1.5. Swelling behaviour	63
1.6. Small Angle Neutron Scattering	66
2. Results and discussion.....	68
2.1. Titration of extractible	68
2.2. Mechanical properties	69
2.3. Swelling properties	73
2.3.1. Swelling kinetics.....	73
2.3.2. Swelling equilibrium.....	76
2.4. Structure of PDMA networks.....	79
3. Conclusion.....	85
References	87

Introduction

This first experimental chapter is dedicated to the synthesis and the structural study of single polymer hydrogels, prepared without silica nanoparticle. The aim of this study is to get an accurate picture of the structure-properties relationships of cross-linked poly(*N,N*-dimethylacrylamide) hydrogels, using complementary techniques based on mechanical, thermodynamical and scattering experiments. These PDMA hydrogels will constitute the base of our study as all the hybrid materials that we will develop later, will derive from the same architecture.

1. Material and methods

1.1. Chemicals

The chemical reactants used in this chapter are listed in **Table 1**. Their main characteristics are also reported here.

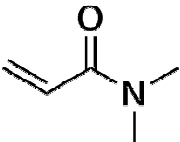
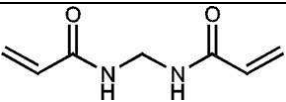
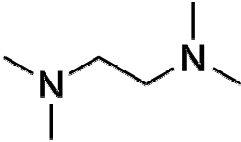
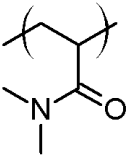
Notation	Chemical name	Semi-developed formula	Molar mass (g.mol ⁻¹)	Purity	Origin
DMA	<i>N,N</i> -dimethyl-acrylamide		99	99%	Aldrich
MBA	<i>N,N'</i> -methylene-bis-acrylamide		154	99%	Aldrich
KPS	Potassium persulfate	K ₂ S ₂ O ₈	270	-	Acros
TEMED	<i>N,N,N',N'</i> -tetramethyl-ethylenediamine		116	99%	Aldrich
D ₂ O	Deuterium oxide	D ₂ O	20	99.85%	Eurisotop
Linear PDMA	Poly(<i>N,N</i> -dimethyl-acrylamide)		Mn 100 000 D=2-3	-	PPMD lab

Table 1: Chemical reactants

All the chemicals were used as received without further purification. For all the experiments, water was purified with a Millipore system by reverse osmosis (Millipore filter Milli Ro3+) followed by deionization (MilliQ+).

1.2. Synthesis of hydrogels

Poly(*N,N*-dimethylacrylamide) hydrogels were prepared in a nitrogen filled and oxygen free glove box at room temperature by *in situ* free radical polymerization of DMA using *N,N'*-methylenebisacrylamide (MBA) as cross-linker. All the reactants were initially deoxygenated and introduced in the glove box in order to prevent any oxygen contamination. After dissolution of MBA and DMA in water, two freshly prepared solutions of KPS and *N,N,N',N'*-tetramethylethylenediamine (TEMED) are added under stirring. The mixture is then rapidly transferred into moulds initially placed under the nitrogen atmosphere of the glove box. The geometry of moulds depends on the characterization techniques used. For all the syntheses the molar ratio (DMA)/(KPS)/(TEMED) was set equal to 100/1/1. Experimentally we observed that the redox initiation starts rapidly (as ever shown by Orakdogan [1]) and the polymerization is let to proceed during 24 hours. After demoulding, hydrogels are immediately characterized or stored into paraffin to avoid drying before analysis.

The following study was mainly based on hydrogels at the preparation state: with a fixed weight ratio between polymer and water equals to 0.14. This corresponds to a fixed polymer concentration equals to 12.5 wt% or to a fixed polymer volume fraction $\phi_0 = 0.118$. In most cases, the gels are studied in this preparation state. The molar ratio of cross-linker (MBA) to monomer varied from 0.1 to 5 mol%. The nomenclature used in this study is: SP x for the Silica to Polymer weight ratio with x from 0 to 5 (in the case of hybrid hydrogels containing silica particles), PW y for the Polymer to Water weight ratio (with y varying between 0.07 and 0.2) and R z for the molar ratio of cross-linker to monomer (from 0.1 to 2 mol%). A gel without silica nanoparticles, with a polymer concentration of 12.5 wt%, and containing 0.1 mol% of MBA will be named:

“SP0_PW0.14_R0.1”.

The formulation of single hydrogels SP0_PW0.14_R z , prepared without silica particles, with a fixed network hydration (corresponding to a polymer to water weight ratio of 0.14) and by varying the cross-linking ratio, is given in **Table 2**.

Samples	DMA (g)	MBA (mg)	KPS (mg)	TEMED (μL)	H ₂ O (g)
SP0_PW0.14_R0.1	1.485	2.3	0.041	22.5	10.62
SP0_PW0.14_R0.5	1.485	11.6	0.041	22.5	10.69
SP0_PW0.14_R1	1.485	23.1	0.041	22.5	10.77
SP0_PW0.14_R1.5	1.485	34.7	0.041	22.5	10.85
SP0_PW0.14_R2	1.485	46.2	0.041	22.5	10.94

Table 2: Formulation of SP0_PW0.14_Rz PDMA hydrogels

1.3. Titration of extractible

The synthesis method that has just been described, with polymerization and cross-linking occurring at the same time, is known to lead to heterogeneous structures with a broad size distribution of chains [2].

In order to quantitatively determine extractible molecules unbound to the gel matrix, a rectangular piece of gel (approximately 4 cm length, 0.5 cm width and 0.2 cm thickness) is immersed in 2 g of a solution of LiNO₃ 0.5M for 2 days. The gel swells in this medium and the uncross-linked material can be extracted from the gel. The supernatant is then analysed by GPC, at room temperature. The molecules that can be detected by this technique are:

- the un-reacted DMA monomer,
- the un-reacted MBA cross-linker,
- the uncross-linked PDMA chains.

A calibration of the GPC is made for each of those three components with well defined solutions, in order to identify them and to quantitatively determine their content.

1.4. Mechanics: tensile test

Tensile tests were used to investigate the elastic properties of hydrogels in relation with their macromolecular architecture that can also be probed by other techniques like swelling

experiments and SANS. Tensile tests are performed on a standard tensile Instron machine, model 5565, using a 10 N load cell and a video extensometer, model SVE, which can precisely follow the local displacement of markers (see **Figure 1**). Strain can be measured using both the video extensometer and the displacement of the crosshead. The relative uncertainties for the load cell and the video extensometer are respectively 0.16% in the range from 0 to 0.1N and 0.11% at the full scale of 120mm.



Figure 1: Left: The Instron equipment. Right: Design of specific clamps. Specimens were dotted for video extensometer recognition.

The gel samples used for mechanical tests are synthesized in home-made moulds consisting of two covered glass plates spaced by a stainless steel spacer of 2 mm thick. The gels are then cut with a punch and their final dimensions are $L_0 = 50$ mm, $w_0 = 5$ mm and $t_0 = 2$ mm. These gel samples are placed in home-made screw side action grips and are marked by two white dots. The video extensometer can measure the initial length between the white marks (L_{e0}) and is able to follow the local displacement during the test.

A constant strain rate is used for the tests: 0.06 s^{-1} , corresponding to an initial velocity of 3 mm.s^{-1} . The measurements are performed at room temperature and the reproducibility is checked, performing at least three tests per sample formulation.

During the test, force (F) and displacement (L) are recorded while the nominal stress (σ) and the strain (ϵ) are calculated. From these data, the classic representation used is the nominal stress as a function of the strain, as shown in **Figure 2**.

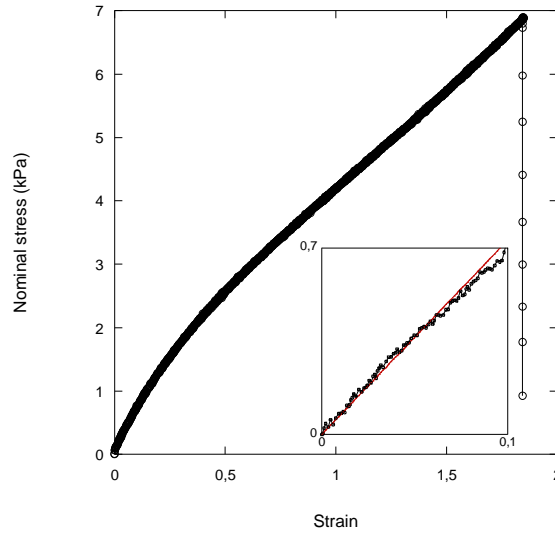


Figure 2: Representation of the experimental method used to define the initial modulus: nominal stress versus strain for SP0_PW0.14_R0.1 sample. Insert: a zoom of the beginning of the stress-strain curve in black and in red the fitting curve.

In this chapter, only initial modulus will be investigated, large strain behaviour being discussed in Chapter 4. The Young's modulus that can be calculated from this representation is the relevant parameter for the evaluation of the stiffness of hydrogels. For that purpose, we have chosen an interval of strain $\Delta\epsilon = 0.02$ where the stress-strain curves are linear, as represented in the insert of the **Figure 2**.

As shown in **Figure 3**, the stress-strain curves coming from the video extensometer and from the global displacement of the cross-bar are fully comparable. This agreement, which has been observed for all the samples, clearly emphasizes the absence of slippage during hydrogel extension and validates the determination of the Young's modulus.

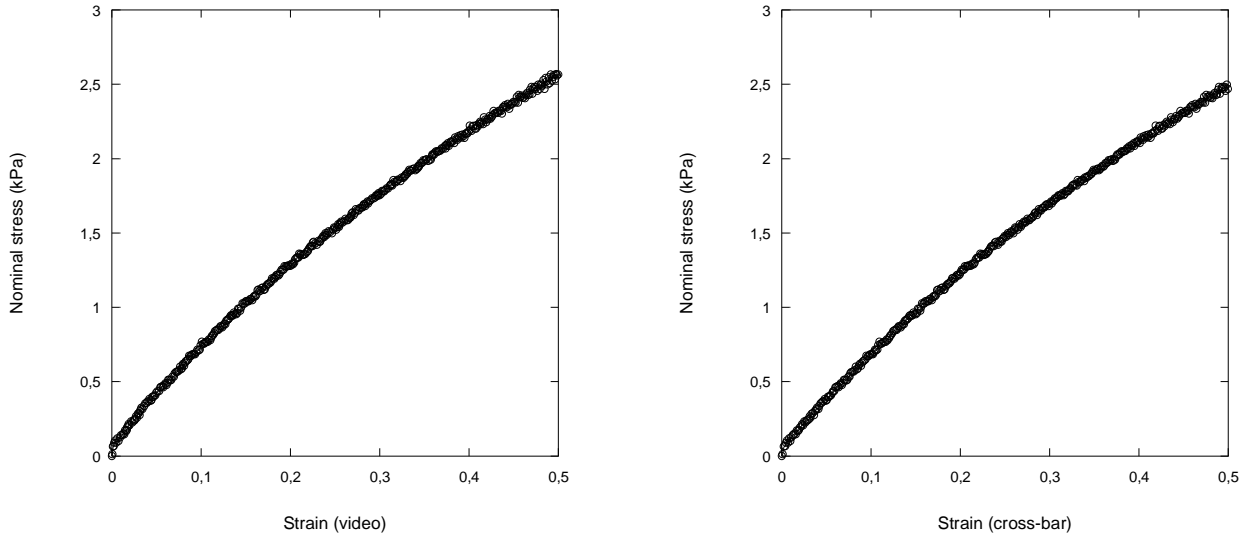


Figure 3: Representation of the experimental procedure: initial modulus was defined using the video extensometer. Comparison of the standard representations used to analyse large strain data: nominal stress versus strain for SP0_PW0.14_R0.1 sample. Left: video extensometer strain and right: cross-bar strain.

1.5. Swelling behaviour

The swelling ability is a classical characterization of polymer networks, depending on temperature, chain length between cross-links, size of the solvent molecules and of course on the affinity of the polymer chains for the surrounding solvent molecules; all these parameters being fixed by the experimental conditions.

The description of the swelling theory of Flory-Rehner is based on the hypothesis of separability of free energy terms [3]. The swelling equilibrium is expressed by the variation of free energy, coming from the combination of a mixing term (ΔF_m) and an elastic one (ΔF_{el}) depending on the elastic deformation of the network:

$$\frac{\Delta F}{V} = \frac{\Delta F_m}{V} + \frac{\Delta F_{el}}{V} \quad \text{Eq. 1}$$

with $\frac{\Delta F}{V}$ the variation of energy density associated to the volume V of the studied system.

The theory of Flory describes the mixing term as:

$$\frac{\Delta F_m}{V} = \frac{RT}{V_1} (\phi_1 \ln \phi_1 + \chi_{12} \phi_1 \phi_2) \quad \text{Eq. 2}$$

where R is the universal gas constant, T is the temperature, V_1 is the molar volume of the solvent, ϕ_1 and ϕ_2 are respectively the volume fractions of the solvent and of the polymer in the gel and χ_{12} is the Flory interaction parameter of this binary system.

Considering the elastic free energy, the elastic term ΔF_{el} can be described by different models, making a link between the macroscopic deformations of the network (due to the swelling) and the local deformation of chains. Flory together with Rehner developed the affine network theory, leading to the well-known elasticity model [4]. The affine network model describes a local deformation of each elastic chain homothetic to the macroscopic deformation, as cross-linking points are supposed to be embedded in the network.

Considering a more relevant network picture in which the junction points can freely move and fluctuate over time on a range which is not affected by the macroscopic deformation, James and Guth proposed the phantom network model [5]. In the case of swelling, supposing that the network deforms isotropically, the phantom theory gives the following free energy density:

$$\frac{\Delta F_{el}}{V} = \left(1 - \frac{2}{f}\right) \frac{3k_B T v_e}{2V} (\alpha^2 - 1) \quad \text{Eq. 3}$$

where α is the isotropic extension ratio defined as $\alpha = (\phi_0 / \phi_2)^{1/3}$, with ϕ_0 the polymer volume fraction in the preparation state and f the functionality of the junction points. The concentration of elastically active chains (v_e/V) for an ideal network can be written as:

$$\frac{v_e}{V} = \frac{\phi_2 N_A}{v_{pol}^{spe} M_C} = \frac{N_A \phi_2}{N V_1} \quad \text{Eq. 4}$$

with N_A the Avogadro's number, v_{pol}^{spe} the specific volume of the dry polymer and N the mean number of "equivalent" units between junction points.

As the thermodynamic behaviour of swollen networks is generally much closer to the phantom model than to the affine model, even under compression and at low extension, the phantom model will be used accordingly to describe the swelling behaviour of PDMA gels [6].

Starting from the variation of the free energy, one can calculate the osmotic pressure inside the gel as follows:

$$\Pi_{gel} = \Pi_m + \Pi_{el} = \phi_2^2 \frac{\partial}{\partial \phi_2} \left(\frac{\Delta F_m + \Delta F_{el}}{V \phi_2} \right) \quad \text{Eq. 5}$$

where Π_m and Π_{el} are respectively, the mixing and the elastic contributions to the osmotic pressure, $|\Pi_{el}| = G$ being the shear modulus. Using equations Eq. 1, Eq. 2 and Eq. 4, we finally obtain:

$$\Pi_{gel} = -\frac{RT}{V_1} \left(\ln(1 - \phi_2) + \phi_2 + \chi_{12} \phi_2^2 + \left(1 - \frac{2}{f} \right) \frac{\phi_0^{2/3} \phi_2^{1/3}}{N} \right) \quad \text{Eq. 6}$$

$$\text{with} \quad -\Pi_{el} = G = \frac{RT}{V_1} \left(1 - \frac{2}{f} \right) \frac{\phi_0^{2/3} \phi_2^{1/3}}{N} \quad \text{Eq. 7}$$

When immersed in a solvent, the polymer network can swell but the elastic cross-linked chains resists to this swelling. The swelling equilibrium ($Q_e = 1/\phi_2$) is reached when the osmotic pressure inside the gel (Π_{gel}) is equal to the osmotic pressure of the surrounding medium (Π_{out}). In the case of neutral networks swollen in a pure solvent, like water, this situation is described by the following equation:

$$\Pi_{gel} = -\frac{RT}{V_1} \left(\ln(1 - \phi_2) + \phi_2 + \chi_{12} \phi_2^2 + \left(1 - \frac{2}{f} \right) \frac{\phi_0^{2/3} \phi_2^{1/3}}{N} \right) = 0 \quad \text{Eq. 8}$$

For each PDMA hydrogel, the initial swelling in the preparation state ($Q_0 = 1/\phi_0$) can be calculated assuming full conversion of monomers and additivity of volumes:

$$Q_0 = 1 + \frac{v_{spe}^w}{v_{spe}^p} \left(\frac{m_{p,w}^0}{m_p^0} - 1 \right) \quad \text{Eq. 9}$$

with v_{spe}^w the specific volume of water ($v_{spe}^w = 1 \text{ mL.g}^{-1}$), v_{spe}^p the specific volume of the dry polymer network ($v_{spe}^p = 0.95 \text{ mL.g}^{-1}$), m_p^0 the mass of the polymer network (with $m_p^0 = m_{DMA} + m_{MBA}$) and $m_{p,w}^0$ the total mass of the swollen gel in the preparation state ($m_{p,w}^0 = m_p^0 + m_w^0$, with m_w^0 the total mass of water).

Experimentally, small pieces of hydrogel, in their preparation state (Q_0), are cut, weighed and placed in a large excess of solvent, at room temperature. In order to investigate the swelling equilibrium of hydrogels, the solvent is changed every day during 2 weeks. The gels, swollen at equilibrium, are then weighed and the equilibrium swelling is calculated. All the measurements, carried out at room temperature are performed in replicate to check the reproducibility. Kinetic studies were also performed on chemical hydrogels by weighting pieces of gel (after removing the excess water on the surface) at regular time intervals during 45 hours.

1.6. Small Angle Neutron Scattering

Small angle neutron scattering experiments have been carried out at the Laboratoire Léon Brillouin (CEA, Saclay) using a small angle neutron spectrometer (PACE), dedicated to isotropic measurements. For that purpose, hydrogenated PDMA networks are prepared in D_2O instead of H_2O , using the same protocol as described previously. From the hydrogel plates in the preparation state, synthesized in the same home-made moulds than the one used for mechanical tests, discs (diameter $d = 14 \text{ mm}$ and thickness $t = 1 \text{ or } 2 \text{ mm}$) are cut with a cylindrical punch. Those discs are then placed between two quartz slides hermetically sealed.

In comparison with PDMA hydrogels, solutions of linear hydrogenated PDMA were also prepared in D_2O , varying the polymer concentration from 6.5 wt% to 12.3 wt% (corresponding to the polymer concentration in PW0.14 hydrogels).

The small angle neutron scattering experiments can be described as follows: an incident radiation of wave vector \vec{k}_0 (with a wavelength λ) is sent through a gel sample, inducing a scattered radiation. The interaction between neutrons and the sample is elastic: the incident

wave vector \vec{k}_0 and the scattered wave vector \vec{k} have the same modulus. The angle between these two wave vectors is named the scattering angle θ . The scattering vector is then defined as $\vec{k} - \vec{k}_0$ and its modulus is:

$$q = \frac{4\pi}{\lambda} \sin\left(\frac{\theta}{2}\right) \quad \text{Eq. 10}$$

Absolute measurements of the scattering intensity $I(q)$ (cm^{-1} or 10^{-8} \AA^{-1}) were obtained from the direct determination of the incident neutron flux and the cell solid angle, the efficiency of the detector cell being normalized by the intensity delivered by a pure water cell of 1 mm thickness. Finally, the coherent scattering intensity of the gel was obtained after subtracting the contribution of the solvent used D_2O . After treatment, the scattering intensity $I(q)$ of elastically scattered neutrons is plotted versus the wave vector modulus q .

Two measurement configurations are used, keeping constant the sample-to-detector distance $D = 4.7 \text{ m}$ and changing the wavelength of the incident neutron beam $\lambda = 12$ and 4.5 \AA . The corresponding values of the scattering vector modulus are ranging between 0.0034 \AA^{-1} and 0.098 \AA^{-1} .

2. Results and discussion

2.1. Titration of extractible

The network formation, taking place during the cross-linking polymerization of DMA with MBA, is far to be ideal and before going deeper into the network properties it is important to check the level of monomer conversion, *i.e.* the efficiency of the polymerization process. Indeed, if the cross-linking polymerization is not total, residual monomers and free polymer chains embedded into the network will impact the mechanical characterization of hydrogels (presence of elastically inactive chains) as well as its swelling properties (release of uncross-linked material in the external medium). For that purpose, a systematic characterization of extractible by GPC has been carried out on every chemical hydrogel, for molar fraction of cross-linker MBA varying between 0.1 and 2 mol%. A typical chromatogram is shown in **Figure 4**, and compared to the reference chromatograms of the hydrogel components.

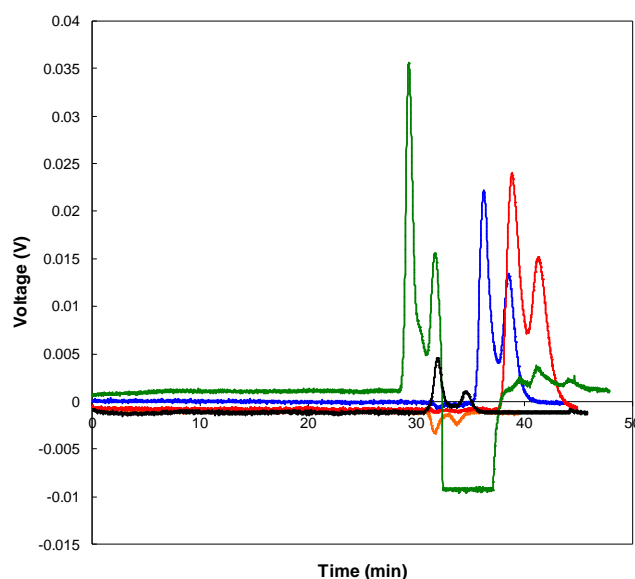


Figure 4: Typical chromatogram obtained from a SP0_PW0.14_R0.1 hydrogel (in black), with the chromatograms of the reference species: the solvent LiNO₃ (in orange), the monomer DMA (in blue), the cross-linker MBA (in red) and the mixing KPS-TEMED (in green).

In the present case of the SP0_PW0.14_R0.1 hydrogel, no extractible species can be observed; only a difference in the LiNO₃ solvent concentration is detected. For all the samples, the

polymerization efficiency is always well above 98% (no more than 2% of residual monomers) and the amount of extractable PDMA chains, when observable, is less than 1 wt% of the total material. In the following, we will thus consider that the conversion of monomers is quantitative and that all the organic material is attached to the polymer network.

2.2. Mechanical properties

The mechanical study of PDMA hydrogels at different cross-linking densities is a convenient method to analyze the network structure in terms of number of elastically active chains. For that purpose a set of experiments has been carried out on a series of PDMA networks with different molar fraction of cross-linker MBA, SP0_PW0.14_Rz, with z varying between 0.1 and 2 mol%. The stress-strain curves of the SP0_PW0.14_Rz hydrogels are represented in **Figure 5**.

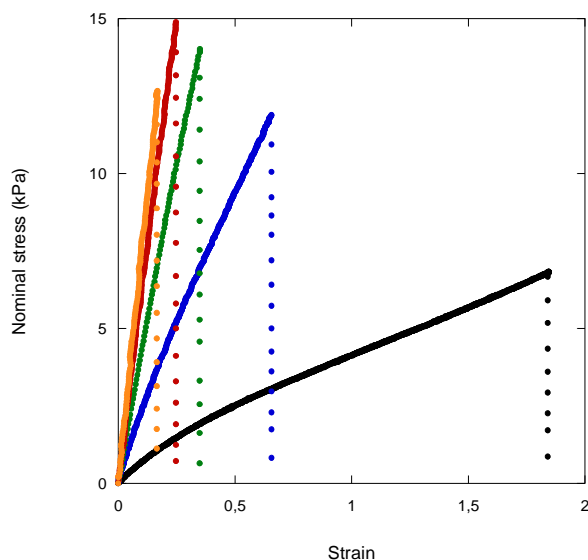


Figure 5: Stress-strain curves of SP0_PW0.14_Rz hydrogels with R0.1 (in black), R0.5 (in blue), R1 (in green), R1.5 (in red) and R2 (in orange).

Without chemical cross-linker MBA, hydrogels can be formed thanks to self-cross-linking reactions [7]. However, in the case of single organic hydrogels (without silica particles), the hydrogel SP0_PW0.14_R0 is too soft and irregular to be handled, and it has not been studied for this reason. From the stress-strain curves, it is clear that increasing the amount of

chemical cross-linker MBA in the hydrogel leads to an increase of the initial slope of the curve and also to a decrease of the maximal strain. The classical tensile tests are not appropriate to the study of failure but these results can give a good idea of the global behaviour of hydrogels with different cross-linking ratio.

The SPx_PW0.14_Rz hydrogels are tested in their preparation state by tensile tests and the shear modulus (G) is obtained from the initial slope of the strain-stress curve as one third of the Young's modulus, assuming incompressibility of the hydrogel:

$$G = \frac{1}{3}E \quad \text{Eq. 11}$$

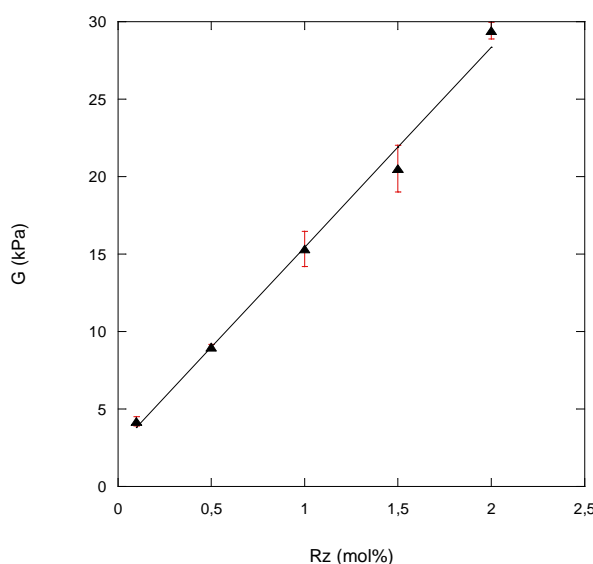


Figure 6: Variation of the shear modulus of PDMA hydrogels (SP0_PW0.14_Rz) with the molar amount of cross-linker MBA.

The representation of the shear modulus as a function of the molar amount of cross-linker (see **Figure 6**) shows a linear variation $G = 2.5 + 12.9 R_z$ (with G in kPa) which highlights the contribution of both entanglements ($G_e = 2.5$ kPa) and covalent cross-links (G_c):

$$G = G_e + G_c \quad \text{Eq. 12}$$

As reported by Obukhov *et al.* [8], the relative contribution of trapped entanglements and chemical cross-links to the elastic modulus strongly depends on the polymer concentration

during the network formation ($G_e \propto \phi_0^{2.3}$) and the level of cross-linker. In the framework of SP0_PW0.14_Rz hydrogels prepared at $\phi_0 = 0.118$, one can notice that trapped entanglements dominate the elastic behaviour at low level of cross-linking ($z = 0.1$ mol%) while they contribute for less than 10% at $z = 2$ mol%. Nevertheless, stress-strain curves do not show any clear evidence of softening.

On the other hand, taking into account the phantom network model [8], the contribution of covalent cross-links is proportional to the effective degree of cross-linking (R_e) and can be expressed by the following relation:

$$G_c = \left(1 - \frac{2}{f}\right) \frac{RTf}{200v_{spe}^p M_0 Q_0} R_e = B.R_e \quad \text{Eq. 13}$$

with R the universal gas constant, T the temperature (here $T = 293K$), f the functionality of the junction points (here $f = 4$), v_{spe}^p the specific volume of the dry polymer network ($v_{spe}^p = 0.95 \cdot 10^{-3} \text{ m}^3 \cdot \text{kg}^{-1}$) and M_0 the molar mass of the monomer units ($M_0 = 99 \cdot 10^{-3} \text{ kg} \cdot \text{mol}^{-1}$ for DMA).

The numerical calculation gives $G_c = 30.5 R_e$ for the pre-factor of the previous equation, this result is much higher than the experimental value calculated from **Figure 6** ($G_c = 12.9 R_e$). This difference is due to the presence of defects inside the polymer network. Several reasons can be accounted for these defects or irregularities and first of all the copolymerization process itself that, carried out in batch conditions, makes the incorporation of monomers and cross-linkers statistic and not random with a drift of M_c along the conversion of the reaction. A broad distribution of molar masses between cross-links is then expected with heterogeneities at the local scale between soft “low cross-linked” domains alternating with “harder” ones. Another important point is the conversion of the polymerization process. As previously mentioned, GPC analysis has shown the absence of residual free monomer at the end of the reaction but remaining double bonds corresponding to MBA attached just by one end could exist. The presence of reactive double bonds embedded inside the network is an important feature that strongly impacts the formation, the architecture and the properties of interpenetrating networks or “double networks” as it has been discussed by Gong *et al.* [9].

Finally, regardless of the previous reasons, we have also to take into account that all cross-links ($f = 4$) do not give rise to elastically active chains, *i.e.* bridges, and that inactive chains like dangling chains or loops are also formed during the polymerization/gelation process (Figure 7).

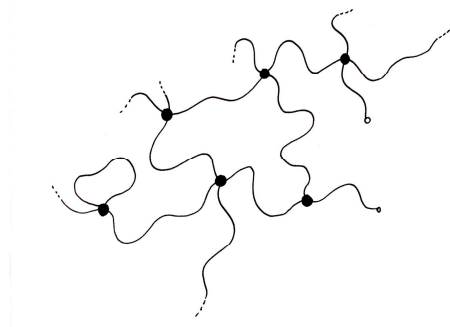


Figure 7: Schematic representation of a real polymer network swollen by a solvent

The probability of cyclization and multiple cross-linking reactions have been calculated by Gundogan *et al.*, showing that a high polymer concentration improves the efficiency [10]. For instance, for PDMA networks prepared in similar conditions, they show that the cross-linking efficiency rapidly increases from 20 to 60% in the concentration range: $0.08 < \phi_0 < 0.3$. Similar results have been obtained by Orakdogan and Okay for both poly(acrylamide) and poly(*N,N*-dimethylacrylamide), showing a cross-linking efficiency of 10-15% at a polymer concentration of 5% [1]. In our case, the comparison between theoretical and experimental slopes indicates a cross-linking efficiency of 42% at $\phi_0 = 0.12$, irrespective of the level of cross-linking. For a hydrogel with a theoretical molar ratio of cross-linker to monomer equal to 0.1 mol%, the real cross-linking density is only 0.042 mol% and the average number of monomer units between covalent cross-links is 1200 instead of 500.

2.3. Swelling properties

2.3.1. Swelling kinetics

The swelling kinetics of hydrogels has been studied in order to investigate the diffusion process occurring during the swelling. The water sorption process has been studied by measuring the change in the amount of water absorbed by the hydrogel at various time periods. Usually, when a piece of gel is immersed in water, two steps can be observed:

- i. the entry of water in the superficial part of the sample, followed by
- ii. the diffusion of the water to the centre of the sample, in the direction of the gradient of concentration.

An example is given in **Figure 8** for two SP0_PW0.14_R0.1 hydrogels swollen in water where the swelling $Q(t)$ is plotted as a function of time.

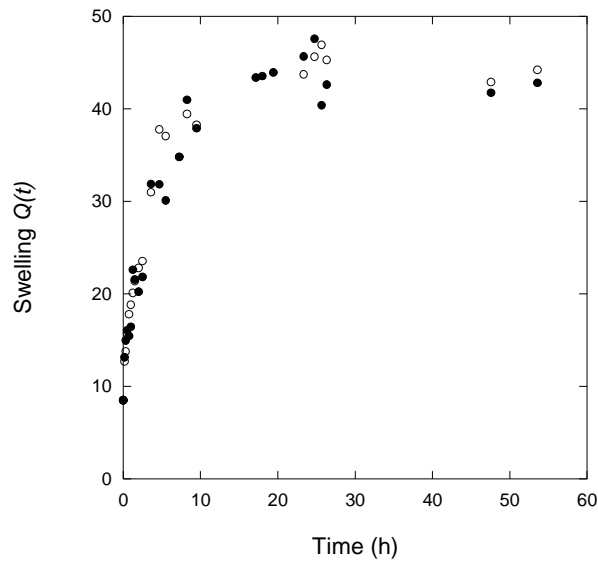


Figure 8: Variation of the swelling $Q(t)$ as a function of time for two SP0_PW0.14_R0.1 hydrogel samples.

One can wonder if the swelling mechanisms of hydrogels can be described in terms of Fickian diffusion or non-Fickian diffusion, also called anomalous transport process. The kinetics of the swelling process is usually determined by the following expression [11]:

$$\frac{M_t}{M_\infty} = kt^n \quad \text{Eq. 14}$$

where M_t and M_∞ are the water uptakes (in grams) at time t and equilibrium time, k is the diffusion constant and n is the swelling exponent which is often used to determine the transport mechanism mode. For a Fickian diffusion, the swelling exponent n is equal to 0.5, while for a non-Fickian transport, it is higher than 0.5.

The situation described by Eq. 14 can be applied when the ratio of water intakes does not exceed 0.50. In the case of our cross-linked PDMA hydrogels, we can represent the mass ratios as a function of the square root of the time (Figure 9).

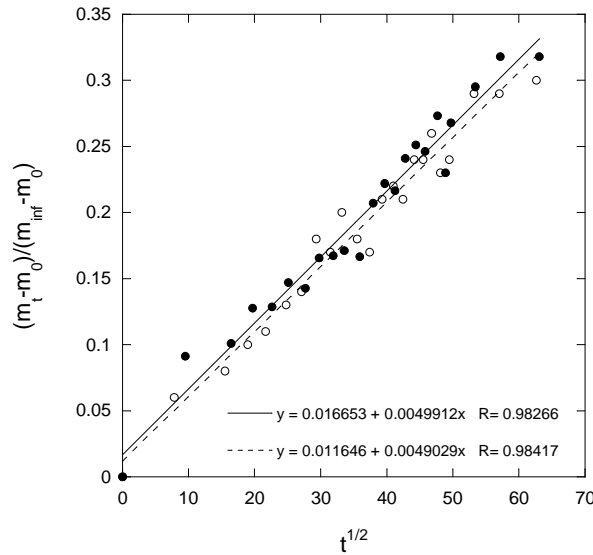


Figure 9: Variation of the mass ratio as a function of the square root of the time for two SP0_PW0.14_R0.1 hydrogels, with the corresponding linear fits.

From the Figure 9, one can conclude that the swelling kinetics of the SP0_PW0.14_R0.1 hydrogels follow a Fickian diffusion, as the linear fits are good. If the swelling exponent (here equal to 0.5) had been higher than 0.5, the diffusion would have been non-Fickian, due to polymer relaxation occurring at a similar rate than the diffusion for example.

Fick's law is given by the following expression:

$$\frac{\partial C}{\partial t} + D\Delta C = 0 \quad \text{Eq. 15}$$

where C is the concentration of the diffusing specie, D the diffusion coefficient (in $\text{m}^2.\text{s}^{-1}$) and Δ the Laplacian operator.

If we suppose that the diffusion through the gel sample is unidirectional, following the x direction, Fick's law becomes:

$$\frac{\partial C}{\partial t} = D \frac{\partial^2 C}{\partial x^2} \quad \text{Eq. 16}$$

Crank and Nicolson [12] developed a finite difference method for numerically solving the partial differential equations. Considering unidirectional diffusion in a thin plate, e being the thickness, and integrating $C(x,t)$ within the thickness, the following expression can be written as:

$$\frac{M_t}{M_\infty} = 1 - \frac{8}{\pi^2} \sum_{n=0}^{\infty} \frac{1}{(2n+1)^2} \exp\left(-D \frac{(2n+1)^2}{e^2} \pi^2 t\right) \quad \text{Eq. 17}$$

with M_t and M_∞ respectively the mass uptake at t and at equilibrium.

In order to calculate this variation, Shen and Springer [13] wrote an approximation for $M_t/M_\infty < 0.5$:

$$\frac{M_t}{M_\infty} = \frac{4}{e} \sqrt{\frac{Dt}{\pi}} \quad \text{Eq. 18}$$

According to this last expression, in the case of a rectangular specimen of hydrogel (50 mm by 5 mm by 2 mm), the corresponding diffusion coefficient can be calculated for the initial part of the curve (where the ratio of water intakes does not exceed 0.50), for a Fickian diffusion, with:

$$D = \frac{\pi}{16} \frac{e^2}{t} \left(\frac{M_t}{M_\infty} \right)^2 \quad \text{Eq. 19}$$

The calculation gives a diffusion coefficient $D \approx 2.10^{-7} \text{ cm}^2 / \text{s}$. After 50-60 hours, the hydrogel may have reached its swelling equilibrium state. This value is in good agreement with the results of Alam *et al.*[14]. Accordingly, we choose to study the swelling equilibrium after 2 weeks, in order to be sure that the hydrogels have reached their maximal swelling.

2.3.2. Swelling equilibrium

While the structure of polymer networks controls the mechanical properties, it also strongly impacts their swelling behaviour. For instance an increase of the cross-linking density, corresponding to a decrease of the average distance (or number of monomer units) between cross-linking points, will reduce the swelling ability of the gel. This qualitative behaviour is clearly depicted in **Figure 10** where the swelling ratio at equilibrium has been plotted versus the effective cross-linking density.

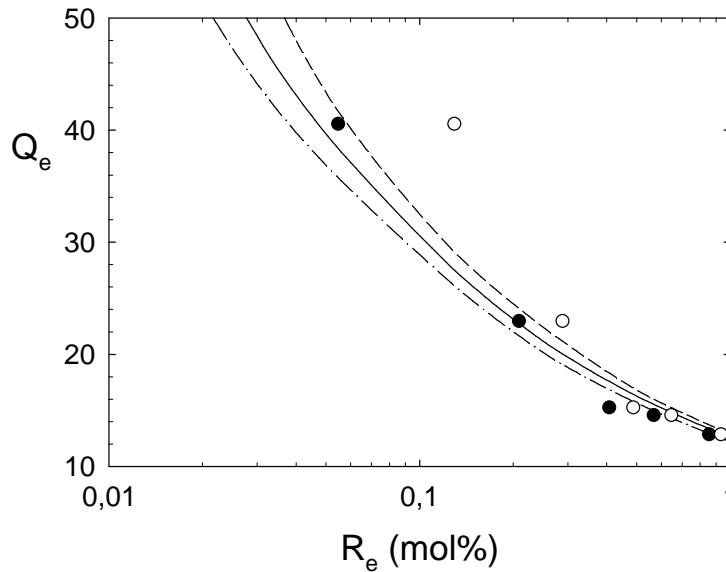


Figure 10: Variation of the swelling ratio at equilibrium Q_e as a function of the effective cross-linking density, R_e calculated by assuming $|\Pi_{el}| = G_c$ (●) or $|\Pi_{el}| = G_c + G_e$ (○). Experimental data are compared to theoretical predictions of the phantom network model with $\chi_{12} = 0.495$ (short line); 0.498 (solid line) and 0.5 (long dash).

From a quantitative point of view, we also compare in **Figure 10** the theoretical swelling behaviour issued from the phantom network model (**Eq. 8**) with experimental data plotted as a function of the effective cross-linking density (R_e). This latter is calculated from moduli obtained by tensile test experiments using **Eq. 6** and taking into account the contribution of both entanglements and covalent cross-links ($G = G_e + G_c$) or only covalent cross-links ($G = G_c$).

As we can see, the best agreement is obtained around the theta-conditions ($\chi_{12} \cong 0.5$) assuming that only covalent cross-links contribute to the swelling properties at equilibrium. The reason for that could be that entanglements are dynamic and not trapped into the covalent matrix and that disentanglement occurs upon dilution (during swelling). Another possibility is that the Flory parameter (χ_{12}) is not constant with the concentration as it was shown recently by Gundogan et al [8] in the case of cross-linked PDMA hydrogels. These authors effectively found that the Flory parameter follows a unique relation $\chi_{12} = 0.47 + 0.36/Q_e$ that evidences an improvement of PDMA/water interactions upon dilution. In our case, being aware of the limited number of data, we get almost the same relation (indeed in our case $\chi_{12} = 0.47 + 0.38/Q_e$) that would indicate that entanglements are effectively trapped into the covalent networks and that polymer-solvent interactions are improved upon swelling. The main conclusion of this thermodynamic study, irrespective of the above assumptions, is that in the preparation state ($\phi_0 = 0.12$) SP0_PW0.14_Rz gels are close to the Θ -conditions and that PDMA chains remain almost Gaussian in water at room temperature.

From these experiments, it is also interesting to consider that working at a given concentration during the preparation of the gel, for instance $\phi_0 = 0.12$ ($Q_0 = 8.5$), it is not possible to increase indefinitely the degree of cross-linking as it should reach a saturation threshold, corresponding to the lowest degree of polymerization between cross-links (P_c) [2, 15]. Beyond these conditions, a syneresis of the gel is generally observed experimentally during the polymerization (leading to an increase of its concentration) due to the stress imposed by the high level of cross-linking. This critical behaviour can be described explicitly from **Eq. 8** assuming that PDMA gels have reached their swelling equilibrium in their preparation state. In this case, the critical degree of polymerization between cross-links (P_c) in the preparation state ($\phi_2 = \phi_0$) can be written as follows:

$$P_c = \frac{-(1-2/f)V_1\phi_0}{M_0 v_{spe}^p (\ln(1-\phi_0) + \phi_0 + \chi_{12}\phi_0^2)} \quad \text{Eq. 20}$$

Taking into account the relation between the degree of polymerization between cross-links (P) and the effective degree of cross-linking ($R_e = 200/fP$), one can obtain the critical value of R_e :

$$(R_e)_c = \frac{-200M_0 v_{spe}^p (\ln(1-\phi_0) + \phi_0 + \chi_{12}\phi_0^2)}{fV_1(1-2/f)\phi_0} = \frac{-522.5(\ln(1-\phi_0) + \phi_0 + \chi_{12}\phi_0^2)}{\phi_0} \quad \text{Eq. 21}$$

This relation, plotted in **Figure 11**, clearly emphasizes the limiting conditions that should be followed to prepare homogeneous hydrogels. Here, the two situations discussed previously ((a) $\chi_{12} = 0.50$ and (b) $\chi_{12} = 0.47 + 0.38 \phi$) have been taken into account with a marked influence of the Flory interaction parameter. Considering the gel series SP0_PW0.14_Rz prepared at $\phi_0 = 0.118$, the maximum degree of cross-linking is expected at about 2.8 and 1.8 mol%, for situations (a) and (b) respectively, which should correspond to about 6.5 mol% or 4.3 mol%, assuming an efficiency of 42% for the bridge formation.

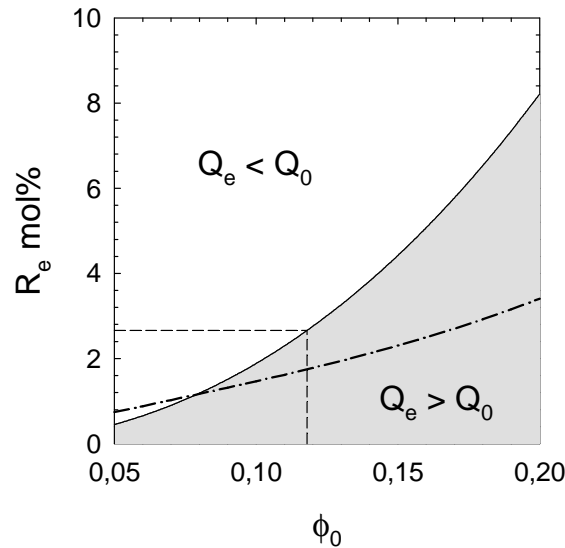


Figure 11: Swelling/deswelling map of PDMA hydrogels in pure water as a function of their initial concentration ϕ_0 and effective degree of cross-linking R_e . The calculation was done according to Eq. 21 with $\chi_{12} = 0.50$ (solid line) and $\chi_{12} = 0.47 + 0.38 \cdot \phi_2$ (dash dot line).

From an experimental point of view all hydrogels prepared in this work are homogeneous except the sample SP0_PW0.14_R5, showing syneresis during preparation, and which degree of cross-linking is very close to the limiting values calculated above.

2.4. Structure of PDMA networks

The theoretical description of the scattering intensity $I(q)$ for swollen polymer networks is generally considers the addition of two main contributions arising from [16], [17]:

- thermal concentration fluctuations as typically observed for semi-dilute polymer solutions. These thermodynamic fluctuations can be described and expressed, in the previously determined Θ -conditions, by a Lorentzian function of the correlation length ξ :

$$I_{sol}(q) = \frac{I_{sol}(0)}{1 + \xi^2 q^2} \quad \text{Eq. 22}$$

- static inhomogeneities due to the presence of cross-links, preventing free motions of polymer segments. Several relations have been proposed to describe the excess scattering observed in polymer gels [17] and more particularly the Debye-Bueche function:

$$I_{ex}(q) = \frac{I_{ex}(0)}{(1 + \Xi^2 q^2)^2} \quad \text{Eq. 23}$$

where Ξ is a length scale characterizing the static inhomogeneities in the gel.

By assuming simple additivity, the scattering intensity of polymer gels can be written as:

$$I_{ex}(q) = I_{sol}(q) + I_{ex}(q) = \frac{I_{sol}(0)}{1 + \xi^2 q^2} + \frac{I_{ex}(0)}{(1 + \Xi^2 q^2)^2} \quad \text{Eq. 24}$$

In this expression, the last term, characteristic of covalent gels and coming from frozen heterogeneities can be enhanced by swelling or stretching: indeed, the more a region is cross-linked, the less it deforms, enhancing the density differences within the gel [18].

However, these static heterogeneities can also be observed in semi-dilute polymer solutions, not only in gels. For instance, on **Figure 12** the Zimm representation of the scattering data obtained with semi-dilute solutions of linear PDMA reveals a strong deviation from the Lorentzian function in the low- q range. This particular behaviour, known as Picot-Benoit effect, is associated with large scale composition fluctuations formed at sample preparation [19, 20]. This excess scattering at low- q may be related to a long time relaxation process that might have been observed in DLS by Blanco [21].

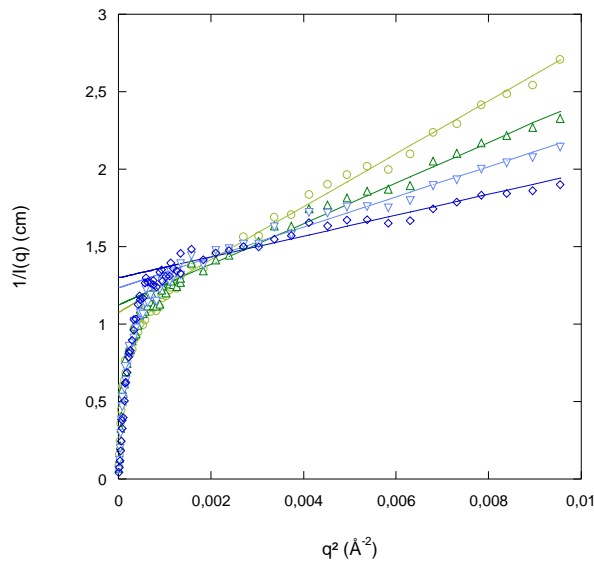


Figure 12: Zimm representation of the scattering data of linear PDMA solutions in D_2O for different PDMA volume fractions: $\phi = 0.068$ (\circ); 0.084 (\triangle); 0.104 (∇) and 0.128 (\diamond).

The correlation length ξ of thermal fluctuations can be obtained from the linear behaviour in the high q -range on the Zimm representation on **Figure 12**. The characteristic length Ξ of static heterogeneities is then calculated using the expression of the scattering intensity (Eq. 24). The values are reported in **Table 3**. As expected for semi-dilute polymer solutions, the correlation length ξ decreases with the polymer concentration, as it scales with the blob size. However, the characteristic length Ξ of static inhomogeneities appears to be constant in this concentration range.

Sample	State	ϕ	$I_{\text{soln}}(0)$ (cm^{-1})	ξ (\AA)	$I_{\text{ex}}(0)$ (cm^{-1})	Ξ (\AA)
PDMA linear	Solution	0.068	0.93	12.6	22.7	221
PDMA linear	Solution	0.084	0.89	10.8	16.7	182
PDMA linear	Solution	0.104	0.81	8.9	20.9	187
PDMA linear	Solution	0.128	0.77	7.2	48.2	201

Table 3: Characteristic lengths of PDMA solutions

By comparison with the solution of linear PDMA, the chemical gels prepared at the same concentration ($\phi_0 = 0.128$) display a rather good superposition of their scattering behavior in the high q range (see **Figure 13**) which means that similar thermal fluctuations are experienced in both linear and cross-linked systems.

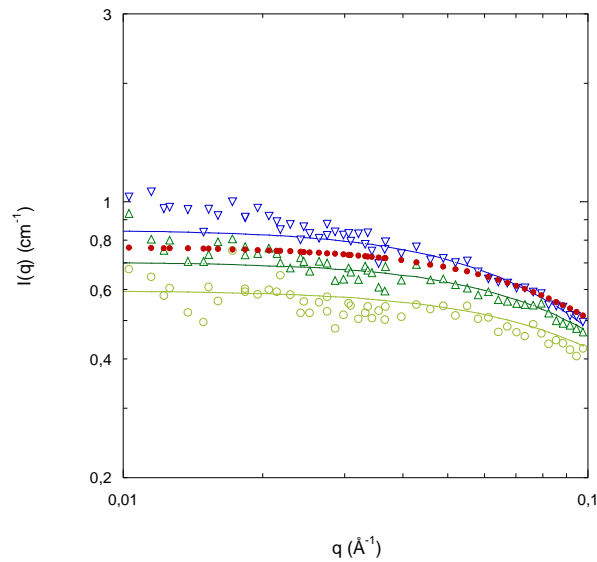


Figure 13: Double logarithmic representation of the scattered intensities of PDMA hydrogels in D_2O (SP0_PW0.14_Rz) for different amount of cross-linker: R0.1 (○); R0.5 (△) and R1 (▽). The thin lines correspond to the fitting results using Eq. 24. The red symbols indicate the fitting of thermal fluctuations alone (Eq. 22) obtained from the semi-dilute PDMA solution at the same volume fraction than PDMA hydrogels at Q_0 ($\phi = 0.128$).

The main difference between the semi-dilute solutions of PDMA and the PDMA cross-linked hydrogels remains in the low q -range: while heterogeneities formed during dissolution are still present in linear PDMA, the PDMA cross-linked hydrogels show only a very weak

scattering excess. The low cross-linking densities of our PDMA networks is certainly the main reason for this absence of static inhomogeneities. Indeed, it has been shown by Shibayama *et al.* that ξ and Ξ remain almost equal at low degree of cross-linking in the case of PNIPAM hydrogels cross-linked with MBA (about 15 Å for $\phi_0 = 0.078$) and that these characteristic lengths start to diverge for MBA amounts above 1 mol% [2].

The contrast between hydrogel heterogeneities (densely and weakly cross-linked domains) remains weak at the preparation state but can be enhanced by swelling the hydrogel: the differences of polymer concentrations within these different domains are revealed [22]. For instance, such behaviour is reported in **Figure 14** for a PDMA hydrogel prepared in D₂O with a cross-linking density of 1 mol%. The scattering intensities are compared for the gel at the preparation state ($\phi = 0.118$) and at the swelling equilibrium ($\phi_2 = 0.057$).

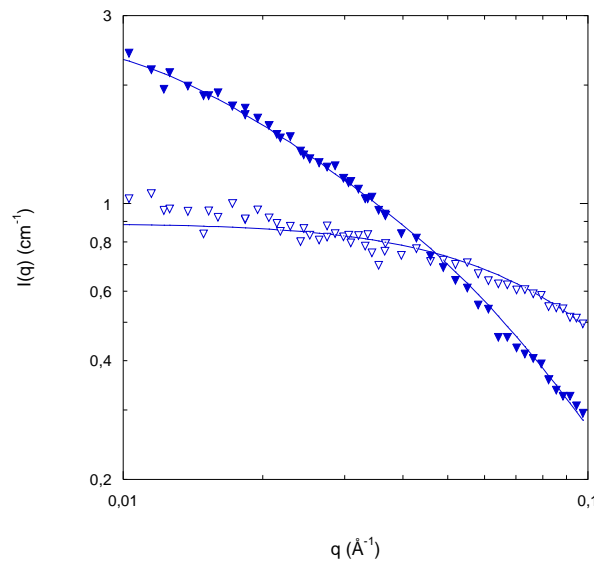


Figure 14: Double logarithmic representation of the scattered intensities of PDMA hydrogels in D₂O SP0_PWy_R1 for different swelling state: Q_0 (∇) and Q_e (\blacktriangledown). The thin lines correspond to the fitting results using Eq. 24.

Swelling the hydrogel clearly emphasizes the difference between Ξ and ξ : the characteristic length Ξ of static inhomogeneities becomes much higher than the correlation length ξ of thermal fluctuations. All the values are reported in **Table 4**.

Sample	State	ϕ	$I_{\text{soln}}(0)$ (cm^{-1})	ξ (Å)	$I_{\text{ex}}(0)$ (cm^{-1})	Ξ (Å)
SP0_PW0.14_R0.1	Gel Q_0	0.128	0.55	5.8	0.046	14.1
SP0_PW0.14_R0.1	Gel Q_e	0.023	0.96	27.4	2.7	74
SP0_PW0.14_R0.5	Gel Q_0	0.128	0.69	7.0	0.014	10.4
SP0_PW0.14_R0.5	Gel Q_e	0.04	1.08	24.5	1.75	67
SP0_PW0.14_R1	Gel Q_0	0.128	0.85	8.8	0.045	13.3
SP0_PW0.14_R1	Gel Q_e	0.057	1.3	19.6	1.61	47

Sample	State	ϕ	$I_{\text{soln}}(0)$ (cm^{-1})	ξ (Å)	$I_{\text{ex}}(0)$ (cm^{-1})	Ξ (Å)
SP0_PW0.07_R1	Gel Q_e	0.031	1.2	28.2	2.7	65
SP0_PW0.20_R0.1	Gel Q_0	0.173	0.54	4.4	0,023	17,8
SP0_PW0.20_R1	Gel Q_0	0.173	0.64	5.6	0,089	23,2

Table 4: Characteristic lengths of PDMA hydrogels at initial swelling Q_0 and at swelling equilibrium Q_e . Up: for the SP0_PW0.14_Rz series and bottom: for other SP0_PWy_Rz series.

Finally, the correlation length ξ of thermal fluctuations is plotted in **Figure 15** as a function of the polymer volume fraction ϕ for all the studied systems: semi-dilute solutions of linear PDMA, cross-linked PDMA hydrogels in the preparation state and at the swelling equilibrium in D₂O. This representation reveals a unique relation $\xi = \alpha\phi^{-0.94}$, with a scaling exponent close to -1 corresponding to the unperturbed conditions and a prefactor $\alpha \cong 1 \text{ Å}$. Quantitatively these results are in good agreement with the correlation length obtained by Shibayama and co-workers for PNIPAM hydrogels prepared and studied in similar conditions below their LCST ($\xi = 15 \text{ Å}$ for $\phi_0 = 0.078$) [2]. From **Figure 15**, the extrapolation of the experimental data to the melt state gives the corresponding correlation length $\xi \approx 1 \text{ Å}$. From this value, the corresponding blob size can be calculated as [23]:

$$\xi_b = \frac{\xi}{0.35} \quad \text{Eq. 25}$$

In our case, the blob size value is around 3 Å , close to the monomer size.

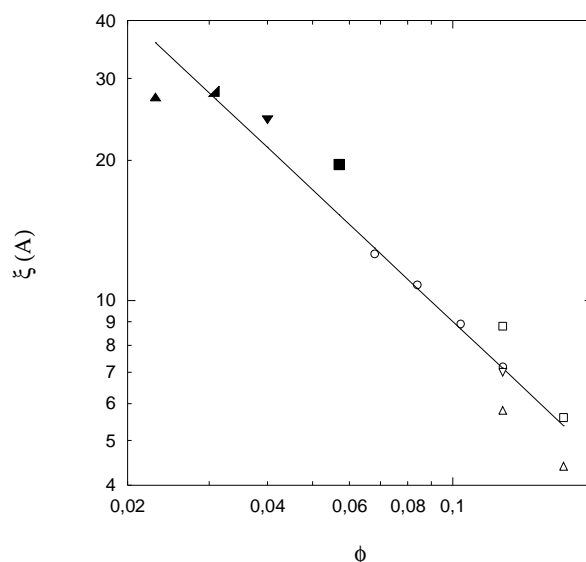


Figure 15: Concentration dependence of the correlation length in PDMA/D₂O binary mixtures. Linear PDMA (○) and PDMA hydrogels (SP0 series) in the preparation state (open symbols) and at equilibrium (filled symbols): △ (PW0.14_R0.1); ▽ (PW0.14_R0.5); □ (PW0.14_R1) and ◇ (PW0.07_R1).

In summary, SANS is a powerful technique to investigate the local structure of hydrogels. Within the small range of cross-linking density explored in this study, SANS shows that PDMA networks are rather homogeneous in their preparation state and reveals the presence of static heterogeneities in the swollen state with densely cross-linked domains surrounded by weakly cross-linked ones. Moreover, it comes out that polymer chains behave as Gaussian coils for all the polymer concentrations investigated.

3. Conclusion

In this chapter, PDMA hydrogels have been synthesized by free radical polymerization of DMA in presence of MBA as cross-linker, with KPS/TEMED as redox initiator, under nitrogen. The synthesis is reproducible and leads to transparent hydrogels which are macroscopically homogeneous. However, as polymerization and cross-linking happen at the same time, the concurrence of these two reactions leads to structural defects such as dangling chains and loops: the obtained materials being softer than the expected ones. The presence of defects was confirmed by mechanical measurements that aimed at characterizing the elastic properties of hydrogels. Using the initial moduli obtained by tensile tests, we showed that both physical entanglements and covalent cross-links contribute to the elastic modulus. Nevertheless, the contribution of covalent cross-links remains lower than the theoretical one: for gels prepared at $\phi_0 = 0.12$, the effective cross-linking density is only 42% of the theoretical one. An increase in the cross-linking density, corresponding to a decrease in the average number of monomer units between cross-links, leads to a reduction of the strain at failure and to an increase of the initial stiffness. Swelling experiments were in good agreement with the mechanical tendency observed for PDMA hydrogels varying the cross-linking density: the swelling ability strongly depends on the preparation state, *i.e.* the initial matrix concentration and its cross-linking density. Swelling experiments also point out that, in the preparation state, PDMA gels are close to their Θ -conditions in water at room temperature.

A detailed investigation of the structural properties of PDMA hydrogels was finally carried out by Small Angle Neutron Scattering. From these experiments, we have shown that the correlation length ξ , related to thermal fluctuations, is inversely proportional to the gel concentration, as expected in unperturbed conditions. Meanwhile, the length scale of static heterogeneities Ξ remains comparable to thermal ones when gels are studied in the preparation state, but Ξ is clearly enhanced in swollen samples.

The overall investigation carried out on PDMA hydrogels allowed us to have a detailed picture of the polymeric matrix (as represented in the **Figure 6** of Chapter 1) which characteristics are reported in **Table 5**.

Sample	ϕ_0	Monomer units between covalent cross-links	Q_e	E (kPa)	ϵ_r	ξ (Å)	Ξ (Å)
R 0.1	0.128	1200	40.5	12.6	1.84	5.8	14.1
R 0.5	0.128	240	22.9	27	0.66	7.0	10.4
R 1	0.128	120	15.2	46	0.34	8.8	13.3
R 1.5	0.128	80	14.5	61.6	0.25	-	-
R 2	0.128	60	12.8	88.3	0.24	-	-

Table 5: Characteristic of PDMA hydrogels prepared at $Q_0 = 8.5$.

Considering this first set of results, we choose to focus more specifically in the following on the R0.1 gel series which offers the best compromise between: a good swelling ability, a high deformability (compared to more cross-linked matrices) and a good stability and reproducibility (compared to the very weak R0 hydrogel). From this well-known polymeric matrix, the effect of the introduction of silica nanoparticles will be studied in the next chapters.

References

1. Orakdogan, N. and O. Okay, *Inhomogeneity in Acrylamide-based Hydrogels*. Journal of Applied Polymer Science, 2007. **103**: p. 3228-3237.
2. Norisuye, T., et al., *Small angle neutron scattering studies on structural inhomogeneities in polymer gels: irradiation cross-linked gels vs chemically cross-linked gels*. Polymer, 2002. **43**: p. 5289-5297.
3. Flory, P.J. and J. Rehner, *Statistical mechanics of cross-linked polymer networks II Swelling*. Journal of Chemical Physics, 1943. **11**: p. 521-526.
4. Flory, P.J. and J. Rehner, *Statistical mechanics of cross-linked polymer networks I Rubberlike elasticity*. Journal of Chemical Physics, 1943. **11**: p. 512-520.
5. Mark, J.E. and B. Erman, *Rubberlike Elasticity - A Molecular Primer*. 1988, New York: John Wiley & Sons.
6. Rubinstein, M. and R.H. Colby, *Polymer Physics*, ed. Oxford. 2003, New York.
7. Carlsson, L., et al., *Nano-hybrid self-crosslinked PDMA/silica hydrogels*. Soft Matter, 2010. **6**(15): p. 3619-3631.
8. Obukhov, S.P., M. Rubinstein, and R.H. Colby, *Network Modulus and Superelasticity*. Macromolecules, 1994. **27**: p. 3191-3198.
9. Gong, J.P., et al., *Double-network hydrogels with extremely high mechanical strength*. Advanced Materials, 2003. **15**(14): p. 1155.
10. Gundogan, N., O. Okay, and W. Oppermann, *Swelling, Elasticity and Spatial Inhomogeneity of Poly(N,N-dimethylacrylamide) Hydrogels Formed at Various Polymer Concentrations*. Macromol. Chem. Phys., 2004. **205**: p. 814-823.
11. Aouada, F.A., et al., *Preparation and Characterization of Hydrophilic, Spectroscopic, and Kinetic Properties of Hydrogels Based on Polyacrylamide and Methylcellulose Polysaccharide*. Journal of Applied Polymer Science, 2011. **120**(3004-3013).
12. Crank, J. and P. Nicolson, *The mathematics of diffusion*, ed. 2nd. 1983: Oxford University Press.
13. Shen, C. and G. Springer, *Environmental effects on composites materials*. Technomic Publishing and Co., 1981.

14. Alam, M.M., M.F. Mina, and F. Akhtar, *Swelling and hydration properties of Acrylamide hydrogel in distilled water*. Polymer-Plastics Technology and Engineering, 2003. **42**: p. 533-542.
15. Panyukov, S. and Y. Rabin, *Statistical physics of polymer gels*. Physics Reports, 1996. **269**: p. 1-131.
16. Horkay, F., et al., *Effect of cross-links on the structure of polymer gels*. Polymer Gels and Networks, 1996. **4**: p. 451-465.
17. Shibayama, M., *Soft Matter Characterization*. Vol. 2. 2008: Springer.
18. Bastide, J. and L. Leibler, *Large-Scale Heterogeneities in Randomly Cross-Linked Networks*. Macromolecules, 1988. **21**: p. 2647.
19. Benoit, H. and C. Picot, *Pure Appl. Chem.*, 1966. **12**: p. 545-562.
20. Koberstein, J.T., C. Picot, and H. Benoit, *Polymer*, 1985. **26**: p. 673-681.
21. Blanco, M.C., et al., *Dynamic Light Scattering in Transient Reversible Gels*. Langmuir, 2000. **16**: p. 8585-8594.
22. Mendes, E., et al., *Experimental evidence for inhomogeneous swelling and deformation in statistical gels*. Phys. Rev. Lett., 1991. **66**: p. 1595-1598.
23. Broseta, D., et al., *Universal Properties of Semi-Dilute Polymer Solutions: Comparison between Experiments and Theory*. Europhys. Lett., 1986. **2**: p. 733-737.

Chapter 3

Hybrid networks: synthesis and structural investigation of hydrogels containing silica nanoparticles

Contents

Contents	90
Introduction.....	91
1. Synthesis and characterization methods.....	92
1.1. Inorganic material	92
1.1.1. Scanning electron microscopy	92
1.1.2. Dynamic light scattering	93
1.1.3. Small angle neutron scattering.....	94
1.2. Synthesis of hybrid hydrogels.....	95
1.3. Titration of extractibles.....	96
1.4. Mechanics: tensile test	97
1.5. Swelling behaviour	97
1.6. Structural investigations by small angle neutron scattering.....	98
2. Characterization of hybrid PDMA hydrogels.....	100
2.1. Titration of extractible chains and silica nanoparticles.....	100
2.2. Structural analysis by Small Angle Neutron Scattering	102
2.2.1. Characterization of silica dispersion	102
2.2.2. Characterization of silica dispersion in hybrid hydrogels	108
2.2.3. Looking for the corona	114
2.3. Mechanical properties: initial elastic modulus	117
2.4. Swelling behaviour	120
3. Conclusions on the structure of hybrid hydrogels.....	123
References	125

Introduction

Now that the PDMA matrix of hydrogels has been characterized in details, the main purpose of this third chapter is to investigate how the introduction of silica nanoparticles will modify the general properties of the network, in terms of structure, mechanical behaviour and thermodynamics.

After a brief presentation and characterization of the inorganic material used in this study, the synthesis procedure of hybrid hydrogels as well as the characterization techniques will be presented. In the following, we will show that silica nanoparticles are physically trapped inside the polymer matrix, even during swelling experiments, and their distribution will be studied in details by small angle neutron scattering. Then, the impact of silica nanoparticles onto the mechanical properties of the gels at small strain will be emphasized and the swelling behaviour of hybrid hydrogels will be discussed in the light of these results.

1. Synthesis and characterization methods

The aim of this experimental part is to make a survey of all the materials and techniques that will be used afterwards. A special attention will be given to the inorganic material that had not been introduced before.

1.1. Inorganic material

Hybrid hydrogels are prepared by polymerizing organic monomers in the presence of silica nanoparticles dispersed in water. One suspension named Ludox-TM50 from Dupont was used for the study. The Ludox suspensions are known to be weakly polydisperse and easily available with several sizes. The main characteristics of the Ludox-TM50, characterized at 25°C, are the following:

- Concentration: 52 wt% in water;
- pH = 9;
- conductivity: 4.9 mS/cm;
- nature of the stabilizing counter ions: Na⁺.

The Ludox-TM50 suspension was used as received, without further purification.

The size of silica nanoparticles was characterized by different techniques such as dynamic light scattering, small angle neutron scattering and scanning electron microscopy.

1.1.1. Scanning electron microscopy

Scanning electron microscopy is a high resolution technique, based on the scanning of a sample with a focused beam of electrons, giving direct information about the shape and size of the nanoparticles (see **Figure 1**). Here, the silica material (Ludox TM-50), coated on a silicon wafer, is conductive enough to avoid additional step of metallization. The acquisition times were short (about 20 seconds) and high voltages were used (10 kV).

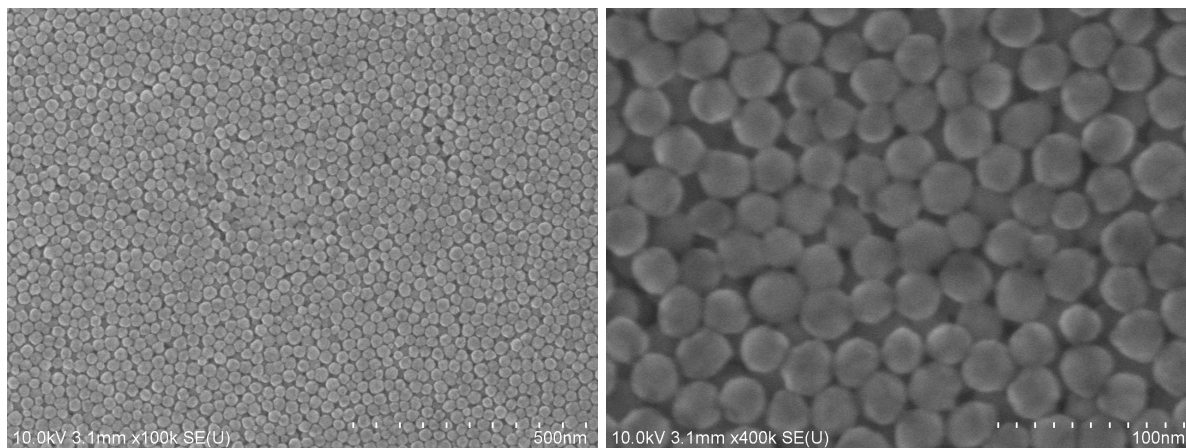


Figure 1: SEM images of silica nanoparticles Ludox-TM50, with two different scales.

The first general observation is that the particles present a spherical shape. This indication will be useful for the following characterizations, when we will need to use some fitting models. The scanning electron microscopy did not provide us clear images of the nanoparticles with sharp contours, due to the size limitation of this technique. However a mean radius of the silica nanoparticles Ludox-TM50 can be measured and is around 14-15 nm.

1.1.2. Dynamic light scattering

The size of silica nanoparticles was also characterized by dynamic light scattering, using an ALV/CGS-3 compact goniometer (ALV, Langer, Germany). The description of this technique will be detailed in Chapter 6 but one possibility offered by the dynamic light scattering technique is the determination of the size distribution of nanoparticles in suspension. This technique can give us the hydrodynamic radius of particles which is different from its real radius. As a matter of fact, the obtained size of the particles includes all the other molecules (such as stabilizer, surfactant, and even solvent molecules) that are surrounding the particles.

The measurements, performed at 25°C and at different scattering angles (30°, 60°, 90°, 120° and 150°) in dilute conditions, gave an average hydrodynamic radius $R_H = 17$ nm, which is a little bit higher than the radius observed by microscopy.

1.1.3. Small angle neutron scattering

Finally, small angle neutron scattering experiments were also performed on diluted suspension of silica nanoparticles (1 wt%). We get a particle radius of 13.2 nm, with a standard deviation of 1.5 nm. The experimental curve and its fit are given in **Figure 2** but a complete description of the technique and of the fitting parameters of these polydisperse spherical particles are detailed further in this Chapter.

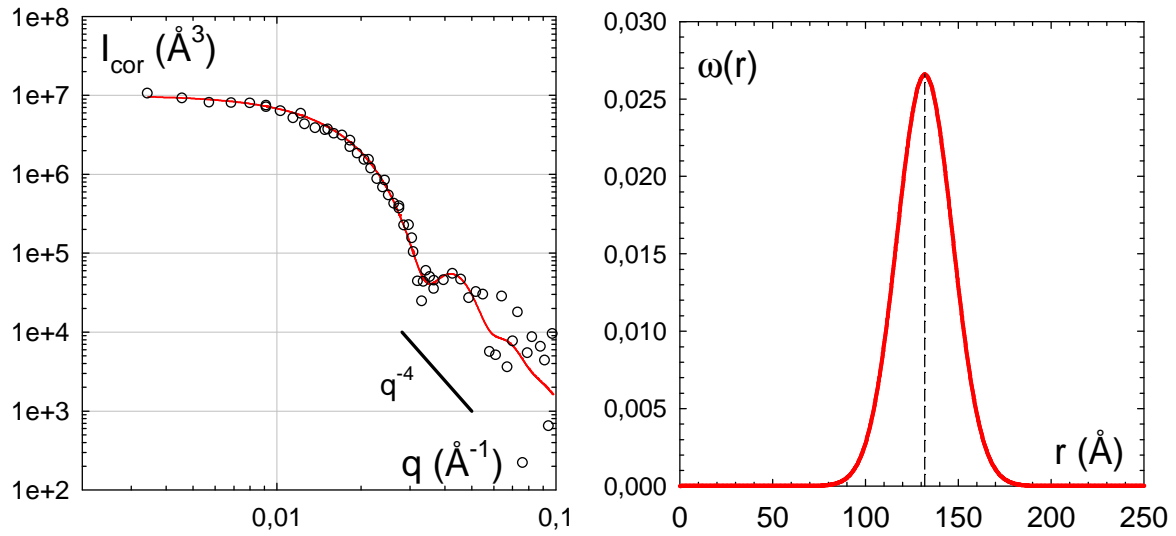


Figure 2: Left: Double logarithmic plot of the reduced scattering intensity (○) obtained from a dilute dispersion of silica nanoparticles Ludox-TM50 ($C = 1$ wt% or $\phi = 0.0044$). The corresponding fit based on a polydisperse sphere model (with a radius $R = 132$ Å and a standard deviation $\sigma = 15$ Å) is indicated in solid red line.

Right: Corresponding size distribution of Ludox-TM50.

The radii obtained by these different techniques are in good agreement with numerous characterizations reported on Ludox-TM50 in the literature [1-3]. As discussed by Orts-Gill and co-workers, which obtained similar values by TEM, DLS and SAXS, the hydrodynamic radius obtained by DLS is generally overestimated in dilute solution due to larger objects that contribute to higher intensity and to the increasing particles repulsions observed by dilution.

Taking into account the radius obtained by SANS for the mean size of Ludox-TM50, we can estimate the specific area of these silica nanoparticles according to:

$$S_{spe} = \frac{3}{\rho_{Si} R} \cong 100 m^2 / g \quad \text{Eq. 1}$$

with ρ_{Si} the density of pure silica, equal to $2.3 \cdot 10^6$ g/m³ and $R = 13.2$ nm the radius of the silica nanoparticles.

1.2. Synthesis of hybrid hydrogels

Poly(*N,N*-dimethylacrylamide) hybrid hydrogels were prepared in a nitrogen filled and oxygen free glove box at room temperature by *in situ* free radical polymerization of DMA using *N,N'*-methylenebisacrylamide (MBA) as cross-linker. All the reactants were initially deoxygenated and introduced in the glove box in order to prevent any oxygen contamination. After dilution of the silica suspension Ludox-TM50 in water, MBA (in solution) and DMA are added. A solution of KPS initially prepared and *N,N,N',N'*-tetramethylethylenediamine (TEMED) are added under stirring. The mixture is then rapidly transferred into moulds initially placed under the nitrogen atmosphere of the glove box. The geometry of moulds depends on the characterization techniques used. As previously mentioned, the polymerization is let to proceed during 24 hours.

This study of hybrid gels was based on the same hydrogel matrix as described in Chapter 2, with a fixed weight ratio between polymer and water equals to 0.14, corresponding to a fixed initial swelling of 8.5 and to a fixed polymer concentration equals to 12.3 wt%. The gels are studied in this preparation state. The molar ratio of cross-linker (MBA) to monomer varied from 0 to 5 mol%. The nomenclature used is still: SP_x for the Silica to Polymer weight ratio with x varying from 0 to 5, PW_y for the Polymer to Water weight ratio (y being equal to 0.14) and R_z for the molar ratio of cross-linker to monomer with z = 0 to 5 mol%. Therefore, a hybrid hydrogel with a polymer concentration of 12.3 wt% and containing 0.1 mol% of MBA will be named:

“SP_x_PW0.14_R0.1”.

Typically, a gel prepared with 2 g of silica particles, 1 g of PDMA, 7.14 g of water and 0.1 mol% of MBA will be named SP2_PW0.14_R0.1. The formulation of hybrid hydrogels used in this chapter is given in **Table 1**. In the following, we will mainly focus on the characterization of SP_x_PW0.14_R0.1 gels, the others being mainly used for comparison purposes.

Sample	Silica (g)	DMA (g)	MBA (mg)	KPS (mg)	TEMED (μL)	H ₂ O (g)
SP0.5_PW0.14_R0.1	0.744	1.485	2.3	0.041	22.5	10.624
SP1_PW0.14_R0.1	1.487	1.485	2.3	0.041	22.5	10.624
SP2_PW0.14_R0.1	2.975	1.485	2.3	0.041	22.5	10.624
SP3.5_PW0.14_R0.1	5.206	1.485	2.3	0.041	22.5	10.624
SP5_PW0.14_R0.1	7.437	1.485	2.3	0.041	22.5	10.624
SP2_PW0.14_R0	2.975	1.485	0	0.041	22.5	10.624
SP2_PW0.14_R1	2.975	1.485	23	0.041	22.5	10.624
SP2_PW0.14_R5	2.975	1.485	115	0.041	22.5	10.624

Table 1: Formulation of PDMA hybrid hydrogels.

1.3. Titration of extractibles

By comparison with organic hydrogels studied in Chapter 2, it is interesting to investigate if the presence of silica particles impacts the cross-linking polymerization of DMA and MBA. For that purpose, a rectangular piece of gel (approximately 4 cm length, 0.5 cm width and 0.2 cm thickness) is immersed in 150 mL of a solution of LiNO₃ at 0.5 mol/L. As the gel swells in these conditions, unreacted monomers (DMA and MBA) as well as uncross-linked chains can be extracted and characterized quantitatively by GPC after calibration of the refractometric detector with standard solutions of DMA, MBA and linear PDMA.

In the case of hybrid hydrogels, it is also interesting to verify that the silica nanoparticles cannot diffuse out of the cross-linked polymer network during swelling experiments. This study was carried out by Thermo-Gravimetric Analysis which can determine changes in weight as a function of temperature due to the vaporization of volatile compounds and/or decomposition of organic materials, under a specific and controlled atmosphere.

Prior to swelling experiments, hybrid hydrogels were studied just after the synthesis in order to define the reference state for both organic and inorganic compounds. Then, a second analysis was carried out with the gel swollen at equilibrium in pure water (after 2 weeks) in order to get information about the diffusion of nanoparticles outside the gel. All the samples were dried before the TGA analyses in order to remove the maximum of water and to improve consequently the accuracy of the organic/inorganic weight ratio determination. For that purpose, the samples were placed during 2 days at 80°C. The TGA analyses were performed under nitrogen atmosphere (with a flow rate of 50 mL/min) between 20 and 1200°C with a heating rate of 20°C per minute. The results were plotted as the fraction of lost weight as a function of the temperature, in order to get a good identification of the different species.

1.4. Mechanics: tensile test

Tensile tests are performed on hybrid hydrogels, following exactly the same procedure as the one described in Chapter 2. The constant strain rate used for the tests is 0.06 s⁻¹, corresponding to an initial velocity equal to 3 mm.s⁻¹.

1.5. Swelling behaviour

In the case of hybrid hydrogels, the silica particles embedded inside the network can have two antagonistic effects. They can interact with the matrix through attractive interactions and reduce the swelling ability of the gel, but at the same time they bring counter ions coming from partial dissociation of silanol groups and these counter ions will contribute positively to the osmotic pressure ($\Pi_{ion} > 0$), like in polyelectrolyte gels. When such a gel is immersed in water, the swelling equilibrium is reached when the osmotic pressure inside the gel (Π_{gel})

becomes equal to that of the surrounding medium (Π_{out}), as described by the following relation:

$$\Pi_{gel} = \Pi_m + \Pi_{el} + \Pi_{int} + \Pi_{ion} = \Pi_{out} \quad \text{Eq. 2}$$

where Π_m , Π_{el} , Π_{int} and Π_{ion} are respectively, the mixing, the elastic, the attractive interactions and the ionic contributions to the osmotic pressure.

With the aim of studying specifically the role of silica beads as potential cross-linkers (Π_{int}), all the swelling experiments were performed at high ionic strength (LiNO_3 ; $C_s = 0.5 \text{ mol/L}$) in order to screen the ionic contribution ($\Pi_{ion} \cong \Pi_{out} = \Pi'_{ion} = 2RTC'_s$).

For each hybrid hydrogel, the initial swelling in the preparation state (Q_0) is calculated assuming full conversion of monomers and additivity of volumes:

$$Q_0 = 1 + \frac{v_{spe}^w}{v_{spe}^p} \left(\frac{m_{p,w}^0}{m_p^0} - 1 \right) \quad \text{Eq. 3}$$

with v_{spe}^w the specific volume of water, v_{spe}^p the specific volume of the dry polymer network ($v_{spe}^p = 0.95 \text{ mL.g}^{-1}$), m_p^0 the mass of the polymer network ($m_p^0 = m_{DMA} + m_{MBA}$) and $m_{p,w}^0$ the total mass of the swollen gel in the preparation state ($m_{p,w}^0 = m_p^0 + m_w^0$, with m_w^0 the total mass of water). It is important to notice that we only consider the polymer in its aqueous environment and the mass of silica nanoparticles is not taken into account in the determination of the swelling.

Experimentally, small pieces of hybrid hydrogel, at their initial swelling Q_0 (preparation state) are cut, weighed and placed in a large excess of solvent (LiNO_3 , 0.5 mol/L), at room temperature. The solvent is changed every day during 2 weeks. The gels, swollen at equilibrium, are then weighed and the equilibrium swelling is calculated.

1.6. Structural investigations by small angle neutron scattering

Small angle neutrons scattering experiments have been carried out at Laboratoire Léon Brillouin (CEA, Saclay) with a small angle neutron spectrometer (PACE) dedicated to

isotropic measurements. In order to investigate the contributions of both organic and inorganic components within the gel, we applied the contrast matching procedure using suitable ratios $\text{H}_2\text{O}/\text{D}_2\text{O}$ to selectively adjust the neutron contrast of the solvent to one of the component either PDMA or silica. Taking into account the scattering length densities of H_2O ($Q_{\text{H}_2\text{O}} = -0.56 \cdot 10^{-6} \text{ \AA}^{-2}$), PDMA ($Q_{\text{PDMA}} = 0.936 \cdot 10^{-6} \text{ \AA}^{-2}$), silica ($Q_{\text{Si}} = 3.48 \cdot 10^{-6} \text{ \AA}^{-2}$) and D_2O ($Q_{\text{D}_2\text{O}} = 6.41 \cdot 10^{-6} \text{ \AA}^{-2}$), the contrast matching of PDMA and silica can be achieved with the following volume ratios:

- a. $\text{H}_2\text{O}/\text{D}_2\text{O} = 0.79/0.21$, for matching the PDMA network, that will be named “solvent p”,
- b. $\text{H}_2\text{O}/\text{D}_2\text{O} = 0.42/0.58$, for matching the silica nanoparticles, that will be named “solvent s”.

For that purpose, hybrid hydrogels were specially prepared, as previously described, in three different aqueous environments: solvent p, solvent s and pure H_2O . For hybrid hydrogels with high amounts of D_2O , Ludox-TM50 was initially dialysed during two weeks in control D_2O environment in order to get a stable and concentrated dispersion of silica in D_2O (with a silica concentration around 40 wt%), with:

- a. $\text{pH} = 9$, or $\text{pH}^* = 8.6$, with pH^* the pH value measured in D_2O ,
- b. 4.9 mS/cm for the conductivity.

From the hydrogel stripes in their preparation state, synthesized in the same home-made moulds than the one used for mechanical tests, discoid samples (diameter $d = 14$ mm and thickness of 1 or 2 mm) were cut with a cylindrical punch. Those discs were placed between two quartz slides hermetically sealed.

As described in Chapter 2, two configurations were used on the spectrometer, keeping constant the sample-to-detector distance $D = 4.7$ m and changing the wavelength of the incident neutron beam $\lambda = 12$ and 4.5 \AA . The resulting values of the scattering vector modulus are ranging between 0.0034 and 0.098 \AA^{-1} .

2. Characterization of hybrid PDMA hydrogels

The synthesis procedure previously described, with polymerization and cross-linking occurring at the same time, is known to lead to heterogeneous structures with a broad size distribution of chains [4]. The presence of silica nanoparticles is another perturbation factor due to possible interactions taking place between silica and other reactants. Experimentally, we observed that increasing the amount of silica nanoparticles leads to an increase of the gelation time of the system. This observation will be explained later in Chapter 6.

2.1. Titration of extractible chains and silica nanoparticles

As discussed in Chapter 2, the polymerization efficiency is always above 98% for single PDMA hydrogels and less than 1 wt% of PDMA chains are extractible from the cross-linked network. In the case of hybrid PDMA hydrogels, we do not observe by GPC any kind of organic extractible, either monomer or polymer chains and again we can conclude that the cross-linking polymerization is quantitative. However, as the silica nanoparticles cannot be characterized by this technique, TGA experiments were also used.

The experimental values of the silica/polymer ratio (SP_x), determined in the preparation state and after swelling at equilibrium are reported in **Table 2** for SP3.5 and SP5 hydrogels.

In the preparation state, we can observe a slight dispersion of the SP values for samples SP3.5 and SP5. As a matter of fact, some samples show a SP value higher than the theoretical value while some others have a lower SP ratio. Surprisingly, for two gel pieces coming from the same initial sample, different SP values can be obtained. For example, we obtained experimental values of 3.1 and 2.1 for a SP3.5 hydrogel and even a SP value of 8 has been obtained for a SP5 hydrogel. This broad dispersion of experimental data is attributed to the drying step priori to TGA measurements. Indeed, samples were systematically dried before testing in order to get a better accuracy in the evaluation of the SP ratio. Before drying, the samples are transparent and homogeneous while they are heterogeneous after drying: some parts of the dried gel are transparent while others are completely white and crumbly. One

can assume that the white parts contain more silica nanoparticles than the transparent ones and indeed the TGA measurements confirm this idea. A segregation of silica nanoparticles takes place during the drying process, leading to parts with different silica amounts at the dried state.

For the study performed with hydrogels in the swelling state, the same observation can be made: no significant difference is observed for the SP3.5 hydrogels before and after swelling, the mean values are identical. In that case, we can conclude that most of silica nanoparticles remain embedded inside the network, even after swelling. For the SP5 hydrogels, a slight decrease of the experimental SP value is observed after swelling: the average values decreasing from 4.7 ± 0.4 to 3.7 ± 0.4 . However, this difference does not seem to be significant as the results strongly depend on the heterogeneity of the dried sample tested. Some improvements of this statistic analysis of the SP ratio would require a soft drying process with a controlled decrease of the environment humidity.

Sample	Theoretical SP	Initial SP	SP after swelling
SP3.5_PW0.14_R0.1	3.5	2.8 ± 0.3	2.9 ± 0.3
SP5_PW0.14_R0.1	5	4.7 ± 0.4	3.7 ± 0.4

Table 2: Experimental values of the Silica/Polymer ratios before and after swelling.

Moreover, a simple observation of the SP5 surface by SEM can illustrate that the silica nanoparticles remain inside the network when hybrid hydrogels are swollen up to equilibrium. In **Figure 3**, we compare the surface of a SP5 sample dried just after synthesis (left) to the surface of a SP5 sample dried after reaching its swelling equilibrium in water (right). The two surfaces seem to be identical, silica nanoparticles do not leach out the sample.

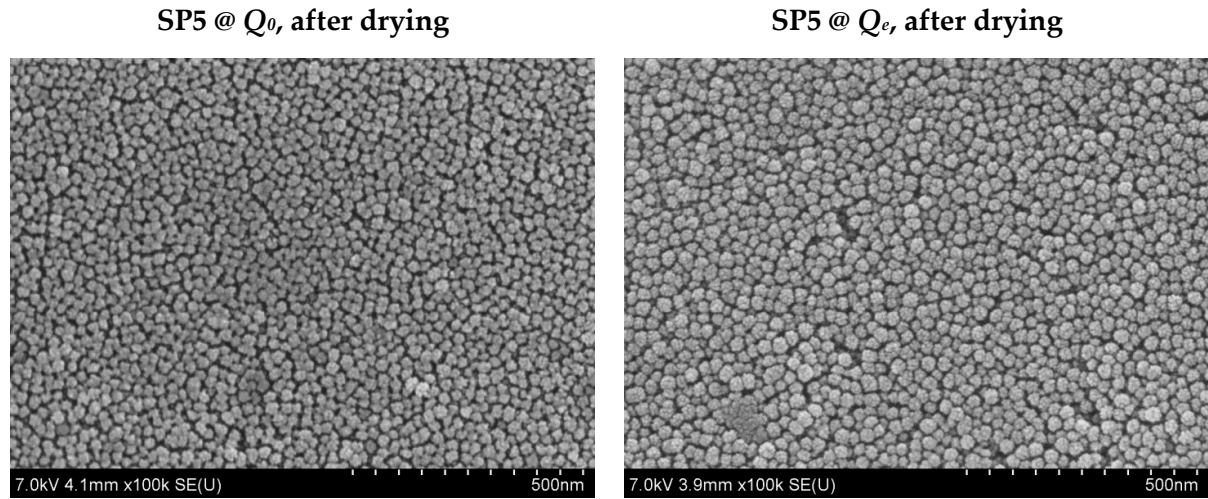


Figure 3: SEM images of SP5 surface. Left: surface of a SP5 sample dried just after synthesis. Right: surface of a SP5 sample dried after reaching its swelling equilibrium in water.

As a conclusion, we will keep in mind that no significant difference of silica content has been observed by TGA measurements. In relation with the specific interactions taking place between silica surfaces and PDMA matrix, most of the nanoparticles remain embedded inside the polymer network during and after swelling. As most of the following experiments are performed in the preparation state, the total amount of silica in the gels is perfectly known.

2.2. Structural analysis by Small Angle Neutron Scattering

2.2.1. Characterization of silica dispersion

SANS experiment is a very interesting tool to investigate the local structure of complex materials such as hybrid hydrogels. For binary systems like silica suspension, where spherical particles (the filler: index f) are dispersed in a homogeneous medium (the solvent: index s), the scattering intensity can be described by the following relation:

$$I(q) = \frac{N_f v_f}{V} \phi_s (\Delta\rho)^2 P(q) S(q) \quad \text{Eq. 4}$$

with q the scattering vector, N_f the number of filler particles of average volume $v_f = 4\pi R_f^3/3$ and radius R_f , V the total scattering volume, $\phi_s = 1 - \phi_f$ the volume fraction of

the solvent ($\phi_f = N_f v_f / V$ being the volume fraction of the filler), $\Delta\rho = \rho_f - \rho_s$ the difference of scattering length densities between the filler and the solvent, $P(q)$ the form factor of the particles and $S(q)$ their structure factor.

A convenient way to compare scattering curves from different formulations is to divide $I(q)$ in Eq. 4 by $\phi_f \phi_s (\Delta\rho)^2$ or by the experimental value of the invariant given by:

$$Q_{\text{exp}} = \int_0^\infty q^2 I(q) dq \quad \text{Eq. 5}$$

Indeed, for an incompressible two-phase system, the invariant is a constant that only depends on the volume fraction and the contrast between the two phases:

$$Q_{\text{th}} = 2\pi^2 (\Delta\rho)^2 \phi_f \phi_s \quad \text{Eq. 6}$$

In the case of particles with sharp interfaces, the scattering intensity as well as $q^2 I(q)$ rapidly decrease at high values of q ($qR > 1$) following the Porod's law ($I(q) \approx q^{-4}$). In these conditions, and more generally when we will be able to readily calculate the integral in Eq. 5 over the experimental q -range, we will use the following relation to describe the scattering data:

$$I_{\text{cor}}(q) = 2\pi^2 \frac{I(q)}{Q_{\text{exp}}} = P(q) \cdot S(q) \quad \text{Eq. 7}$$

From a general point of view, this correction of the scattering intensity by the experimental value of the invariant is also an interesting way to minimize experimental uncertainties related to concentration and contrast. Nevertheless, the main feature of this relation is that $I_{\text{cor}}(q)$ only depends now on the two main functions: $P(q)$ and $S(q)$.

$P(q)$ represents the interference of neutron scattered from different parts of the same object ($P(q)$ tends to v for $qR < 1$) and gives geometrical information about the size and shape of the scatterers. In the same way, $S(q)$ describes the interference of neutron scattered from different

objects and provides details about their correlation. $S(q)$ is the Fourier transform of the correlation function of the mass centre of the particles.

For Ludox-TM50, which contains polydisperse spherical particles, the form factor can be described by the following expression:

$$P(q) = \int_{-5\sigma}^{+5\sigma} \frac{4\pi r^3}{3} [F(q, r)]^2 \omega(r) dr \quad \text{Eq. 8}$$

with

$$F(q, r) = 3 \frac{\sin(qr) - qr \cos(qr)}{(qr)^3} \quad \text{Eq. 9}$$

and

$$\omega(r) = \frac{1}{\sqrt{2\pi}\sigma} \exp\left(-\frac{(r-R)^2}{2\sigma^2}\right) \quad \text{Eq. 10}$$

where $\omega(r)$ is the Gaussian size distribution function, with σ the standard deviation here.

In dilute condition, when interactions between particles are negligible, $S(q) = 1$ over the whole range of q and the scattering intensity $I_{cor}(q)$ is equal to the form factor. An example is given in **Figure 2** with a dilute dispersion of Ludox-TM50 (1 wt%) along with the fit obtained from the polydisperse sphere model. Even if the reduced scattering intensity, equal in these conditions to the form factor, is very noisy at large q because of the subtraction of the solvent, this first set of data allows a good assessment of the particle size; their volume being extrapolated at $q \rightarrow 0$: $I_{cor}(0) = P(0) = V_f \approx 10^7 \text{ \AA}^3$. The best fitting is obtained here with a particle radius $R_f = 132 \text{ \AA}$ and a standard deviation $\sigma = 15 \text{ \AA}$; the corresponding size distribution of the particles being shown in **Figure 2**.

At higher silica concentrations, typically in the range where hybrid hydrogels are prepared, colloidal interactions take place and $S(q)$ is no longer equal to 1 over the whole q -range. If the particles have a liquid-like order, the structure factor has a correlation peak at q_{max} which characterizes the average distance between the particles. This situation is clearly depicted in **Figure 4** (left) with the scattering pattern of a concentrated suspension of Ludox-TM50 ($C = 20 \text{ wt\%}$ or $\phi_f = 0.099$). A maximum of scattering intensity is actually observed at $q_{max} = 0.015 \text{ \AA}^{-1}$ but this maximum can be different from that of the structure factor as it can be shifted by

the decreasing function of $P(q)$. Assuming that the form factor previously determined in dilute conditions corresponds to the one of isolated particles, we can deduce the structure factor from more concentrated dispersions by dividing $I_{cor}(q)$ by $P(q)$. Such treatment presented in **Figure 4** (right) leads to a large dispersion of data, especially at large q where the statistics of scattering intensities of the dilute suspension is rather poor, but with a clear correlation peak can be observed around $q_{max} = 0.017 \text{ \AA}^{-1}$. Moreover, the sharp decrease of $S(q)$ below 1 at low q , which corresponds to the reduction of the osmotic compressibility ($\chi = S(0)$) of the suspension with increasing concentration, clearly points out the repulsive nature of interactions between silica particles.

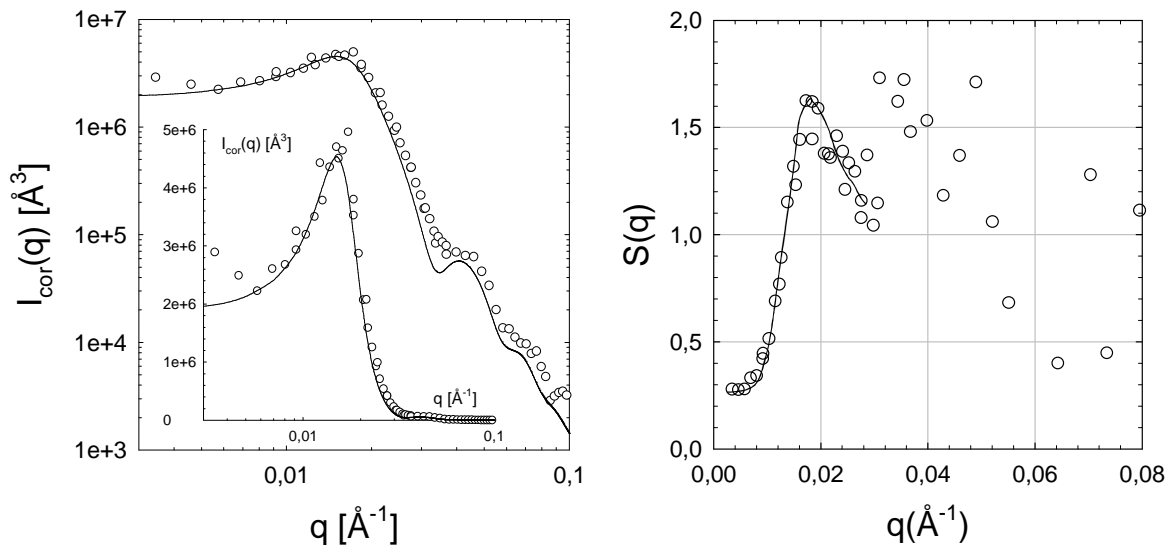


Figure 4: Left: Double logarithmic plots of the reduced scattering intensity (○) obtained from a concentrated dispersion of silica particles ($C = 20 \text{ wt\%}$ or $\phi_f = 0.099$). The corresponding fit based on a polydisperse sphere model with hard sphere repulsions is indicated in solid black line. Experimental data and model fitting are also shown under a semi-log form at the bottom of the figure.

Right: Representation of the experimental structure factor obtained by dividing the reduced scattering intensity of concentrated silica suspension ($\phi_f = 0.099$) by the reduced scattering intensity of dilute silica suspension ($\phi_f = 0.0044$).

The value of q_{max} corresponds in the real space to an effective centre-to-centre distance between particles $d = 2\pi/q_{max} = 370 \text{ \AA}$. By comparison with the average spacing between

particles at this concentration ($\phi_f = 0.099$), assuming a perfectly ordered dispersion like simple cubic ($d_{sc} = 470 \text{ \AA}$), it appears that silica beads interact in our experimental conditions (pH and ionic strength) mostly through short-range repulsive inter-particle forces.

In order to model the scattering behaviour of our different systems (both dispersions and hybrid hydrogels) with a minimum number of adjustable parameters, we have assumed a hard sphere potential between particles. Considering the Percus-Yevick approximation of the Ornstein-Zernike equation, the structure factor for hard spheres can be calculated using the following set of equations:

$$S(q) = \frac{1}{1 + \frac{24\phi_{HS}G(2qR_{HS})}{2qR_{HS}}} \quad \text{Eq. 11}$$

with R_{HS} the radius of hard spheres with volume fraction ϕ_{HS} , and G a trigonometric function depending on q , R_{HS} and ϕ_{HS} as follows:

$$G(x) = \alpha \frac{(\sin x - x \cos x)}{x^2} + \beta \frac{2x \sin x + (2 - x^2) \cos x - 2}{x^3} + \gamma \frac{\left\{ -x^4 \cos x + 4 \left[(3x^2 - 6) \cos x + (x^3 - 6x) \sin x + 6 \right] \right\}}{x^5} \quad \text{Eq. 12}$$

$$\text{with} \quad \alpha = \frac{(1 + 2\phi_{HS})^2}{(1 - \phi_{HS})^4} \quad \beta = -6\phi_{HS} \frac{(1 + (\phi_{HS}/2))^2}{(1 - \phi_{HS})^4} \quad \gamma = \frac{(\phi_{HS}/2)(1 + 2\phi_{HS})^2}{(1 - \phi_{HS})^4} \quad \text{Eq. 13}$$

Working with absolute scattering intensities and known formulation parameters, like the volume fraction of silica particles (ϕ_f) and the nature of the diluent, it is possible to fit the experimental data according to **Eq. 7** by using a simple set of unequivocal variables: R , σ and R_{HS} ; ϕ_{HS} being given by $\phi_{HS} = \phi_f (R_{HS}/R)^3$.

The application of this previous model, taking into account polydisperse spheres interacting with a hard sphere potential, is given in **Figure 4** for the Ludox-TM50 suspension ($C = 20$ wt%). In that case, the fitting procedure gives:

- $R = 134 \text{ \AA}$ for the radius of the particles that is similar to the one previously extrapolated in dilute conditions,
- an average polydispersity $\sigma(R)/R$ of about 10% in good agreement with the literature data [O],
- a hard sphere radius of 175 \AA that evidences short-range repulsive interactions between silica particles.

As the effective hard sphere radius is larger than the physical one, we can assume that weak electrostatic repulsions exist between silica nanoparticles and that the range of these interactions is of the order of the Debye length; *i.e.* 20 to 30 \AA in our conditions. Qualitatively we can mention that these two parameters R and $R_{HS} = d/2$ can be roughly extrapolated from the scattering curve without mathematical treatment, assuming that the first maximum is related to the most probable distance between particles ($q_{max} = 0.0172 \text{ \AA}^{-1}$ and $R_{HS} = 182 \text{ \AA}$) and that the following “minimum”, related to the oscillations of the form factor, is $q_{min}R = 4.5$; *i.e.* $R = 128 \text{ \AA}$ for $q_{min} = 0.035 \text{ \AA}^{-1}$.

2.2.2. Characterization of silica dispersion in hybrid hydrogels

As far as hybrid hydrogels are concerned, we have to consider the study of a ternary system composed of cross-linked polymer (p), filler (f) and solvent (s). This situation cannot longer be described by the previous general structure factor; the three components must be taken into account as:

$$I(q) = (\rho_p - \rho_s)^2 \bar{S}_{pp}(q) + (\rho_f - \rho_s)^2 \bar{S}_{ff}(q) + 2(\rho_p - \rho_s)(\rho_f - \rho_s) \bar{S}_{pf}(q) \quad \text{Eq. 14}$$

with ρ_i the scattering length density of each component and $\bar{S}_{ij}(q)$ the partial scattering functions: $\bar{S}_{pp}(q)$ and $\bar{S}_{ff}(q)$ are respectively the self-correlations of the polymer and the silica filler and $\bar{S}_{pf}(q)$ represents the cross-correlation between the polymer and the filler.

From this complex expression, it is clear that $I(q)$ must be measured using at least three different values of the solvent scattering length ρ_s in order to solve the three partial scattering functions [5]. Alternatively, one can perform contrast variation experiments by tuning the scattering length density of the solvent mixture (H₂O/D₂O) in order to focus more specifically on the silica nanoparticles ($\rho_p = \rho_s$) or on the polymer network ($\rho_f = \rho_s$). For that purpose, scattering experiments have been performed either in solvent p ($\rho_p = \rho_{PDMA} = 0.936 \cdot 10^{14} \text{ m}^{-2}$ with $\rho_{D2O} = 0.21$ and $\rho_{H2O} = 0.79$) or in solvent f ($\rho_f = \rho_{Si} = 3.48 \cdot 10^{14} \text{ m}^{-2}$ with $\rho_{D2O} = 0.58$ and $\rho_{H2O} = 0.42$).

In the case of solvent p, where both polymer and solvent mixture have the same scattering length density, **Eq. 14** is reduced to **Eq. 4** and all the procedure previously described with silica suspension can be readily applied to hybrid hydrogels.

As shown in **Figure 5** (left), where the scattering behaviour of hybrid networks and silica suspension are compared at the same filler concentration, we get a very good superposition of the curves in the high q -range which is mainly dominated by the form factor of silica particles ($S(q) \cong 1$).

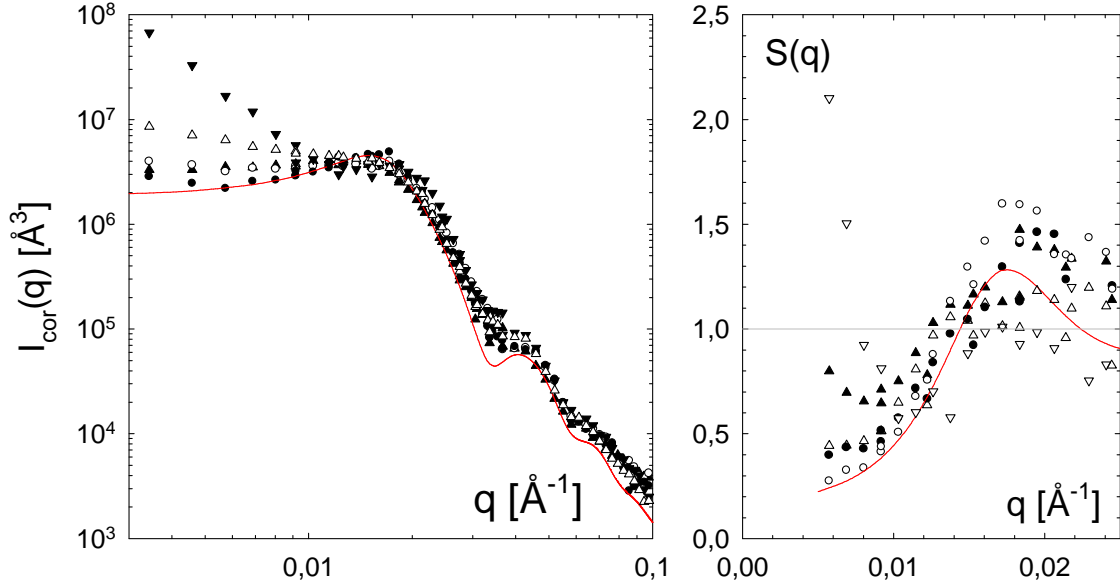


Figure 5: Left: Double logarithmic plots of the reduced scattering intensity of PDMA/silica hydrogels (SP2_PW0.14_Rz) prepared in solvent p (silica scattering) with different amounts of cross-linker: R0 (○); R0.1 (▲); R1 (△) and R5 (▼). By comparison, the scattered intensity of silica particles without PDMA but at the same volume fraction ($\phi_f = 0.099$) and in the same solvent conditions is shown (●) with the fit (solid red line) obtained from the hard sphere model.

Right: Representation of the experimental structure factor obtained by dividing the reduced scattering intensity of hybrid formulations by the reduced scattering intensity of dilute silica suspension ($\phi_f = 0.0044$).

The main difference arises at low- q where the scattering intensity increases when silica beads are embedded into the PDMA network with increasing level of cross-linking. This behaviour is taken into account within the hard sphere model with lower values of R_{HS} obtained with hybrid networks (see **Table 3**) but this comparison remains only qualitative as it is difficult, even impossible, to fit the scattering data of highly cross-linked samples with a hard core potential.

Sample	ρ_f	R (Å)	σ (Å)	R _{HS} (Å)
Silica suspension	0.0044	132	15	---
Silica suspension	0.099	134	15	175
SP2_PW0.14_R0	0.099	135	15	155
SP2_PW0.14_R0.1	0.099	135	15	155
SP2_PW0.14_R1	0.099	138	15	152
SP2_PW0.14_R5	0.099	135	15	---

Table 3: Fitting parameters related to silica scattering obtained from hybrid hydrogels prepared in solvent p ($\rho_{D_2O} = 0.21$; $\rho_{H_2O} = 0.79$).

Obviously, this difference originates from the structure factor of the particles and we tried to extrapolate $S(q)$ as previously described in the case of the concentrated silica suspension. The plots of $S(q)$ versus q are shown in **Figure 5** in a limited range of q where the dispersion of data is not too high to allow a quantitative discussion. By comparison with the silica suspension, the polymerization of DMA without cross-linker ($z = 0$ mol%) or with a low level of cross-linker ($z = 0.1$ mol%) only slightly increases the osmotic compressibility of the system which remains repulsive in nature. At higher level of cross-linking ($z = 1$ and 5 mol%) $S(q)$ goes upward at low q and becomes even higher than 1 for the highest level of cross-linker. In that case the potential between particles becomes clearly attractive: the system becomes more compressible and tends towards phase transition (aggregation). The destabilization of silica particles in the presence of polymers can be understood on the basis of enthalpic or entropic contributions.

Enthalpic contribution could prevail when there is a strong attractive potential between polymer and particles, like between silica and cationic polymers, or as it was observed by Shibayama and co-workers [6] during the polymerization of *N*-isopropylacrylamide at low pH (between 3 and 6) in the presence of silica particles.

Entropic effects are generally described by the existence of a depletion layer of polymer chains near hard particles. The weak flocculation of colloidal particles induced by non-

adsorbing polymers has been widely reported in the literature [7, 8] and was typically observed in this work for hybrid hydrogels prepared by polymerizing acrylamide in the presence of silica particles (see Chapters 5 and 6). In the case of PDMA/silica, which is characterized by attractive interactions, we can assume that a layer of cross-linked PDMA is rapidly formed (adsorbed) at the silica interface during the first stage of the polymerization. This layer provides an additional steric stabilization of the particles, but it is also known that sterically stabilized particles can undergo weak flocculation when suspended in a polymer solution of the same composition [7, 8]. In that case the flocculation is explained by the existence of a depletion of mobile chains near the steric layer, similar to the depletion layer next to a hard wall. This phenomenon strongly depends on the relative polymer concentration inside and outside the adsorbed layer; the depletion layer decreasing with the decreasing imbalance between concentrations and vanishing when concentrations are almost the same. In the case of hybrid hydrogels, we can reasonably assume that the spatial distribution of silica nanoparticles in the polymer network is rapidly fixed; as soon as the system reaches the gelation threshold. That means that the structure observed in the hydrogels by small angle neutron scattering mirrors the first stage of the polymerization. If we assume that at the beginning of the reaction the first polymerized chains are adsorbed onto the silica nanoparticles, this polymerization/adsorption mechanism will rapidly drive a concentration imbalance between the polymer layer and the bulk. If the concentration of the polymer layer is controlled by the degree of cross-linking during the first stage of the polymerization, following the C^* theorem, it follows that the depletion mechanism should increase with the degree of cross-linking with a higher tendency towards aggregation as it was shown in **Figure 5**. The aggregation mechanism is particularly favourable at high degree of cross-linking, typically for z above 2mol%, where syneresis has been observed with a final concentration of the gel higher than the initial one.

The adsorption of PDMA chains at the surface of silica beads is responsible for the formation of an attractive potential between particles and we can reasonably assume that the bridging forces induced by PDMA chains and then the level of heterogeneity of the hybrid network will increase with parameters such like binding energy or cross-linking density.

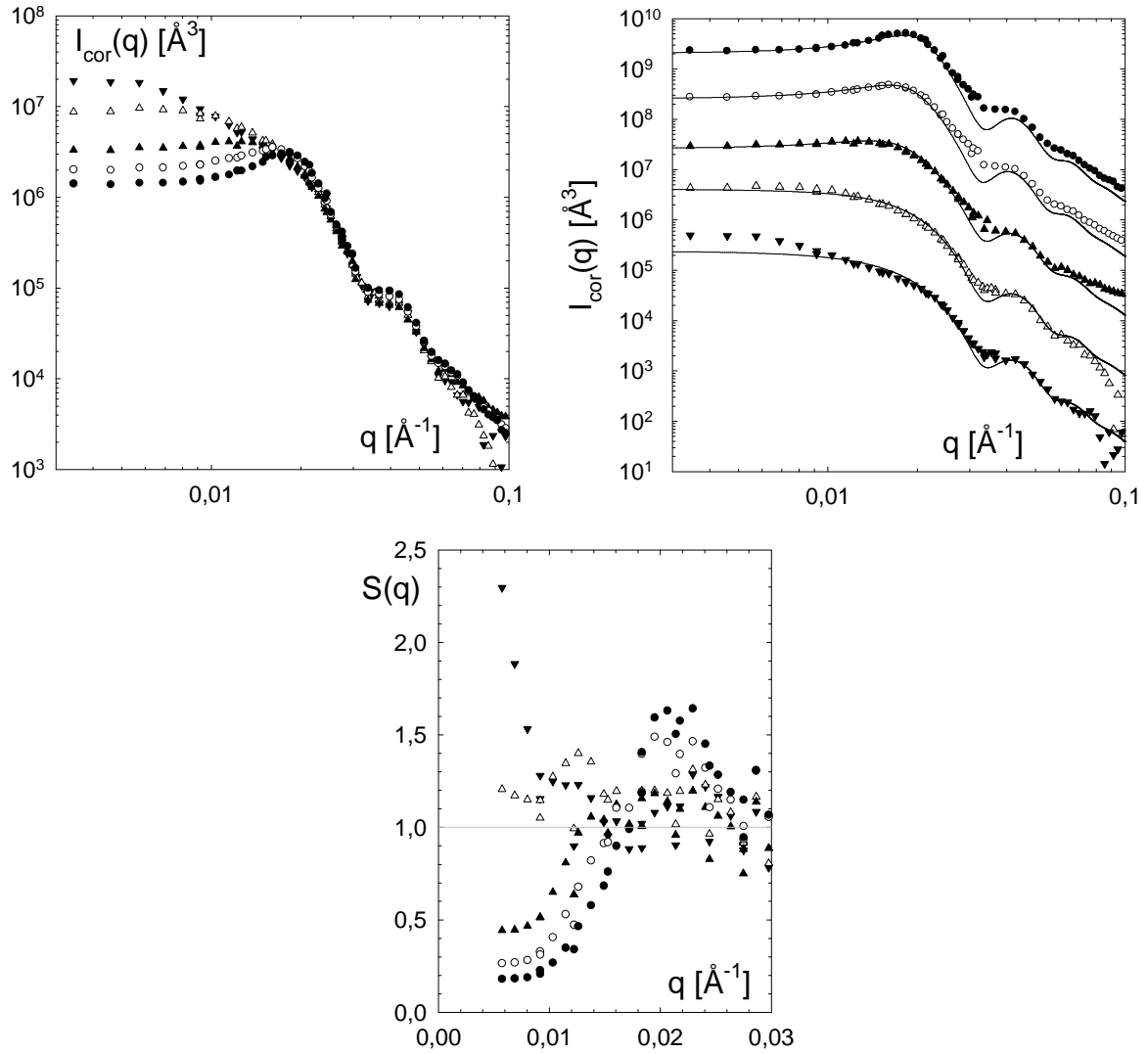


Figure 6: Up left: Double logarithmic plot of the normalized scattered intensity of PDMA/silica hydrogels (SPx_PW0.14_R0.1) prepared in solvent p (silica scattering) with different amounts of silica: SP0.5 (\blacktriangledown); SP1 (\triangle) SP2 (\blacktriangle), SP3.5 (\circ) and SP4.8 (\bullet).

Up right: Similar plot with fittings obtained. The curves are shifted from one to another by a factor 10; the bottom one (\blacktriangledown) being the reference position.

Down: Experimental structure factor obtained by dividing the reduced scattering intensity of hybrid formulations by the reduced scattering intensity of dilute silica suspension ($\phi_f = 0.0044$).

With increasing the fraction of filler inside the network, we can observe in **Figure 6**:

- the same scattering pattern in the high q -range, in relation with the form factor of individual particles, and

- a sharp decrease of $I(q)$ at low q due to increasing interferences between particles.

In that case, a correlation peak is readily observed from 10 vol%. As shown in **Figure 6** (up left), the experimental data can be reasonably fitted with the hard sphere model, showing a decrease of R_{HS} with decreasing the fraction of filler (**Table 4**).

Nevertheless, there is a clear discrepancy between the model and experimental data for the lowest filler concentration where attractive interactions are not taken into account within the hard sphere potential. The reduction of scattering curves by the form factor in **Figure 6** (down) emphasizes the variation of the osmotic compressibility ($S(0)$) with the concentration of filler. Whereas the potential is clearly repulsive for volume fraction equal and higher than 10 vol%, it progressively turns attractive at lower concentration and especially at 2.5 vol%. One of the main differences between hybrid hydrogels prepared at “high” and “low” filler concentration is the dilution of the original dispersion of Ludox-TM50 suspension initially stabilized at pH 9. While the silica suspension is diluted only 1.4 times to formulate the sample SP5, the dilution is 14 times for the SP0.5. As higher dilution means lower pH and then stronger interactions between PDMA and silica surfaces (SiOH), this could explain the variation of $S(q)$ with the filler content.

Formulation	ρ_f	R (Å)	σ (Å)	R_{HS} (Å)
SP0.5_PW0.14_R0.1	0.027	135	15	135
SP1_PW0.14_R0.1	0.052	135	15	135
SP2_PW0.14_R0.1	0.099	135	15	155
SP3.5_PW0.14_R0.1	0.161	135	15	148
SP4.8_PW0.14_R0.1	0.206	135	15	148

Table 4: Fitting parameters related to silica scattering obtained from hybrid hydrogels prepared in solvent p ($\rho_{D_2O} = 0.21$; $\rho_{H_2O} = 0.79$).

As for polymer-polymer systems that can undergo different type of phase transitions like segregation or complex formation depending on interactions, the formation of hybrid networks thermodynamically stable during their formation results from the same subtle

balance involving adsorption and depletion forces. In agreement with our macroscopic observations concerning the transparency of hybrid hydrogels that remain comparable to initial dispersions, we have shown by small angle neutron scattering that it is possible to get well dispersed silica particles inside a PDMA network so long as we work with reasonable level of cross-linker. For these systems, we assume that there is an attractive potential between silica and PDMA, mainly driven through hydrogen bonds and hydrophobicity as it has been widely reported for polymer coating on fused silica capillaries [9, 10], and that this potential is not too high to avoid any phase transition. During the discussion, we were talking about the PDMA layer adsorbed at the silica interface. This adsorption layer was experimentally evidenced from adsorption isotherm measurements [11] and we have tried to get more information by small angle neutron scattering, especially about the layer concentration.

2.2.3. Looking for the corona

Working in solvent f , the filler and the solvent have the same scattering length densities and the situation is now similar to a PDMA hydrogel with solvent holes replacing the silica nanoparticles. This case is nevertheless different from the previous one as we assume that PDMA chains interact with the silica surface and we have to consider a 3-phase model with:

- the filler (index f),
- the adsorbed polymer layer at the interface (index l) and
- the PDMA matrix which does not interact directly with the particles (index m).

In order to take into account this situation we have used the form factor describing the scattering of the hard sphere interface between the core and the corona (adsorbed polymer layer) and between the corona and the surrounding polymer matrix. The scattering amplitude of the core-shell particle is given by:

$$A(q) = V_l (\rho_l - \rho_m) F(q, R_l) + V_f (\rho_f - \rho_l) F(q, R_f) \quad \text{Eq. 15}$$

or
$$A(q) = (\rho_p - \rho_s) \left\{ (\phi_l - \phi_m) V_l F(q, R_l) - \phi_l V_f F(q, R_f) \right\} \quad \text{Eq. 16}$$

with ϕ_l and ϕ_m the volume fraction of polymer in the layer and out of the layer, $F(q, R_i)$ the scattering amplitude of spheres of radius R_i defined by **Eq. 9**, $V_i = 4\pi R_i^3/3$ the volume of spheres with $R_i = R_f + t$ where t is the thickness of the adsorbed polymer layer.

In order to describe the whole scattering intensity, we have to take into account the structure factor of the particles. As the position of the mass centre of the silica beads coincides with that of the polymer layer, the structure factor $S(q)$ should be the same as the previous one and $I(q)$ can be given as follows:

$$I(q) = \frac{N_f}{V} \phi |A(q)|^2 S(q) \quad \text{Eq. 17}$$

with $\phi = 1 - (N_f V_i / V)$. In this relation, we did not introduce the Ornstein-Zernike equation, taking into account the inhomogeneities of the polymer network in the solvent, as this contribution remains very weak in solvent f.

In order to get an idea about the scattering profile of core-shell particles, we have carried out simulations using **Eq. 16** by changing either the thickness of the polymer layer or its concentration.

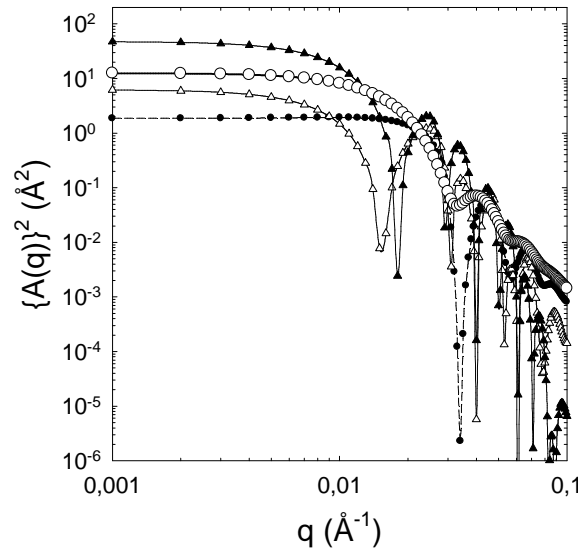


Figure 7: Variation of the square of the scattering amplitude of core-shell particles for various concentrations and thicknesses of the polymer layer: $t=0$ Å with $\phi_l=\phi_p=0.124$ (O); $t=20$ Å with $\phi_l=0.25$ and $\phi_p=0.116$ (●); $t=20$ Å and $\phi_l=0.50$ and $\phi_p=0.101$ (Δ) and $t=30$ Å and $\phi_l=0.50$ and $\phi_p=0.070$ (▲).

The plots given in **Figure 7** point out dramatic changes of scattering patterns due to:

- large variations of the scattering volume of particles (proportional to $A(0)$) as a function of the characteristics of the polymer layer and
- interferences within the shell that give rise to additional oscillations in the scattering spectrum.

Whereas the same pattern is expected from **Eq. 17** for $I(q)$ versus q , we do not observe large modifications of the scattering profiles with contrast variation of the solvent. An example is given in **Figure 8** for the same formulation SP2_PW0.14_R0.1 prepared in three different conditions: H₂O, solvent p and solvent f.

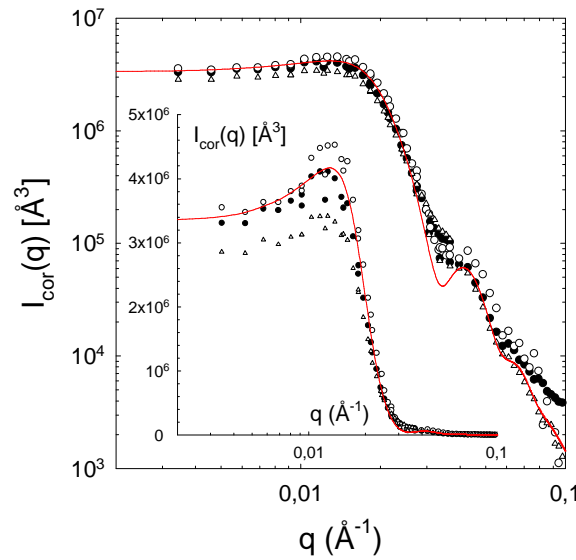


Figure 8: Double logarithmic plots of the normalized scattered intensity of PDMA/silica hydrogels (SP2_PW0.14_R0.1) prepared in various solvents: (●) p ($\phi_{D2O} = 0.21$; $\phi_{H2O} = 0.79$), (○) s ($\phi_{D2O} = 0.58$; $\phi_{H2O} = 0.42$) and (△) pure H₂O. The corresponding fit based on a polydisperse sphere model with hard sphere repulsions is indicated in solid red line. Experimental data and model fitting are also shown under a semi-log form at the bottom of the figure.

As we can see in **Figure 8**, the three plots have qualitatively the same signature and the fit initially obtained by contrast matching the polymer in solvent p (**Figure 6** down) describes pretty well the other scattering curves. This behaviour is quite general and has been observed for all the formulations of the R0.1 series which have been studied in 3 different

solvents. Obviously, although PDMA chains interact with silica surfaces they do not form a concentrated layer at the interface, or at least if there is a concentrated layer its thickness remains very low and beyond the experimental accuracy. By comparison, Shibayama and co-workers, who worked with silica particles embedded into a PNIPAm gel matrix prepared at lower concentration (around 5 to 6 vol%), could determine a polymer layer with a thickness of about 30 Å with a volume fraction of 15 to 17 % [6]. Even with PNIPAm, which is known to strongly interact with silica particles, especially at low pH as it was the case in their study, the concentration of the polymer layer is not very high and finally of the same order of our gel formulation (12 to 13 vol%).

2.3. Mechanical properties: initial elastic modulus

The aim of this chapter is to study the effect of the presence of silica nanoparticles on various properties of hydrogels. Here we focus on the mechanical reinforcement of hybrid hydrogels. Thus, the initial modulus of hybrid hydrogels, with a fixed chemical cross-linking ratio and varying the amount of silica nanoparticles, were investigated by uniaxial tensile tests to failure. The hybrid hydrogels SP_x_PW0.14_R0.1, with *x* values between 0 and 5, were tested in their preparation state at a nominal strain rate equal to 0.06 s⁻¹.

The typical stress-strain curves obtained for the different silica amounts are represented in **Figure 9**. The first observation that can be done is that the general shape of the curves is highly non-linear for hybrid hydrogels. The general “S-shaped” curve is classically attributed to the rubber elasticity [12]. The second observation made during the mechanical tests is that the deformation process remained homogeneous along the sample: no necking was observed.

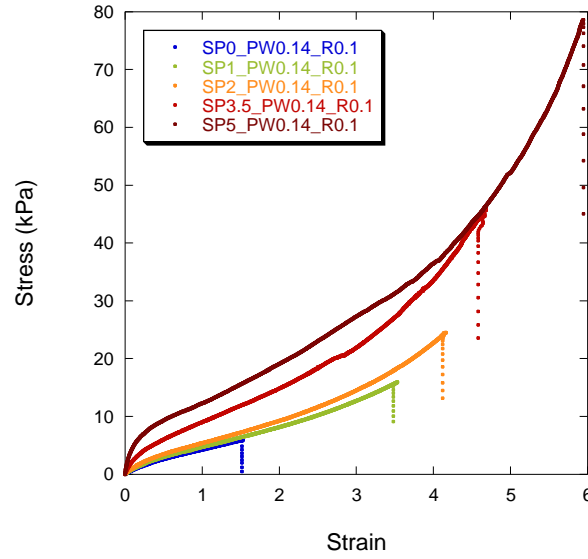


Figure 9: Effect of the silica content on tensile mechanical behaviour with a nominal strain rate of 0.06 s^{-1} for $\text{SP}_x\text{PW0.14_R0.1}$ with $x = 0$ (blue); 1 (green); 2 (orange); 3.5 (red) and 5 (brown).

From the low strain part of the curves, the Young's modulus can be determined and plotted as a function of the silica volume fraction, as reported in **Table 5**. It is obvious that an increase of the initial modulus is observed when the silica volume fraction is increased. This enhancement of the initial stiffness can be explained in terms of attractive interactions between PDMA and the silica nanoparticles. A classical comparison can be used with the model that Guth, Gold and Simha [13, 14] developed for spherical rigid fillers embedded in a rubbery matrix. This model derives from the earlier work of Einstein on viscosity of particle-filled viscous fluids and predicts the small-strain modulus enhancement due to the presence of rigid fillers. The conditions of use of this model are: an incompressible matrix and hard spherical particles without specific interaction with the matrix. This model can be used for low volume fractions of filler ($\phi \leq 0.2$) and the Young's modulus of the reinforced material E is then:

$$E = E_0 \left(1 + 2.5\phi + 14.1\phi^2 \right) \quad \text{Eq. 18}$$

with E_0 the Young's modulus of the unfilled matrix.

Sample	Silica volume fraction	Young's modulus E (kPa)
SP0_PW0.14_R0.1	0	10.5 ± 0.4
SP1_PW0.14_R0.1	0.051	13.8 ± 1.3
SP2_PW0.14_R0.1	0.097	19.8 ± 1.6
SP3.5_PW0.14_R0.1	0.158	44.5 ± 5.6
SP5_PW0.14_R0.1	0.212	102.0 ± 9.2

Table 5: Young's modulus E (kPa) of hybrid PDMA hydrogels obtained at a nominal strain rate of 0.06 s^{-1} for SP x _PW0.14_R0.1 with $x = 0; 1; 2; 3.5$ and 5 .

As presented in **Figure 10**, the model of Guth and Gold (dotted line) largely underestimates the experimental values of the initial modulus, revealing that specific interactions are taking place between the PDMA matrix and the silica nanoparticles. For high values of silica volume fraction (between 0.1 and 0.2), the reinforcement is obvious. Silica nanoparticles provide a strong anchorage of polymer chains at their surface. This strong adhesion leads to an efficient reinforcement effect of silica nanoparticles.

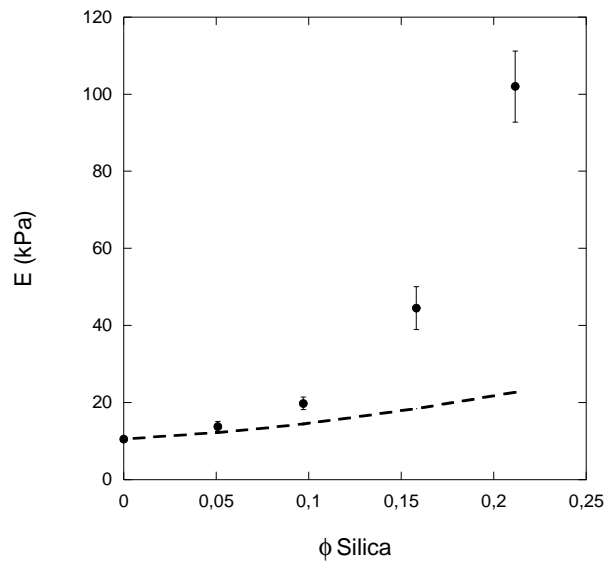


Figure 10: Comparison of experimental values of initial modulus E (dots) and theoretical values from Guth and Gold's model (dotted line), for a nominal strain rate of 0.06 s^{-1} , for samples SP x _PW0.14_R0.1 with $x = 0; 1; 2; 3.5$ and 5 .

More remarkably, focusing on the global shape of the curves and on the hydrogels' behaviour at failure, the attractive interactions between PDMA and silica nanoparticles induce not only an increase in initial stiffness but also an increase in the strain at failure: this value is 4 times higher for the SP5_PW0.14_R0.1 hybrid hydrogel than for the corresponding non-hybrid SP0_PW0.14_R0.1 hydrogel. As a comparison, the behaviour of Haraguchi's hybrid hydrogels containing clay platelets [15] is different: no increase of deformability is observed when the clay content is increased. This interesting feature of PDMA/silica hybrid hydrogels will be discussed in more details in Chapter 4.

2.4. Swelling behaviour

Swelling a polymer network is a common experiment in the world of filled elastomers. The physical consequences (on both mechanical and swelling properties) of the presence of fillers in a polymer matrix have been widely studied. Many research teams have been interested in the addition of fillers for the reinforcement of mechanical properties of elastomers. As a matter of fact, swelling experiment is an easy tool to investigate interactions between a polymer network and its fillers. In the case of attractive interactions (*i.e.* an adhesion) between the polymer matrix and the filler, the swelling ability of the system will be reduced in comparison with the swelling equilibrium of the unfilled system. In fact, strong interactions at the interface give rise to geometrical constraints which restrict the swelling of the polymer network. In contrast, the absence of interaction would slightly increase the estimated swelling equilibrium, as a consequence of the formation of cavities filled with solvent around the particles. These situations have been analytically described by Berriot *et al.* [16], using a continuous media mechanics approach. A schematic representation is given on **Figure 11**.

In the case of adhesion, the interaction and the physico-chemical parameters can induce the formation of a less swollen polymer layer at the surface of the spherical fillers. For the three situations described by Berriot, the following analytical model can be used to describe swelling at equilibrium:

$$Q_e = \frac{1}{1-\phi} \left[\left(Q_{ref}^{1/3} + \frac{3(1-Q_{ref}^{1/3})(1-v)}{2(1-2v)+(1+v) \left(\frac{0.64}{\phi(1+t/r_0)^3} \right)} \right)^3 - \phi \right] \quad \text{Eq. 19}$$

with ϕ the volume fraction of filler particles, Q_{ref} the swelling equilibrium value of the pure polymeric hydrogel (SP0_R0.1 hydrogel), v the Poisson coefficient taken equal to 0.5, r_0 the radius of neat particles and t the thickness of the adsorbed polymer layer.

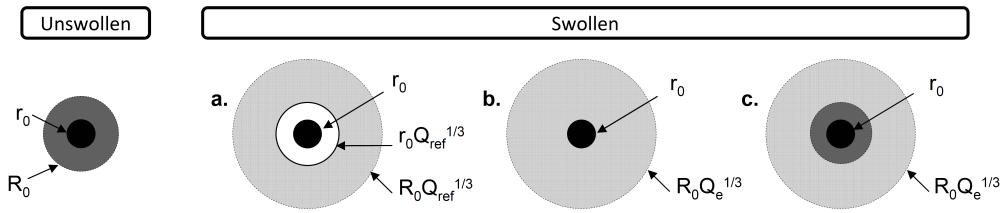


Figure 11: Schematic representation of the swelling behaviour of a polymer layer (initial radius R_0) surrounding a hard sphere (r_0) : a) swelling without adhesion between the particle and the polymer matrix, swelling with adhesion without b) or with c) an un-swollen polymer layer.

Swelling experiments carried out on cross-linked PDMA hybrid hydrogels containing silica nanoparticles Ludox-TM50 at different amounts are represented on **Figure 12**. The obvious trend of this representation is a clear decrease of the swelling equilibrium values as the silica content is increased. The presence of silica nanoparticles in the polymer network provides two opposite contributions to the swelling properties at equilibrium. As a matter of fact, the main effect is a decrease of the swelling ability of the network as a consequence of the attractive interactions between the silica nanoparticles and the PDMA network. The second effect is a slight increase of the swelling ability due to the additional osmotic pressure generated by the counter-ions present at the surface of the silica nanoparticles. For that reason, all the experiments have been carried out in an aqueous medium of LiNO_3 (0.5 mol/L) in order to screen the ionic contribution of the silica suspension. We are thus able to focus on the specific interactions between silica nanoparticles and PDMA.

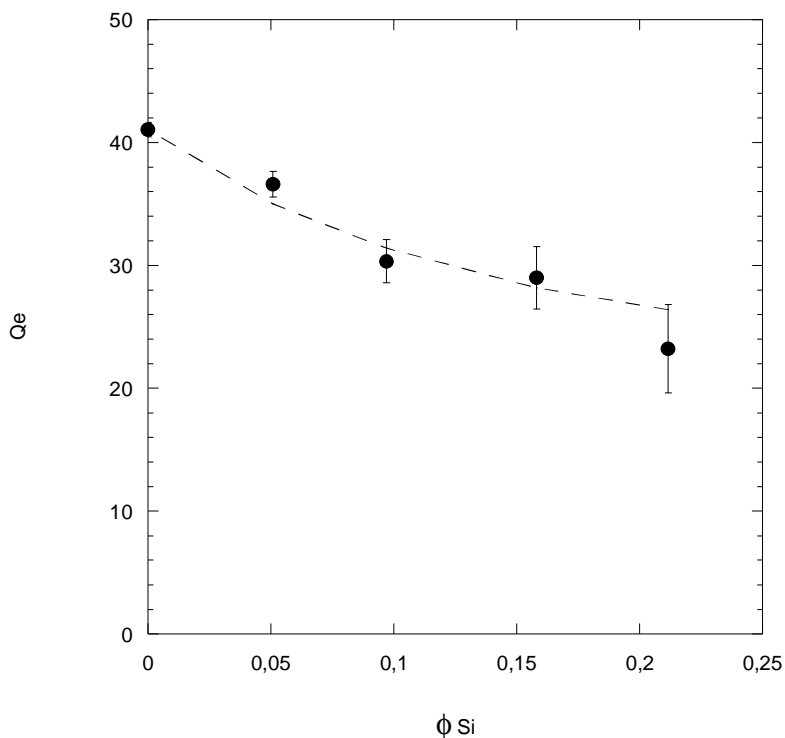


Figure 12: Variation of the swelling ratio at equilibrium Q_e in LiNO_3 0.5M, as a function of the volume fraction of silica ϕ_{Si} . Experimental data (black dots) are compared to theoretical predictions of the model developed by Berriot *et al.* with no adsorbed polymer layer (long dash).

Starting from an initial swelling value of $Q_0 = 8.5$, the hybrid hydrogels swell and reach equilibrium values between 42 (for the pure polymer matrix without silica) and 23 (for the higher silica content). The observed deswelling can be compared to the model developed by Berriot *et al.*. With our results, the best fitting curve is obtained without considering the formation of a dense polymer layer adsorbed at the interface. These results are qualitatively in good agreement with the structure and the mechanical behaviour previously described.

3. Conclusions on the structure of hybrid hydrogels

In this chapter, hybrid hydrogels have been synthesized following a very simple procedure involving the free radical copolymerization of DMA and MBA, with KPS/TEMED as redox initiators in the presence of silica nanoparticles. The formulation of hybrid hydrogels was defined as follows:

- a polymer network slightly cross-linked (0.1 mol%),
- a high and constant water/polymer weight ratio equal to 7,
- a variable silica content, up to five times the polymer weight.

From SEM and Small Angle Neutron Scattering analyses it was shown that silica nanoparticles are low polydispersed spheres forming stable suspensions stabilized by short-range repulsive interactions. When the cross-linking polymerization is carried out in the presence of nanoparticles, the silica beads remain well dispersed as long as the level of cross-linker is not too high and this is typically the case for our reference series R0.1. Concerning the ternary systems “PDMA/silica/water”, it appears that the attractive potential between organic and inorganic components is not too high in our pH conditions and prevents the hydrogel from phase separation during its preparation. The attractive potential still exists between PDMA and silica particles and we have shown that most of the particles remain embedded inside the network during swelling experiments. Moreover, these attractive interactions between PDMA and silica surfaces are responsible for the decrease of the swelling at equilibrium of hybrid hydrogels but it appears that the adsorbed layer is not very dense as it does not emerge from contrast matching experiments. A layer of comparable density with the polymer matrix will be assumed in the following with intermediate “adhesive” properties that will play a major role in the viscoelastic behaviour. From preliminary tensile tests performed on hybrid hydrogels, it was shown that this attractive potential gives rise to a dramatic reinforcement of the mechanical behaviour, with higher initial modulus and strain at failure.

Now that the structure of hybrid hydrogels has been investigated, the mechanical properties will be studied in details in Chapter 4.

References

1. Goertz, V., N. Dingemouts, and H. Nirschl, *Part. Part. Syst. Charact.*, 2009. **26**: p. 17-24.
2. Hould, N., R. Lobo, and N. Wagner, *Part. Part. Syst. Charact.*, 2010. **27**: p. 89-99.
3. Orts-Gil, G., et al., *Characterisation of silica nanoparticles prior to in vitro studies: from primary particles to agglomerates*. Journal of Nanoparticle Research, 2010.
4. Norisuye, T., et al., *Small angle neutron scattering studies on structural inhomogeneities in polymer gels: irradiation cross-linked gels vs chemically cross-linked gels*. Polymer, 2002. **43**: p. 5289-5297.
5. Hecht, A.M., F. Horkay, and E. Geissler, *Structure of polymer solutions containing fumed silica*. Phys. Rev. E, 2001. **64**(402-407).
6. Suzuki, T., et al., *Dynamics and Microstructure Analysis of N-isopropylacrylamide/Silica Hybrid Gels*. Langmuir, 2009. **25**(15): p. 8824-8832.
7. Gast, A.P. and L. Leibler, *Effect of Polymer Solution on Sterically Stabilized Suspensions*. Journal of Physical Chemistry, 1985. **89**(19).
8. Gast, A.P. and L. Leibler, *Interactions of Sterically Stabilized Particles Suspended in a Polymer Solution*. Macromolecules, 1986. **19**: p. 686-691.
9. Doherty, E.A.S., et al., *Critical factors for high performance physically adsorbed (dynamic) polymeric wall coatings for capillary electrophoresis of DNA*. Electrophoresis, 2002. **26**(16): p. 2766-2776.
10. Lin, S.C. and C.W. Whang, *Capillary electrophoretic separation of tricyclic antidepressants using a polymer-coated capillary β -cyclodextrin as an electrolyte additive*. Journal of Separation Science, 2008. **31**(22): p. 3921-3929.
11. Petit, L., et al., *Responsive hybrid self-assemblies in aqueous media*. Langmuir, 2007. **23**(1): p. 147-158.
12. Treloar, L.R.G., *The Physics of Rubber Elasticity*, ed. Oxford. 1978, New York.
13. Guth, E., *Theory of filler reinforcement*. Journal of Applied Physics, 1945. **16**: p. 20-25.
14. Guth, E. and R. Simha, *Explorations of the viscosity of suspensions and solutions 3 The viscosity of sphere suspensions (The calculation of wall influence and the exchange effect in viscosity as well as in rotating spheres)*. Kolloid-Zeitschrift, 1936. **74**(3): p. 266-275.

15. Haraguchi, K. and H.J. Li, *Mechanical properties and structure of polymer-clay nanocomposite gels with high clay content*. *Macromolecules*, 2006. **39**(5): p. 1898-1905.
16. Berriot, J., et al., *Evidence for the shift of the glass transition near the particles in silica-filled elastomers*. *Macromolecules*, 2002. **35**(26): p. 9756-9762.

Chapter 4

From covalent networks to hybrid hydrogels: time-dependence of mechanical reinforcement, dissipation and recovery

Contents

Contents	128
Introduction and general strategy	130
1. Material and methods.....	133
1.1. Synthesis of hybrid hydrogels.....	133
1.2. Rheology	133
1.3. Large strain experiments in tensile mode – rubber elasticity	134
1.3.1. Tensile tests	136
1.3.2. Cycling	136
1.3.3. Stress relaxation.....	137
1.3.4. Fracture	137
1.4. Small angle neutron scattering under deformation	138
2. Stiffening effect of nanoparticles and time-dependence	141
2.1. Rheology: small strain linear viscoelasticity	141
2.2. Tensile behaviour	144
3. Dissipation processes.....	147
3.1. Dissipation by stress relaxation.....	147
3.1.1. Stress relaxation behaviour related to the silica content	148
3.1.2. Toward a characteristic time-identification.....	150
3.2. Dissipation upon loading-unloading cycles.....	151
3.3. Recovery processes	155
3.3.1. Strain recovery and effect on successive moduli.....	155
3.3.2. Cycling at large strains	159
4. Damage and fracture	161
4.1. Failure properties: effects of silica content and strain rate.....	161
4.2. Fracture properties	165
5. Small angle neutron scattering under deformation	170
5.1. Strain visualisation.....	171

5.2. Reversibility	177
6. Conclusions on the mechanical reinforcement of hybrid hydrogels: picture and simple model.....	180
References	187

Introduction and general strategy

As described in Chapter 3, the hybrid hydrogels based on PDMA networks containing large amounts of water and silica nanoparticles that we developed here are complex materials. The idealized architecture of this series of gels is schematically pictured in **Figure 1**.

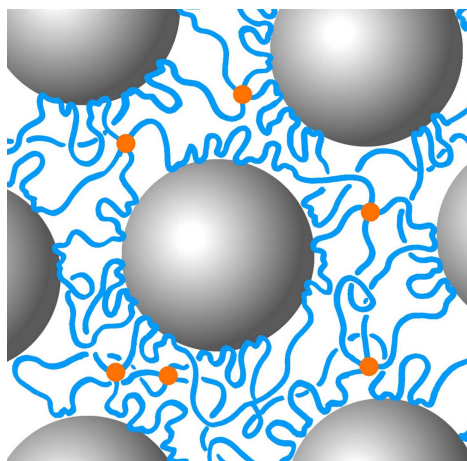


Figure 1: Schematic representation of hybrid hydrogels combining covalent cross-links (in orange dots ●) and physical interactions sketched by polymer chains (in light blue lines) adsorbed at the surface of silica nanoparticles (the grey spheres). Note that the mean diameter of the silica particles is about 30 nm.

The strategy consists of coupling a covalent network with reversible interactions using silica nanoparticles as physical cross-linker. Indeed, based on pioneering studies in semi-dilute solutions, macromolecular assemblies demonstrated strong adsorption of polymer chains (poly(*N*-alkylacrylamide) or polyethers) onto the surface of silica nanoparticles [1]. Emphasizing on the strong particle-chain interaction by varying the silica volume fraction, Chapter 3 reported on the very promising mechanical properties: initial modulus, together with stretchability until fracture, were seen to be simultaneously enhanced by increasing the silica nanoparticle volume fraction. Yet several questions remained: is the PDMA/silica association reversible? What are the characteristic times involved?

The objective of the present chapter is to investigate the mechanical response of nano-hybrid gels, focusing on two main aspects: strain rate dependent dissipation and recovery. Evidently, adsorption can provide an efficient anchorage of polymer chains onto the silica particles, but conceptually this process is reversible [2, 3]. Thus, as previously described, the silica nanoparticles could act as multi-functional cross-linkers, but potentially the polymer/silica associations could play the role of exchangeable sacrificial bonds upon stretching. That way, adsorption could promote “recoverable” dissipative processes, depending on the probed time-scale relative to the particle/polymer association characteristic time.

This chapter will emphasize on the particle-chain interaction and particularly on its life-time. The silica nanoparticles content in the gel will be varied to tune the gel architecture: from pure organic network to hybrid gel.

The main characteristics of these hybrid hydrogels are:

- Monodisperse spherical silica nanoparticles are homogeneously distributed in the polymer gel matrix and act as physical cross-linkers by strongly adsorbing polymer chains to their surface;
- A small amount of chemical cross-linker (0.1 mol%) stabilizes the network dimensionality and controls the “shape-memory” properties. This small value is a compromise to overcome the self cross-linking reaction that takes place during DMA polymerization (leading to a more controlled cross-linking process) and to avoid a dramatic reduction of network extensibility;
- The gel matrix hydration is maintained at 87.8 wt%, to specifically characterize the synergistic impact of silica nanoparticles on the mechanical properties of hybrid gels. Gels will be tested at their preparation conditions.

After a description of the characterization methods (the classical ones and the specific ones that we developed for the study of hydrogels), the rheological properties, within the viscoelastic regime, and the large strain mechanical behaviour of hybrid hydrogels will be described. A particular attention will be given to the time-dependence of the reinforcement

induced by the silica nanoparticles. The discussion will be focused on the determination of a characteristic time of the silica-PDMA interaction. For that purpose, stress relaxation and loading-unloading cycles will be studied. A special focus will be given to recovery processes. The mechanical study will be completed by two-dimensional small angle neutron scattering experiments. Damage and fracture properties on notched specimens will then be studied. Finally, this chapter will end with a brief modelling part taking into account the structure and the viscoelastic nature of the system.

1. Material and methods

1.1. Synthesis of hybrid hydrogels

The synthesis and structure of hybrid hydrogels have been described in details in Chapter 3. Here the materials studied are hybrid hydrogels based on *N,N*-dimethylacrylamide monomer, keeping the same hydrogels matrix, as described in Chapter 2. The gels are studied in their preparation state (at $Q_0 = 8.5$). The molar ratio of cross-linker (MBA) to monomer studied in this part is equal to 0.1 mol%. The nomenclature used is still:

"SPx_PW0.14_R0.1".

As mentioned in Chapter 2, the geometry of the moulds that are used during the synthesis depends on the characterization techniques. In the case of mechanical tests, home-made moulds have been designed and consist of two covered glass plates spaced by a stainless steel spacer of 2 mm thick and a film of tri-cellulose acetate to make the demoulding easier. The hydrogels are then cut with a punch and their final dimensions are $L_0 = 50$ mm, $w_0 = 5$ mm and $t_0 = 2$ mm.

1.2. Rheology

The visco-elastic properties of hybrid hydrogels have been studied on a strain-controlled rheometer (Rheometrics RFSII, TA Instruments). A sinusoidal strain (γ^*) of very low amplitude γ_0 is applied and the response of the material in producing a resulting sinusoidal stress (σ^*) of amplitude σ_0 is recorded. The phase difference between the stress and the strain δ (from 0 to $\pi/2$) is characteristic of the dissipative properties of the constrained material: a strictly elastic material will have no phase difference whereas a purely viscous material will have a phase difference equal to $\pi/2$.

For visco-elastic materials and for shear strains, Hooke's law can be written as:

$$\sigma^* = G^* \gamma^* \quad \text{Eq. 1}$$

where G^* is the complex shear storage modulus which is defined as: $G^* = G' + iG''$.

In this last equation, the first term G' is the elastic component of the modulus; it characterizes the elasticity of the material:

$$G' = \frac{\sigma_0}{\gamma_0} \cos \delta \quad \text{Eq. 2}$$

The second term G'' is the loss component of the modulus:

$$G'' = \frac{\sigma_0}{\gamma_0} \sin \delta \quad \text{Eq. 3}$$

We used a rotational parallel-plate geometry with a diameter of 25 mm, as schematically represented on **Figure 2**. The thickness of the plates did not exceed 2 mm. Discs of diameter 24 mm were cut out of the hydrogel plate with a punch. Specific alumina plates were designed and machined. Experimentally a special attention was given to the absence of air between the surface of the gel and the plates. A stabilized normal force of 0.5 N (corresponding to a normal stress around 1 kPa) was applied. Gels were deformed at a distortion of $\gamma = 0.03$ within the linear visco-elastic regime as determined using a frequency of 1 Hz. Then, the samples were immersed in the paraffin oil to avoid drying. We studied the hybrid hydrogels with a frequency sweep between 0.1 rad.s^{-1} and 100 rad.s^{-1} (*i.e.* 0.016 Hz and 16 Hz).

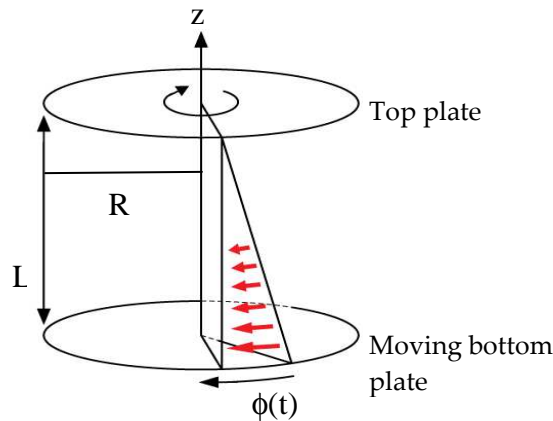


Figure 2: Schematic representation of the parallel-plate geometry

1.3. Large strain experiments in tensile mode – rubber elasticity

Tensile mode was used to investigate the mechanical properties of hydrogels. Tests were performed on a standard tensile Instron machine, model 5565, using a 10 N load cell and a

video extensometer, model SVE, which can precisely follow the local displacement of markers and a BlueHill software. Strain can be measured using both the video extensometer and the displacement of the crosshead. The relative uncertainties for the load cell and the video extensometer are respectively 0.16% in the range from 0 to 0.1 N and 0.11% at the full scale of 120 mm.

All the gel samples were placed in home-made screw side action grips and marked by two white dots. The video extensometer can measure the initial length between the white marks (L_{e0}) and then follow it during the test. Force (F) and displacement (L) are recorded. The sample geometry has been chose in order to reduce the volume of material. The sample size has been kept constant with a rectangular shape: gauge length $L_0 = 25$ mm, width $w = 5$ mm and thickness of 2 mm.

Nominal stress σ_N was defined as the tensile force per unit of non deformed area and true stress σ_T was calculated assuming iso-volume deformation, thanks to the following relation:

$$\sigma_T = \sigma_N \cdot \lambda \quad \text{Eq. 4}$$

$$\lambda = \frac{L}{L_0} \quad \text{Eq. 5}$$

with λ the strain ratio.

The classical rubberlike elasticity model gives a non-linear stress – elongation response. Experimental deviations from the model are often read in Mooney plots, using the Mooney stress defined as:

$$\sigma_{Mooney} = \frac{\sigma_N}{\left(\lambda - \frac{1}{\lambda^2}\right)} \quad \text{Eq. 6}$$

This reduced stress normalizes the measured stress by the predicted rubberlike behaviour in uniaxial extension and is usually plotted as a function of $1/\lambda$. Softening and stress hardening are therefore well-identified.

For long-term experiments (*i.e.* elapsed times greater than hundreds of seconds), the main experimental problem that arose was the possible water exchange during the test. As a matter of fact, when exposed to ambient air, the hydrogels rapidly dry and a long-time experiment cannot make sense without an appropriate set-up to prevent drying. For that purpose, the long tests were conducted in a home-made set-up consisting of a paraffin oil bath surrounding the sample, as pictured in **Figure 3**. The grip immersion into the paraffin oil induces a non negligible contribution to the measured force. Indeed, to correct the buoyancy, blank tests were systematically carried out for each experimental condition.



Figure 3: Picture of the experimental set-up designed for long-time mechanical tests.

1.3.1. Tensile tests

For tensile tests, the nominal strain rate was varied from $3 \cdot 10^{-4} \text{ s}^{-1}$ to 0.6 s^{-1} .

1.3.2. Cycling

Loading-unloading cycles were performed in order to investigate the self-recovery process of the gels, using the following strain rates: $3 \cdot 10^{-4} \text{ s}^{-1}$, 0.06 s^{-1} and 0.6 s^{-1} . Cycles were applied from 0 to a maximal strain ε_0 and then the sample was unloaded. For each measurement, three cycles were done.

1.3.3. Stress relaxation

Stress relaxation experiments consisted of maintaining a fixed strain level and recording the mechanical response of the material in terms of stress. For SPx_PW0.14_R0.1 samples, the strain level was varied between 0.02 and 2.

Concerning the strain rate used for loading the samples, we decided to fix the duration of the loading step equal to 2 seconds. The loading strain rate was then calculated depending on the initial length of the sample.

1.3.4. Fracture

Fracture tests were performed using the classical single edge notch geometry, which is known as Single Edge Notch Tensile (SENT), using the Instron machine. For that purpose, a cut was made in the centre of the rectangular samples using a blade. An example of hybrid hydrogel specimen is represented in **Figure 4**.

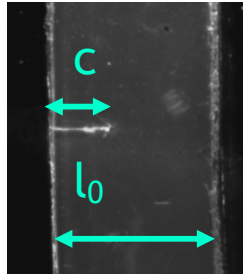


Figure 4: Optical microscopy picture of a single edge notch sample. The typical dimensions used were the one mentioned at the beginning of this chapter.

Each notch was measured by optical microscopy in order to determine its exact length (c), approximately 1 mm. The same procedure as the one used for tensile tests was performed: the two strain rates were fixed equal to 0.06 s^{-1} and 0.6 s^{-1} , the force and the displacement data were recorded.

1.4. Small angle neutron scattering under deformation

Small angle neutron scattering experiments under deformation have been carried out at Laboratoire Léon Brillouin (CEA, Saclay) with a small angle neutron spectrometer (PAXY) dedicated to anisotropic measurements. As explained in Chapter 3, we used the contrast matching procedure with suitable ratios $\text{H}_2\text{O}/\text{D}_2\text{O}$ to selectively adjust the neutron contrast of the solvent to one of the component, either PDMA or silica:

- $\text{H}_2\text{O}/\text{D}_2\text{O} = 0.79/0.21$, for matching the PDMA network,
- $\text{H}_2\text{O}/\text{D}_2\text{O} = 0.42/0.58$, for matching the silica nanoparticles.

The hybrid hydrogels were specially prepared, according to the procedure previously described in Chapter 3, in two different aqueous environments: in the solvent matching the PDMA network and in the solvent matching the silica nanoparticles. For hybrid hydrogels with high amounts of D_2O , the Ludox-TM50 suspension was initially dialysed during two weeks in control D_2O environment in order to get a stable and concentrated dispersion of silica in D_2O (with silica concentration around 40 w%), with:

- $\text{pH} = 9$, or $\text{pH}^* = 8.6$, with pH^* the pH value measured in D_2O ,
- 4.9 mS/cm for the conductivity.

As described in Chapter 2, two configurations were used on the spectrometer, keeping constant the sample-to-detector distance $D = 4.7$ m and changing the wavelength of the incident neutron beam $\lambda = 12$ and 4.5 \AA . The resulting values of the scattering vector modulus are ranging between 0.0034 and 0.098 \AA^{-1} .

Concerning the experimental setup, we developed a special cell, in collaboration with the Laboratoire Léon Brillouin. We had to design the setup in order to use it in the automatic sample changer of the PAXY spectrometer, with specific materials. The main experimental characteristics that we had to take into account were:

- a precise fixation system for the sample that prevents sliding;
- a fine control of the elongation of the sample, with micrometric screws;
- a closed antechamber with a fine control of the environment, such as temperature, solvent or humidity;

- two windows tightly closed, transparent for neutrons, with good hermetic properties and with a sufficient diameter for the neutrons beam (about 7.3 mm).

With the previous characteristics, we developed the following device, presented in **Figure 5**.

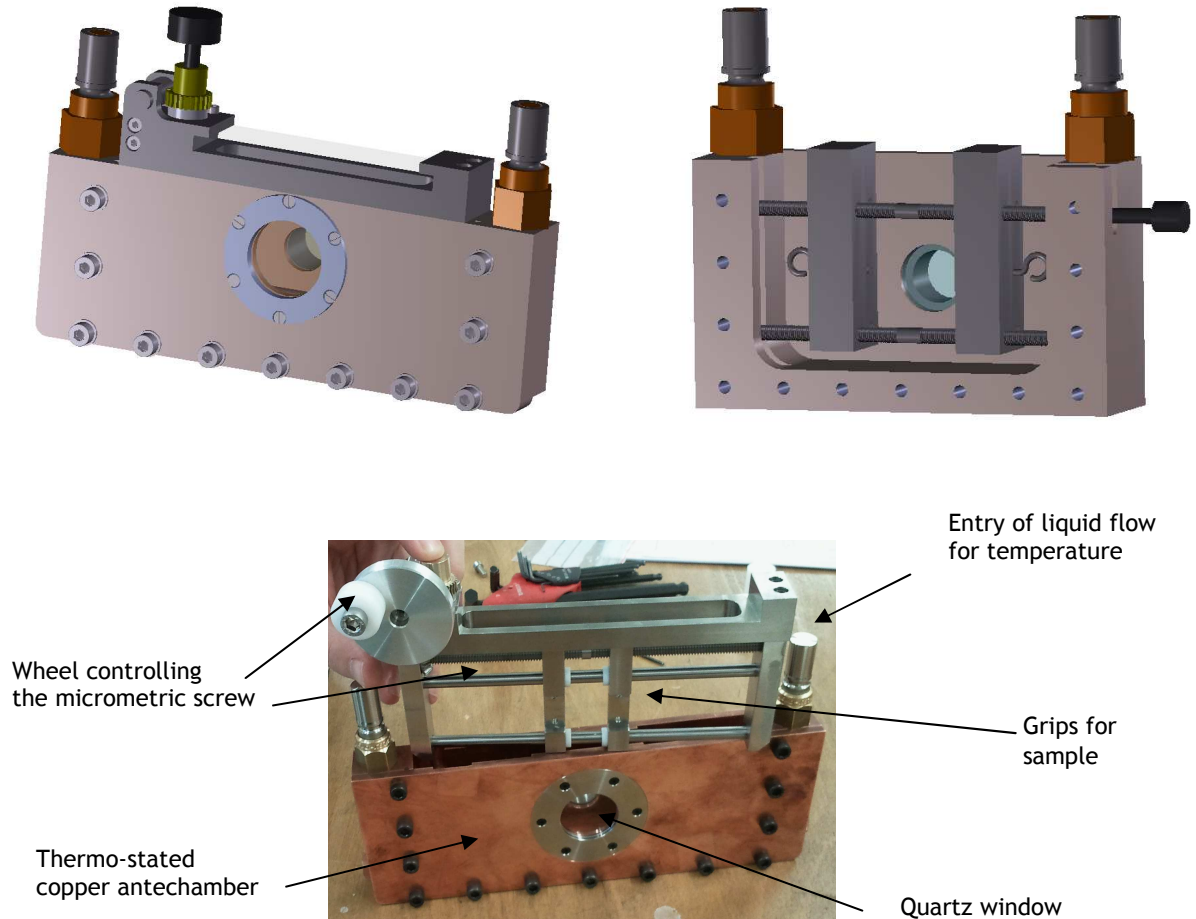


Figure 5: Up: Schematic representations of the 2D SANS device, with top left: the entire device, and top right: an internal view. Down: picture of the experimental device with legends.

In 2D SANS experiments, the incident neutron flux, recorded on a two dimensional detector constituted of 15500 cells of 25 mm², is directly converted into an image with a colour guide. After treatment (as described in Chapter 2 and 3) the collected data can be qualitatively analyzed in terms of diffusion pattern. From the anisotropic properties of the samples, the collected data coming from all the detection cells cannot be summed over all the surface of

the detector. For that reason, the acquisition times must be longer than the usual ones for isotropic SANS measurements (about four times longer). In the case of our hybrid hydrogels, containing large amounts of water, a long stay in air induces drying, changing the state of the PDMA chains, even more when the samples are stretched. In order to prevent hybrid hydrogels from drying during the SANS measurements, we chose to fill the sample antechamber with a fluorinated oil and to immerse the samples in it: the octadecafluorodecahydronaphthalene (also called perfluorodecalin), represented in **Figure 6**. We verified that the mechanical properties of our hybrid hydrogels were not changed by possible interactions with this fluorinated oil and that the hydrogels remained stable in such immersed conditions. Furthermore, the scattered intensity of the perfluorodecalin has been measured, in order to make the corrections to the scattered intensities of samples studied in the oil environment.

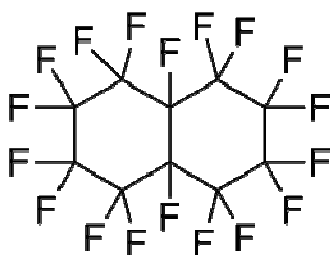


Figure 6: Representation of the octadecafluorodecahydronaphthalene.

2. Stiffening effect of nanoparticles and time-dependence

In Chapter 3, the mechanical properties of hybrid hydrogels based on PDMA and silica nanoparticles have been briefly exposed with the study of the tensile behaviour at a constant strain rate of 0.06 s^{-1} . In this chapter a special interest will be given to the detailed study of the mechanical properties of our hybrid hydrogels, with the aim to probe time-scale effects on the PDMA/silica associations. Let us start by a shear study of hybrid hydrogels in order to explore the viscoelastic signature at small deformations and tensile behaviour.

2.1. Rheology: small strain linear viscoelasticity

Linear viscoelastic analysis has been extensively used to investigate physical or chemical sol/gel transitions in soft materials, but this technique is less frequently used for characterizing stiff gels above their gel point. Indeed, large discrepancies between moduli obtained from tensile measurements and those obtained from shear experiments have already been observed [4, 5]. In our case, the viscoelastic properties of the hybrid PDMA-silica hydrogels have been studied in a plate-plate rheometer, within the linear viscoelastic regime (see **Annex 1**). The mechanical spectra are given in **Figure 7**. G' and G'' show a power-law frequency dependence, respectively $G' \sim \omega^n$ and $G'' \sim \omega^m$.

The frequency-dependence of the storage and the loss moduli was investigated from 0.1 to 100 rad.s^{-1} . For all our hybrid hydrogels, G' was greater than G'' over the entire frequency range, which is consistent with the solid-like elastic nature of the gel. The storage modulus of the unfilled hydrogel, SP0 is independent of the frequency as expected for a purely elastic system. As shown in **Figure 7**, the introduction of silica nanoparticles leads not only to an increase of G' , but also to an enhancement of the frequency dependence. Similarly, the loss modulus G'' , mainly negligible for SP0 (below 100 Pa at 100 rad.s^{-1}), strongly increases for hybrid systems and reaches several thousands Pascals for similar frequencies with SP2 and SP5 filled hydrogels. The dynamic moduli follow a power-law frequency response, as those reported in physical gels [6] [7, 8] or hydrophobically modified gels [9-12]. The presence of the nanoparticles in the network tunes the rheological signature from a chemical gel

response (SP0_PW0.14_R0.1 gel) to that of a physical gel (SP2, SP3.5 and SP5_PW0.14_R0.1 gels). Experimental results show that storage and loss moduli scale as $G' \sim \omega^n$ and $G'' \sim \omega^m$. The obtained loss tangents are relatively constant over the three frequency decades and are related to the silica concentration: typically from 0.106 (for SP2) and up to 0.211 (for SP5). The dissipative component was seen to monotonically increase with the silica content, as reported elsewhere for polyacrylamide-clay nanocomposite gels [13, 14].

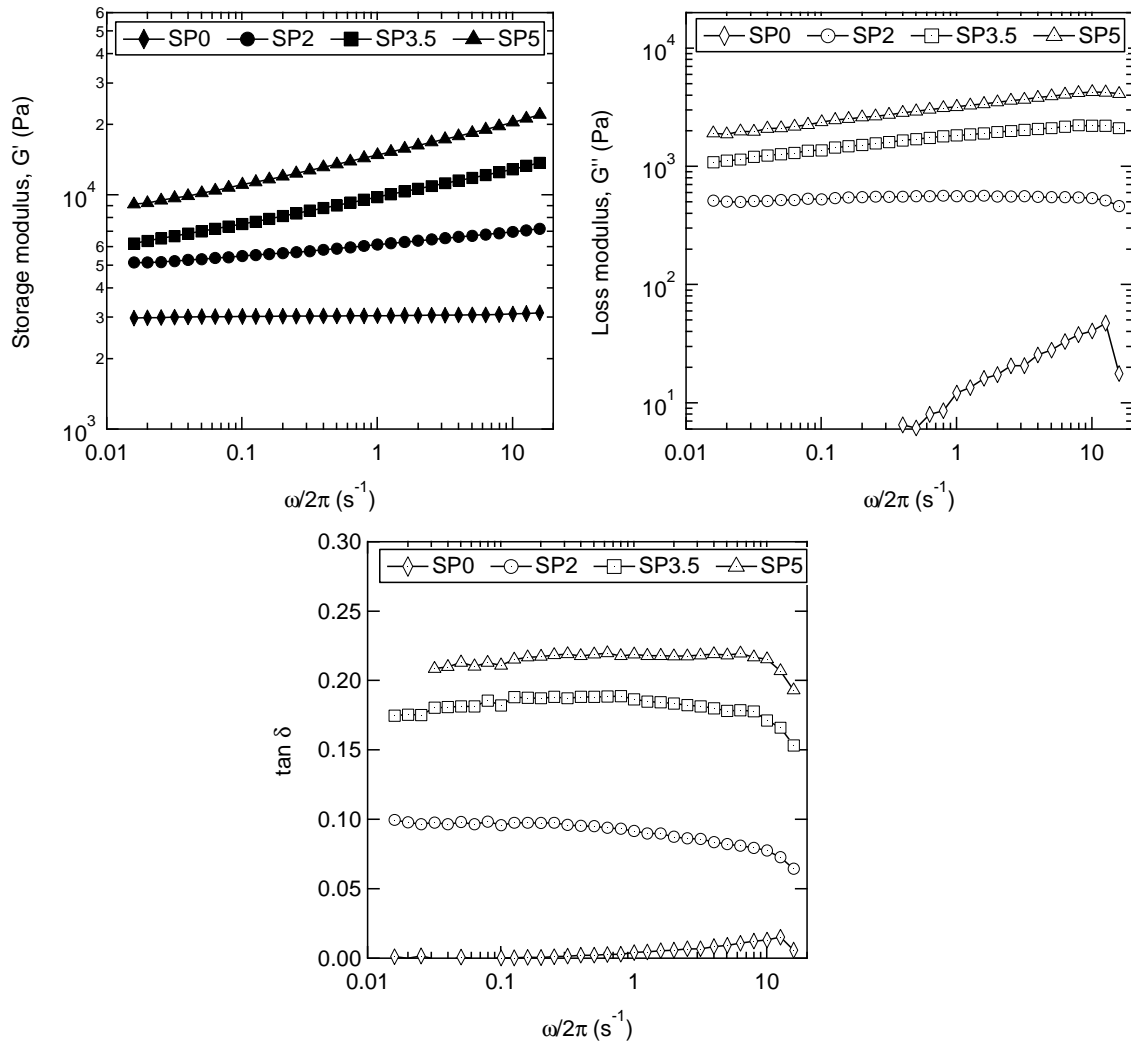


Figure 7: Storage G' modulus (filled symbols), loss modulus G'' (open symbols) and phase angle (bottom) obtained from rheological measurements ($\gamma = 0.03$, at 25°C) for hybrid hydrogels SP x _PW0.14_R0.1, with $x = 0, 2, 3.5$ and 5 .

	SP0	SP2	SP3.5	SP5
n ($G' \sim \omega^n$)	0.005 ± 0.002	0.051 ± 0.005	0.116 ± 0.005	0.132 ± 0.003
m ($G'' \sim \omega^m$)	-	0.008 ± 0.002	0.101 ± 0.002	0.124 ± 0.008
$E^* = 3(G'^2 + G''^2)^{1/2}$	9 kPa	16 kPa	22 kPa	32 kPa
E (tensile tests)	10.5 ± 0.4 kPa	19.8 ± 1.6 kPa	44.5 ± 5.6 kPa	102 ± 9.2 kPa

Table 1: Experimental values of power laws of storage and loss moduli at 0.06 s^{-1} , corresponding value of modulus, compared to experimental values of initial modulus obtain in tensile tests at 0.06 s^{-1} , for SPx_PW0.14_R0.1, with x = 0; 2; 3.5 and 5.

Contrary to specific associating systems, like telechelic polymers or more recently in hydrophobically modified gels [11], the dynamic measurements did not give us the possibility to reveal a well defined characteristic time, corresponding to a maximum in the loss modulus. The dissipative component was seen to monotonically increase with the silica content, traducing rather broad spectra of relaxation times, as reported elsewhere for polyacrylamide-clay nanocomposite gels [13, 14]. This absence of maximum corresponds to a large distribution of characteristic times related to the large population of PDMA sections more or less adsorbed onto the silica surface. As a matter of fact, between two cross-linking points, the PDMA chain can be adsorbed onto the silica surface by one or more sites, giving rise to a complex and wide range of characteristic times.

The quantitative agreement between tensile and storage moduli was observed for SP0 and SP2 hydrogels, as reported in **Table 1**. Higher discrepancies were noticed for the stiffest gels, SP3.5 and SP5_PW0.14_R0.1, as ever reported [15]. Surface effects are presumably at the origin of this difference.

Thanks to shear measurements, we confirmed the solid-like elastic nature of the gels and we probed the effect of silica nanoparticles on the mechanical properties. We will now go further on the large strain behaviour with detailed tensile tests.

2.2. Tensile behaviour

In Chapter 3, we studied the impact of silica nanoparticles on properties of hydrogels. Particularly, we focused on the reinforcement effect for a unique nominal strain rate equal to 0.06 s^{-1} . Here the typical tensile stress-strain responses are studied investigating both time-dependence and silica content. True stress-strain curves are given in **Figure 8**, varying the strain rate by a decade.

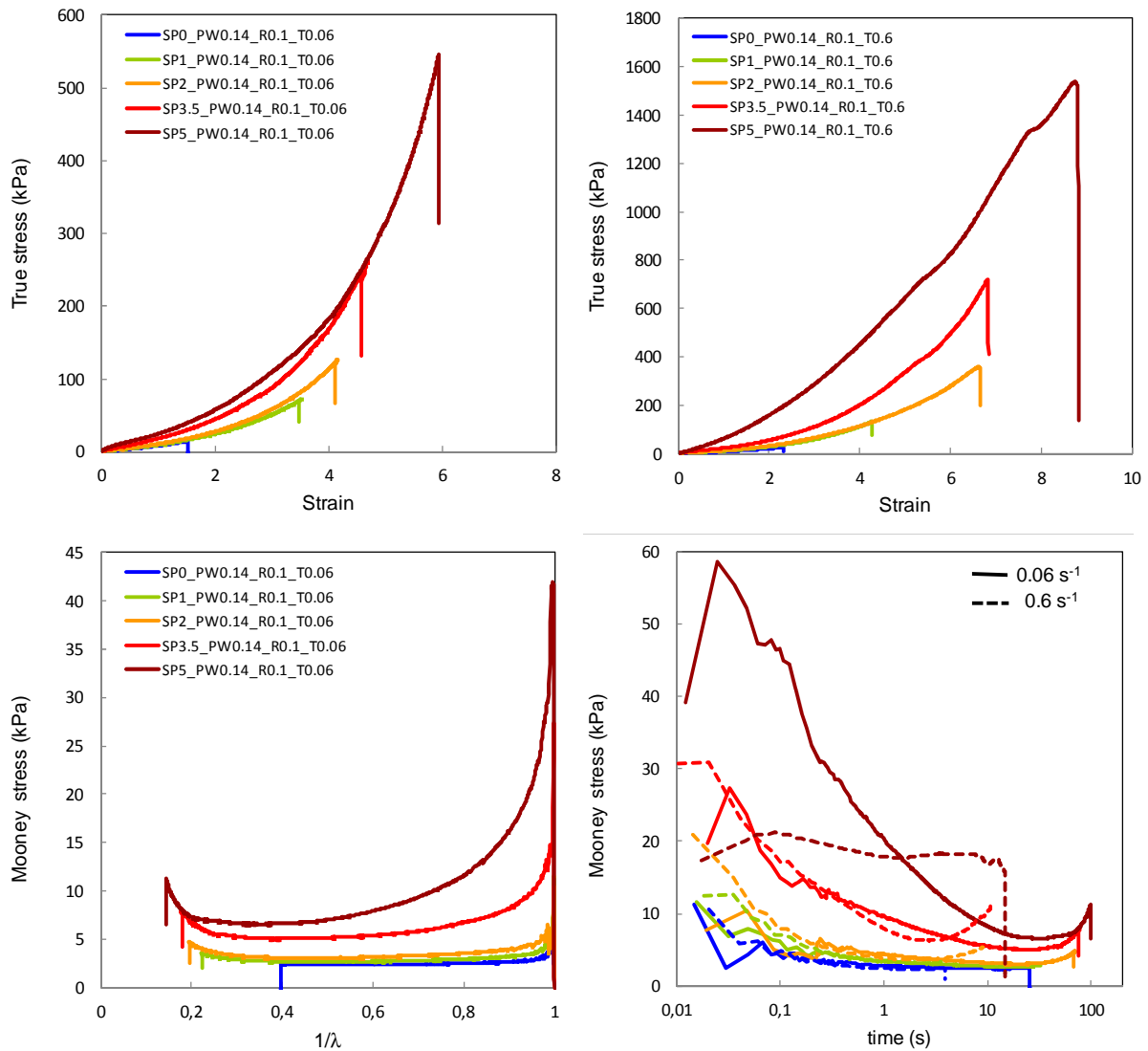


Figure 8: Effect of the silica content on tensile mechanical behaviour for SPx_PW0.14_R0.1, with $x = 0$ (blue); 1 (green); 2 (orange); 3.5 (red) and 5 (brown). Up: true stress-strain curves at two nominal strain rates: 0.06 s^{-1} (left) and 0.6 s^{-1} (right). Down left: corresponding Mooney plot for the nominal strain rate of 0.06 s^{-1} . Down right: Mooney plots versus time for both strain rates 0.06 s^{-1} (solid line) and 0.6 s^{-1} (dashed line).

During the mechanical tests, the deformation process remained homogeneous along the sample: no necking was observed. For both strain rate conditions, the stress-strain behaviour presented a highly non-linear general shape, classically attributed to the rubbery behaviour. Nevertheless, as shown in **Figure 8** down left, the curves show some deviations from the classical model of rubber elasticity by a large strain softening at intermediate strains and strain hardening at large strains. In this case, the softening effect is related to silica/PDMA associations, since no softening is observed for SP0_PW0.14_R0.1. The Mooney stress plotted as a function of time (**Figure 8** down right) shows that the observed softening is mostly induced by stress relaxation upon loading. Finite extensibility of the polymer chains is observed at high strain levels by an upturn of the Mooney stress. The silica nanoparticles concentration does not clearly impact the strain position of this upturn. However, interestingly the SP5_PW0.14_R0.1 presents a unique behaviour compared to other formulations: at high strain rate (0.6 s^{-1}) the softening seems to be fully screened.

Sample	Silica volume fraction	$E @ 0.06 \text{ s}^{-1}$ (kPa)	$E @ 0.6 \text{ s}^{-1}$ (kPa)	$E @ 3.10^{-4} \text{ s}^{-1}$ (kPa)
SP0_PW0.14_R0.1	0	10.5 ± 0.4	11.2 ± 0.3	--
SP1_PW0.14_R0.1	0.051	13.8 ± 1.3	20.2 ± 0.1	--
SP2_PW0.14_R0.1	0.097	19.8 ± 1.6	28.1 ± 0.6	--
SP3.5_PW0.14_R0.1	0.158	44.5 ± 5.6	55.0 ± 4.0	--
SP5_PW0.14_R0.1	0.212	102.0 ± 9.2	170.0 ± 9.3	25 ± 2.7

Table 2: Strain rate effect on reinforcement: initial moduli E (kPa) of hybrid PDMA hydrogels obtained at different strain rates for SP x _PW0.14_R0.1, with $x = 0; 1; 2; 3.5$ and 5 .

As reported in **Figure 9**, for a nominal strain rate of 0.06 s^{-1} , the model of Guth and Gold (in dotted line) is far below the experimental values of the initial modulus, revealing the strong interactions taking place between the PDMA matrix and the silica nanoparticles. For high volume fractions of silica (between 0.1 and 0.2), the reinforcement is obvious. Increasing the strain rate by a decade, the hybrid hydrogels behave even more stiffly. This result reveals an important viscoelastic contribution which is correlated to the content of nano-filler, since SP0

was unaffected by the change of strain rate compared to the filled systems. But more interestingly, at low strain rate (*i.e.* 3.10^{-4} s^{-1}) the initial modulus of the highly filled hybrid hydrogel (SP5_PW0.14_R0.1) is in good agreement with Guth and Gold's model. The obtained Young's modulus is equal to 25 kPa and the strong reinforcement effect of nanoparticles, observed for higher time-scales, vanishes at such low strain rate.

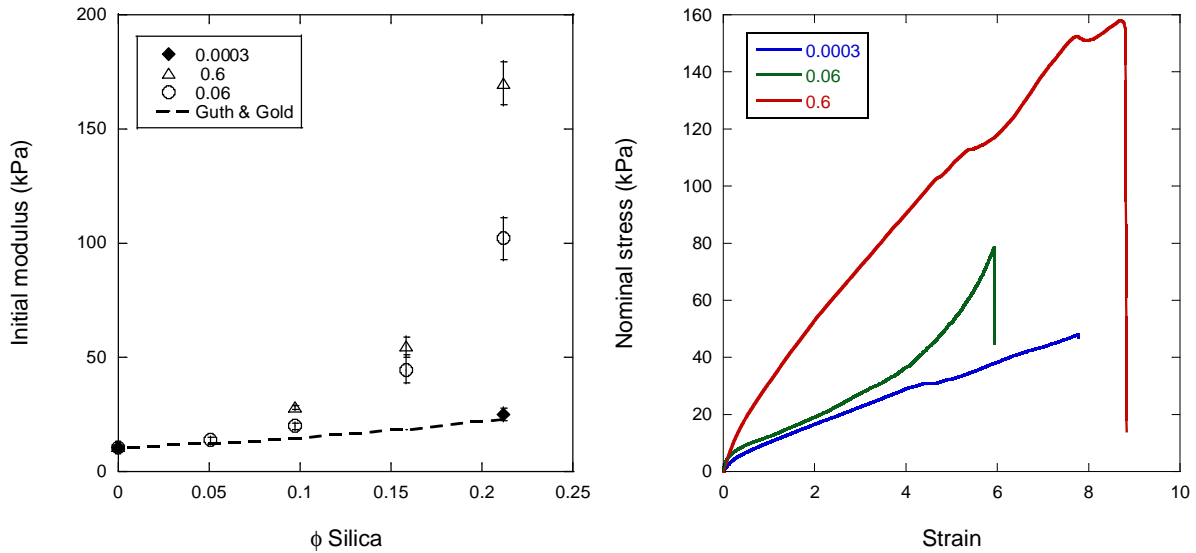


Figure 9: Left: comparison of experimental values of initial modulus E for a nominal strain rate of 0.06 s^{-1} (open circles), 0.6 s^{-1} (open triangles) and 3.10^{-4} s^{-1} (filled symbols). Theoretical values from Guth and Gold's model (dotted line) are given by the following expression $E = E_0 (1 + 2.5\phi + 14.1\phi^2)$ with E_0 the Young's modulus of the unfilled matrix. Right: comparison of tensile behaviour for SP5_PW0.14_R0.1 at the three strain rates: 3.10^{-4} s^{-1} (blue), 0.06 s^{-1} (green) and 0.6 s^{-1} (red).

From the global shape of the curves and the hydrogels behaviour at failure, the interactions between PDMA and silica nanoparticles induce not only an increase in initial stiffness but also an increase in the strain at failure. Thus at 0.06 s^{-1} , this value is around 4 times higher for the SP5_PW0.14_R0.1 hybrid hydrogel than for the corresponding organic matrix SP0_PW0.14_R0.1 hydrogel. This is a remarkable feature within the fields of nano-composite engineering as well as nanocomposite gels developed by Haraguchi *et al.* [16] for which no increase of deformability is observed when the clay content is increased. Damage mechanisms and fracture properties will be discussed later in this chapter.

3. Dissipation processes

The dynamics of PDMA segments association at the surface of silica particles is the key aspect of the mechanical reinforcement induced by silica that can also be studied in terms of energy dissipation and recovery. For that purpose, stress relaxation and strain-controlled tensile loading-unloading cycles were used and are described in the following part.

3.1. Dissipation by stress relaxation

As described by Gent [17], stress relaxation is a common tool to investigate the mechanical behaviour of polymer materials and especially to observe how the materials relieve stress under constant strains. In rubber science, relaxation mechanisms are generally classified in two categories. First one can consider the physical relaxation, which is associated to reorientation of the stretched network. These reorientations can be: rearrangements of entanglements of chains, breaking of physical bonds, such as hydrogen bonds, between chains, between particles or between chains and particles. Physical relaxation is known to decrease linearly with the logarithm of time and to strongly depend on the temperature (indeed on the gap between the experimental temperature and the glass transition temperature T_g) but also on the degree of cross-linking. The presence of fillers is also a key parameter, at the origin of higher physical relaxation rates, but the mode of deformation should not impact the relaxation rates. The second category of relaxation mechanisms is the chemical relaxation, consisting of the breaking of chemical bonds (in the polymer chains or in the cross-link points). The chemical relaxation strongly depends on the temperature, as oxidative reactions are activated at higher temperatures. For that reason, the size of the sample is a key factor, and more particularly its surface.

Concerning the relaxation mechanisms in hydrogels, the literature is quite poor. Only few groups have studied the long-time behaviour of hydrogels [18-21]. Stress relaxation has been principally investigated on covalently cross-linked gels immersed in water [19-21]. The experiment consisted in compressing suddenly a piece of gel between two rigid plates and keeping fixed the displacement subsequently while the force was recorded as a function of

time. Results in these purely elastic gels showed an instantly rise of the force and then a relaxation process relied to water migration outside the gel, until gel approaches a new state of equilibrium. The recorded relaxation is in that case the result of the compression-driven deswelling (or stretching-driven swelling). The concurrent deformation process and migration of the solvent is known as poroelasticity. This feature is intrinsically due to the nature of polymer gels that behave as semi-open systems (*i.e.* exchange of solvent with surroundings).

In order to forestall such effects, we developed an experimental setup preventing solvent exchanges upon stretching that could be induced by a long stay in a non-controlled environment. As described in the first part of this chapter, the relaxation tests in tension were conducted in a home-made setup consisting of a paraffin oil bath surrounding the sample, presented in **Figure 3**.

3.1.1. Stress relaxation behaviour related to the silica content

Stress relaxation mechanisms can be compared within our series of hybrid hydrogels, varying the silica concentration in the gels. The results obtained for a series of SP_x_PW0.14_R0.1 hydrogels (with *x* equal to 0, 2 and 5) are presented in **Figure 10** for an initial strain of 100%, with a constant loading-time equal to 2 seconds. First, we can notice that the presence of silica nanoparticles is decisive for the relaxation mechanism: no relaxation is observed for the pure PDMA cross-linked hydrogel. The SP0_PW0.14_R0.1 response is purely elastic. The amplitude of stress relaxation strongly depends on the silica concentration. This observation can be attributed to the PDMA/silica interaction and more particularly to possible rearrangement processes occurring at the particle interface (desorption-adsorption processes). When PDMA hydrogels contain silica nanoparticles, stress relaxation becomes possible, by release of strained polymer chains at the particle surface. Thus for SP5, the amplitude of stress relaxation is very high, since stress relaxed from 20 kPa (the maximal stress, at 2 seconds) to 5 kPa (for elapsed times of 10 000 seconds). Typically, the stress is reduced by a factor 2 within the first 50 seconds of experiment.

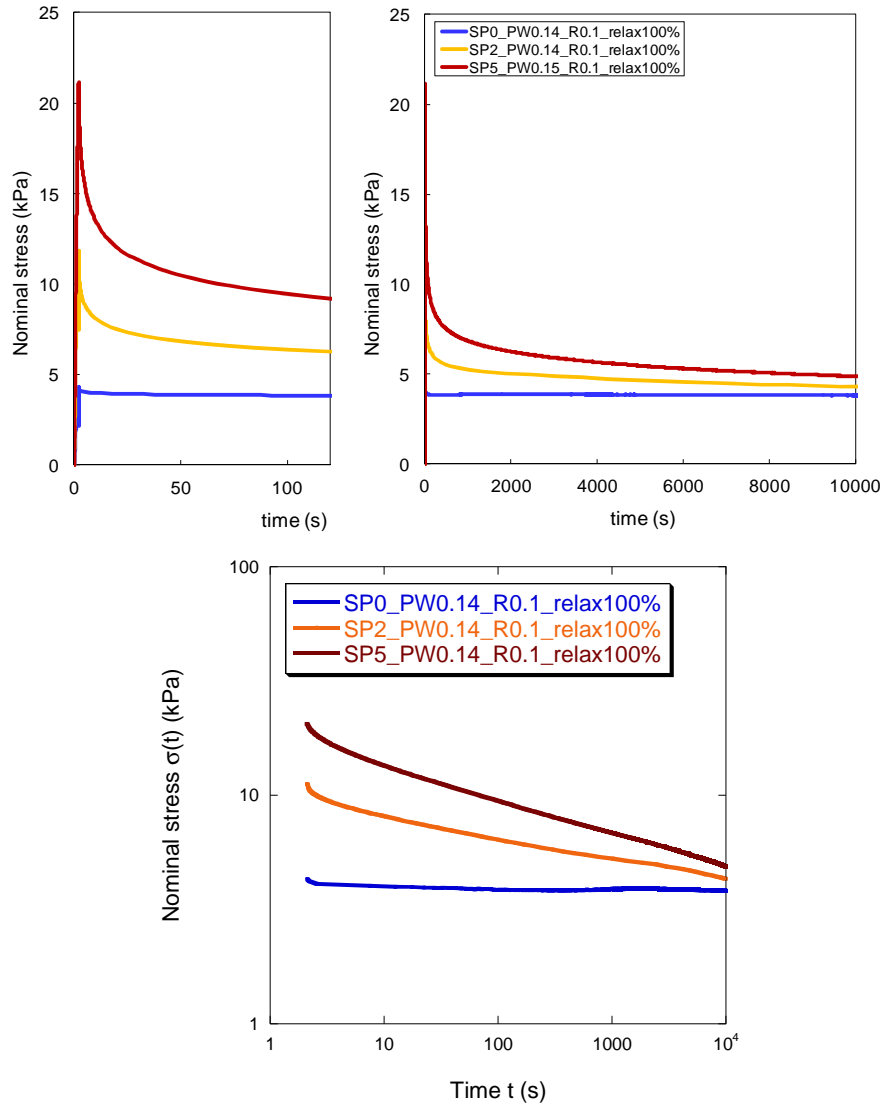


Figure 10: Relaxation experiments with an initial strain equal to 100%, on SP_x_PW0.14_R0.1 hydrogels, with x = 0, 2 and 5: evolution of the nominal stress as a function of time.

Concerning the stress relaxation at long-time scales, the **Figure 10** indicates that all the SP_x_PW0.14_R0.1 hydrogels converge to the signature of the pure organic matrix (*i.e.* SP0_PW0.14_R0.1). Thus, the results demonstrated that the physical network is fully relaxed at large time-scales and, as expected, the chemical network maintains the network topology. This result corroborates the quantitative agreement obtained at low strain rate (3.10^{-4} s^{-1}) for SP5_PW0.14_R0.14 initial modulus with the Guth and Gold's mechanical model. It confirms the efficiency of the chemical cross-linking process, which is not strongly affected by the presence of silica nanoparticles: composite's matrix is analogous to SP0_PW0.14_R0.1.

3.1.2. Toward a characteristic time-identification

Despite the power-law dependence of G'' evidenced by rheology within the linear viscoelastic regime that suggests a rather broad distribution of relaxation times, stress relaxation curves demonstrated an important stress relaxation process within the first tens of seconds of testing. Focusing typically below 50 seconds, which corresponds to the SP5 half-life stress relaxation, we have considered an exponential decay of stress relaxation (see **Figure 11**), with the general form:

$$\sigma(t) = A \exp\left(-\frac{t}{\tau}\right) + \sigma|_{t=50s} \quad \text{Eq. 7}$$

with τ a characteristic time, t the time and A a fitting parameter to adjust the vertical position of the curve.

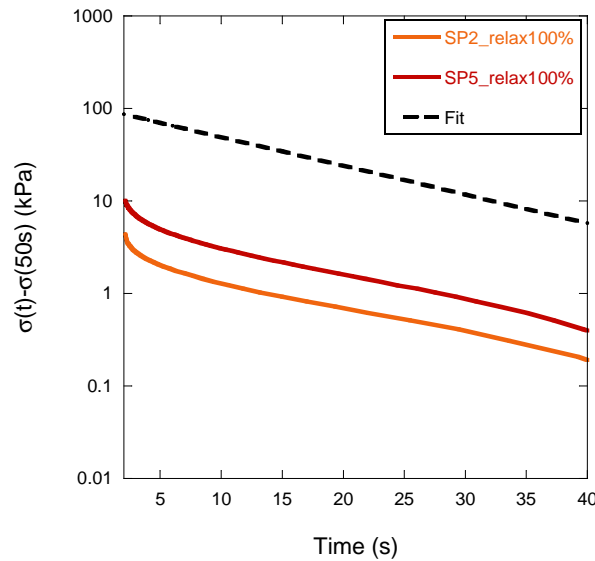


Figure 11: Relaxation experiments on SPx_PW0.14_R0.1 hydrogels with an initial strain of 100%: logarithmic representation of the modified nominal stress $\sigma'(t) = \sigma(t) - \sigma(50s)$ as a function of time compared to an exponential fit with a characteristic time equal to 14s, as a guide line.

From the representation given in **Figure 11**, we evidenced a common characteristic time of the relaxation process at short time-scale. This characteristic time is about 14 seconds for the hybrid hydrogels containing different amounts of silica nanoparticles. The same estimate of

characteristic time was also obtained independently of the level of applied strain (from 2% to 200%), as shown in **Figure 12**.

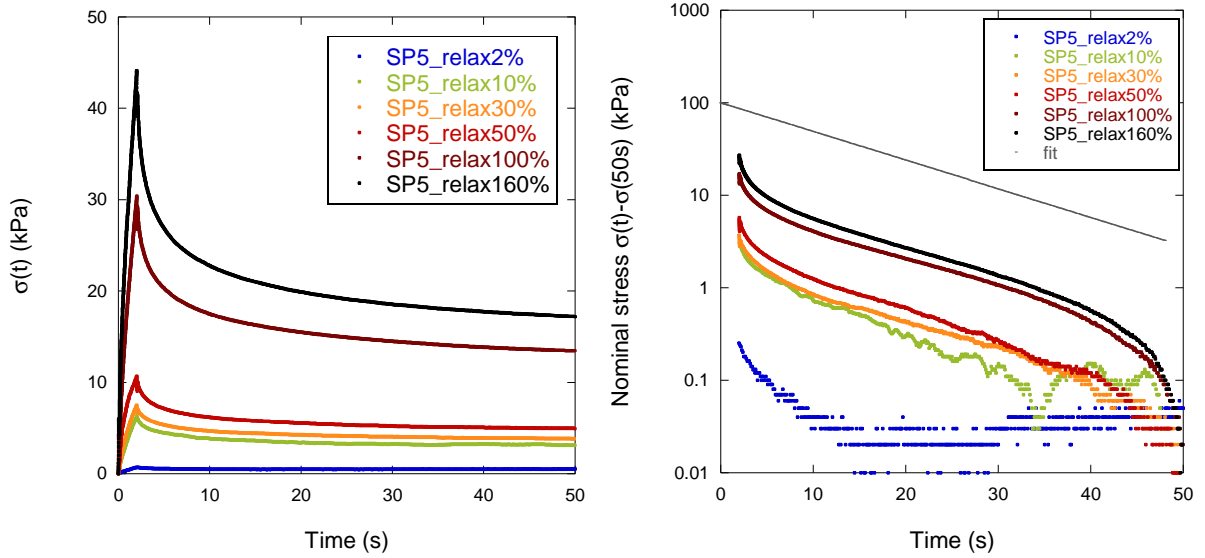


Figure 12: Relaxation experiment of SP5_PW0.14_R0.1 hydrogels, with increasing initial strain, from 2% to 160%: evolution of the nominal stress as a function of time.

Left: representation of the nominal stress. Right: logarithmic representation of the modified nominal stress $\sigma'(t) = \sigma(t) - \sigma(50s)$ as a function of time. The dotted line is an exponential fit with a characteristic time equal to 14s, as a guide line.

Qualitatively experimental curves are well ordered as a function of the initial strain: the higher the initial strain, the higher the relaxation amplitude (see **Figure 12**). Note that for initial strain of 2%, the experimental error made on its deformed length can be non negligible. This characteristic time, τ around 14 seconds, should be related to the kinetics of exchange processes of the PDMA chains at the silica surface.

3.2. Dissipation upon loading-unloading cycles

Strain-controlled tensile loading-unloading cycles have been carried out in order to investigate the dissipative mechanisms existing in hybrid hydrogels SP x _PW0.14_R0.1, from $\varepsilon_0 = 0$ to 0.25, to stay far from possible particle/particle contacts in compression in the transverse direction upon stretching. As a matter a fact, a simple estimation can be used in order to determine the strain of the contact between nanoparticles, considering that the

arrangement of the silica nanoparticles is described by a simple cubic structure, as represented in **Figure 13**. This critical deformation at which contacts between particles become effective is:

$$\varepsilon_{cr} = \left(\frac{\pi}{6\phi_{Si}} \right)^{2/3} - 1 \quad \text{Eq. 8}$$

In the case of the SP5_PW0.14_R0.1 formulation (corresponding to a volume fraction of silica equal to 0.21), the distance between two silica nanoparticles from centre to centre is equal to 406 Å. With a radius equal to 150 Å, the available distance between two particles is 106 Å. The contact of the particles is then reached when the sample is stretched of $\varepsilon_{cr} = 83\%$.

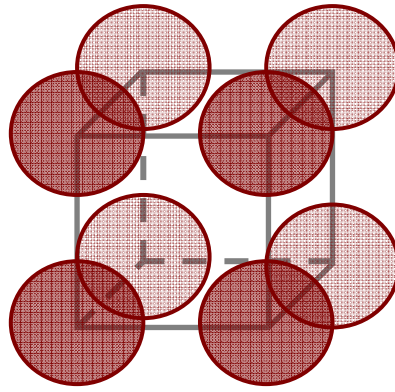


Figure 13: Schematic representation of a simple cubic arrangement of the silica nanoparticles in a SP5_PW0.14_R0.1 unstrained hybrid hydrogels.

Cycles of strain were applied first at a constant strain rate of 0.06 s^{-1} , which implies that the mean duration of one loading-unloading cycle is around 8 seconds. This loading-unloading cycle was repeated 2 times. The typical obtained curves, depending on silica content, are represented on **Figure 14**.

From the curves presented in **Figure 14** left, the dissipated strain energy can be calculated for each cycle: it corresponds to the area within the loop. This dissipated strain energy per cycle is related to the stress relaxation process upon loading. Dissipation is correlated to the presence of silica nanoparticles in the material as shown in **Table 3**. Without silica nanoparticle (the blue curve), the hydrogel SP0_PW0.14_R0.1 behaves as a purely elastic

matrix; the dissipation of the gel matrix is therefore negligible. As soon as silica nanoparticles are present in the hydrogels, the dissipated strain energy E_d significantly increases; visually it corresponds to an opening of the stress-strain curves.

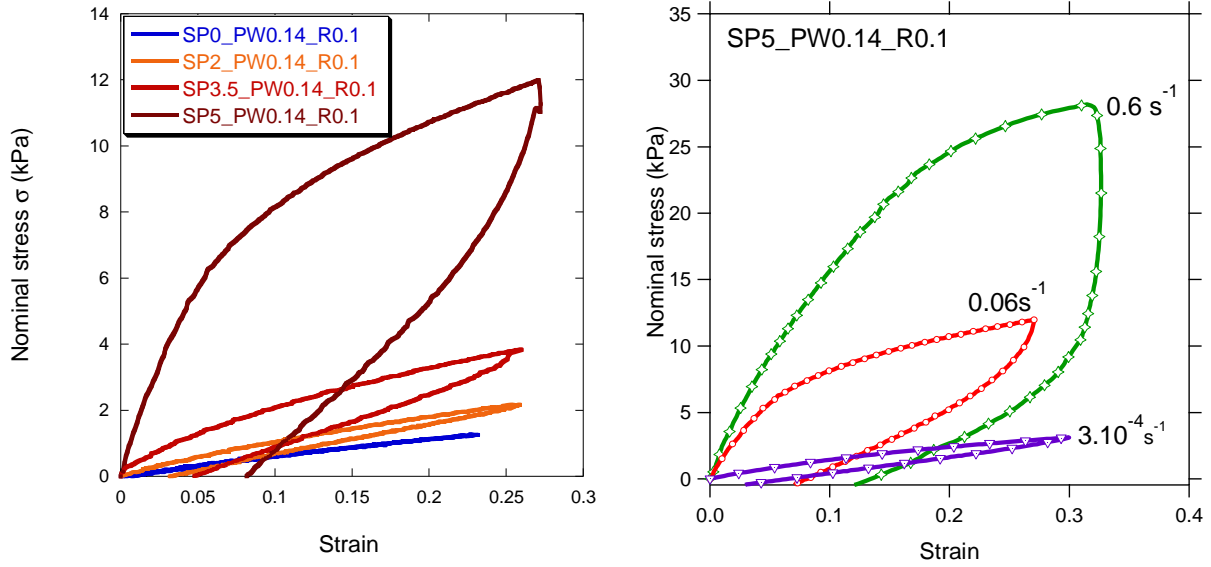


Figure 14: Left: effect of the silica content on the first loading-unloading cycle at 0.06 s^{-1} for $\text{SP}_x\text{-PW0.14_R0.1}$, with $x = 0; 1; 2; 3.5$ and 5 .
Right: effect of strain rate on the first loading-unloading cycle for SP5_PW0.14_R0.1 hybrid hydrogel.

Strain rate effects on modulus have been quite extensively studied for viscoelastic hydrogels [22-24]. In contrast, strain rate effects on large strain cycling behaviour (*i.e.* dissipation) have not been addressed so far. Interestingly, as shown in **Figure 14** (right), dissipation depends on both silica volume fraction and strain rate. **Figure 14** (right) displays cycling behaviour of SP5_PW0.14_R0.1 hybrid hydrogel for three different strain rates from 3.10^{-4} s^{-1} to 0.6 s^{-1} . Thus, the dissipative capabilities of such nano-hybrid gels appear to be highly strain rate dependent. Note that the minimum instantaneous residual strain was obtained at low strain rates (for 3.10^{-4} s^{-1}), confirming the efficiency of the chemically cross-linked matrix.

As the dissipated energy strongly increases with the complex modulus (*i.e.* the initial modulus) we estimate the dissipative component normalizing E_d by the strain energy for the fully relaxed behaviour E_∞ , *i.e.* the corresponding area under the SP5 loading curve obtained

at 3.10^{-4} s^{-1} . The values of E_d/E_∞ are presented in **Table 3** and plotted in **Figure 15**. For higher silica content at high strain rate (0.6 s^{-1}), the hybrid hydrogel can dissipate more than 10 times the amount of energy than the pure polymeric matrix is able to store at the same strain level, which is quite remarkable. Part of the dissipated strain energy at such high strain rate could be involved in damage processes, particularly for experiments carried out far below the characteristic time of PDMA/silica interaction. Thus, non linear processes, such as damage, could explain the unexpected feature of the unloading curve at 0.6 s^{-1} (see **Figure 14** right).

Sample	Silica vol. fraction, Φ_{si}	@ 0.06 s^{-1}		@ 0.6 s^{-1}		@ 3.10^{-4} s^{-1}	
		E_d / kJ.m^{-3}	E_d/E_∞	E_d / kJ.m^{-3}	E_d/E_∞	E_d / kJ.m^{-3}	E_d/E_∞
SP0	0	0	0	0	0	0	0
SP2	0.097	0.33 ± 0.18	0.54 ± 0.29	2.00 ± 0.35	3.28 ± 0.55	-	-
SP3.5	0.158	0.43 ± 0.13	0.70 ± 0.21	-	-	-	-
SP5	0.212	1.47 ± 0.24	2.41 ± 0.39	6.51 ± 0.25	10.67 ± 0.40	0.41 ± 0.14	0.67 ± 0.22

Table 3: Strain rate dependence on dissipated strain energy during the first cycle (E_d), i.e. For SP5, normalized dissipated strain energy (E_d/E_∞) with E_∞ the strain energy for the fully relaxed gel, i.e. the area under the SP5 loading curve at 3.10^{-4} s^{-1} .

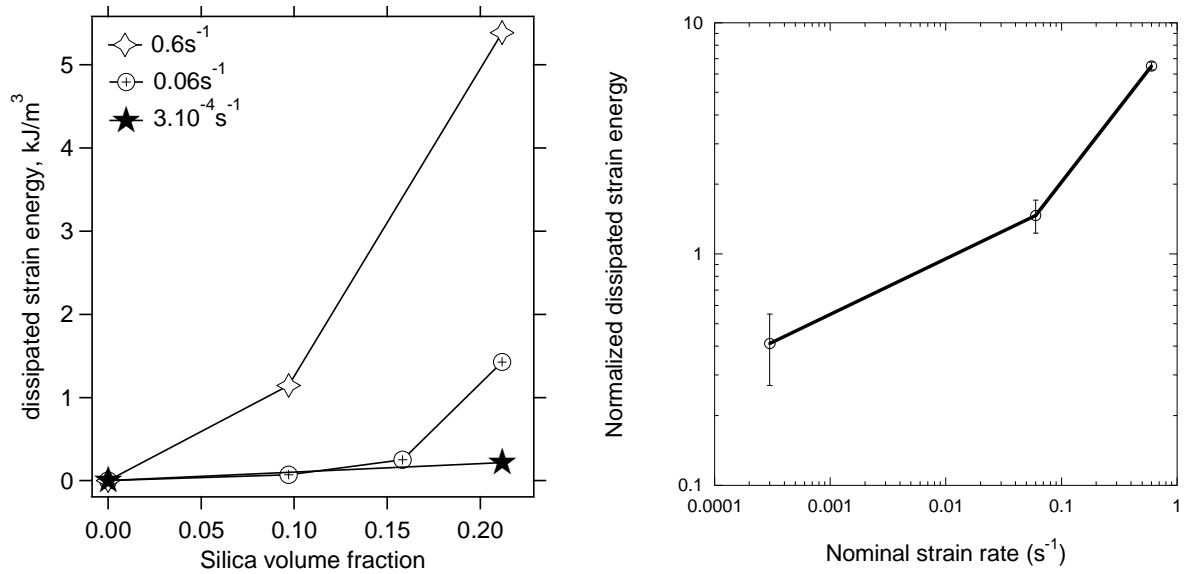


Figure 15: Left: dissipated strain energy as a function of silica volume fraction, at 0.06 s^{-1} , 0.6 s^{-1} and 3.10^{-4} s^{-1} . Right: time-dependence of the normalized dissipated strain energy, E_d/E_∞ , defined as the ratio of the dissipated strain energy at large strain during the first cycle (*i.e.* area under the loop with a maximal applied strain of 0.25), normalized by the strain energy of the fully relaxed gel (*i.e.* the area under the SP5 loading curve at 3.10^{-4} s^{-1}) with a power law fit in red ($n=0.34$).

3.3. Recovery processes

Concerning recovery processes, two aspects will be discussed: strain recovery and recovery of successive initial moduli. Moreover, two strain ranges will be investigated: cycling up to 25% of strain (to exclude particle/particle contact in the transverse direction) and cycling at large strains.

3.3.1. Strain recovery and effect on successive moduli

As presented in **Figure 16** for the SP5_PW0.14_R0.1 system, the loading-unloading cycles lead to a non-negligible instantaneous residual strain. This instantaneous residual strain can also be noticed for the other hybrid hydrogels (with lower SP values) but in a lower extent, whereas for the pure PDMA hydrogel (without silica), there is no residual strain at all. Interestingly, the residual strain is fully recovered after few seconds. Indeed, in **Figure 16**, we present a stress-strain curve corresponding to a first loading-unloading cycle at 0.06 s^{-1}

followed by 30 seconds wait and then a second loading-unloading cycle at 0.06 s^{-1} . It is obvious that this pause gives enough time to the system to recover its initial length but also recover its initial stiffness as the second cycle is identical to the first one. Remarkably, the initial modulus is fully recovered in an elapsed time of 10 seconds, which is consistent with the characteristic time identified in relaxation experiments.

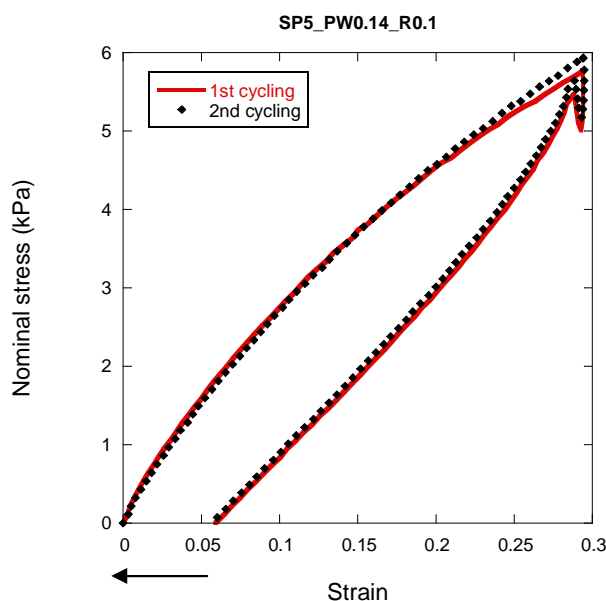


Figure 16: Effect of a 30 seconds pause on the loading-unloading cycles at 0.06 s^{-1} for a SP5_PW0.14_R0.1 hybrid hydrogel: the first cycle (red line) is followed by 30 seconds of pause and then a second cycle (black dots).

As far as the successive initial moduli are concerned, a strong effect of the strain rates can be revealed. For the unfilled hydrogel SP0_PW0.14_R0.1, the stress-strain curve remains unaffected by the cycling: there is no difference between the three successive cycles, whatever the strain rate. However, for the hybrid hydrogel with the highest amount of nanoparticles SP5_PW0.14_R0.1, a large softening of the initial modulus at large strain rates is observed while at low strain rates the initial moduli were unchanged. The complete curves for the SP5_PW0.14_R0.1 hybrid hydrogel are plotted on **Figure 17**. The evolution of the initial moduli during the consecutive loading is represented in details in **Figure 18**, with a comparison of SP0_PW0.14_R0.1 and SP5_PW0.14_R0.1.

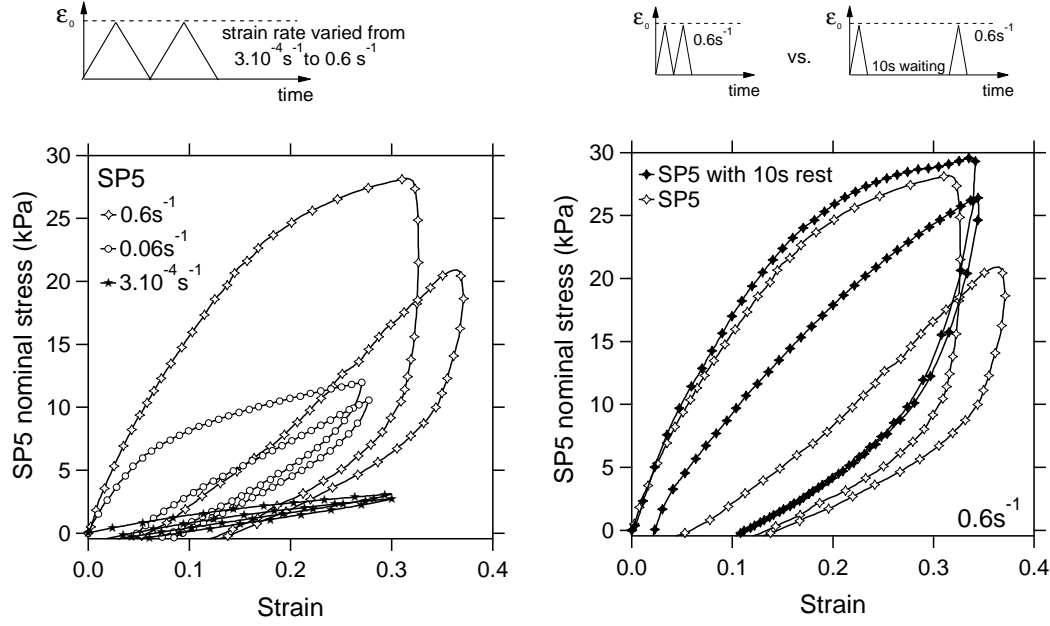


Figure 17: Cycling behaviour of the hybrid hydrogel SP5_PW0.14_R0.1. Left: two consecutive loading-unloading cycles for the three strain rates: 3.10^{-4} s^{-1} , 0.06 s^{-1} and 0.6 s^{-1} . Right: effect of a 10 seconds rest on the cycling behaviour at 0.6 s^{-1} .

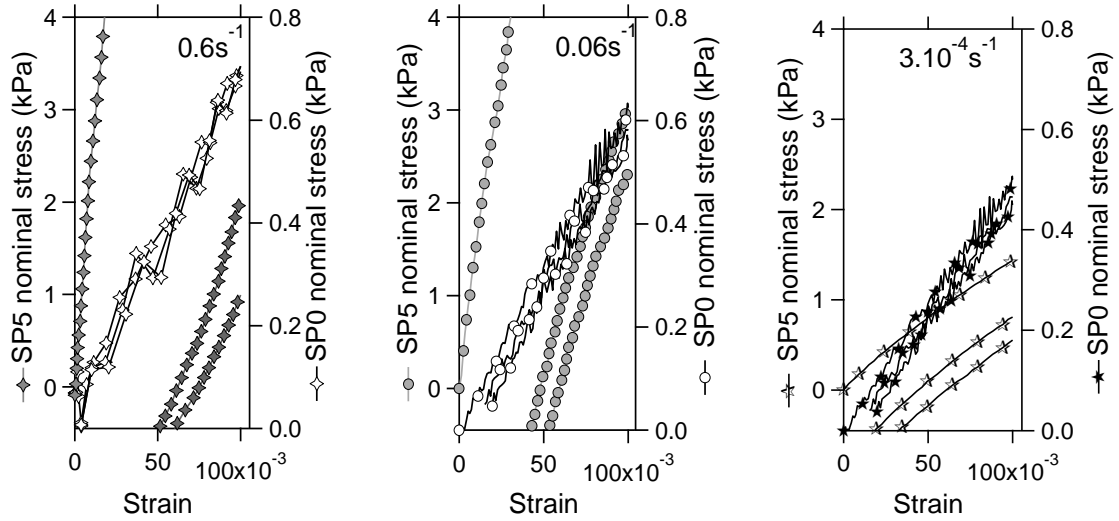


Figure 18: Comparison of the initial moduli during three subsequent loadings (with $\varepsilon_0=0.25$) for the unfilled hydrogel SP0_PW0.14_R0.1 (white markers, see right axis) and the highly filled hybrid hydrogel SP5_PW0.14_R0.1 (grey markers, see left axis) for the three nominal strain rates: 0.06 s^{-1} (left) and 0.6 s^{-1} (middle) and 3.10^{-4} s^{-1} (right). Note that only the loading portion of the cycle is reported here in order to simplify the reading.

The values of the initial moduli can be considered as a global parameter to analyze the cross-linking density of the network (considering both chemical and physical cross-links), since the modulus of the gel matrix is related to the density of elastically-active chains. Then, a decrease of stiffness can be considered as a reduction in the connectivity of the transient network. For comparative purposes, a recovery parameter, noted R , can be defined as follows:

$$R = \frac{E^{2nd}}{E^{1st}} \quad \text{Eq. 9}$$

with E^{2nd} the initial modulus during the second loading cycle and E^{1st} the initial modulus during the first loading cycle.

This recovery parameter R has been calculated for the investigated strain rates and the results are presented in **Figure 19**. The recovery of the initial modulus was seen to be complete when the experiment is carried out within the timescale of the characteristic time (*i.e.* low strain rate, 0.06 s^{-1}), while it strongly decreased for $t \ll \tau$ (*i.e.* at high strain rate 0.6 s^{-1}). As a matter of fact, in the case of the lower strain rate, the elapsed time between two loadings (typically 10 s for 0.06 s^{-1} tests) was long enough to enable a complete modulus recovery. The cycling loading-unloading tests are then in general agreement with the characteristic time identified in the relaxation process.

Ten seconds appear to be a characteristic time for recovery, since a sequence of one high strain rate cycle, followed by 10 seconds rest and then another sequence of one 0.6 s^{-1} cycle showed perfect recovery of initial stiffness (see **Figure 19**). This 10 seconds rest enables the bulk material to self-reorganize and to recover an equivalent density of elastically active chains. The gel is mending in the bulk within this time-scale. Depending on time-scale compared to the characteristic time of the polymer/silica association, the silica/polymer interaction can break and, even more importantly, be reformed, enlarging therefore very efficiently the dissipative processes.

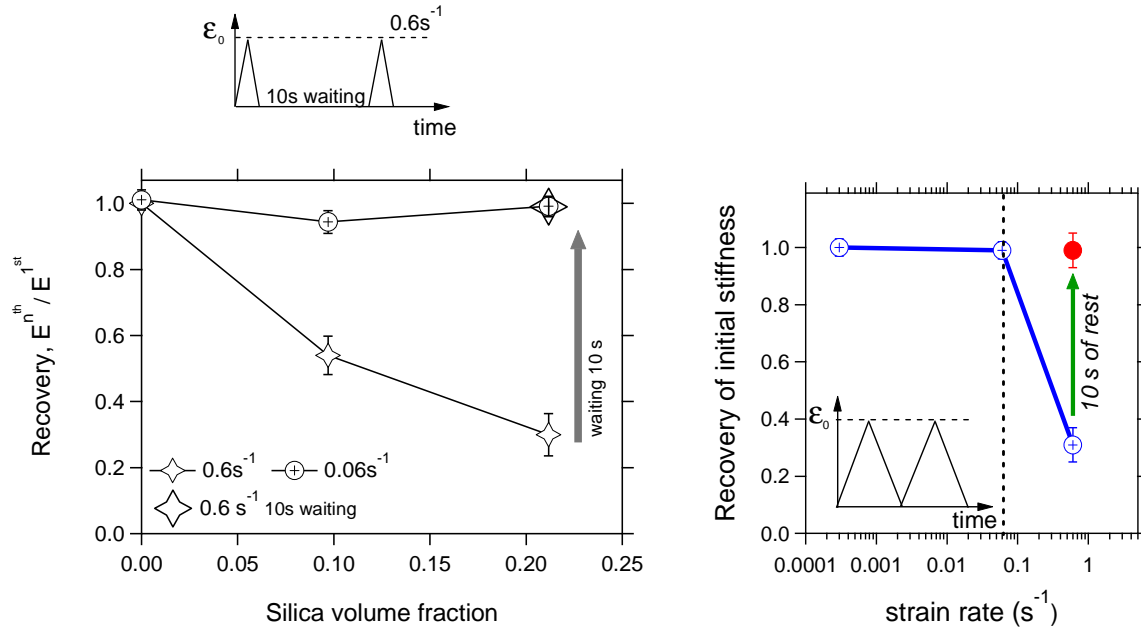


Figure 19: Left: recovery in modulus as a function of the silica volume fraction for cycling stress-strain experiments performed at different strain rates: 0.06 s^{-1} (circles) and 0.6 s^{-1} (stars). Right: recovery in connectivity as a function of the strain rate for cycling stress-strain experiments performed on SP5_PW0.14_R0.1 hybrid hydrogels, effect of a ten seconds rest.

3.3.2. Cycling at large strains

From the tensile tests previously presented, we evidenced the high deformability of the hybrid hydrogels and especially for the highest amounts of silica nanoparticles. Indeed, the SP5_PW0.14_R0.1 hydrogel can reach very high strain levels: up to 700%. Knowing that, we studied the cycling behaviour of hybrid hydrogels at large strains (500% here) followed by a tensile test at a strain rate of 0.06 s^{-1} , as presented in **Figure 20**.

First we can notice that the high strain level induces a non-negligible residual strain that partially recovers: the following tensile test starts at a partially recovered initial strain. This partial recovery (obtained without any resting time) can be attributed to the presence of the silica nanoparticles that come in contact while the strain is increased. Concerning the initial modulus, we observed a loss of 65% of the initial modulus between the first cycle and the tensile test. The damage of the system is evidently important and can also be a consequence

of an irreversible contact between the silica nanoparticles. Above a critical nominal strain of about 80%, contact of the particles is reached upon stretching.

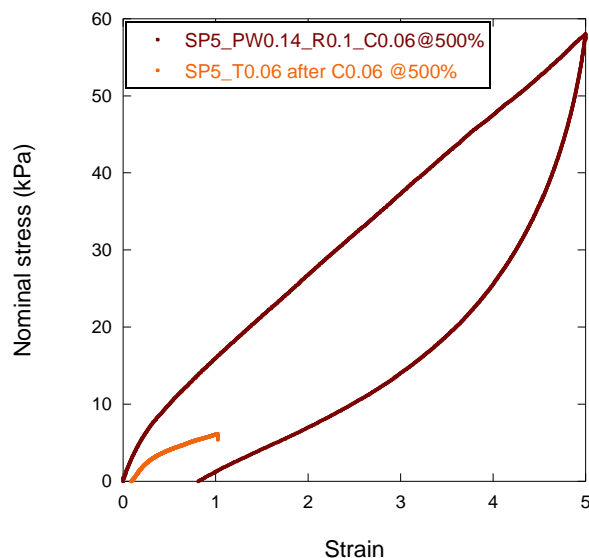


Figure 20: Cycling behaviour up to a strain of 500% of the hybrid hydrogel SP5_PW0.14_R0.1, at 0.06 s^{-1} (red), followed by a tensile test at 0.06 s^{-1} (orange).

From this value of strain, it is clear that loading the SP5_PW0.14_R0.1 sample up to 500% of strain leads to a contact of the silica nanoparticles that can be irreversible. This situation is not as easy as it can appear because of the interactions between the silica nanoparticles and the effect of the contact between particles will be discussed later in this chapter.

Moreover, giving a special attention to the strain at failure during the subsequent tensile test, we observe that the value is particularly low compared to the one obtained in tensile tests on un-stretched SP5_PW0.14_R0.1 samples (up to 700%). This drastic reduction is clearly due to a damage in such a high strain range of loading, up to 500%. During deformation, both the PDMA network and the silica dispersion could be damaged, giving rise to an even more complex interpretation.

4. Damage and fracture

In section 2 of this Chapter, we evidenced the effect of strain rate on the large strain mechanical behaviour of hybrid hydrogels. The general reinforcement was seen to be highly time-dependent. Within the appropriate time-window, the resulting mechanical behaviour of such highly stretchable nano-hybrid hydrogels highlighted a very unusual combination of properties induced by the incorporation of silica nanoparticles: elasticity, dissipation, but also strain at failure were seen to be enhanced simultaneously.

4.1. Failure properties: effects of silica content and strain rate

From the nominal stress-strain curves presented in **Figure 21**, a simple estimation of the work of extension can be done considering the area under the tensile curve (at 0.06 s^{-1}). The obtained values are:

- $W_{ext} \cong 8 \text{ kJ.m}^{-3}$ for SP0_PW0.14_R0.1;
- $W_{ext} \cong 210 \text{ kJ.m}^{-3}$ for SP5_PW0.14_R0.1.

These values clearly reveal that the physical interactions taking place between PDMA and silica efficiently dissipate energy during the fracture process, implying an increase in fracture toughness. The fracture process will be studied later in this Chapter, with a more appropriate geometry: single edge notch tensile tests.

The nominal strain at break determined from the stress-strain curves largely underestimates the nominal strain undergone by the gel matrix itself. In order to appreciate this increase in strain at failure, it is crucial to note that the local average strain in the polymer matrix is necessarily amplified over that of the macroscopic sample [25]. As a matter of fact, the high contrast in modulus between the soft polymeric matrix and the rigid silica filler implies strain amplification effects, associated with the volume occupied by the non-deformed particles. A strain amplification factor, X , can be easily calculated as follows [26, 27]:

$$X = \frac{\epsilon_{matrix}}{\epsilon} = \left(1 - \phi^{1/3}\right)^{-1} \quad \text{Eq. 10}$$

with ϕ the volume fraction of filler, ε_{matrix} the strain undergone by the matrix and ε the nominal strain.

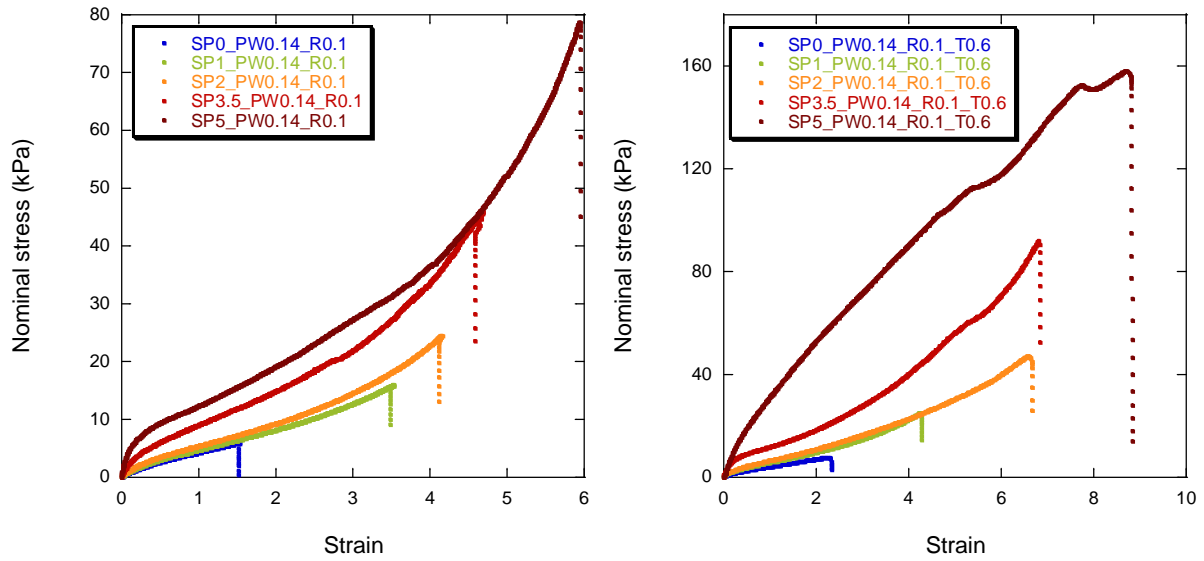


Figure 21: Effect of the silica content on tensile mechanical behaviour for SP x _PW0.14_R0.1, with $x = 0$ (blue); 1 (green); 2 (orange); 3.5 (red) and 5 (brown). Left: true stress-strain curves at a nominal strain rate equal to 0.06 s^{-1} (left) and at of 0.6 s^{-1} (right).

In the case of the SP5_PW0.14_R0.1 hydrogel, the previous equation gives a strain amplification factor value of $X = 2.5$, meaning that the strain at failure within the gel matrix reaches approximately 1700%, compared to the mean nominal strain at failure of 700% for the sample. This increase in stretchability at break is huge in comparison with the mean strain at failure obtained for the unfilled hydrogel SP0_PW0.14_R0.1. This effect can be explained by the synergy between the silica nanoparticles and the polymeric PDMA matrix, allowing exchanges of polymer partners with the surrounding nanoparticles. This is clearly a key-aspect of the strong toughening observed.

Strain rate effects on cycling behaviour were investigated in part 2 of this chapter and revealed a mechanical reinforcement which is highly time-dependent. Compared to the results obtained at 0.06 s^{-1} , the values of Young's moduli at 0.6 s^{-1} were greatly higher; the hybrid hydrogels behave more stiffly at high strain rate. However, we obtained very low

values of initial moduli at very low nominal strain rate (3.10^{-4} s^{-1}), the hybrid hydrogels followed the Guth and Gold's model.

One can wonder if the strain rate can have an effect on the mean strain at failure and if a choice of the strain rate could induce an early failure of the gel. For that purpose, **Figure 22** compares the general shape of the tensile curves at 0.06 s^{-1} and 0.6 s^{-1} for all the SPx_PW0.14_R0.1 gel formulations.

From the mean values of strain and true stress at failure reported in **Table 4**, we can first observe that the SP5 hydrogel reaches values of true stress σ_T of almost 1.5 MPa at high strain rates. Results suggest that the strain at failure increases as the strain rates is increased. However, the obtained stress and strain at break induce a statistic distribution of defects in the sample and very often fracture occurred in the clamp vicinity. In order to overcome the crack initiation from imperfections inadvertently present or introduced in the body of the material or on its surface, the approach developed by fracture mechanics consists in the analysis of failure processes on notched specimen. Fracture experiments will be discussed in the next part.

Sample	Silica volume fraction, ϕ_{Si}	@ 0.06 s^{-1}		@ 0.6 s^{-1}		@ 3.10^{-4} s^{-1}	
		ϵ_R	σ_T (kPa)	ϵ_R	σ_T (kPa)	ϵ_R	σ_T (kPa)
SP0	0	1.9 ± 0.1	24.4 ± 10.4	2.6 ± 0.1	35.6 ± 11.9	-	-
SP1	0.051	4.0 ± 0.3	134 ± 27	4.8 ± 0.4	244 ± 81	-	-
SP2	0.097	4.2 ± 0.8	306 ± 79	6.0 ± 0.3	610 ± 127	-	-
SP3.5	0.158	5.9 ± 0.8	671 ± 113	6.3 ± 0.4	913 ± 126	-	-
SP5	0.212	6.2 ± 0.6	995 ± 125	7.6 ± 0.8	1403 ± 120	5.9 ± 1.3	306 ± 6

Table 4: Effect of the strain rate on tensile mechanical behaviour of SPx_PW0.14_R0.1 hydrogels: effect on the average true strain at failure and on the average stress at failure.

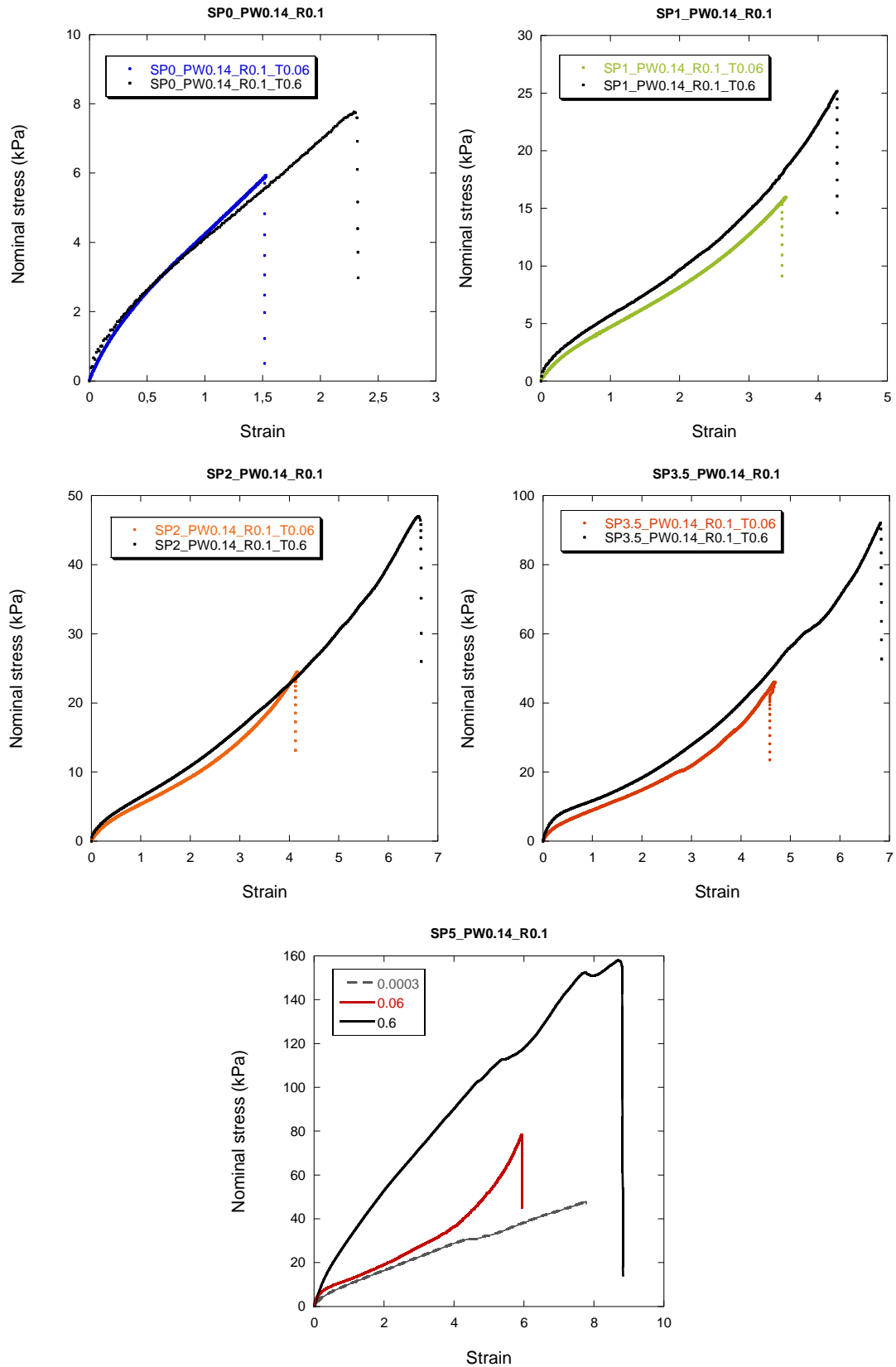


Figure 22: Effect of the strain rate on tensile mechanical behaviour of SPx_PW0.14_R0.1 hydrogels at different strain rates, with x = 0 (blue); 1 (green); 2 (orange); 3.5 (red) and 5 (brown).

4.2. Fracture properties

Fracture mechanics approach has been based on the energy necessary to propagate a crack. For rubbers, several approaches have been developed [17] to quantify the mechanical toughness, or the fracture energy, as deterministic parameters. Thus, Rivlin and Thomas [28] and later Greensmith [29] addressed a rather simple method for determination of the strain energy release rate or fracture energy, G_{IC} in the case of a single edge notched specimen:

$$G_{IC} = 2KW(\lambda_c)c \quad \text{Eq. 11}$$

with $W(\lambda_c)$ the strain energy density, λ_c the extension ratio at break, c the initial length of the crack and K a strain-dependent correction associated to the lateral contraction of the sample in extension.

The strain dependence of K has been studied by Greensmith [29] and is approximated by:

$$K = \frac{3}{\sqrt{\lambda_c}} \quad \text{Eq. 12}$$

Hence, Eq. 11 and Eq. 12 were used in the experimental part to determine the fracture energy at the onset of crack propagation:

$$G_{IC} = \frac{6cW}{\sqrt{\lambda_c}} \quad \text{Eq. 13}$$

Concerning the fracture behaviour of our nano-hybrid gels, from simple tensile behaviour the general trend is a strong toughening effect by the presence of silica. To estimate this effect, reading out the distribution of defects, we carried out some fracture tests on notched specimen. The typical stress-strain curves of notched samples tested at two strain-rates (0.06 s^{-1} and 0.6 s^{-1}) are plotted on **Figure 23**. Here the stress is defined as the force measured during the test, normalized by the initial cross-section area of the un-notched part of the sample (*i.e.* 2 mm per 5 mm). From the curves, we can clearly see that the presence of silica nanoparticles strongly enhances the fracture properties of hydrogels. As a matter of fact, the curve of the SP5 sample is far above the one of the un-filled system. Moreover, fracture appears to propagate in a more controlled manner at low strain rate and for the highest silica content (and less rapidly), since a decrease of stress is observed. In spite of the presence of

the notch, the SP5 sample almost reaches 500% of strain, while the mean nominal strain at failure of the un-notched sample reaches approximately 700%.

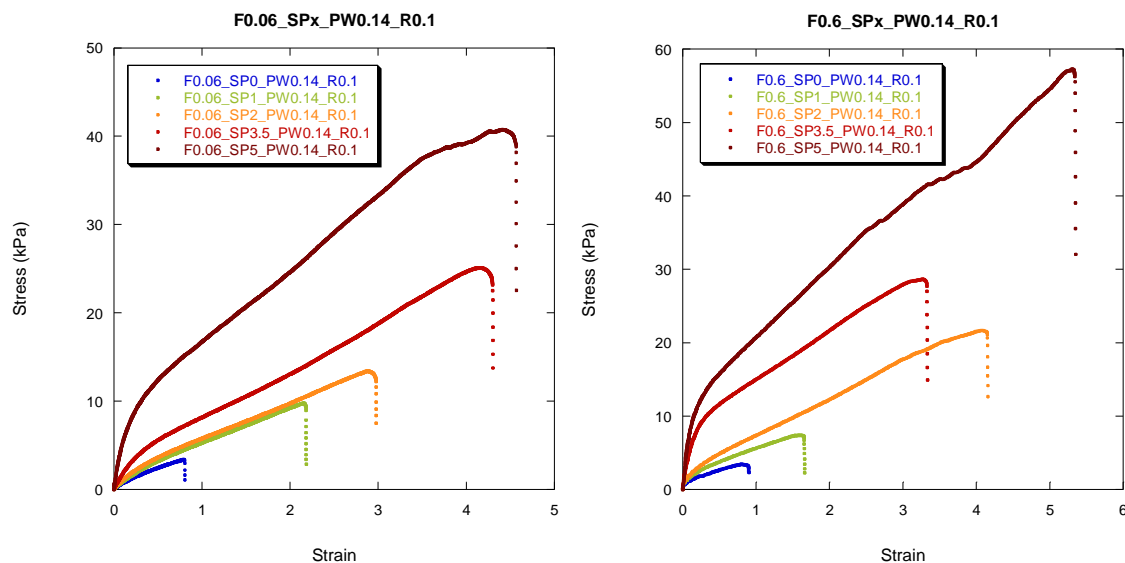


Figure 23: Effect of the silica content on fracture behaviour of SP_x_PW0.14_R0.1, with x = 0 (blue); 1 (green); 2 (orange); 3.5 (red) and 5 (brown). Left: with a nominal strain rate of 0.06 s⁻¹. Right: with a nominal strain rate of 0.6 s⁻¹. Values of c/l_0 (see Figure 4) are given for 0.06 s⁻¹: 0.34 for SP0; 0.33 for SP1; 0.4 for SP2; 0.29 for SP3.5; 0.26 for SP5; and for 0.6 s⁻¹: 0.13 for SP0; 0.14 for SP1; 0.1 for SP2; 0.15 for SP3.5; 0.19 for SP5.

The calculated fracture energies for both strain rates are represented in **Figure 24** and values are reported in **Table 5**. From this representation, one can see that, whatever the strain rate, the addition of silica nanoparticles significantly increases the energy release rate. As the polymeric matrix has a low cross-link density, the effect of the silica nanoparticles is very important. If the PDMA matrix had been more cross-linked, the presence of silica nanoparticles would have influenced the energy release rates in a weaker manner. This aspect will be discussed in Chapter 5, in a study of SP_x_PW0.14_R1 hydrogels.

First, let us focus on the values of fracture energies obtained for the unfilled system, we can observe that at the two strain rates, the curves and the values are very similar: 10.2 J/m² at 0.06 s⁻¹ and 5.1 J/m² at 0.6 s⁻¹. A comparison can be done with the theoretical prediction of Lake and Thomas, developed in the 60's for elastomers [30] and exposed in more details in

Annex 2. From the basic picture of a network formed by a collection of long and flexible chains, Lake and Thomas proposed an estimate of the threshold energy G_{LT} to propagate crack in unfilled rubbers:

$$G_{LT} = \Sigma J N_c \quad \text{Eq. 14}$$

where Σ is the surface density of chains crossing the fracture plane, N_c is the number of monomer units between cross-links, and J is the energy required to break one covalent bond. Such argument is based on the assumption that the transmitted load throughout the network brings each bond in a polymer strand crossing the interface close to its maximal free energy (*i.e.* the dissociation energy of the weakest bond in the monomer unit).

In our case, the calculation of this fracture energy G_{LT} gives about 1.2 J/m², taking the effective cross-linking density calculated in Chapter 2. This value is in a good agreement with our experimental results for the SP0_PW0.14_R0.1 hydrogel.

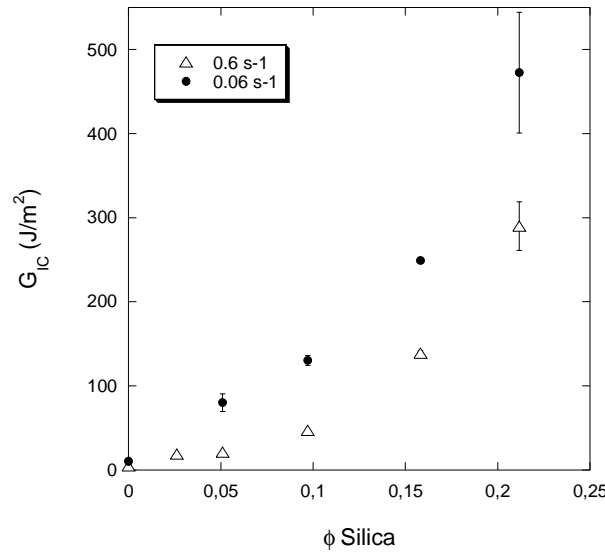


Figure 24: Effect of the strain rate on fracture behaviour of SPx_PW0.14_R0.1 hydrogels: low strain rate 0.06 s⁻¹ (filled circles) and high strain rate 0.6 s⁻¹ (unfilled triangles).

Sample	Silica volume fraction, ϕ_{Si}	G_{IC} (J.m ⁻²) @ 0.06 s ⁻¹	G_{IC} (J.m ⁻²) @ 0.6 s ⁻¹	G_{LT} (J.m ⁻²)
SP0_PW0.14_R0.1	0	10.2 ± 1.2	5.1 ± --	1.2
SP1_PW0.14_R0.1	0.051	80.3 ± 10.6	21.1 ± --	--
SP2_PW0.14_R0.1	0.097	130.2 ± 6.0	46.8 ± --	--
SP3.5_PW0.14_R0.1	0.158	249.1 ± 3.5	138.7 ± 3.0	--
SP5_PW0.14_R0.1	0.212	472.4 ± 71.8	289.9 ± 29.1	--

Table 5: Experimental values of fractures energies at 0.06 s⁻¹ and 0.06 s⁻¹, compared to the Lake and Thomas calculation (G_{LT}), for SPx_PW0.14_R0.1 hybrid hydrogels.

Concerning the strain rate effect on the fracture tests, the level of energy release rates is lower with the high strain rates, for all the SPx values. This result is in good agreement with the interpretation of the mechanical reinforcement, the characteristic times of interactions and the relaxation experiments. As a matter of fact, within the large strain regime when a SP5_PW0.14_R0.1 sample is stretched with a high strain rate, the time allocated to the desorption/re-adsorption phenomenon occurring at high strains is not long enough, the system cannot resist to the crack propagation as much as for the low strain rate. In these frequency and large strain domains, polymer/silica associations are frozen.

Note that this behaviour differs from the one classically observed for elastomers. For unfilled non-crystallizing rubbers, the effect of the strain rate on fracture energies leads to an increase of G_{IC} with the strain rate [17]. Indeed, this variation parallels closely the variation of viscoelastic properties with rate: the fracture energy increasing with increasing viscoelastic energy dissipation and the fracture process is in that case entering in the monomer-monomer friction regime.

With this quantitative analysis of the fracture experiments, one can clearly notice that the effect of the presence of silica nanoparticles highly toughens the hydrogel. However, the fracture experiments conducted here was not as conventional as expected since the notched samples underwent very high strains: very large deformations, crack blunting and

presumably large dissipative volume were induced, making the fracture analysis complex. The silica nanoparticles interact efficiently with the PDMA matrix and the crack propagation is delayed. Depending on the time-window, a “healing” or “recovery” phenomenon seems to appear: as the hybrid hydrogel sample is stretched, the PDMA chains are desorbed from the silica surface and can be re-adsorbed onto other silica surface, reaching, that way, very high dissipation before final fracture. This characteristic time controls the fracture toughness.

5. Small angle neutron scattering under deformation

SANS is widely used to analyze the structure of polymer network under deformation as thermal fluctuations of polymer chains and/or frozen inhomogeneities give rise to very informative anisotropic patterns [31-34]. A first kind of deformation is the phenomenon of swelling-deswelling of hydrogels, leading to an enhancement of the structure inhomogeneities. The second kind of deformation is the mechanical stretching of hydrogels. The complex spatial distribution of strains and stresses in a deformed nanocomposite material is a crucial problem for understanding the reinforcement mechanisms.

By following the evolutions of structural parameters of fillers (spatial evolution, contact threshold, state of dispersion...) and of polymer chains (spatial distribution, adsorption-desorption phenomenon, conformation under strain...), SANS experiments under deformation are very useful in the study of interactions matrix-fillers, making a link between macroscopic properties (in our case the mechanical reinforcement) and the spatial organization of the components. For that purpose, we used a small angle neutron spectrometer dedicated to anisotropic measurements with a load cell specially designed for these experiments. In the framework of this study we mainly investigate the structure of silica particles which are used in this case as local probes (or tracers) during the deformation of the hydrogel. Indeed, as already described with static SANS experiments, the characterization of the polymer matrix in hybrid hydrogels by contrast matching of silica does not really provide quantitative information as the scattering of the polymer matrix is very weak in these conditions and the “ghost” scattering of silica particles strongly interferes in the scattering spectrum.

As described in the experimental part of this chapter, a special load cell has been designed for this set of experiments carried out on a 2D spectrometer dedicated to anisotropic measurements. The main advantage of our set-up is the possibility to work with hydrogel samples immersed in a thermostatic bath of perfluorodecalin. In these conditions, where the fluorinated liquid and water are totally non-miscible, scattering experiments can be performed without any risk of hydrogel drying during hours, even days. These conditions

are critical, especially in 2D scattering as a high signal/noise ratio is needed over the whole frame of the detector. In the following, all the scattering experiments have been carried out during at least 1 hour for each sample in a given deformation state. For all the scattering patterns, the direction of the uni-axial deformation is along the horizontal axis.

The interpretation of the 2D scattering images is not as easy as it could be. As a matter of fact, in the reciprocal q -space, the intensity of scattering depends on the form factor of the particles. Usually, the 2D intensity data are analyzed thanks to circular-averaging (in this case we obtain a classical SANS plots) or to sector-averaging [35].

5.1. Strain visualisation

A first set of experiments is shown in **Figure 25** with the hybrid hydrogel SP5_PW0.14_R0.1 studied under incremental strain, from $\varepsilon = 0$ to 200 %. As expected, the unstrained sample displays an isotropic pattern with a circular diffraction ring corresponding to the maximum of the scattering curve previously discussed in Chapter 3. This isotropic scattering can also be observed in **Figure 26** where the 2D data have been plotted after sector-averaging, considering three different sectors of 10° width: the horizontal one (0° : with X the stretching direction), the vertical one (90° ; Y being the transverse direction) and the intermediate direction at 45° . At rest, all the scattering curves are superimposed whatever the angular sector is.

At low deformation, typically for strains of 10 % and 45 %, a double wing pattern (or butterfly pattern) appears in **Figure 25** as a consequence of an increase of the scattering intensity in the parallel direction and a decrease along the perpendicular one. This situation is clearly emphasized in **Figure 26** where the intensity increases in the X-direction with a shift of q_{max} towards low q -vectors, while it decreases in the perpendicular direction with a maximum pushed to higher q . In the meanwhile, the scattering profile at 45° remains almost unchanged if we compare $\varepsilon = 0$, 10 and 45%.

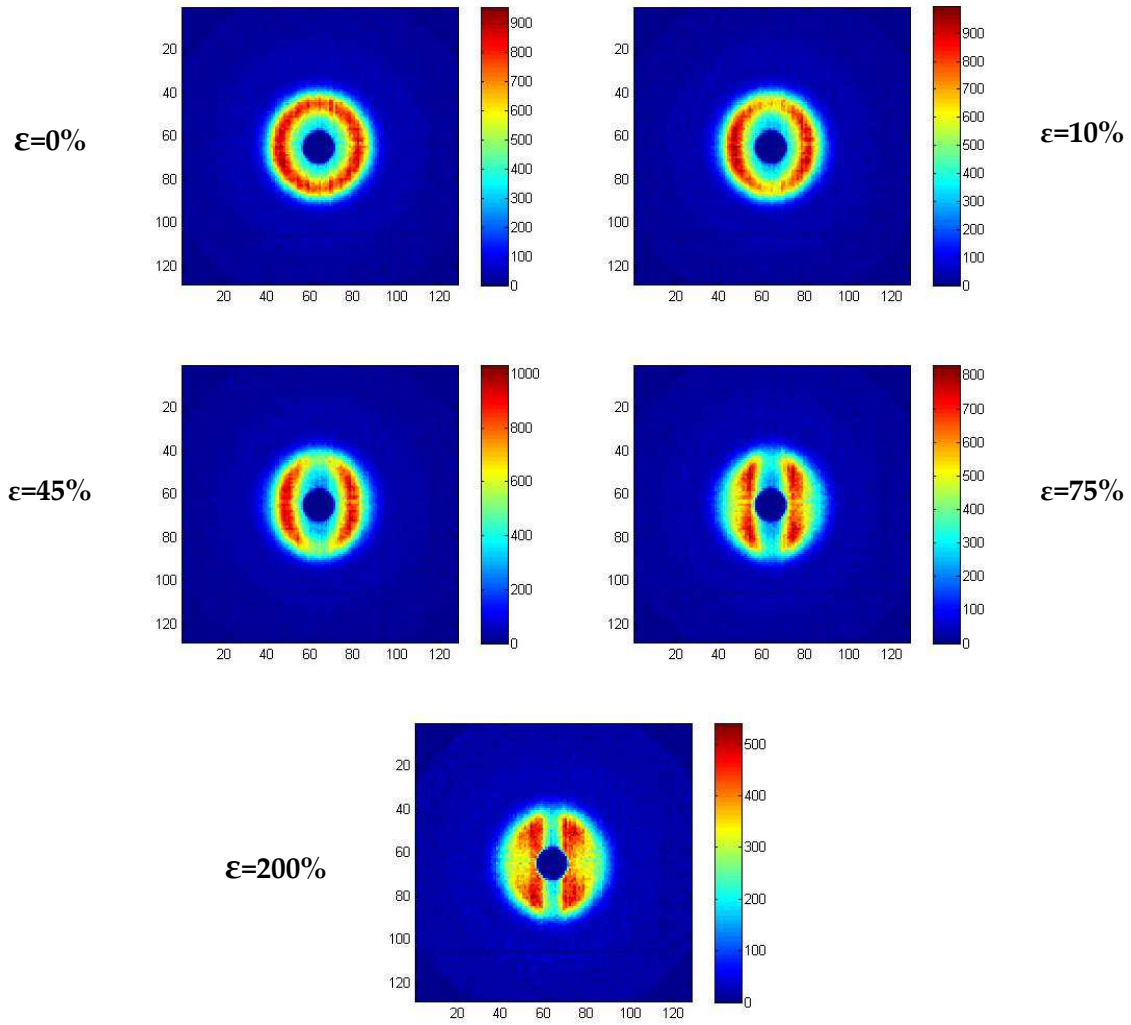


Figure 25: 2D-SANS images of a step-by-step loading of SP5_PW0.14_R0.1 hybrid hydrogel.

It is worth noting that similar patterns have been reported with nanocomposite hydrogels [36-38] and hybrid materials reinforced with silica particles like polyacrylate [39] or polyisoprene [40]. These patterns, which originate from the anisotropic space displacement of scatterers, here the silica particles, have also been described by computer simulation by Boué and co-workers [39, 41].

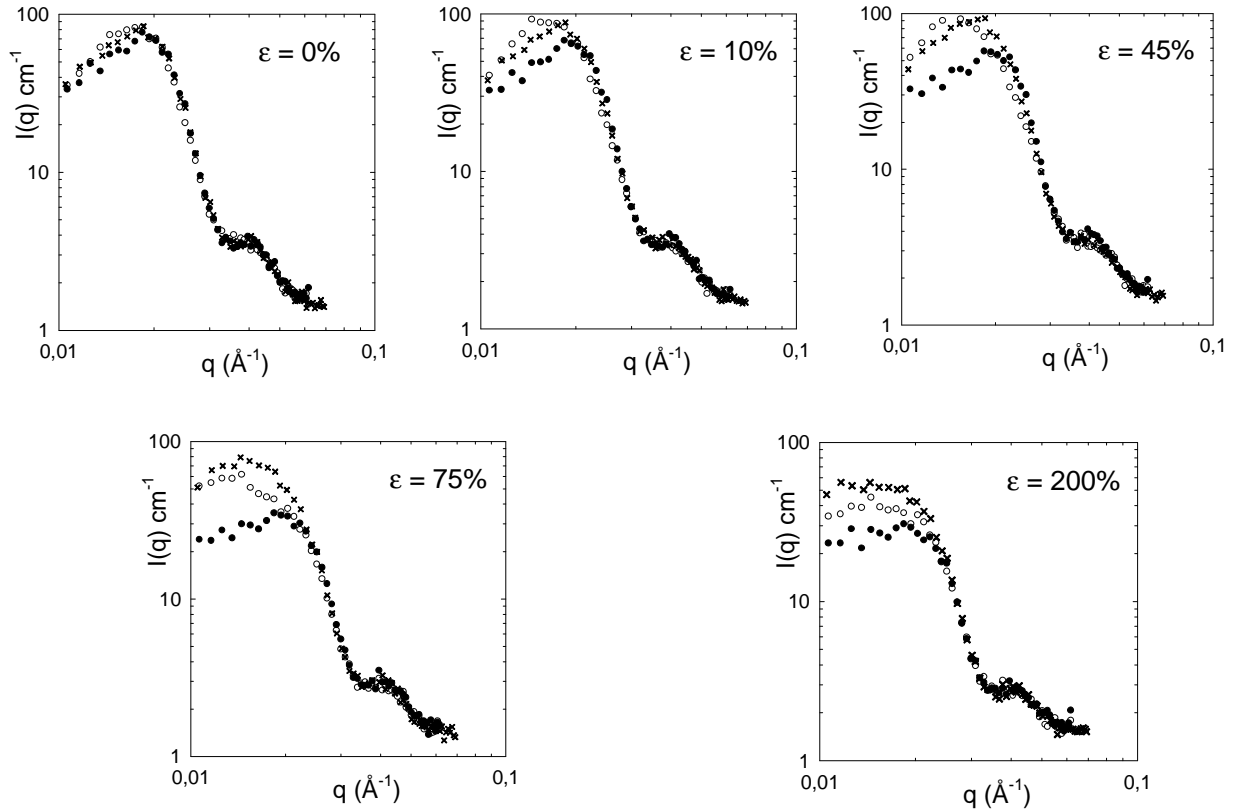


Figure 26: Double logarithmic plot of the scattering intensity of SP5_PW0.14_R0.1 hydrogel studied at different strains: from 0% to 200%. The data have been obtained from 2D-SANS images according to different sector-averaging patterns of 10° width: 0° (○), 45° (×) and 90° (●).

As schematically sketched in **Figure 27**, the stretching of the sample along the X-direction, involves an increase of the average distance between silica particles along the same direction while this distance decreases in the perpendicular direction, due to transverse compression. As the particles are brought closer in the Y-direction, their effective concentration increases and the scattering maximum is reduced and shifted towards higher q . Conversely, in the parallel direction, the particles are diluted and the maximum is enhanced at lower q . As shown in **Figure 25**, the modification of the scattering pattern under deformation is mainly observed in the intermediate q -range. Indeed, as the polymer matrix is totally screened in this contrast matching experiment (solvent p), the scattering intensity observed in the high q -range, which is the signature of the form factor ($S(q) \approx 1$), remains unchanged as silica particles are non-deformable. The circular ring obtained at high q gives also evidence that

silica particles remain dispersed in the polymer matrix and do not form aggregates that could be oriented during stretching.

When the deformation increases (for $\varepsilon = 75$ and 200%) the double wing pattern evolves into a set of four maxima which points out some reorganization of the nanoparticles. This morphological change originates from the transverse compression that pushes the particles towards each other. As shown by computer simulation by Rharbi *et al.*, if the particles coming into contact remain stuck in the relative position they had when they hit, the particles would then aggregate in horizontal bands which progressively separate from each other along the stretching direction. In that case the scattering pattern should be reduced in two spots in the stretching direction. The four-spot pattern implies that the silica particles, which are pushed towards each other by the deformation of the matrix, may avoid each other by localized shear displacements. Accordingly, a re-densification (or “re-population”) is expected in the X-direction with a decrease of the correlation length along X and a shift of the correlation peak at higher q , thus weakening the diffusion along this axis. This scenario, schematically described in the real space in **Figure 27**, strongly depends on the excluded volume, on the size, polydispersity, concentration and state of aggregation of particles. According to computer simulation [41], it was shown that the number of collisions between particles raises immediately with the deformation in the case of a random hard sphere distribution while it starts at higher deformation for a liquid-like order distribution.

A rough estimation of the critical deformation at which collisions between particles become effective, can be calculated assuming the simple cubic lattice of silica particles previously described. For SP5_PW0.14_R0.1 hydrogels, this critical strain is $\varepsilon_{cr} = 0.83$ which has to be compared with the experimentally observed values of $\varepsilon_{cr} = 0.45$ - 0.75 (see **Figure 25**). Under this consideration, a similar behaviour would be expected for SP2 hydrogels at higher deformation ($\varepsilon_{cr} = 2.08$).

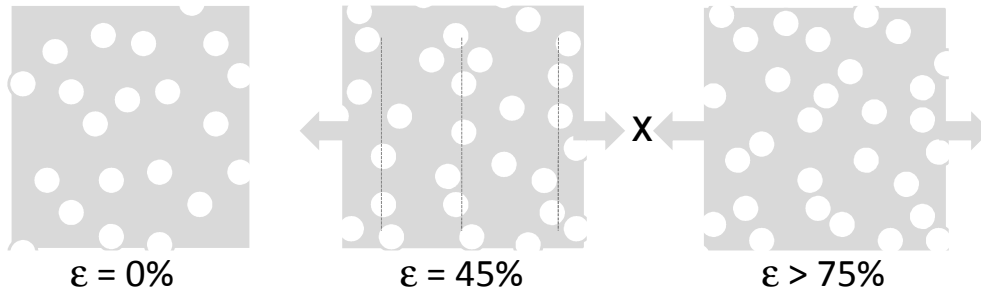


Figure 27: Schematic representation of the average distance between silica particles in hybrid hydrogels for un-stretched (left) and stretched materials, before ($\varepsilon = 45\%$) and during ($\varepsilon > 75\%$) shear reorganization. The dotted lines shown at $\varepsilon = 45\%$ highlight the alignment of particles under transverse compression.

In **Figure 26**, we have seen that for strained samples ($\varepsilon < 75\%$), the position of the scattering maximum (q_{max}) was shifted towards low q in the stretching direction and high q in the perpendicular direction. Using q_{max} as a rough estimation of the average distance between particles ($d = 2\pi/q_{max}$), this scaling parameter has been plotted in **Figure 28** as a function of strain. In the absence of collision, if we assume that the displacement of silica particles is affine with the macroscopic deformation, the opposite of the average distance from centre to centre (q_{max}) will decrease by a factor $\varepsilon + 1$ in the X-direction and increase with $(\varepsilon + 1)^{1/2}$ in the perpendicular one. Although we do not have a lot of data to plot in these conditions, the comparison with affine deformation suggests some deviation that can be attributed to the short-range repulsive inter-particle forces that have been pointed out previously. Indeed, for an initial random distribution of hard spheres (without aggregation), the probability of having spheres close to one another without contact is non-zero. This implies that even under very small deformations, silica particles will come into contact and their motion will not be affine anymore. Moreover, the possibility for polymer chains to exchange reversible contacts between particles when they are close to each other, certainly introduces additional relaxation effects that move the particles away from their affine displacement.

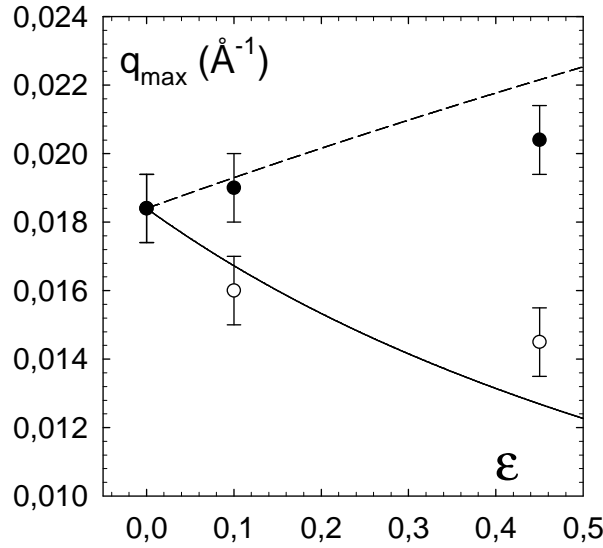


Figure 28: Strain dependence of q_{\max} for SP5_PW0.14_R0.1 hydrogel in the parallel (○) and perpendicular (●) directions of stretching. The solid line and short-dash line are the theoretical plots calculated for affine deformation in the parallel direction and perpendicular one, respectively.

The same anisotropic scattering pattern has also been observed for SP2_PW0.14_R0.1 hybrid hydrogels under uniaxial stretching. As shown in **Figure 29**, the double wing patterns is preserved at $\epsilon = 100\%$ as the volume fraction of silica particles is about two times less in that case compared to SP5 formulation. Nevertheless a four spot pattern is obtained at higher deformation ($\epsilon = 370\%$); *i.e.* well above the critical value roughly calculated from **Figure 13**: $\epsilon_{cr} = 208\%$. We can also notice that when the sample is maintained under high deformation ($\epsilon = 370\%$) during a long period (10 hours) there is mainly no change in the scattering pattern of the sample and consequently in the distribution of silica particles under large strain. This could be different for the polymer chains.

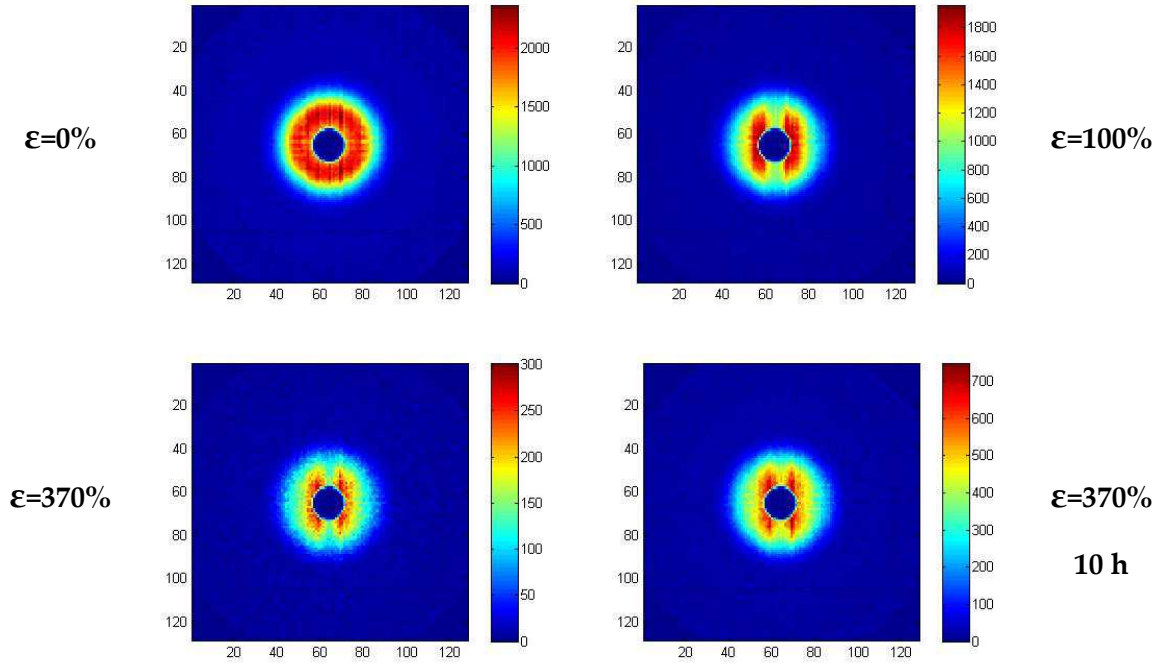


Figure 29: 2D-SANS images of SP2_PW0.14_R0.1 hybrid hydrogel. Top left: unstrained sample ($\epsilon=0\%$); top right ($\epsilon=100\%$); bottom left ($\epsilon=370\%$); bottom right ($\epsilon=370\%$) after 10 hours loading at this strain.

5.2. Reversibility

In order to study the recovery of the samples, through the distribution of silica nanoparticles in the polymer matrix, loading/unloading experiments were carried out on samples SP2 and SP5 at intermediate strains. The scattering spectra given in **Figure 30** compare the same samples: 1) initially unstrained, 2) stretched during one hour under uni-axial deformation (at $\epsilon = 100\%$) and 3) just after unloading ($\epsilon = 0\%$). We can notice that in these conditions the silica nanoparticles recover after unloading their initial isotropic pattern and we can reasonably assume that the same holds for the polymer matrix and the mechanical properties as well. By comparison with SP2, for which the 2D image obtained after unloading is totally similar to the initial one, SP5 displays a longer time dependence for its recovery. This can originate from the higher level of particles shearing induced by the transverse compression discussed previously.

As shown in **Figure 31**, when the sample SP5_PW0.14_R0.1 is stretched well above its critical condition (for instance at $\varepsilon = 200\%$) during half an hour and then unloaded back to $\varepsilon = 45\%$, the recovery is not complete and the four-spot pattern remains observable even after 3 hours. For comparison, the same sample gently loaded at $\varepsilon = 45\%$, is characterized by a double wing pattern. In this case, where the sample is highly deformed, the unloading was stopped at a strain level of 45% which corresponds to the deformation that is immediately recovered by the sample.

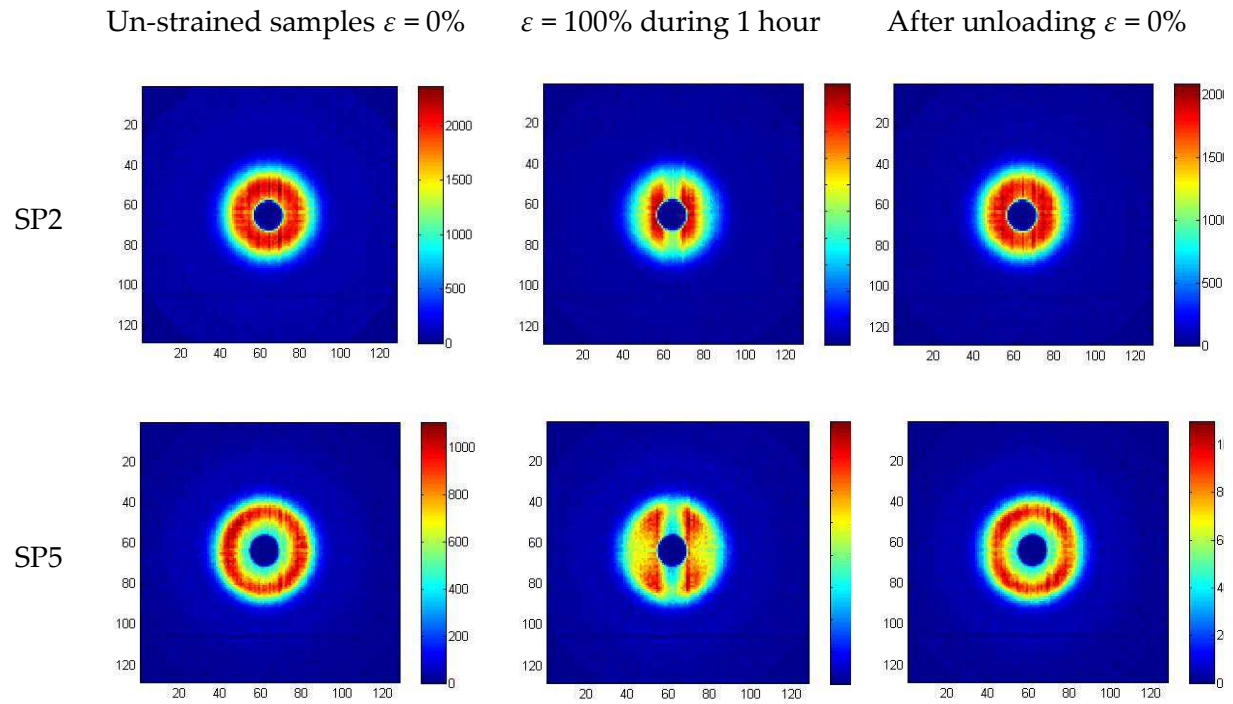


Figure 30: 2D-SANS patterns of SP2_PW0.14_R0.1 (up) and SP5_PW0.14_R0.1 (down) hybrid hydrogels before loading ($\varepsilon=0\%$; left), under loading (middle; $\varepsilon=100\%$) and after unloading (right; $\varepsilon=0\%$).

The main conclusion of this set of experiments is that silica particles embedded into the polymer matrix undergo various mechanical stresses under uni-axial deformation. Following the macroscopic deformation of the sample, the particles display affine motions at low strain but rapidly, the close contact between particles and their polymer layer induced by transverse compression gives rise to non affine displacement with local shearing. The loading process appears to be reversible, on time scale that could not be probed by SANS, as

soon as the strain level is not too high and does not imply a high level of confinement of silica beads. For larger deformations, the particles do not recover their initial distribution, revealing that some irreversible or long-term mechanisms are involved.

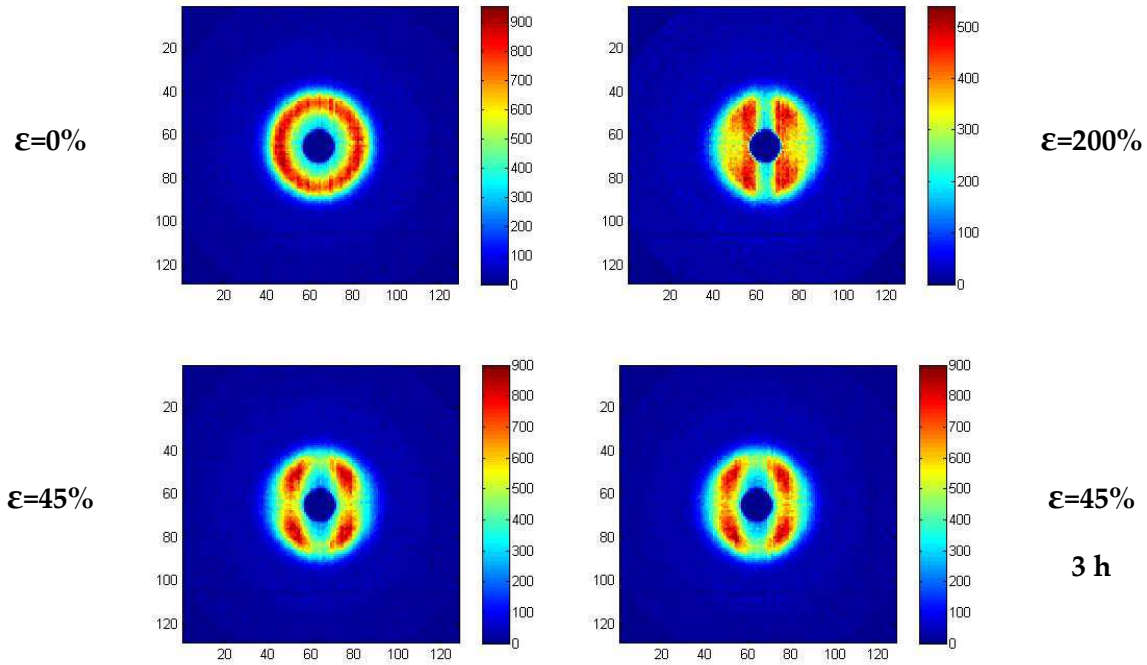


Figure 31: 2D-SANS patterns of SP5_PW0.14_R0.1 hybrid hydrogel. Top left: unstrained sample ($\epsilon=0\%$); top right: loading at $\epsilon=200\%$; bottom left: unloading from $\epsilon=200\%$ to $\epsilon=45\%$; bottom right: 3 hours after unloading to $\epsilon=45\%$.

Concerning the structure of the polymer network, we did not succeed in characterizing it properly. As a matter of fact, in the case of the silica matching, the poor contrast would have implied very long times of acquisition (several hours). For that reason we did not study the polymer network by 2D SANS.

6. Conclusions on the mechanical reinforcement of hybrid hydrogels: picture and simple model

Time-dependent dissipative mechanisms and recovery of highly stretchable nano-hybrid hydrogels have been investigated in this Chapter 4 on a model system with i) spherical well-dispersed silica particles, ii) 0.1 mol% of chemical cross-linker to obtain a low and homogeneous crosslinking process and iii) a fixed polymer/water ratio and variable particle content.

The silica nanoparticles served as multifunctional physical cross-linkers, allowing the transient anchoring of surrounding chains. As shown in Chapter 3 by swelling experiments, the PDMA chemical network was strongly adsorbed onto the silica nanoparticles surface: particles do not leach out and constrain swelling. Whereas the unfilled gel matrix behaved elastically, the silica/polymer interactions were responsible for the viscoelastic character of the hybrid gels. Indeed, the strain rate dependence of the dissipation during cycling and of the loss modulus amplitude was seen to be related to the presence of polymer/silica associations. Thanks to contrast matching experiments, the structure of these hybrid hydrogels has been followed by small angle neutron scattering experiments, with results in a very good agreement with mechanical properties.

We demonstrated that nano-hybrid gels can be considered to some extent as double networks, as schematically represented in **Figure 32**. The covalent network, prepared by chemically cross-linked polymer chains, controls the elasticity recoverability and we verified that it controls the long time behaviour. The physical network formed by reversible adsorption of polymer chains onto silica surface is responsible for the strong stiffening effect at small strain, but is highly time-dependent. The process involved in transient silica/polymer interactions clearly governs the dynamics of the gel: below the association characteristic time (for $t \ll \tau$), the hybrid gel response is governed by the double network whereas at long time-scale (for $t \gg \tau$), the physical network appears to be fully relaxed by a release in polymer chains constrained and the mechanical response remains purely

controlled by the chemical network. In such time-scale, the contribution of the nano-particle/polymer interactions vanishes.

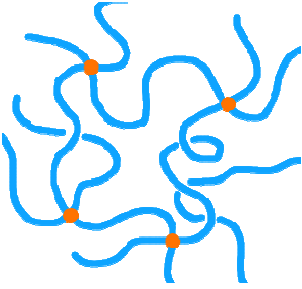
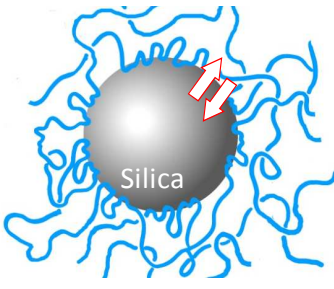
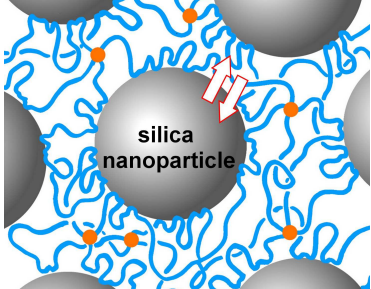
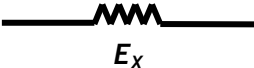
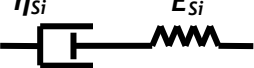
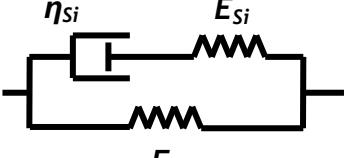
Structure / mechanical response	Covalent network = SP0_PW0.14_R0.1	Physical interactions (adsorption)	Double network = (SP5_PW0.14_R0.1)
			
Model	= strain recovery	= "recoverable" sacrificial bonds (exchanges)	Nano-hybrid gels
	Elasticity  E_x = covalent cross-links	Dissipation  E_{Si} = silica cross-links	Viscoelastic model  E_x

Figure 32: Schematic representation of hybrid hydrogels combining covalent cross-links (•) and physical interactions sketched by polymer chains adsorbed at the surface of silica nanoparticles. The structure is analogous to a double network: the chemical network controls the strain recovery thanks to the entropic restoring forces and silica nanoparticles promote transient and recoverable connectivity.

A simple description of the viscoelastic behaviour of hybrid hydrogels can be made by using classical linear viscoelastic models. In these models, springs hold for the elastic contribution while dashpots take into account the viscous dissipation. In order to mimic the complex behaviour of our hybrid hydrogels, we used the generalized Maxwell model. In this model several Maxwell elements are assembled in parallel. It takes into account that the relaxation does not occur at a single time but in a set of times. This generalized model has been developed in order to describe viscoelastic materials with dynamical properties between purely solids and purely liquids and is based on combinations of springs and dashpots as represented in **Figure 33**.

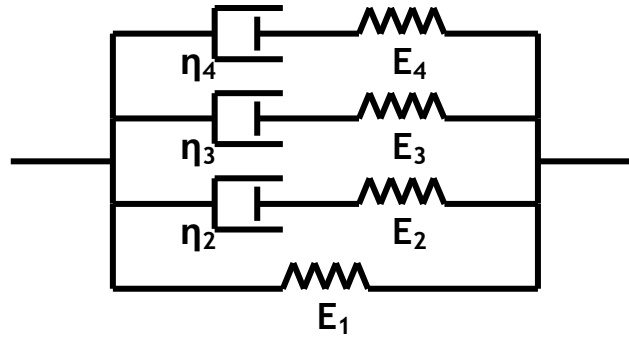


Figure 33: Picture of the generalized Maxwell model, with 3 characteristic times defines as $\tau_i = \eta_i/E_i$.

This generalized Maxwell model is more suited than the two classical models of Maxwell and Kelvin-Voigt. As a matter of fact, the Maxwell model, consisting of one spring and one dashpot in series, does not describe the recovery. On the other hand, the Kelvin-Voigt model, which is the combination of one spring and one dashpot in parallel, does not take into account the stress relaxation of the described materials. The springs obey Hooke's law (Eq. 15) while the dashpots obey Newton's law (Eq. 16), with σ_s the stress of the spring, E its modulus, σ_d the stress of the dashpot, η the viscosity and ε the strain:

$$\sigma_s = E \cdot \varepsilon \quad \text{Eq. 15}$$

$$\sigma_d = \eta \frac{d\varepsilon}{dt} \quad \text{Eq. 16}$$

Through combinations of springs and dashpots, standard viscoelastic behaviours are obtained, with a limited number of elements. Thanks to this model, it is possible to introduce several relaxation times τ_i in order to characterize the system. In the example presented in **Figure 33**, the relaxation times, τ_i , are defined as:

$$\tau_i = \eta_i / E_i \quad \text{Eq. 17}$$

Assuming linear viscoelasticity, the model defines the stress, σ , to the strain ε by the following relation:

$$\sigma(t) = \int_0^t 2G(t-\tau) \dot{\varepsilon}(\tau) d\tau + \frac{1}{3} \int_0^t K(t-\tau) \text{Trace}(\dot{\varepsilon}) d\tau \quad \text{Eq. 18}$$

with e the deviator of the strain tensor ε . The terms G and K are relaxation functions defines by Prony series:

$$G(t) = G_{\infty} - (G_{\infty} - G_0) \psi_1(\tau) \quad \psi_1(\tau) = \sum_{i=1}^n \omega_i \exp\left(-\tau/\tau_i\right) \quad \text{Eq. 19}$$

$$K(t) = K_{\infty} - (K_{\infty} - K_0) \psi_2(\tau) \quad \psi_2(\tau) = \sum_{i=1}^n \omega_i \exp\left(-\tau/\tau_i\right) \quad \text{Eq. 20}$$

with the sum of the coefficients ω_i for modulus terms must equal to one. G_0 and G_{∞} are shear modulus coefficients respectively for short and long time. K_0 and K_{∞} are bulk modulus coefficients respectively for short and long time.

In our case, we decided to define a basic model that enables to better understand the mechanical response relied to the architecture. We will focus on the SP5_PW0.14_R0.1 structure and illustrating the use of our model on a dip-test, consisting of one first loading up to a strain of 20% maintained during 80 seconds followed by an unloading to a strain of 10% also maintained during 80 seconds, as presented in **Figure 34** left. First, concerning the loading part of the dip-test, the initial modulus corresponds to the one measured by tensile tests at high strain rate (0.6 s^{-1}): 170 kPa. This initial modulus includes the connectivity of the chemically cross-linked PDMA network and the signature of the physical cross-linking induced by the presence of silica. In this way, these 170 kPa are the sum of 10 kPa coming from the chemical network (the initial modulus of the SP0_PW0.14_R0.1 hydrogel) and 160 kPa coming from the reinforcement due to silica:

$$E_t = E_x + E_{Si} \quad \text{Eq. 21}$$

Thus, we used a generalized Maxwell model with the following assumptions:

- E_{∞} characterizing the long-time behaviour of the gel will be fixed at 10 kPa, that corresponds to the chemical network (SP0_PW0.14_R0.1);
- E_0 , the short-time modulus will be fixed at 170 kPa, which corresponds to the modulus obtained at 0.6 s^{-1} ;
- three characteristic times will be considered. The first one, evidenced experimentally by relaxation experiments and cycling tests, will be fixed at 10 seconds. To cover a wide range of scale-time, the two other times will be arbitrary fixed at 1 second and 800 seconds, respectively.

All the fitting parameters are summarized in **Table 6**.

Parameters	Fixed values	Experimental determination
E_0	170 kPa	Initial modulus of SP5 at 0.6 s ⁻¹
E_∞	10 kPa	Initial modulus of SP0 and relaxation experiments
τ_1	1 s	-
τ_2	10 s	Relaxation experiments
τ_3	800 s	-
ω_1	-	-
ω_2	-	-
ω_3	-	-
$\sum_{i=1}^3 \omega_i$	1	-

Table 6: Fitting parameters of our generalized Maxwell model.

As a result only three coefficients ω_i for modulus will be optimized, constraining that the sum of ω_i terms must equal to one. Optimization of ω_i parameters has been carried out on the dip-test, conducted on a SP5_PW0.14_R0.1 hybrid hydrogel. The true stress-relaxation curve as a function of time and the comparison to the model are given in **Figure 34**. The optimized fitting curve is in very good agreement with the experimental dip-test, but contains some minor deviations. A fair fitting result was obtained for the following set of weights ω_i :

- a short one $\tau_1 = 1$ second, with a relative weight $\omega_1 = 0.7$,
- a middle one $\tau_2 = 10$ seconds, with a relative weight $\omega_2 = 0.18$ and
- a longer one $\tau_3 = 800$ seconds with a relative weight $\omega_3 = 0.12$.

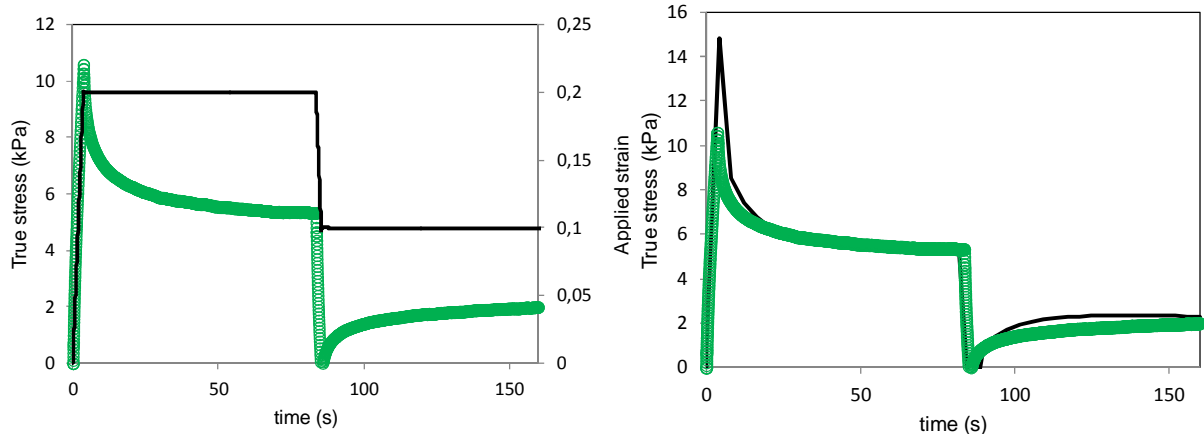


Figure 34: Dip-test on SP5_PW0.14_R0.1 sample. Left: the applied strain and gel response are plotted versus time. Right: Comparison of experimental data (in green) and the viscoelastic model (black line).

From the parameters of this model, we try to validate such choice of parameters by modelling cycling tests at the three studied strain rates: model is compared to experimental data in **Figure 35**.

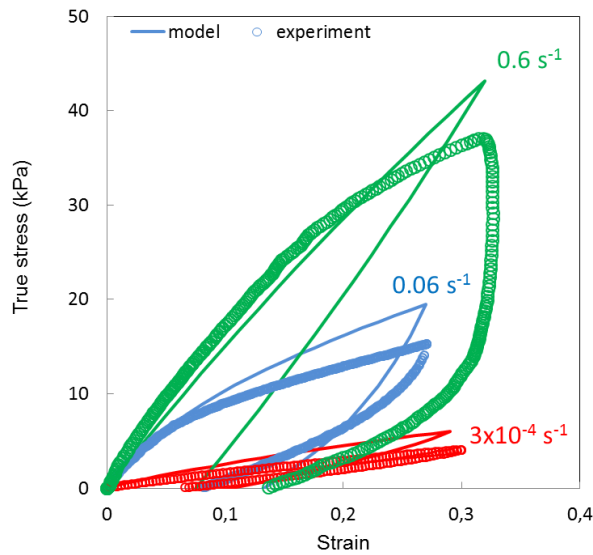


Figure 35: Comparison of modelling (lines) and experimentation (dots) of cycling tests at three strain rates: 0.6 s^{-1} (in green), 0.06 s^{-1} (in blue) and 3.10^{-4} s^{-1} (in red).

First, one can notice that the general shape of the curves is very similar to the experimental ones. Especially in the case of the two lower strain rates, the modelling curves are in a very good agreement in terms of shape but also in terms of dissipated energy. Concerning the curves at 0.6 s^{-1} , higher discrepancies are noticeable. While the loading part of the modelling curve follows the experimental one, the unloading one does not look like the experiments: at a given strain, higher values of true stress are modelled. Another lack of correspondence in this model is the residual strain at high strain rates.

As a conclusion to this brief modelling part, even if our model is based on very basics assumptions and some choices of fitting, the good agreement with experimental results is a token of the relevance of the model. If this thesis had initially included a modelling part, fractional calculus based on generalized visco-elastic models could have been of interest [42, 43]. We succeeded in testing a simple model, taking into account our mechanical characterization, which includes the structural picture of our double network gels: the adsorption-desorption phenomenon on PDMA at the silica nanoparticles surface and a covalent network. These exchange mechanism should present a wide distribution of characteristic times and are much more complex than what we have taken into account in our model. Many associating polymers with multiple stickers are characterized by such a broad distribution of relaxation times [44-48]. In our PDMA/silica system, the chain detachment at the silica surface and exchange with other polymer chains that occur under strain probably occur through multiple step mechanisms which are responsible for such a large distribution of relaxation times evidenced by rheology within the linear viscoelastic regime. In our system, the strength of the silica/polymer physical junctions is far weaker than those of covalent bonds. The mechanical force accumulated under large strains within the polymer chains, above a critical strain energy, can be released through the yielding of these physical cross-links. To this extent, our nano-hybrid hydrogels can be considered as double networks. Such a combination of time-dependent bonds and permanent bonds may be relevant for other soft material systems [49-53] where two populations of bonds exist and stress the need to understand the role played by these time scales on more complex processes such as fracture. The remarkable role played by the silica nanoparticles leads to promising applications of toughening, self-recovery and self-healing properties [49, 51, 52].

References

1. Petit, L., et al., *Responsive hybrid self-assemblies in aqueous media*. Langmuir, 2007. **23**(1): p. 147-158.
2. Frantz, P. and S. Granick, *Kinetics of polymer adsorption and desorption*. Physical Review Letters, 1991. **66**(7): p. 899-902.
3. Pefferkorn, E., A. Carroy, and R. Varoqui, *Dynamic behavior of flexible polymer at a solid liquid interface*. Journal of Polymer Science Part B - Polymer Physics, 1985. **23**(10): p. 1997-2008.
4. Okumura, Y. and K. Ito, *The Polyrotaxane Gel: A Topological Gel by Figure-of-Eight Cross-links*. Advanced Mater., 2001. **13**(7): p. 485.
5. Sudre, G., *Adhésion stimulable d'hydrogels*, in *Chimie et Physico-chimie des Polymères*. 2011, UPMC: Paris.
6. Kong, H.J., E. Wong, and D.J. Mooney, *Independent control of rigidity and toughness of polymeric hydrogels*. Macromolecules, 2003. **36**(12): p. 4582-4588.
7. Ng, T.S.K. and G.H. McKinley, *Power law gels at finite strains: The nonlinear rheology of gluten gels*. Journal of Rheology, 2008. **52**(2): p. 417-449.
8. Ng, T.S.K., G.H. McKinley, and R.H. Ewoldt, *Large amplitude oscillatory shear flow of gluten dough: A model power-law gel*. Journal of Rheology, 2011. **55**(3): p. 627-654.
9. Hao, J.K. and R.A. Weiss, *Viscoelastic and Mechanical Behavior of Hydrophobically Modified Hydrogels*. Macromolecules, 2011. **44**(23): p. 9390-9398.
10. Haraguchi, K., T. Takehisa, and S. Fan, *Effects of clay content on the properties of nanocomposite hydrogels composed of poly(N-isopropylacrylamide) and clay*. Macromolecules, 2002. **35**(27): p. 10162-10171.
11. Abdurrahmanoglu, S., M. Cilingir, and O. Okay, *Dodecyl methacrylate as a crosslinker in the preparation of tough polyacrylamide hydrogels*. Polymer, 2011. **52**(3): p. 694-699.
12. Miquelard-Garnier, G., C. Creton, and D. Hourdet, *Strain induced clustering in polyelectrolyte hydrogels*. Soft Matter, 2008. **4**(5): p. 1011-1023.
13. Abdurrahmanoglu, S. and O. Okay, *Rheological Behavior of Polymer-Clay Nanocomposite Hydrogels: Effect of Nanoscale Interactions*. Journal of Applied Polymer Science, 2010. **116**(4): p. 2328-2335.

14. Xiong, L., et al., *Network chain density and relaxation of in situ synthesized polyacrylamide/hectorite clay nanocomposite hydrogels with ultrahigh tensibility*. *Polymer*, 2008. **49**(23): p. 5064-5071.
15. Meyvis, T.K.L., et al., *Rheological monitoring of long-term degrading polymer hydrogels*. *Journal of Rheology*, 1999. **43**(4): p. 933-950.
16. Haraguchi, K. and H.J. Li, *Mechanical properties and structure of polymer-clay nanocomposite gels with high clay content*. *Macromolecules*, 2006. **39**(5): p. 1898-1905.
17. Gent, A.N., *Engineering with Rubber*. 2000: Hanser.
18. Zhao, X., et al., *Stress-relaxation behavior in gels with ionic and covalent crosslinks*. *Journal of Applied Physics*, 2010. **107**.
19. Cai, S., et al., *Poroelectricity of a covalently crosslinked alginate hydrogel under compression*. *Journal of Applied Physics*, 2010. **108**(11).
20. Konda, A., K. Urayama, and T. Takigawa, *Strain-Rate-Dependent Poisson's Ratio and Stress of Polymer Gels in Solvents Revealed by Ultraslow Stretching*. *Macromolecules*, 2011. **44**(8): p. 3000-3008.
21. Zhao, X., et al., *Stress-relaxation behavior in gels with ionic and covalent crosslinks*. *Journal of Applied Physics*, 2010. **107**(6).
22. Carlsson, L., et al., *Nano-hybrid self-crosslinked PDMA/silica hydrogels*. *Soft Matter*, 2010. **6**(15): p. 3619-3631.
23. Gaharwar, A.K., et al., *Highly Extensible, Tough, and Elastomeric Nanocomposite Hydrogels from Poly(ethylene glycol) and Hydroxyapatite Nanoparticles*. *Biomacromolecules*, 2011. **12**(5): p. 1641-1650.
24. Sun, J.-Y., et al., *Highly stretchable and tough hydrogels*. *Nature*, 2012. **489**: p. 133-136.
25. Mullins, L. and N.R. Tobin, *Theoretical Model for the Elastic Behavior of Filled-Reinforced Vulcanized Rubbers*. *Rubber Chemistry and Technology*, 1957. **30**(2): p. 555-571.
26. Bueche, F., *Molecular basis for the Mullins effect*. *Journal of Applied Polymer Science*, 1960. **4**(10): p. 107-114.
27. Bueche, F., *Mullins effect and rubber-filler interaction*. *Journal of Applied Polymer Science*, 1961. **5**(15): p. 271-281.

28. Rivlin, R.S., *Large Elastic Deformations of Isotropic Materials .4. Further Developments of the General Theory*. Philosophical Transactions of the Royal Society of London Series a-Mathematical and Physical Sciences, 1948. **241**(835): p. 379-397.
29. Greensmith, H.W., *Rupture of rubber. X. The change in stored energy on making a small cut in a test piece held in simple extension*. Journal of Applied Polymer Science, 1963. **7**(3): p. 993-1002.
30. Lake, G.J. and A.G. Thomas, *The Strength of Highly Elastic Materials*. Proceedings of the Royal Society London, 1967. **300**(1460): p. 108-119.
31. Bastide, J. and L. Leibler, *Large-Scale Heterogeneities in Randomly Cross-Linked Networks*. Macromolecules, 1988. **21**: p. 2647.
32. Karino, T., et al., *SANS Studies on Deformation Mechanism of Slide-Ring Gel*. Macromolecules, 2005. **38**: p. 6161.
33. Shibayama, M., et al., *Small-Angle Neutron Scattering Study on Charged Gels in Deformed State*. Macromolecules, 1998. **31**: p. 2586-2592.
34. Shibayama, M., et al., *Small-angle neutron scattering studies on chain asymmetry of coextruded poly(vinyl alcohol) film*. Macromolecules, 1990. **23**: p. 1438-1443.
35. Shibayama, M., et al., *Evaluation of Incoherent Neutron Scattering from Softmatter*. Journal of the Physical Society of Japan, 2005. **74**(2728-2736).
36. Nishida, T., et al., *Deformation mechanism of nanocomposite gels studied by contrast variation small-angle neutron scattering*. Physical Review E, 2009. **80**(3): p. 4.
37. Miyazaki, S., et al., *Clay Concentration Dependence of Microstructure in Deformed Poly(N-isopropylacrylamide)-Clay Nanocomposite Gels*. Macromolecules, 2006. **39**: p. 8112-8120.
38. Shibayama, M., *Small-angle neutron scattering on polymer gels: phase behavior, inhomogeneities and deformation mechanisms*. Polymer Journal, 2011. **43**: p. 18-34.
39. Rharbi, Y., et al., *Modes of deformation in a soft/hard nanocomposite: A SANS study*. Europhys. Lett., 1999. **46**: p. 472-478.
40. Ikeda, Y., et al., *Study on two-dimensional small-angle X-ray scattering of in situ silica filled nanocomposite elastomer during deformation*. Journal of Applied Crystallography, 2007. **40**: p. s549-s552.

41. Oberdisse, J., Y. Rharbi, and F. Boué, *Simulation of aggregate structure and SANS-spectra in filled elastomers*. Computational and Theoretical Polymer Science, 2000. **10**: p. 207-217.
42. Schiessel, H., et al., *Generalized viscoelastic models: their fractional equations with solutions*. J. Phys. A: Math. Gen., 1995. **28**: p. 6567-6584.
43. Cao, L., et al., *Time domain analysis of the fractional order weighted distributed parameter Maxwell model*. Computers and Mathematics with Applications, 2013. **in press**.
44. Buhler, E., et al., *Dynamical properties of semidilute solutions of hydrogen-bonded supramolecular polymers*. Physical Review E, 2007. **76**(6): p. 8.
45. Candau, F., E.J. Regalado, and J. Selb, *Scaling behavior of the zero shear viscosity of hydrophobically modified poly(acrylamide)s*. Macromolecules, 1998. **31**(16): p. 5550-5552.
46. Feldman, K.E., et al., *Model Transient Networks from Strongly Hydrogen-Bonded Polymers*. Macromolecules, 2009. **42**(22): p. 9072-9081.
47. Ng, W.K., K.C. Tam, and R.D. Jenkins, *Lifetime and network relaxation time of a HEUR-C20 associative polymer system*. Journal of Rheology, 2000. **44**(1): p. 137-147.
48. Xu, D.H. and S.L. Craig, *Scaling Laws in Supramolecular Polymer Networks*. Macromolecules, 2011. **44**(13): p. 5465-5472.
49. Haraguchi, K., K. Uyama, and H. Tanimoto, *Self-healing in Nanocomposite Hydrogels*. Macromolecular rapid communications, 2011. **32**(16): p. 1253-8.
50. Salib, I.G., et al., *Role of Parallel Reformable Bonds in the Self-Healing of Cross-Linked Nanogel Particles*. Langmuir, 2011. **27**(7): p. 3991-4003.
51. Wang, Q., et al., *High-water-content mouldable hydrogels by mixing clay and a dendritic molecular binder*. Nature, 2010. **463**(7279): p. 339-343.
52. Cordier, P., et al., *Self-healing and thermoreversible rubber from supramolecular assembly*. Nature, 2008. **451**(7181): p. 977-980.
53. Hui, C.Y. and R. Long, *A constitutive model for the large deformation of a self-healing gel*. Soft Matter, 2012. **8**(31): p. 8209-8216.

Chapter 5

Tunability of the system

Contents

Contents	192
Introduction.....	193
1. Tuning the PDMA matrix	194
1.1. Changing the cross-linking density	194
1.1.1. Synthesis of hybrid hydrogels.....	194
1.1.2. Swelling measurements.....	195
1.1.3. Mechanical properties	197
1.2. Changing the swelling state.....	204
1.2.1. Mechanical properties at swelling equilibrium	205
1.2.2. SANS under deformation.....	208
2. Changing the dispersion state of silica particles.....	211
2.1. Synthesis of hybrid hydrogels.....	211
2.2. Swelling measurements.....	213
2.3. Mechanical properties	214
3. Playing with the magnitude of interactions	217
3.1. Changing the monomer.....	217
3.1.1. Synthesis of hybrid hydrogels.....	218
3.1.2. Structural investigations	218
3.1.3. Swelling properties	220
3.1.4. Mechanical properties	221
3.2. Introducing a hydrogen-bonding competitor	222
3.2.1. Swelling behaviour in urea	223
3.2.1. Synthesis of hybrid hydrogels with urea.....	224
3.2.2. Mechanical properties	224
4. Conclusion.....	227
References	229

Introduction

As presented in Chapter 2 and then shown in Chapter 4, the choice of the system is critical for the aimed properties. As far as the mechanical behaviour is concerned, elasticity, dissipation and fracture properties are strongly dependent of the structure of the network and on the silica/polymer network association life-time. In Chapter 2, we studied various architectures of single organic networks, changing the cross-linking density or the matrix/water content. Now that the reference SPx_PW0.14_R0.1 system has been well characterized, we propose to focus on the modification or alteration of this system in order to explore the impact of critical parameters, giving a particular attention to the versatility of the system to the desired physico-chemical and mechanical behaviours.

Here, three main components of the hybrid network system will be changed. First, the PDMA matrix will be concerned, in terms of cross-linking density and of swelling state: a ten times higher cross-linker content and the swelling equilibrium will be studied. Then the impact of the state of dispersion of the silica nanoparticles will be investigated in the framework of the macroscopic properties: a study based on aggregated silica nanoparticles will be described. Finally, we will pay attention to the physical interactions which are at the origin of the mechanical reinforcement. Two routes of tuning the polymer/silica interaction will be studied: changing the nature of the monomer and introducing a hydrogen-bond competitor in the formulation.

1. Tuning the PDMA matrix

1.1. Changing the cross-linking density

In Chapter 2, we characterised the PDMA matrix of hydrogels in details, with a special interest given to the effect of the cross-linking density. Moreover, pioneer works at the origin of this thesis concerned hybrid hydrogels based on PDMA and silica nanoparticles prepared without chemical cross-linker. The macroscopic properties of such systems were qualitatively similar to those of chemically cross-linked hydrogels but with a weaker contribution of the covalent matrix [1]. Starting from this preliminary work, we first choose to focus on the R0.1 system which offers the best compromise to carry out a comprehensive study on hydrogels with: a good ability to swell, an important deformability (compared to the other more cross-linked matrices) and a good reproducibility of the synthesis avoiding self-cross-linking process (in the case of the R0 hydrogels). The following step aims at investigating the impact of the same physical interactions in the framework of a harder PDMA matrix using 1 mol% of MBA, *i.e.* 10 times more than in the previous series.

1.1.1. Synthesis of hybrid hydrogels

The synthesis of these hybrid PDMA hydrogels is similar to the one described in Chapter 3 (1.b) with a fixed weight ratio between polymer and water equals to 0.14, corresponding to a fixed initial swelling of 8.5 that is used as a reference state for the mechanical analyses. The gels are also studied in this preparation state. The only difference is the molar ratio of cross-linker (MBA) to monomer which was set equal to 1 mol%. Therefore, a classical gel with a polymer concentration of 12.3 wt% and containing 1 mol% of MBA will be named:

“SP_x_PW0.14_R1”.

Typically, a gel prepared with 2 g of silica particles, 1 g of PDMA, 7.14 g of water and 1 mol% of MBA will be named SP2_PW0.14_R1. The formulation of hybrid hydrogels used in this chapter is given in **Table 1**.

Sample	Silica (g)	DMA (g)	MBA (mg)	KPS (mg)	TEMED (μ L)	H ₂ O (g)
SP0_PW0.14_R1	0	1.485	23	0.041	22.5	10.624
SP0.5_PW0.14_R1	0.744	1.485	23	0.041	22.5	10.624
SP1_PW0.14_R1	1.487	1.485	23	0.041	22.5	10.624
SP2_PW0.14_R1	2.975	1.485	23	0.041	22.5	10.624
SP3.5_PW0.14_R1	5.206	1.485	23	0.041	22.5	10.624
SP5_PW0.14_R1	7.437	1.485	23	0.041	22.5	10.624

Table 1: Formulation of PDMA hybrid hydrogels “SP_x_PW0.14_R1”.

1.1.2. Swelling measurements

The swelling theory of hydrogels and hybrid hydrogels as already been explained in Chapter 2 and Chapter 3. Swelling measurements of filled systems are a classical test to probe the level of interactions inside the network and an analytical model has been proposed by Berriot *et al.* [2].

Swelling experiments of PDMA hybrid hydrogels, with a cross-linking density of 1 mol% and containing silica nanoparticles Ludox-TM50 are represented on **Figure 1**. By comparison with the R0 and R0.1 series, we observe a weaker dependence of the swelling at equilibrium with the silica fraction. Contrary to the R0.1 system, with an obvious decrease of the swelling equilibrium values as the silica content is increased, most of the hybrid hydrogels of the R1 system swell in a very similar manner and reach an equilibrium value Q_e around 14. As shown in Chapter 2, this value is in good agreement with the phantom network theory, assuming a 42% cross-linking efficiency in the conditions of preparation and θ -conditions for the binary system PDMA/water. Experimental data (black dots) are compared to theoretical predictions of the model developed by Berriot *et al.* without considering the formation of a dry polymer layer at the particle interface (dotted line).

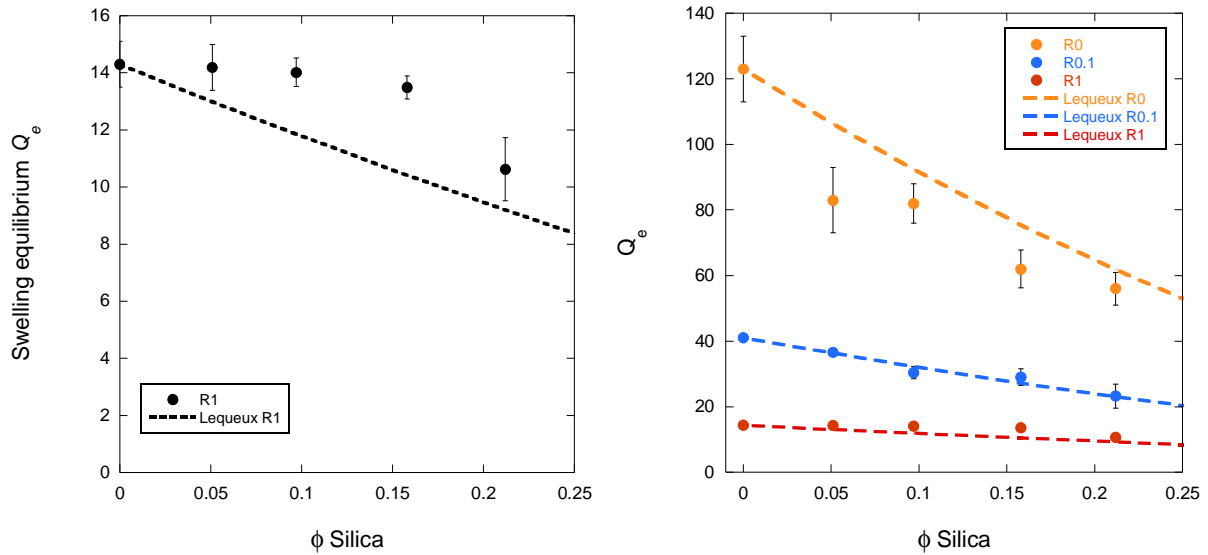


Figure 1: Left: variation of the swelling ratio at equilibrium Q_e in LiNO_3 0.5 M as a function of the volume fraction of silica for SPX_PW0.14_R1 hydrogels. Right: comparison of the normalized swelling equilibrium as a function of the volume fraction of silica for SPX_PW0.14_R0 (black triangles), SPX_PW0.14_R0.1 (white dots) and SPX_PW0.14_R1 (black dots) hybrid hydrogels.

From the right part of **Figure 1**, we can compare the relative deswelling induced by the presence of silica nanoparticles, as a function of the cross-linker density (for R0, R0.1 and R1). The swelling of the uncross-linked matrix (R0) is clearly the most affected by the silica content with a relative deswelling of 50% for 20 vol% of added silica. In the meantime, the R0.1 and R1 matrices deswell of 40 and 20%, respectively. The main reason of this difference comes from the cross-linking density which constrains the PDMA network and decreases the relative contribution of physical interactions. From a general point of view, we can consider that the swelling model of Berriot *et al.* describes fairly well the whole set of data, with certainly a poorer accuracy for the SP0_PW0.14_R0 sample that is used as reference to fit the R0 series.

As an intermediate conclusion of this part, we will keep in mind that silica nanoparticles still behave as adhesive filler inside the PDMA network, but not to the same relative extent as in the R0.1 system, and now we will investigate the mechanical properties of these nanocomposite hydrogels.

1.1.3. Mechanical properties

Reinforcement and time-dependence

The mechanical behaviour of hybrid hydrogels was investigated for the series of SP_x_PW0.14_R1 hydrogels, with *x* varying from 0 to 5. The typical stress-strain curves obtained at 0.06 s⁻¹ are represented in **Figure 2**.

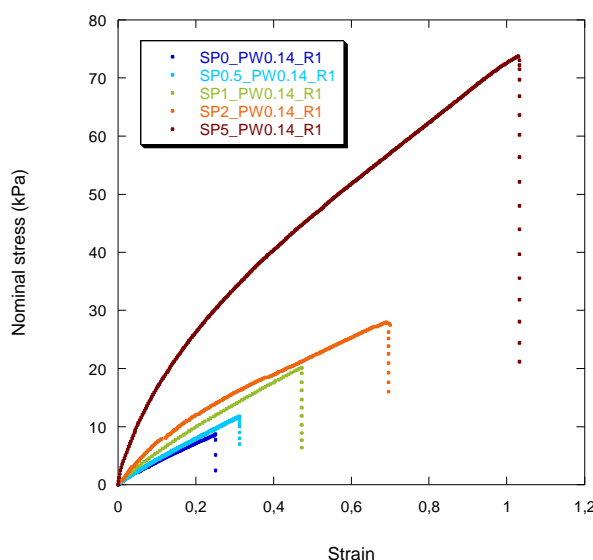


Figure 2: Effect of the silica content on tensile mechanical behaviour at 0.06 s⁻¹ for SP_x_PW0.14_R1, *x* = 0 (blue); 0.5 (light blue); 1 (green); 2 (orange); and 5 (brown).

Concerning the general mechanical behaviour, tensile properties strongly depend on silica content. As for the R0.1 matrix, a significant increase of the initial stiffness is observed as the volume fraction of nanoparticles gets higher. Moreover, the end of the curves, corresponding to the fracture of the sample, is also seen to increase in terms of strain at failure with the amount of silica. Interestingly, the presence of silica nanoparticles increases the strain at failure for both cross-linking density (in tensile tests) in the same extent: at 0.06 s⁻¹, the strain at failure of the SP5 system is around 4 times higher than the one of the SP0 matrix. From a general point of view, silica nanoparticles not only lead to a reinforcement of the initial modulus (presented in **Figure 3**) but also to a toughening of the material.

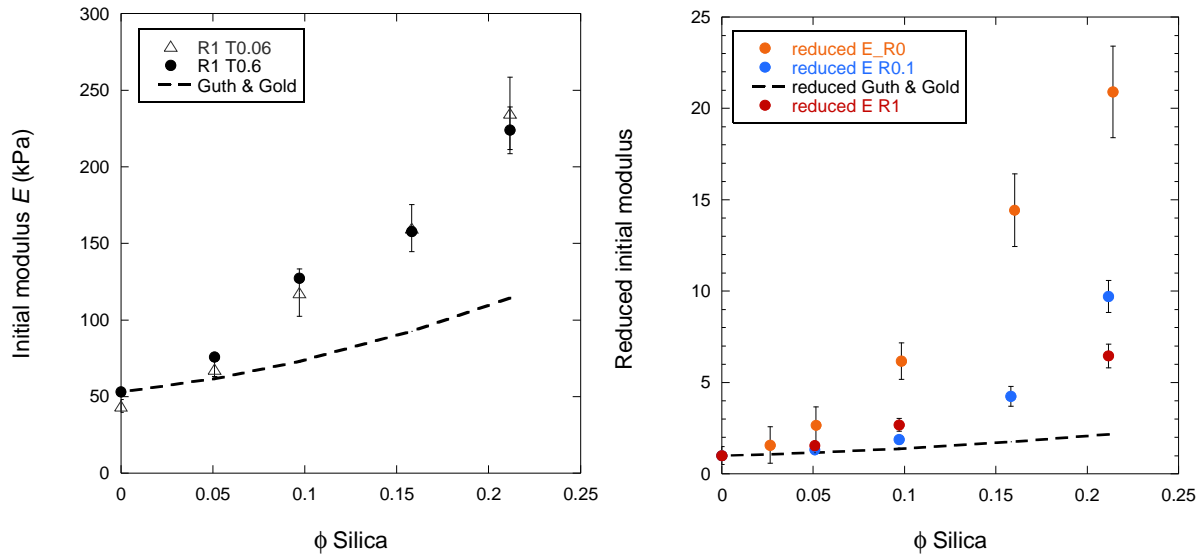


Figure 3: Left: Comparison of experimental values of initial modulus E for two nominal strain rates (0.06 s^{-1} in circles and 0.6 s^{-1} in open triangles) and theoretical values from Guth and Gold's model (dotted line).

Right: Comparison of reduced initial moduli for R0 (orange dots), R0.1 (blue dots) and R1 (red dots) series, obtained at 0.06 s^{-1} . The results are compared with Guth and Gold's model (in dotted line).

Nevertheless it is important to notice that the hydrogel series R1, which contain 1 mol% of chemical cross-linker, does not withstand high deformations ($\epsilon_{max} \leq 1$), contrary to the R0.1 series ($\epsilon_{max} \approx 7$) and to the uncross-linked hybrid networks ($\epsilon_{max} \approx 10$) [1]. This characteristic has ever been discussed in Chapter 2 concerning the pure PDMA matrix (SP0_PW0.14_Rz series) and was at the origin of our choice to study in details the SPx_PW0.14_R0.1 system. This difference of deformability of the matrix is also at the origin of the difference observed in the relative intensity of the reinforcement. As a matter of fact, the effect of the silica nanoparticles on the initial modulus of the different cross-linked systems can be seen by comparing the normalized initial moduli, as presented in the right part of **Figure 3**.

Note that the strain rate effect on initial modulus is relatively weak as the values of initial modulus obtained at 0.06 s^{-1} and 0.6 s^{-1} are relatively close, as represented in **Figure 3** left.

As explained for the SP_x_PW0.14_R0.1 system in Chapter 4, we assumed that the concept of double network structure is correct, coming from the presence of permanent chemical cross-linking points and dynamic physical ones (see **Table 2**). Then, at short time-scales, the behaviour is controlled by the integrity of the network:

$$E_{t \rightarrow 0} = E_x + E_{Si} \left(\frac{n_x + n_{Si}}{n_x} \right) \frac{k_B T}{V_0} \quad \text{Eq. 1}$$

with E_x the initial modulus of the covalent matrix, E_{Si} the modulus of the transient network, respectively proportional to the numbers of cross-linking points of both nature (chemical in the case of n_x and physical for n_{Si}).

	SP0	SP5_PW0.14_Rz			
Rz (mol%)	E_x (kPa)	$E @ 0.6 \text{ s}^{-1}$ (kPa)	$E @ 0.06 \text{ s}^{-1}$ (kPa)	$E/E_x @ 0.6 \text{ s}^{-1}$ (kPa)	$E/E_x @ 0.06 \text{ s}^{-1}$ (kPa)
0	1	74.2	22	74	22
0,1	10	170	102	17	10
1	44	224	220	5	5

Table 2: Initial moduli values for SP5_PW0.14_Rz at 0.06 s^{-1} and 0.6 s^{-1} as a function of the cross-linking ratio, E_x being the modulus of the pure chemical network (SP0).

Figure 4 reports the evolution of the initial moduli of SP5 as a function of the chemical cross-linking density. For comparison purpose, the moduli of the corresponding pure chemical networks are plotted (in blue). It appears that the number of elastically active chains involved in transient junctions (E_{Si}) does not appear to be strongly affected at 0.6 s^{-1} by the cross-linking density of the matrix from R0.1 to R1. However, reducing the distance between chemical cross-links implies a drastic reduction in the ratio of elastic chains bridged by nanoparticles to the number of elastic chains of the covalent network. For a given distance between particles (*i.e.* a fixed volume fraction of silica corresponding to SP5), the ratio E_{Si}/E_x is observed to decrease with Rz, as expected from the deswelling behaviour previously discussed.

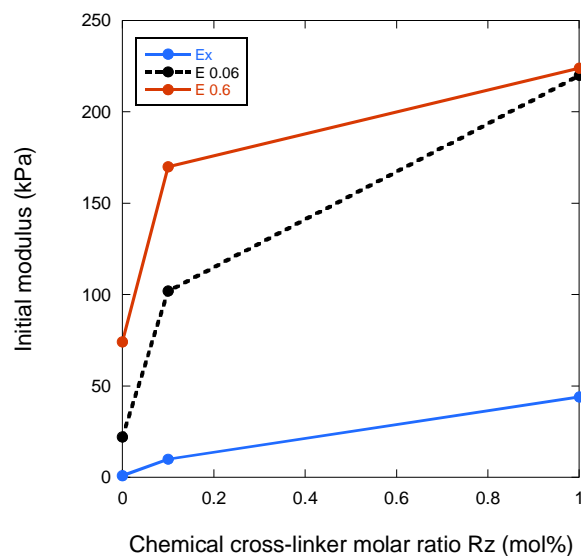


Figure 4: Initial moduli of SP5_PW0.14_Rz versus chemical cross-linker ratio (at 0.06 s^{-1} in black dots and at 0.6 s^{-1} in red dots). SP0_PW0.14_Rz initial moduli E_x is given in blue dots.

Dissipation processes

Relaxation experiments were carried out on the R1 series (see **Figure 5** left) reducing the initial strain to 10% compared to the R0.1 series, in order to avoid fracture during testing, especially of the SP0_PW0.14_R1 hydrogel.

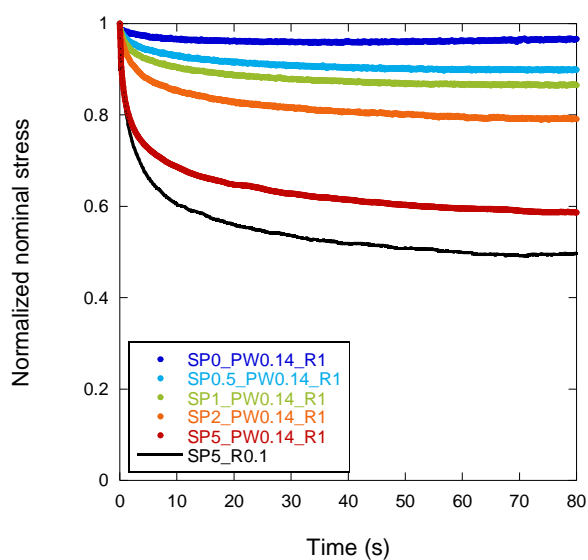


Figure 5: Relaxation experiments with an initial strain equal to 10%, on SPx_PW0.14_R1 hydrogels. Left: evolution of the normalized nominal stress as a function of time. Comparison with SP5_PW0.14_R0.1 (in black) with an initial strain of 30%.

Focusing at intermediate time-scales, typically below 50 seconds, a common characteristic time of the relaxation process has been evidenced: this characteristic time is about 14 seconds as the one obtained for the SPx_PW0.14_R0.1 system. This result shows that changing the cross-linking density by a factor 10 does not lead to a significant change in the association but only to a decrease of the amplitude of the stress relaxation process.

Strain-controlled tensile loading-unloading cycles were carried out up to 10% of strain. The typical obtained curves obtained at 0.06 s^{-1} are represented on **Figure 6** left.

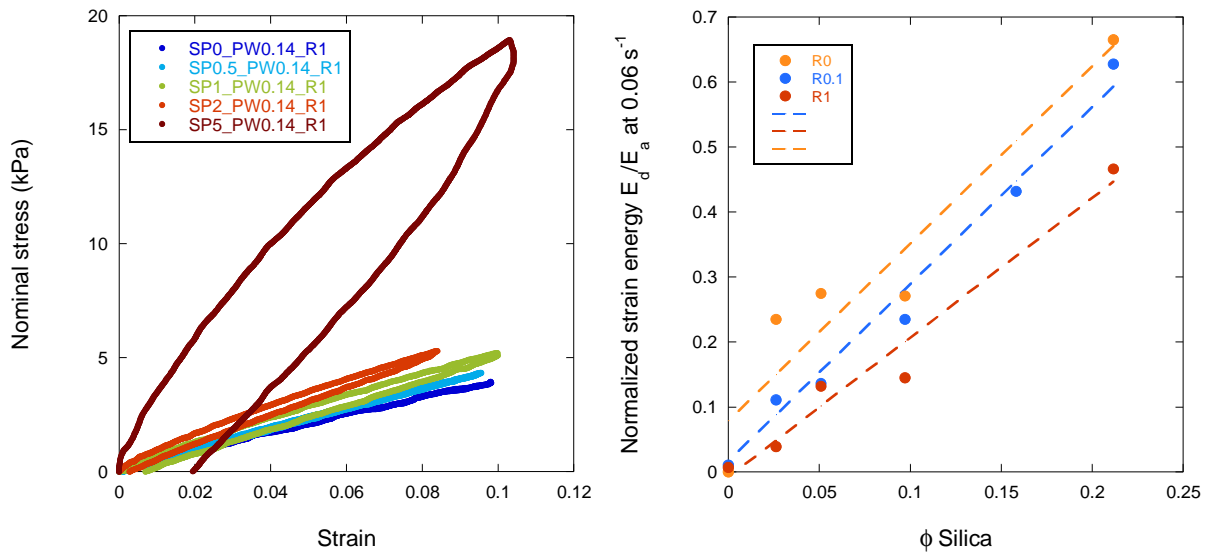


Figure 6: Left: effect of the silica content on the first loading-unloading cycle at 0.06 s^{-1} for SPx_PW0.14_R1, with $x = 0; 0.5; 1; 2$ and 5 .

Right: normalized strain energy E_d/E_a for SPx_PW0.14_Rz series at 0.06 s^{-1} , E_a being the applied strain energy. The maximal strain was varied from 50 %, 30 % and 10 % for R0 (in orange), R0.1 (in blue) and R1 (in red) respectively.

From the curves presented in **Figure 6** left, the dissipated strain energies, E_d , were calculated for each cycle, as explained in Chapter 4, plotted and compared to the other series with different cross-linking densities, in **Figure 6** right. E_d was normalized by the strain applied energy E_a (the area under the loading curve). The general trend is almost the same as for the reference system but with a weaker dependence with the silica volume fraction. Indeed,

hybrid hydrogels prepared with a high level of cross-linking display a lower amplitude of the dissipation component as well as a reduction of the residual strain after loading.

On the other hand, no damage mechanisms have been pointed out (at the standard strain rate 0.06 s^{-1}) in the strain range investigated, since the D values obtained are typically in the uncertainty of the modulus determination. As far as the recovery is concerned, the SPx_PW0.14_R1 hydrogels behave like the reference system ten times less cross-linked: at low strain rate almost no damage is observed, the difference of successive moduli is on the same order than the standard deviation. The typical duration of a loading cycle up to 10% of strain provides enough time to the system to recover its initial properties.

Fracture experiments

The fracture behaviour of SPx_PW0.14_R1 hydrogels is shown in **Figure 7**. The factor ten in the cross-linking density leads to values of fracture energies ten times lower than in the SPx_PW0.14_R0.1 case (**Figure 7** right). Even if the polymer network is very constrained by the high level of covalent cross-links, the attractive interaction between the silica nanoparticles and the PDMA matrix is responsible for the remarkable fracture toughness.

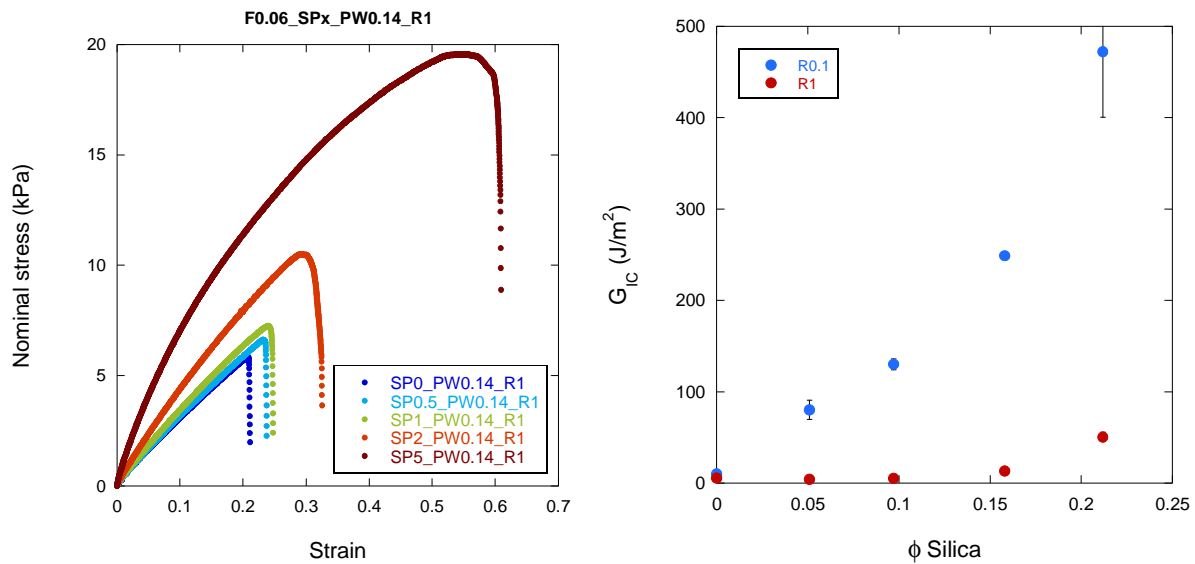


Figure 7: Left: effect of the silica content on fracture behaviour, at 0.06 s^{-1} for SPx_PW0.14_R1.
Right: comparison of fracture energies for R0.1 and R1 series, at 0.06 s^{-1} .

For a comparison purpose, fracture experiments are difficult to perform on the R0 series because of the very high strains reached by those chemically uncross-linked samples: SP5_PW0.1_R0 samples can reach fracture energies of more than 850 J/m².

As observed for the SP_x_PW0.14_R0.1 series, increasing the strain rate by a decade leads to a decrease in fracture energies.

SANS under deformation

2D SANS patterns of the SP5_PW0.14_R1 hybrid hydrogel under deformation are presented in **Figure 8**.

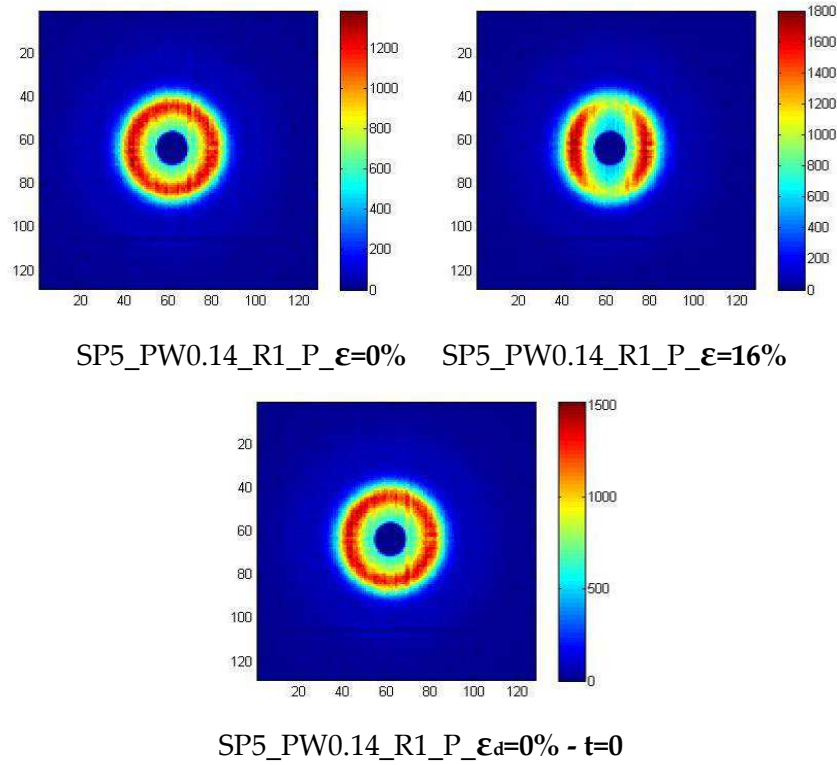


Figure 8: 2D-SANS images of SP5_PW0.14_R1 hybrid hydrogel. Left up: isotropic spectrum of unstrained sample ($\epsilon=0\%$) Right up: loading of $\epsilon=16\%$. Down: unloading to $\epsilon=0\%$.

First, we can verify that the sample had not been pre-stretched as the first SANS image is isotropic. As soon as the hybrid hydrogel is stretched, a double wing pattern appears: in other words, there is an increase of the scattering intensity in the parallel direction and a

decrease along the perpendicular one. Then the sample is unloaded and the isotropic pattern is recovered.

The visualisation of the total recovery of the isotropic shape for SP5_PW0.14_R1 hybrid hydrogel loaded up to 16% of strain is in agreement with the mechanical behaviour previously studied. As a matter of fact, no aggregation of the silica nanoparticles is observed, the aggregation would have induced a modification of the initial stiffness. In the case of the SPx_PW0.14_R0.1 filled hydrogels, the loading of hybrid samples up to high strains, above the critical deformation at which collisions between particles are effective (83% for SP5 samples), lead to irreversible damages. The same level of deformation is difficult to observe with the SPx_PW0.14_R1 system as it is close to its breaking limit.

1.2. Changing the swelling state

The aim of this part is to study of the mechanical properties of hybrid hydrogels fully swollen in water. First, the effect of pH has been studied in order to prevent any experimental error coming from a difference of pH. For that reason, we used four different aqueous media for swelling: pure deionized water, water at pH 5, water at pH 9 and water at pH 11. Experimentally, no difference in swelling equilibrium has been observed at the four different pH values for all the SPx_PW0.14_R0.1 hydrogel formulations: the experimental values are in the error bars. Moreover, the mechanical tensile tests performed on hydrogels swollen at different pH do not show any difference. From these preliminary results, we chose to focus our study on hybrid hydrogels swollen in pure water, without any control of the pH.

It is important to remind that the silica nanoparticles remain into the swollen hydrogels, as shown in Chapter 3 by titration of extractible and by the comparison of SEM images of the SP5 surface before and after swelling.

1.2.1. Mechanical properties at swelling equilibrium

Our first strategy consisted on testing the properties of gels at well-defined conditions, implying mechanical characterisation in the so-called preparation state. As demonstrated by swelling measurements, the preparation state is far from the thermodynamic equilibrium. Now we will focus our study on the fully swollen hydrogels, *i.e.* with swelling ratio at equilibrium. In **Table 3**, some characteristics of the gels are compared at the preparation state and at the swelling equilibrium.

	SP0_PW0.14_R0.1		SP5_PW0.14_R0.1	
	at Q_0	at Q_e	at Q_0	at Q_e
Swelling ratio	8.5	42 ± 0.8	8.5	33 ± 1.1
Silica volume fraction ϕ_{Si}	0	0	0.21	0.05
Q_e/Q_0 ratio	4.9		3.9	
Pre-stretch ratio $\lambda = \left(Q_e/Q_0\right)^{1/3}$	1.0	1.7	1.0	1.6
Initial modulus (kPa)	10.5 ± 0.4	5.1 ± 0.5	102 ± 9.2	8.0 ± 0.8
E_d (kJ.m⁻³)	0	-	1.47 ± 0.24	-

Table 3: Physico-chemical parameters of SP0 and SP5_PW0.14_R0.1 hydrogels at the preparation and swollen states.

As presented in **Figure 9**, the tensile behaviour is highly impacted by the swelling state with a large decrease of the initial moduli (**Table 3**) and the strain at break. The effect of swelling is clear: at swelling equilibrium both modulus and strain at failure decrease. The general tensile behaviour is also deeply modified: initial softening observed at Q_0 is fully removed at Q_e . More interestingly, the decrease of the initial modulus goes together with a total loss of dissipation fully vanishes at Q_e , as presented in **Figure 10**. In the right part of **Figure 10**, cycles were normalized by the maximal stress for comparison purpose. With this representation, the effect of swelling on the loss of reinforcement and dissipation is even more noticeable, in terms of initial modulus and energy dissipation.

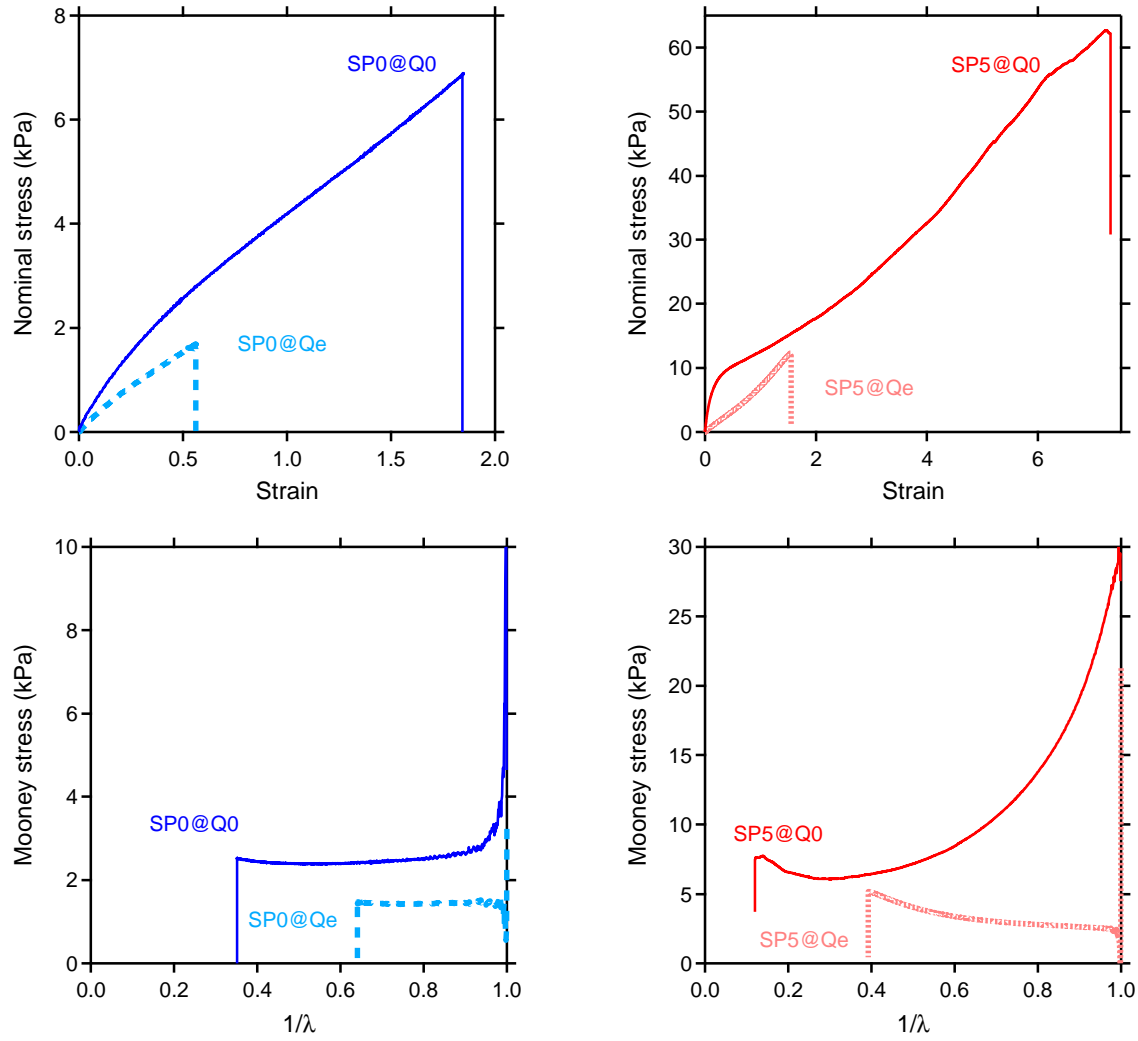


Figure 9: Comparison of the tensile behaviour (at 0.06 s^{-1}) at Q_0 and Q_e for the covalent SP0 gel and the SP5 hybrid one. Up: classical representation. Down: Mooney stress.

Stress relaxation experiments showed a similar behaviour. The stress relaxation experiments were conducted on swollen hydrogels but with an adaptation of the imposed initial strain: indeed, the strain at failure of the swollen samples is dramatically decreased compared to the reference system, as represented in **Figure 9**. A comparison of the curves for the SP5_R0.1 gel is given in **Figure 11**. Concerning the SP0 sample, we did not observe any effect of swelling on the relaxation experiment as the unfilled hydrogel does not relax, whatever its swelling state.

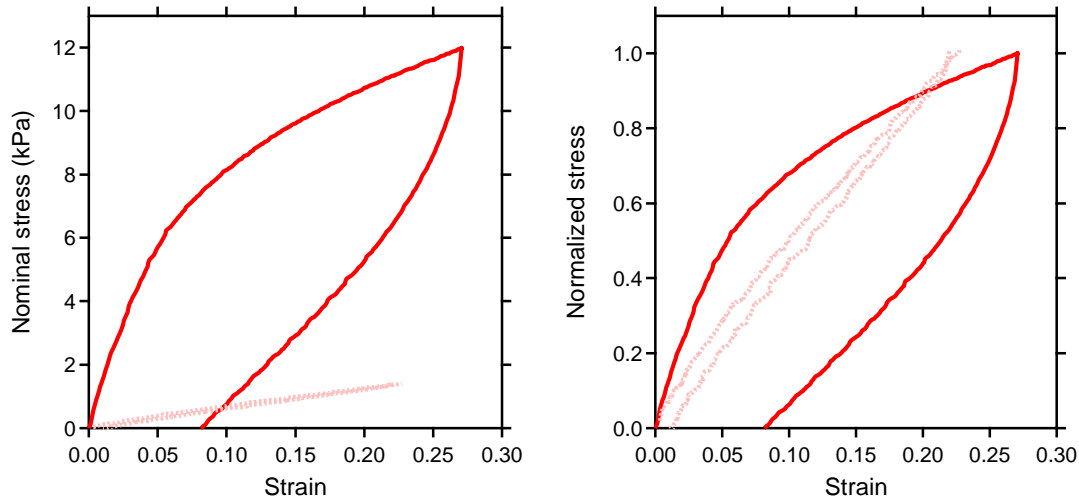


Figure 10: Effect of swelling conditions on the dissipation under cycling (at 0.06 s^{-1}): at preparation conditions Q_0 (red solid line) and at swelling equilibrium Q_e (pink dotted line). Left: nominal stress versus strain. Right: normalized stress versus strain.

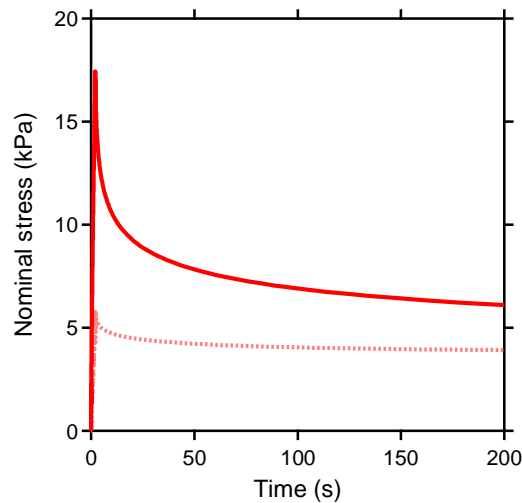


Figure 11: Effect of swelling conditions on relaxation experiments: preparation conditions Q_0 (red line) and swelling equilibrium Q_e (dotted line) for the SP5_R0.1 formulation.

As far as the relaxation experiments performed at high silica content are concerned, the comparison with the reference state is interesting. Concerning the amplitude of relaxation, the difference between the two systems is very important. Both cycling and relaxation experiments evidenced that exchange processes described in Chapter 4 are screened at the swelling equilibrium state.

1.2.2. SANS under deformation

A set of experiments on swollen hydrogels has been conducted by SANS, using the load-cell specially designed and previously described in Chapter 4. For that purpose, a SP5_PW0.14_R0.1 sample has been swollen in the solvent matching the PDMA network (solvent P) in order to follow the scattering of the silica nanoparticles under deformation.

The results are shown in **Figure 12** with the hybrid hydrogel SP5_R0.1 studied under incremental strain, from $\varepsilon = 0$ to 34 %. In these swelling conditions, particles are very far from each other and dramatic collisions between particles in the transverse direction are not expected during stretching.

First we can notice that the swelling of the hydrogel up to the equilibrium does not affect the silica state of dispersion. The unstrained sample always displays an isotropic pattern with a circular diffraction ring corresponding to the maximum of the scattering curve. This maximum is shifted at low q (larger distances between particles) by comparison with the sample in the preparation state. When the sample is stretched along the X-direction, we observe an increase of the average distance between silica particles along the same direction while this distance decreases in the perpendicular direction, due to transverse compression. This phenomenon is progressively observed when the strain is increased.

A simple estimation of the critical deformation at which collisions between particles appear can be calculated assuming the simple cubic lattice of silica particles described in Chapter 4. For swollen SP5_R0.1 hydrogels, the critical strain is $\varepsilon_{cr} = 351\%$ which has to be compared with the strain at failure experimentally observed which was always below 200%: the silica nanoparticles contact cannot be observed by SANS because of the limited stretchability of the swollen system.

After stretching the swollen SP5 sample up to 34%, its SANS spectrum was recorded again immediately after unloading to 0%, as presented shown in the last image of **Figure 12**. The isotropic figure was almost immediately recovered: only a slight difference is noticeable with the image of the initial unstrained state. This observation is in good agreement with the cycling tests previously presented.

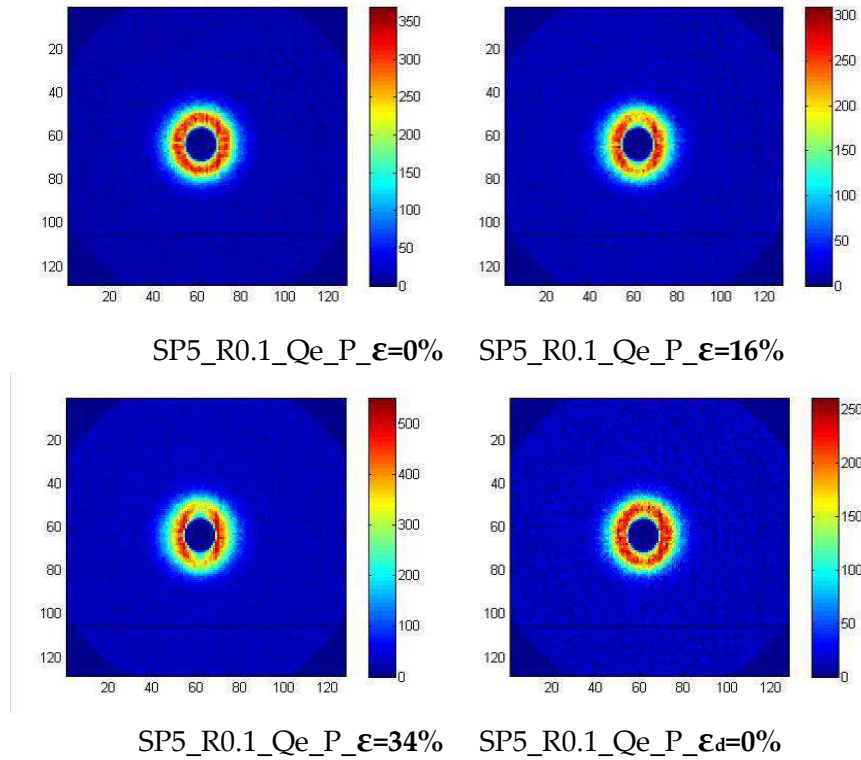


Figure 12: 2D-SANS images of SP5_R0.1_Qe hybrid hydrogel. Left up: isotropic spectrum of unstrained sample ($\epsilon=0\%$). Right up: loading to $\epsilon=16\%$. Left bottom: loading to $\epsilon=34\%$. Right bottom: unloading to $\epsilon=0\%$.

As a conclusion, we can say that the role of silica nanoparticles in the reinforcement of mechanical properties is much weaker when the hydrogel is swollen although it has not totally disappeared. Only the amplitude of physical associations is reduced, due to the dilution of PDMA chains and silica nanoparticles. By comparison with associating systems, it seems that the formation of a percolating network based on PDMA/silica interactions is critical to get macroscopic properties. Below a certain concentration of silica particles, as initially prepared for a given polymer/water ratio (see SP0.5 or SP1) or as obtained after swelling the SP5 sample, the level of physical connectivity becomes too low to provide any efficient reinforcement effect.

An interesting study would be to investigate hybrid hydrogels at different intermediate levels of swelling, between Q_0 and Q_e , in order to analyse the reinforcement behaviour as a function of concentration for a fixed polymer/silica content. A progressive diminution of reinforcement could be expected in this case.

Finally, a schematic picture of the swollen system is suggested in **Figure 13**, comparing the fully swollen state to the preparation state. The two representations have been reproduced in order to give an accurate idea of the swelling effect on the size of samples. At the preparation state, dissipation has been evidenced, coming from PDMA/silica exchanges. At the swelling equilibrium state, there is no dissipation, proof of the screening of the PDMA/silica exchanges.

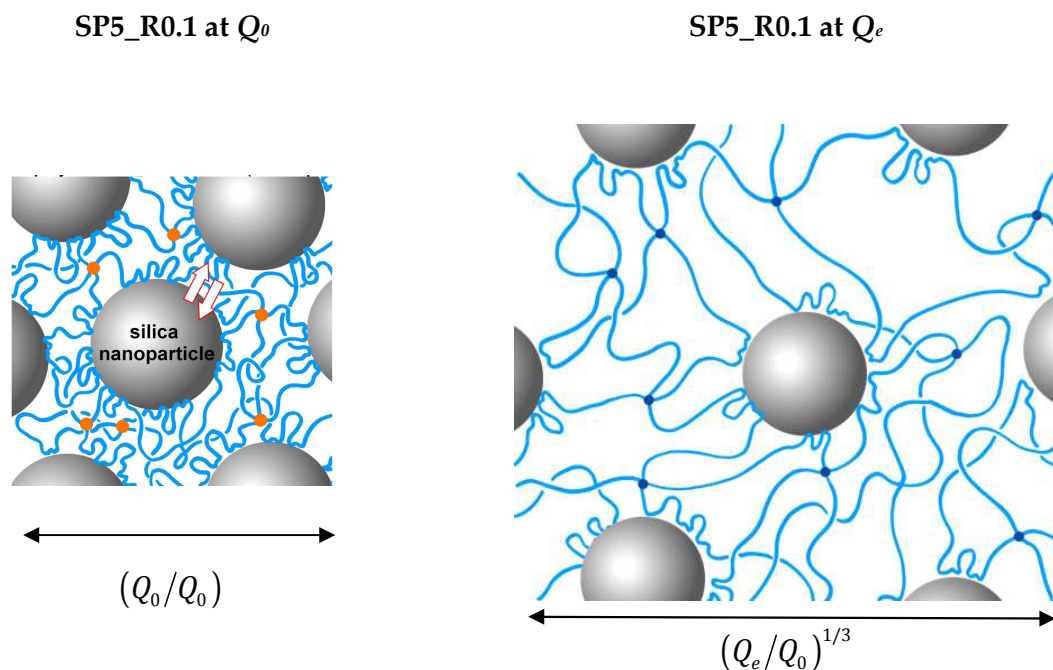


Figure 13: Schematic representations hybrid hydrogel SP5_R0.1. Left: at the preparation state (Q_0). Right: at the swelling equilibrium state (Q_e).

2. Changing the dispersion state of silica particles

As described in Chapter 1, the pH is a key factor for the formulation of hybrid hydrogels since it strongly impacts the stability of silica dispersion, before and during the synthesis. Here, we chose to prepare hybrid hydrogels at pH 5 in order to destabilize the silica particles with the aim of forming a complex material made of one inorganic silica network embedded into a polymer cross-linked matrix. In the following, we will mainly focus on the impact of the inorganic network on the macroscopic behaviour of the gels (swelling properties and mechanical properties).

2.1. Synthesis of hybrid hydrogels

The synthesis of hybrid PDMA hydrogels at pH 5, with Ludox-TM50 is quite different from the one described in Chapter 3. As a matter of fact, preliminary tests of synthesis of hybrid hydrogels at pH 5 led to the observation that when KPS and TEMED are used to initiate the polymerization, the reaction starts immediately. Thus, it is not possible to introduce the mixture into the moulds. For that reason, we used the thermal decomposition of KPS to initiate the radical polymerization.

PDMA hybrid hydrogels were prepared at 80°C by in-situ free radical polymerization of DMA using *N,N'*-methylenebisacrylamide (MBA) as cross-linker. After dilution of the silica suspension Ludox-TM50 in water, the pH is set equal to 5. MBA (in solution), DMA and KPS (in solution) are added and the mixture is deoxygenated under nitrogen flow during 15 minutes. The mixture is then transferred through a needle into sealed moulds initially filled by nitrogen gas. The hole created by the needle is rapidly closed in order to prevent any entry of oxygen. The moulds containing the mixture are placed in an oven at 80°C during 24 hours.

This hydrogels matrix of the studied systems is quite similar to the “SPx_PW0.14_R0.1” one, with a fixed weight ratio between polymer and water equals to 0.14. The gels are studied in this preparation state. The molar ratio of cross-linker (MBA) to monomer was set equal to 0.1

mol%. The weight ratio between silica and polymer is varied from 0 to 5. The nomenclature used is quite similar to the classical one: a gel with a polymer concentration of 12.3 wt% and containing 0.1 mol% of MBA will be named:

“SP_x_PW0.14_R0.1_pH5”.

Typically, a gel prepared at pH 5 with 2 g of silica particles, 1 g of PDMA, 7.14 g of water and 1 mol% of MBA will be named SP2_PW0.14_R0.1_pH 5. The formulation of hybrid hydrogels used in this chapter is given in **Table 4**.

Samples	Silica (g)	DMA (g)	MBA (mg)	KPS (mg)	TEMED (μL)	H ₂ O (g)
SP0_PW0.14_R0.1_pH5	0	1.485	2.3	0.041	22.5	10.624
SP2_PW0.14_R0.1_pH5	2.975	1.485	2.3	0.041	22.5	10.624
SP5_PW0.14_R0.1_pH5	7.437	1.485	2.3	0.041	22.5	10.624

Table 4: Formulation of PDMA hybrid hydrogels at pH 5 “SP_x_PW0.14_R0.1_pH5”.

After the synthesis, the PDMA hybrid hydrogels synthesized at pH 5 look very different from the reference PDMA hybrid hydrogels. Contrary to the transparent and colourless PDMA/silica gels previously studied, opaque hydrogels are obtained at pH 5, as shown in **Figure 14**.



Figure 14: Pictures of hybrid hydrogels synthesized at pH 5. Left: SP0, centre: SP2, right: SP5.

This turbidity comes from the destabilization of the silica suspension when the pH is lowered by adding hydrogen chloride. As presented in Chapter 1, the stability of a colloidal system is a complex balance between antagonistic forces. Changing the pH of an initially

stable colloidal suspension can lead to the aggregation of the particles into clusters; in this case, the interparticle attractive interactions (such as Van der Waals forces) prevail over the repulsive ones (such as electrostatic forces).

2.2. Swelling measurements

The swelling ability of these hybrid hydrogels synthesized at pH 5 appears to be complex. As a matter of fact, the inorganic network that was formed by the aggregation of the silica nanoparticles has a strong effect on the macroscopic behaviour of the material. In **Figure 15** the evolution of the normalized swelling equilibrium in water is represented as a function of the silica volume fraction: no major difference is revealed as the swelling equilibrium values are close to the reference PDMA hydrogel.

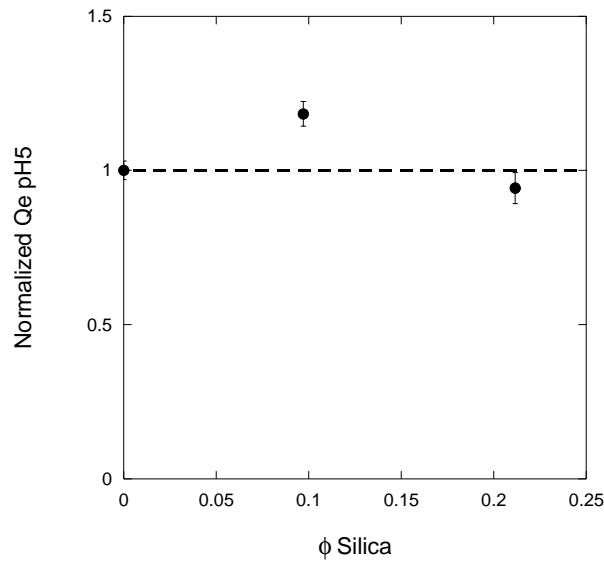


Figure 15: Variation of the normalized swelling ratio at equilibrium Q_e as a function of the volume fraction of silica for SPX_PW0.14_R0.1_pH5 hydrogels in water.

In spite of attractive interactions between PDMA and silica surface that are expected at pH 5, it seems that the aggregation of silica particles (inducing a large decrease of the specific surface of inorganic materials offered to PDMA) is responsible for the weaker sensitivity of the swelling behaviour to these specific interactions. On the other hand, the swelling ability

of the hybrid networks prepared at pH 5 also demonstrates that the clusters of aggregated particles are able to dissociate under osmotic stress.

2.3. Mechanical properties

The impact of the aggregation of silica nanoparticles on the mechanical properties of hybrid hydrogels has been investigated by tensile tests carried out at 0.06 s^{-1} as presented on **Figure 16**. We can observe that the general shape of the curves is identical to the one of the reference system. Concerning the first part of the curves, the SP5_PW0.14_R0.1_pH5 specimen shows a very high initial modulus that is drastically higher compared to the SP5_PW0.14_R0.1, the same behaviour being observed at 0.6 s^{-1} . The mean values of initial moduli are given in **Table 5**.

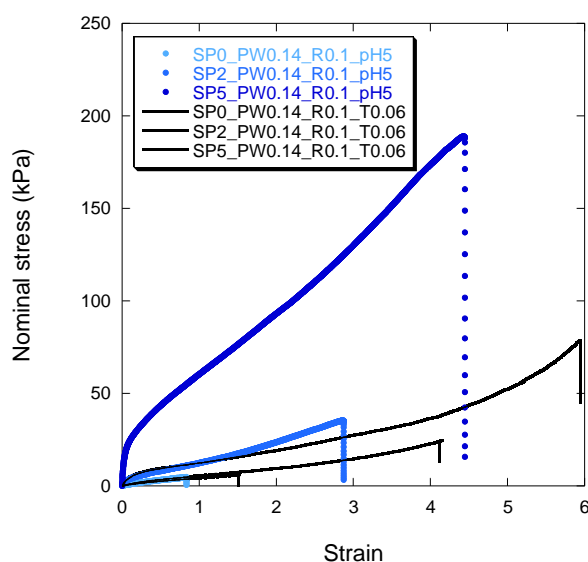


Figure 16: Tensile mechanical behaviour of hybrid PDMA hydrogels synthesized at pH 5, with a nominal strain rate of 0.06 s^{-1} , for SPx_PW0.14_R0.1_pH5 with $x = 0$ (in light blue); 2 (in blue) and 5 (in dark blue). The black curves are given for a comparison purpose as it corresponds to the reference system SPx_PW0.14_R0.1.

The presence of an aggregated network of silica particles has the same consequence on the large strain mechanical properties, at the two strain rates. The hard silica network first prevents the polymer chains from stretching, but as soon as this inorganic network is broken, the PDMA chains are extended and provide high strains before break. The high values of

initial modulus correspond to the silica network, much harder than the polymer part of the system. The breakage of the silica network has been verified by cyclic experiments at two different strain rates. The curves of the first cycles are presented in **Figure 17** at 0.06 s^{-1} , the general trend was identical at 0.6 s^{-1} .

	$E \text{ (kPa) at } 0.06 \text{ s}^{-1}$		$E \text{ (kPa) at } 0.6 \text{ s}^{-1}$		Guth and Gold's model
	SPx_PW0.14_R0.1	at pH 5	SPx_PW0.14_R0.1	at pH 5	
SP0	10.5 ± 0.4	11.2 ± 0.3	11.2 ± 0.3	15.9 ± 2.6	10.5
SP2	19.8 ± 1.6	71.0 ± 4.9	28.1 ± 0.6	56.2 ± 0.7	14.4
SP5	102 ± 9.2	1917 ± 88	170.0 ± 9.3	1357 ± 80	22.7

Table 5: Comparisons of initial moduli E (in kPa) for hybrid PDMA hydrogel synthesized at pH 5, hybrid PDMA hydrogel and theoretical values from Guth and Gold's model, at 0.06 s^{-1} and 0.6 s^{-1} .

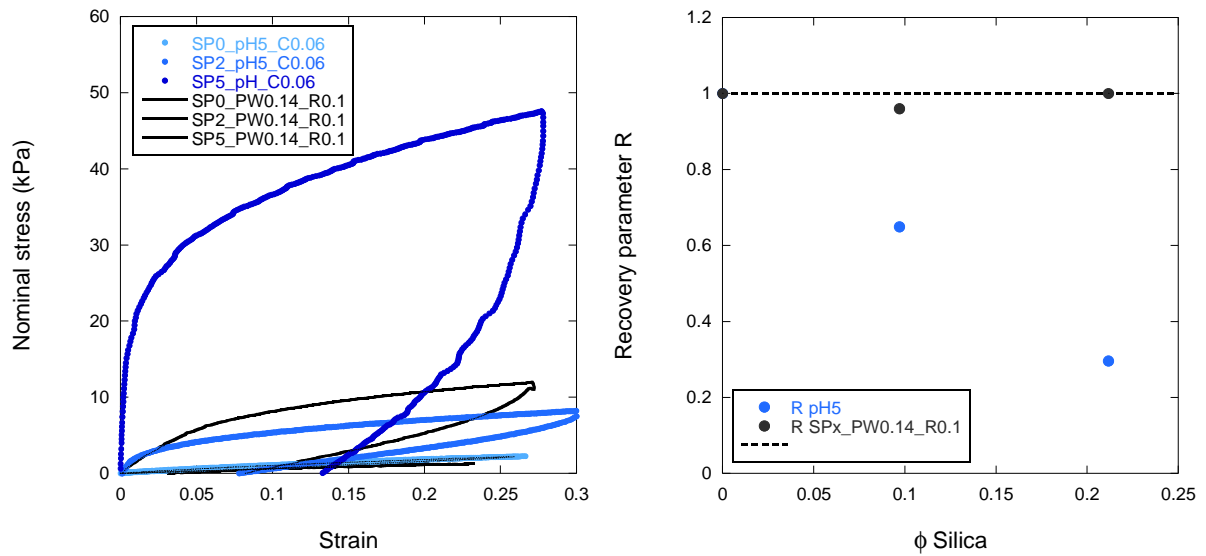


Figure 17: Left: cycling experiments on hybrid PDMA hydrogels synthesized at pH 5, with a nominal strain rate of 0.06 s^{-1} , for SPx_PW0.14_R0.1_pH5 with $x = 0$ (in light blue); 2 (in blue) and 5 (in dark blue). The black curves are given for a comparison purpose as it corresponds to the reference system SPx_PW0.14_R0.1.

Right: Recovery parameter R for hybrid PDMA hydrogel synthesized at pH 5 at 0.06 s^{-1} (blue dots) compared to the one obtained at the synthesis state (black dots).

As discussed on the tensile tests, the initial modulus is much higher in the case of the gels synthesized at pH 5, inducing an important hysteresis. From the shape of the curves at small strains, we can imagine that the silica networks breaks rapidly as the initial slope starts to decrease around a strain of 0.01. This macroscopic transition can be verified by the determination of the initial moduli of the following loading cycles. From the values, the recovery parameter can be calculated; it is presented for 0.06 s^{-1} in **Figure 17** (right). As a matter of fact, the recovery parameter between the first and the second cycle strongly decreases when the silica content is increased: the loading up to 30% strain leads to a break of the silica network.

As a conclusion, we succeeded in building an inorganic network of silica, from silica nanoparticles in suspension, combined to a PDMA network. The state of dispersion of silica particles is an interesting tool to tune the macroscopic properties of hybrid hydrogels. Even if we do not really control the aggregation process of the silica nanoparticles, the mechanical tests clearly emphasized that the percolating network of silica provides a very high toughness at low strain. However, it rapidly breaks, leading to a softer behaviour at high strains as described for hybrid hydrogels. The strain at break drastically decreased compared to the reference system, certainly due to the strong heterogeneity of the silica dispersion. Nevertheless, the level of dissipated energy is very high and ultimate properties are not so bad compared to the organic network.

3. Playing with the magnitude of interactions

In the first part of this chapter, we studied the structure/properties relationships of hybrid networks by changing some physical parameters of the polymer matrix such as the cross-linking density and the swelling state. Then in a second part, we modified the filler distribution by aggregating the silica nanoparticles at lower pH. Another way to change our reference system is to directly modify the interactions involved in the mechanical reinforcement. One possibility to tune the polymer/silica interactions is to exchange the DMA monomer against acrylamide, which is known to weakly interact with silica. Another simple possibility is the introduction of a hydrogen-bonding competitor in the system like urea.

3.1. Changing the monomer

Acrylamide forms polymer chains that do not interact with silica nanoparticles. This behaviour, which is very well-known in electrophoresis applications [3], has been used by Petit *et al.* to design hybrid associating systems. These physical assemblies shown in **Figure 18** are based on specific interactions between silica nanoparticles and PNIPAm or PDMA side-chains grafted onto an “inert” backbone of poly(acrylamide-co-sodium acrylate) or PAAm [4].

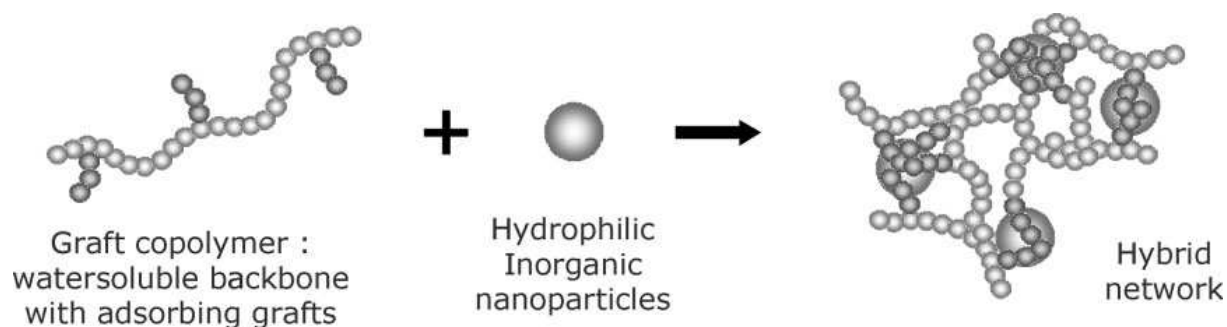


Figure 18: Schematic representation of hybrid network obtained from self-assemblies between adsorbing grafts (dark side chains) and inorganic nanoparticles [4].

3.1.1. Synthesis of hybrid hydrogels

Hybrid hydrogels based on homopolymers and copolymers of acrylamide and *N,N*-dimethylacrylamide were synthesised as follows. Hybrid hydrogels were prepared by in-situ free radical polymerization of DMA and AAm using *N,N'*-methylenebisacrylamide (MBA) as cross-linker and thermal dissociation of KPS as initiator, at 80°C. Two aqueous solutions are prepared: KPS at 4.5wt% and MBA at 1.2 wt%. First, MBA solution and DMA and/or AAm were dissolved at 25°C in water, in presence of an aqueous suspension of silica particles. The KPS solution is added and the homogeneous suspension is purged with nitrogen during 15 minutes under magnetic stirring. The mixture is finally transferred, under nitrogen atmosphere, into appropriate laboratory-made moulds previously sealed and put under nitrogen atmosphere. The sealed moulds are placed in an oven at 80°C for 24 hours. The samples were left for 24 h in a closed vessel under nitrogen atmosphere before use.

This formulation of these new hydrogels is similar to the “SP_xPW0.14_R0.1” one. Since the total monomer concentration was kept to 12.3 wt%, the DMA concentration to the total gel weight is $12.3 \cdot \omega_{\text{DMA}}$ (wt%). The composition of the polymer matrix is named using the weight fraction of DMA:

$$\text{“SP}(\omega_{\text{DMA}} 0.7)\text{x_PW0.14_R0.1”}.$$

3.1.2. Structural investigations

The use of a thermal initiation in the case of the AAm hydrogels comes from preliminary experiments. As a matter of fact, even without silica particles, redox initiation of acrylamide led to turbid PAAm hydrogels, revealing a higher heterogeneity of the polymer matrix. This observation is in good agreement with the work of Okay *et al.* who show that, in similar concentrations and cross-linking conditions, PAAm hydrogels are less homogeneous than PDMA ones [5]. Moreover, when AAm is polymerized in the presence of silica nanoparticles, a weak aggregation process is also observed. This aggregation behaviour is emphasized in **Figure 19** with the comparison of SANS data obtained with two SP2_PW_R0.1 hybrid hydrogels synthesized by redox initiation, either with DMA or AAm. Changing the monomer nature from an interacting one to a non-interacting one leads to an increase of the

scattered intensity at low- q values. As discussed in Chapter 3, the flocculation of colloidal particles induced by non adsorbing polymers can originate from the formation of a depletion layer of polymer chains near the particles.

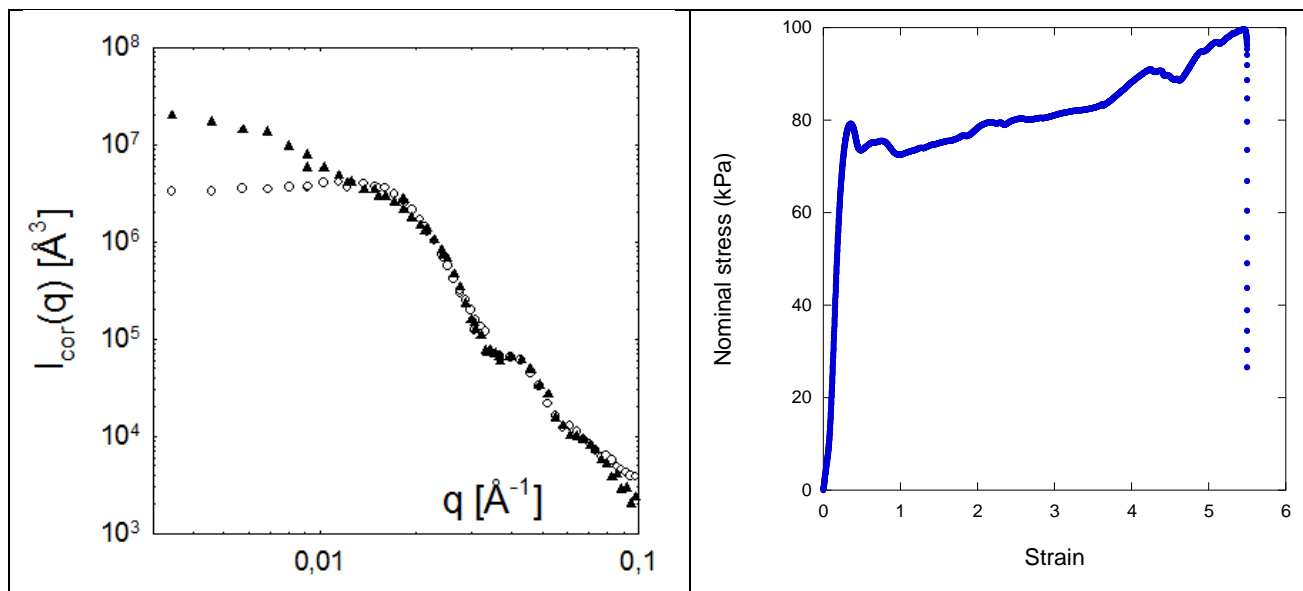


Figure 19: Double logarithmic plot of the normalized scattered intensity of hybrid SP2_PW0.14_R0.1 hydrogels with different monomers: DMA (O) and AAm (▲). The gels have been synthesized in solvent “p”, screening the polymer.

Left: tensile test on a SP(ω_{DMA} 0)5_PW0.14_R0.1 at a strain rate of 0.06 s^{-1} : striction phenomenon due to aggregation of the silica nanoparticles in the case of a redox initiation.

The aggregation of the silica nanoparticles induced by the redox polymerization of acrylamide was also evidenced by cycling tensile tests: the initial modulus of the first loading cycle was far above the initial moduli of the second and third cycles (these two last moduli being equal). Moreover, the tensile tests performed on these heterogeneous hybrid hydrogels exhibit an unusual mechanical behaviour close to the one of semi-crystalline polymers: striction appeared, as represented on **Figure 19**.

The synthesis of hybrid hydrogels using thermal initiation instead of redox led to transparent and homogeneous samples, as it will be shown by DLS in the next chapter. Mechanically, these homogeneous samples present reasonable and reproducible values of

initial modulus and no signature of macroscopic silica aggregation. We have no sound explanation for these different behaviours but perhaps that the fast formation of organic clusters during redox polymerization could destabilize the silica nanoparticles. This peculiar behaviour has not been studied in details in the framework of this PhD but obviously it would deserve further analysis.

3.1.3. Swelling properties

The swelling ability of the pure PAAm hybrid hydrogels in LiNO_3 0.5M (without DMA) is presented in **Figure 20**.

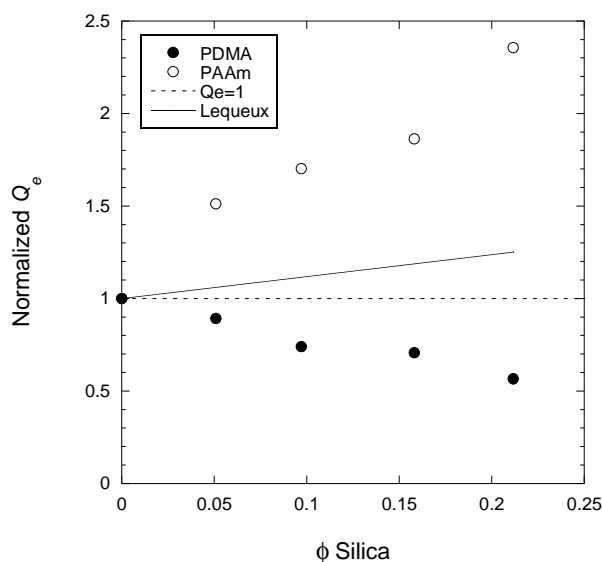


Figure 20: Variation of the normalized swelling ratio in LiNO_3 0.5M at equilibrium Q_e as a function of the volume fraction of silica for $\text{SP}(\omega_{\text{DMA}} 0)\text{x_PW0.14_R0.1}$ hydrogels (pure PAAm hydrogels), in water. The model of Lequeux is represented in the case of a non-reinforcing filler.

The results are in a good agreement with the poor interactions existing between acrylamide and silica nanoparticles. Indeed, the presence of non-interacting filler in the swollen polymer matrix leads to an increase of the swelling at equilibrium by comparison with the reference PAAm hydrogel. Although this tendency is in good agreement with the model developed by Berriot *et al.* in the absence of adhesion between the filler and the matrix, the relative increase

of swelling seems rather high to be attributed only to the formation of solvent cavities around the particles[2]. In the present case of non-adsorbing polymers the impact of counter ions. As a matter of fact, in the case of a polymeric matrix filled by unlinked nanoparticles (no covalent bond nor physical interaction), the immersion in a good solvent induces a swelling of the matrix, without restriction. As a consequence of the swelling, cavities are formed around each particle and are filled with solvent. By determining the expression of an apparent swelling of the sample, Berriot *et al.* evidenced that the swelling of the filled sample is higher than the one of the polymer alone because of the voids filled by solvent around the particles.

The swelling properties of the PAAm hybrid hydrogels compared to the ones of PDMA hybrid hydrogels is an experimental confirmation of the absence of interaction with silica nanoparticles.

3.1.4. Mechanical properties

Working at a given silica concentration, the evolution of the initial modulus was studied as a function of the AAm ratio in the copolymer gel. In **Figure 21**, the values of initial modulus of this system are plotted as a function of the silica volume fraction. The introducing of the non-adsorbing monomer AAm into the polymer network induces a clear decrease of the mechanical properties compared to the reference PDMA system. As we can see, the loss of stiffness scales with the incorporation of AAm monomer into the network: from 0% to 100% of AAm in the polymer matrix, the initial modulus decreases from a hundred of kPa to about 20kPa at the highest silica volume fraction corresponding to the SP5 formulation.

As a conclusion, we succeeded in tuning the reinforcement process in hybrid hydrogels through the polymer composition, playing with the molar ratio between adsorbing (DMA) and non-adsorbing (AAm) monomers.

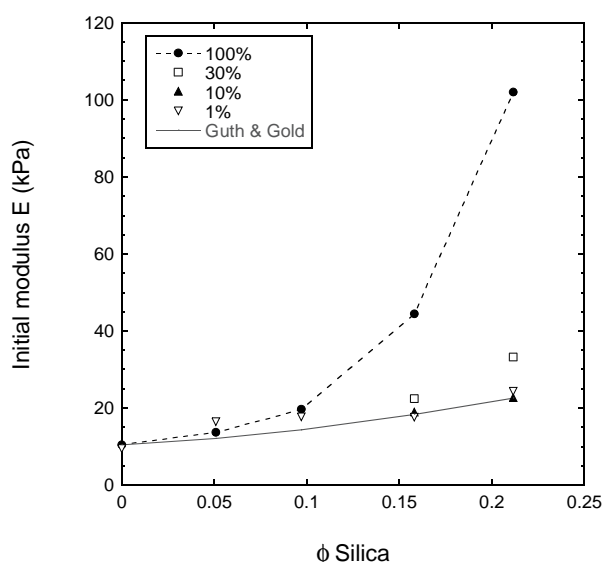


Figure 21: Comparison of experimental values of initial modulus E (in kPa) for hybrid PDMA hydrogel containing various amounts of DMA, at a nominal strain rate of 0.06 s^{-1} : in the legend, \bullet for the reference system with 100 wt% of DMA, \square for 30 wt% of DMA, \blacktriangle for 10 wt% of DMA, ∇ for 1 wt% of DMA, in grey line is represented Guth and Gold's model.

3.2. Introducing a hydrogen-bonding competitor

We saw that the interaction at the origin of the enhanced properties of hybrid hydrogels can be modified by changing the nature of the polymer. Now, we will study the impact of a hydrogen-bonding competitor on the macroscopic properties. For that purpose, we chose to work with urea, a common molecule easily available and presenting two amino -NH_2 groups joined by a carbonyl C=O group, as presented in **Figure 22**. Urea is known to form hydrogen bounds and is widely used in supramolecular chemistry. We can cite the works of two research laboratories: the one of Bouteiller *et al.* [6-9] and also the one of Leibler *et al.* [10-12].

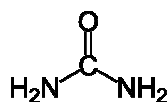


Figure 22: Semi-developed representation of urea.

3.2.1. Swelling behaviour in urea

Preliminary experiments have been carried out with the reference series of hybrid hydrogels, prepared without urea, in order to investigate the influence of urea. For that purpose 3 hydrogels of this series, SP0, SP2 and SP5, were immersed into urea (3 mol/L) during two weeks, the solvent being changed every day. For comparison purpose, we have plotted in **Figure 23** the relative swelling (Q_R) of these gels by dividing the swelling in urea by the swelling initially determined in salt conditions (LiNO_3 0.5 mol/L). While the hydrogel without silica particles does not show any significant volume variation between these two conditions ($Q_R \cong 1$), hybrid hydrogels display a much higher swelling in urea compared to salt ($Q_R \cong 2$). This interesting result emphasizes the role of urea in the hydrogen-bonding competition with the silanol groups. In a large excess of urea molecules, PDMA chains lose their adsorption properties with silica surfaces and the polymer network re-swells. In the present case the swelling at equilibrium in urea measured for SP2 and SP5 ($Q_e \cong 70$) is much higher than the swelling of the reference SP0 as silica nanoparticles embedded into the network carry their counter-ions which are not screened in these conditions.

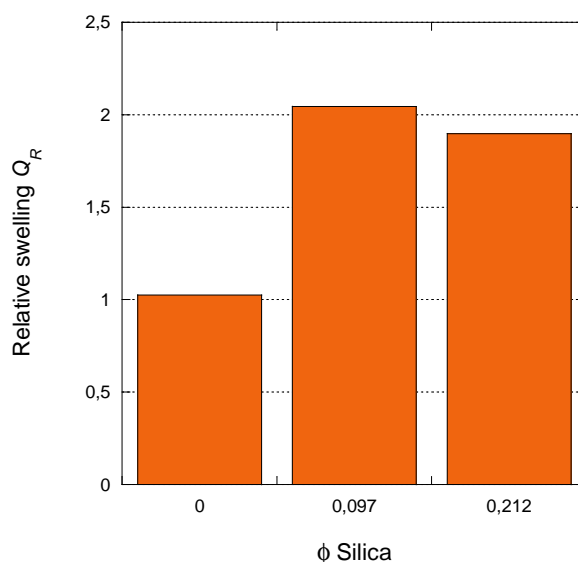


Figure 23: Variation of the relative swelling at equilibrium Q_R as a function of the volume fraction of silica for SPx_PW0.14_R0.1 hydrogels: is the swelling at equilibrium in urea divided by the swelling at equilibrium in LiNO_3 (0.5 mol/L).

In order to probe the impact of urea on the mechanical properties of hybrid networks, hybrid hydrogels were synthesized in the presence of urea. In this case, we have used a lower concentration of urea, typically a stoichiometric amount relative to DMA (about 1.2 mol/L) to avoid any dramatic deviation from our standard polymerization process.

3.2.1. Synthesis of hybrid hydrogels with urea

The synthesis of hybrid PDMA hydrogels containing urea and Ludox-TM50 is similar to the one described in Chapter 3, introducing urea with the silica suspension Ludox-TM50, MBA and DMA. The formulation of hybrid hydrogels used in this chapter is given in **Table 6** and the classical nomenclature used is:

“SPx_PW0.14_R0.1_urea”.

Samples	Silica (g)	DMA (g)	MBA (mg)	KPS (mg)	TEMED (μ L)	urea (g)	H ₂ O (g)
SP0_PW0.14_R0.1_urea	0	1.485	2.3	0.041	22.5	0.9	10.624
SP2_PW0.14_R0.1_urea	2.975	1.485	2.3	0.041	22.5	0.9	10.624
SP5_PW0.14_R0.1_urea	7.437	1.485	2.3	0.041	22.5	0.9	10.624

Table 6: Formulation of PDMA hybrid hydrogels with urea “SPx_PW0.14_R0.1_urea”.

After the synthesis, the PDMA hybrid hydrogels synthesized in presence of were transparent and colourless.

3.2.2. Mechanical properties

The effect of urea on the mechanical properties has been investigated by tensile tests performed at 0.06 s⁻¹ and at 0.6 s⁻¹. No strain effect has been observed. The mean values of initial moduli at 0.06 s⁻¹ are given in **Table 7** and represented on **Figure 24** with a comparison to Guth and Gold’s model.

Samples	Silica volume fraction	$E @ 0.06 \text{ s}^{-1}$ (kPa)
SP0_PW0.14_R0.1_urea	0	10.2 ± 0.2
SP2_PW0.14_R0.1_urea	0.097	22.8 ± 3.8
SP5_PW0.14_R0.1_urea	0.212	27.7 ± 2.4

Table 7: Young's modulus E (kPa) for SPx_PW0.14_R0.1_urea series, at 0.06 s^{-1} .

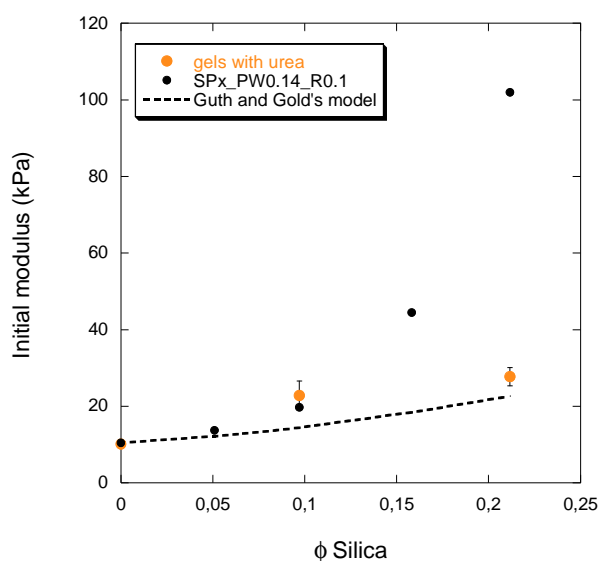


Figure 24: Comparison of initial modulus E for the SPx_PW0.14_R0.1_urea series (orange dots), SPx_PW0.14_R0.1 series (black dots) and Guth and Gold's model (dotted line), at 0.06 s^{-1} .

As previously discussed with the swelling behaviour, addition of urea into the system clearly screens the interactions between PDMA and silica as the initial moduli correspond to the predictions of Guth and Gold (calculated for non-reinforcing fillers in a polymer matrix). This absence of reinforcing interaction is also noticeable in the study of energy dissipation by cycling tests, as presented in **Figure 25**. As a matter of fact, the hysteresis present for charged hydrogel is far below the ones of the reference system but a slight dissipation exists. The mechanism of adsorption/desorption evidenced in Chapter 4 is strongly inhibited at small strain. As expected in the case of a non-reinforced system, the successive loading cycles are similar: the value of recovery parameter at both strain rates is around 1 for all the silica contents.

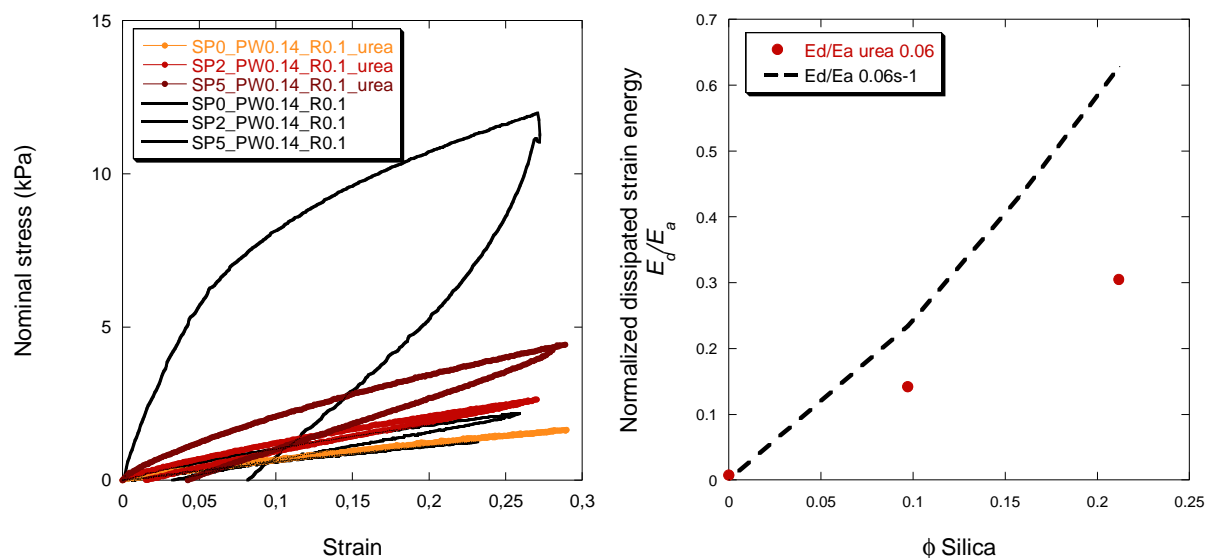


Figure 25: Left: effect of the silica content on the first loading-unloading cycle at 0.06 s⁻¹ for SPx_PW0.14_R0.1_urea, compared to the references SPx_PW0.14_R0.1 (in black curves). Right: effect of urea on the normalized dissipated strain energies E_d/E_a : with urea (red dots) and without urea (dotted line) at 0.06 s⁻¹.

As a conclusion, the introduction of urea in hybrid hydrogels strongly reduces the PDMA/silica interactions at the origin of the reinforcement. The physical adsorption of PDMA chains onto the silica surface can be efficiently suppressed in the presence of a hydrogen bonding competitor, such as urea. As previously discussed in the case of DMA-AAm copolymers, it should be possible to gradually tune the adsorption properties of PDMA onto silica by changing the amount of urea added into the network.

4. Conclusion

The aim of this chapter was to investigate different ways to tune the mechanical properties of hybrid hydrogels. In the first part, we kept the PDMA matrix and we mainly focussed on its physical characteristics. For instance, working at a fixed concentration (preparation state), we have shown by changing the cross-linking density that physical interactions always play a major role in the viscoelastic behaviour but their relative contribution decreases with increasing level of covalent cross-links. We evidenced that the dynamics of the silica-PDMA interaction governs most of the properties. Conversely, working at a fixed level of cross-linking and changing the gel concentration by swelling the polymer matrix at equilibrium, the contribution of both covalent and physical cross-links strongly decrease. This study performed at the swelling equilibrium state opens several interesting questions: a loss of reinforcement and dissipation has been evidenced, suggesting that the exchange processes described in Chapter 4 are screened at this diluted state. The weak signature of the physical interactions between PDMA and silica is quite similar to what is currently observed in associating systems upon dilution with a shift from inter-chain to intra-chain associations.

In the second part of this last chapter, we studied the impact of the state of dispersion of the silica nanoparticles on the macroscopic properties of hybrid hydrogels. Two main parameters seem to be crucial in the reinforcement properties. First, the aggregation/percolation of the silica nanoparticles induces very high values of initial modulus at small strains. Then, the PDMA/silica interactions improve the extensibility at break but due to the aggregation of the particles, only a small part of the initial silica surface remains available, drastically lowering the possibilities of reinforcement.

In the last part of this chapter, two different strategies were used to lower the physical interactions taking place in hybrid hydrogels. For that purpose, we first explored the use of acrylamide as a co-monomer, known to interact weakly with silica surfaces. Secondly, we introduced a hydrogen-bond competitor in order to reduce the number of physical bonds between the silica surface and PDMA. In both cases, the mechanical properties of hybrid

hydrogels were strongly decreased, even cancelled for high amount of added internal or external inhibitors.

As a conclusion, all the strategies explored in this chapter gave us the opportunity to test and to prove that the adaptability of the system is very large. By modifying some of the three categories (the PDMA matrix, the dispersion state of silica and the physical interactions), we opened a wide range of properties. Now that the feasibility of this properties adaptation has been probed, the strategies could be investigated in more details and a larger number of ideas could be tested.

References

1. Carlsson, L., et al., *Nano-hybrid self-crosslinked PDMA/silica hydrogels*. *Soft Matter*, 2010. **6**(15): p. 3619-3631.
2. Berriot, J., et al., *Reinforcement of model filled elastomers: experimental and theoretical approach of swelling properties*. *Polymer*, 2002. **43**(23): p. 6131-6138.
3. Horvath, J. and V. Dolnik, *Polymer wall coatings for capillary electrophoresis*. *Electrophoresis*, 2001. **22**: p. 644-655.
4. Petit, L., et al., *Responsive hybrid self-assemblies in aqueous media*. *Langmuir*, 2007. **23**(1): p. 147-158.
5. Orakdogan, N., M.Y. Kizilay, and O. Okay, *Suppression of inhomogeneities in hydrogels formed by free-radical crosslinking copolymerization*. *Polymer*, 2005. **46**(25): p. 11407-11415.
6. Bouteiller, L., *Assembly via Hydrogen Bonds of Low Molar Mass Compounds into Supramolecular Polymers*, in *Hydrogen Bonded Polymers*, W. Binder, Editor. 2007, Springer Berlin Heidelberg. p. 79-112.
7. Bellot, M. and L. Bouteiller, *Thermodynamic description of bis-urea self-assembly: competition between two supramolecular polymers*. *Langmuir*, 2008. **24**(24): p. 14176-14182.
8. Shikata, T., et al., *Structure and Dynamics of a Bisurea-Based Supramolecular Polymer in n-Dodecane*. *Journal of Physical Chemistry B*, 2008. **112**(29): p. 8459-8465.
9. Roberto Francisco, K., et al., *Tuning the Viscoelastic Properties of Bis(urea)-Based Supramolecular Polymer Solutions by Adding Cosolutes*. *Langmuir*, 2012. **28**(41): p. 14531-14539.
10. Cordier, P., et al., *Self-healing and thermoreversible rubber from supramolecular assembly*. *Nature*, 2008. **451**: p. 977-980.
11. Montarnal, D., et al., *Versatile one-pot synthesis of supramolecular plastics and self-healing of rubbers*. *Journal of the American Chemical Society*, 2009. **131**(23): p. 7966-7967.
12. Maes, F., et al., *Activation and deactivation of self-healing in supramolecular rubbers*. *Soft Matter*, 2012. **8**: p. 1681-1687.

Chapter 6

Diluted approach: study of hybrid hydrogels by Dynamic Light Scattering

Contents

Contents	232
Introduction.....	234
1. Light scattering	235
1.1. Presentation and principle	235
1.1.1. Static Light Scattering	235
1.1.2. Dynamic Light Scattering and Laser Light Scattering	236
1.2. Single Light Scattering in gels	240
1.3. Gelation process.....	243
1.3.1. Gelation of polymeric hydrogels.....	243
1.3.2. Gelation of hybrid hydrogels.....	245
1.4. Dynamics of particles.....	245
2. Dynamics of PAAm hybrid hydrogels studied by DLS	248
2.1. Abstract and introduction	248
2.2. Synthesis and characterization methods.....	251
2.2.1. Synthesis of PAAm hybrid hydrogels.....	251
2.2.2. Dynamic light scattering measurements	252
2.2.3. Microrheology by diffusing-wave spectroscopy	252
2.3. Effect of chemical cross-linking.....	253
2.4. Effect of silica nanoparticles concentration	261
2.5. Conclusions	267
3. Dynamics of PDMA hybrid hydrogels studied by DLS	269
3.1. Abstract and introduction	269
3.2. Synthesis and characterization methods.....	272
3.2.1. Synthesis of P(AAm-co-DMA) hybrid hydrogels	272
3.2.2. Dynamic light scattering measurements	272
3.2.3. Hydrogels synthesis for mechanical measurements.....	273
3.2.4. Mechanical measurements.....	273

3.3.	Effect of DMA/silica interactions on the dynamics	273
3.4.	Conclusions	287
4.	Conclusion on the DLS studies	289
References	291

Introduction

As mentioned in the previous chapters, many experimental approaches have been developed in order to investigate hybrid hydrogels and the specific interactions leading to their unique properties. Among the classical methods developed to study hydrogels (such as nuclear magnetic resonance, Fourier transform infrared spectroscopy, differential scanning calorimetry, static and dynamic light scattering, small angle X-ray scattering and small angle neutron scattering), light scattering experiments have been widely used to study the dynamics of colloids but also the dynamics of gels. Light is an electromagnetic radiation able to probe structures and dynamics on the basis of differences in refractive indices; while SANS technique deals with a different form of radiation since neutrons have mass. Nevertheless, the scattering principles are essentially identical.

In this chapter we will present the light scattering techniques generally used in the gel studies in a first part. Thanks to these techniques, we will try to answer questions about the dynamic behaviours of cross-linked networks and of nanoparticles embedded in networks. Chemically and/or physically networks will be studied, containing/or not silica nanoparticles presenting different interactions with monomers. Then this chapter will deal with two series of experiments of dynamic light scattering. The first one presents a study of the dynamics of polyacrylamide hydrogels, varying the chemical cross-linker concentration and the silica content. The impact of these two factors on the homogeneity of the network was investigated and revealed some transfer mechanisms. In the second one, the introduction of DMA and its consequences on the dynamics is studied, making a link between the observed enhancements of hydrogel properties described in Chapters 3 and 4.

1. Light scattering

1.1. Presentation and principle

1.1.1. Static Light Scattering

In 1802, the observation of a light scattering phenomenon from a sol of colloidal gold made by Richter was the beginning of the light scattering as investigation technique [1]. The works of Tyndall (for his experimentations on vapours crossed by a beam of light [2]), Lord Rayleigh (for his explanation of the blue colour of the sky in terms of diffraction [3] and his theoretical study of light scattering [4]), Einstein (for his adaptation of the fluctuation theory applied to light scattering [5]) and Mie (for his theory of light scattering by large particles whose refractive indices were different from those of the dispersing medium [6]) happened to be essential contributions to the understanding and the development of light scattering techniques. Later, the works of Debye showed how light scattering can be used to determine the molecular weight of weakly interacting particles or polymer molecules in dilute solutions [7]. The principle of the static light scattering technique is a measurement of the time-averaged scattered intensity as a function of the scattering angle at a fixed wavelength of light. This technique can be used in order to obtain the average molecular weight of macromolecules, the second Virial coefficient (which is a quantitative measurement of the solvent-polymer interactions) and also to calculate the radius of gyration of objects. For colloidal suspensions, light scattering is a major experimental tool to study their statistical properties.

Experimentally, a laser beam illuminates a suspension of nano-objects (macromolecules or particles) and the scattered light is measured by detector(s) as a function of time at a certain angle, as schematically represented in **Figure 1**.

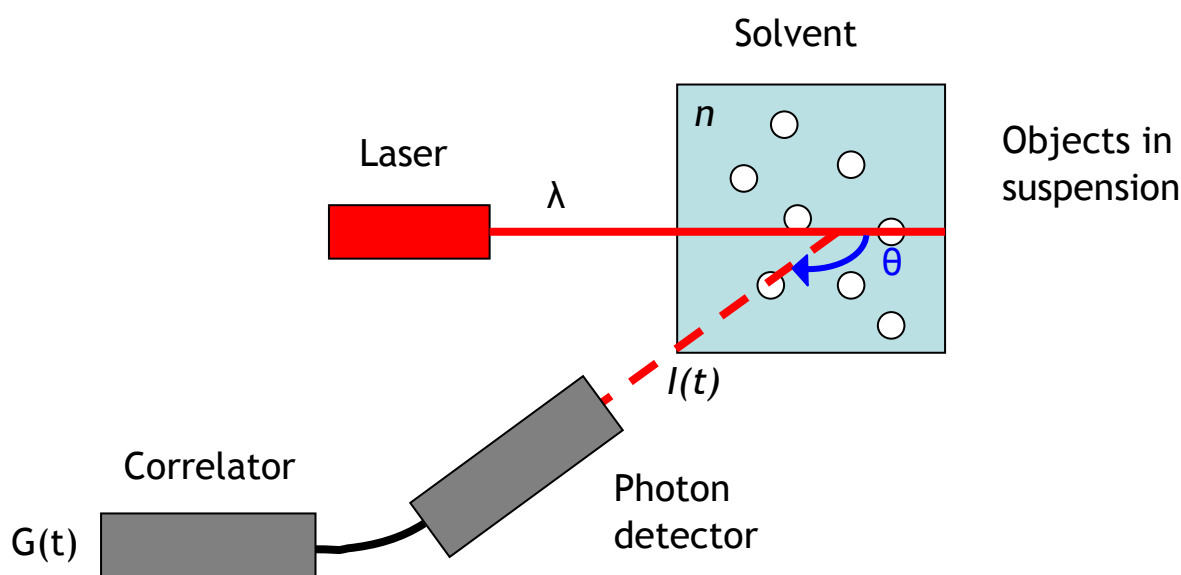


Figure 1: Schematic representation of the experimental setup.

In the static light scattering theory, one assumes that every photon has only been scattered once. This situation corresponds to very dilute solutions where the photons are not scattered several times before the detection. Experimentally, the cases of very dilute solutions are limited and it is often difficult to ignore multiple scattering.

1.1.2. Dynamic Light Scattering and Laser Light Scattering

In Dynamic Light Scattering (DLS) experiments, the aim is the measurement of the time dependence of the fluctuations of the scattered intensity (due to translational and/or internal motions of particles or molecules) rather than the mean intensity as measured in Single Light Scattering (SLS) experiments. This technique is born thanks to the development of laser and especially to the coherent properties of laser light. As a matter of fact, with the spatial and temporal coherence of laser lights, time-dependent measurements became possible. A schematic representation of a Light Scattering experiment on a polymer solution and schematic plot of the measured intensity as a function of time are given on **Figure 2**.

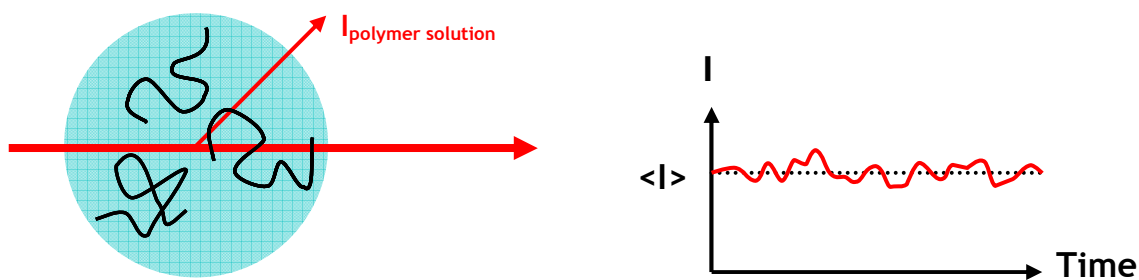


Figure 2: Left: schematic representation of a light scattering experiment on a polymer solution. Right: schematic plot of the measured intensity (in red) as a function of time, with the average intensity (in dotted line).

Concerning the experimental setup, the development of the light scattering technique led to the use of a goniometer equipped with lasers. In our case, we performed our measurement with an ALV CGS-3 goniometry system (ALV, Langen, Germany), equipped with a He-Ne laser (22 mW at $\lambda = 632.8$ nm). The system measures the time-averaged autocorrelation function of the scattered light intensity by varying the scattering angle.

Nowadays, the two techniques of static and dynamic light scattering are often combined and are referred as Laser Light Scattering. Dynamic light scattering is widely used in many academic fields, such as polymer science, colloid chemistry, biochemistry, medical science and also in product development and quality supervision in industry. The aim of this physical technique is to determine both static time-averaged characteristics thanks to static light scattering: molecular weight, radius of gyration, information on polymer-solvent interactions, and time-dependent properties based on dynamic light scattering: translational diffusion coefficient, hydrodynamic radius and its size distribution, rotational and internal motions thanks to local intensity fluctuations of the scattered light.

After collecting the scattered intensity, a calculation of a correlation function is carried out in order to translate the dependency of the intensity to time. In our case, the considered correlation function deals with a random intensity representing the same quantity measured at two different times. For that reason, we will call it the intensity autocorrelation function $g_2(t)$ which can be written as:

$$g_2(t) = \frac{\langle I(t) \cdot I(t+t') \rangle}{\langle I(t)^2 \rangle} \quad \text{Eq. 1}$$

where $I(t)$ and $I(t+t')$ are respectively the scattered intensities at an instant t and $t+t'$.

The brackets denote ensemble average over the orientations and positions of the objects. Experimentally, for ergodic samples, this ensemble average is obtained as a time average. The intensity autocorrelation function is converted into field autocorrelation function $g_1(t)$ by Siegert relation given as:

$$g_2(t, q) = 1 + \beta |g_1(t, q)|^2 \quad \text{Eq. 2}$$

where β is the coherence factor which depends on the experimental set-up.

From the representation of the field autocorrelation function, one can determine characteristic times (τ) that can be analyzed in terms of diffusion of polymer chains or particles. Experimentally, the intensity must be recorded over a time duration that is larger than the decay time τ of the sample, in order to probe all accessible configurations. The sizes of the macromolecular objects or particles can be evaluated if the viscosity of the medium is known. The type of dynamics of the studied objects can be determined: by checking the angular dependence of the system, one can know whether the diffusion follows a Brownian law or not. In the case of a Brownian diffusion, the field autocorrelation decays exponentially and the characteristic time τ can be determined as:

$$g_1(t, q) = \exp\left(-\frac{t}{\tau}\right), \quad \tau = \frac{1}{D \cdot q^2} \quad \text{Eq. 3}$$

where D is the diffusion coefficient (in $\text{m}^2 \cdot \text{s}^{-1}$) and q the modulus of the scattering vector (in m^{-1}). As expressed in Chapter 2, in the case of neutron scattering experiments, the modulus of the scattering vector q is:

$$q = \frac{4\pi n}{\lambda} \sin\left(\frac{\theta}{2}\right) \quad \text{Eq. 4}$$

where λ is the wavelength of the light (in m), n the refractive index and θ the scattering angle.

An example of the field autocorrelation function and the determination of the diffusion coefficient are given in **Figure 3**.

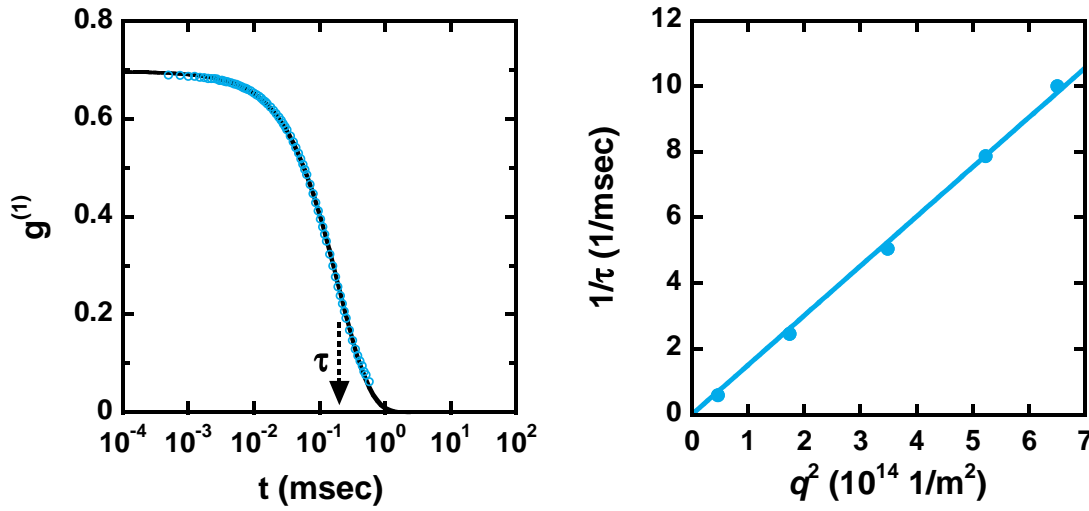


Figure 3: Left: representation of a field autocorrelation function as a function of time.

Right: the function is fit with Eq. 3 to determine the characteristic time τ .

In the case of a Brownian diffusion, the diffusion coefficient D can be related to the hydrodynamic radius according to the Stokes-Einstein equation:

$$D = \frac{k_B \cdot T}{6\pi \cdot \eta \cdot R_H} \quad \text{Eq. 5}$$

with k_B the Boltzmann constant (in J/K), T the temperature (in K), η the viscosity (in Pa.s) and R_H the hydrodynamic radius (in m).

The hydrodynamic radius R_H determined by dynamic light scattering experiments corresponds to the radius of a theoretical hard sphere having the same diffusion coefficient as the real measured particle (or polymer chain). In the case of a polymer coil, this hydrodynamic radius is the radius of a sphere where the solvent cannot enter. For a charged particle, this sphere contains the particle and any other molecules or solvent molecules moving with the particle. This overestimated radius can be compared to the radius observed by optic measurements.

1.2. Single Light Scattering in gels

The main particularity of light scattering in gels comes from the non-ergodicity of the light scattered by the system (**Figure 4**). As a matter of fact, the term ergodic describes a dynamical system in which the average over time behaviour is identical to the averaged over space behaviour. For hydrogels and especially for cross-linked hydrogels, we are in the case of non-ergodic systems as the cross-linked structure can be related to a frozen structure: the concentration gradient of the polymer is specially frozen due to the cross-link. Experimentally the time average scattered intensity is not same as the ensemble average.

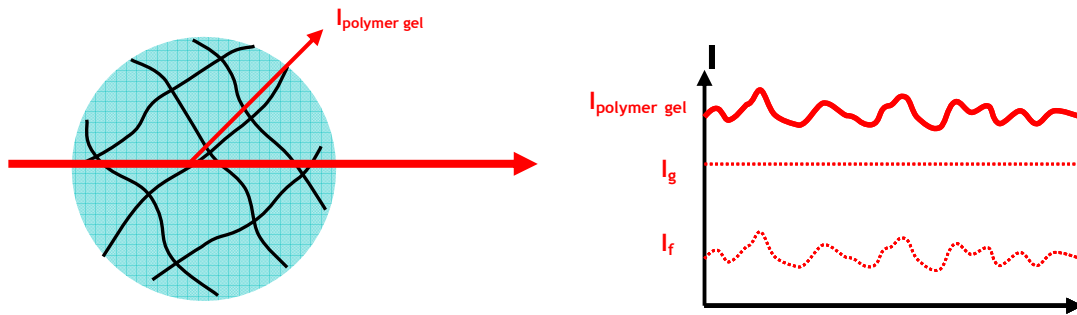


Figure 4: Schematic representation of a light scattering experiment on a polymer gel

The induced frozen structure is at the origin of the measurement of a non-fluctuating intensity that depends on the position of the measurement; that is the direct expression of the non-ergodicity. The scattering intensity from polymer gels is always higher than that from the solution of the same polymer at the same concentration [8]. As a matter of fact, the measured intensity is composed of a fluctuation contribution I_f and of another contribution from the frozen structure of the gel I_g : the inhomogeneous distribution of the polymer material along the gel sample. As discussed in Chapter 2, inhomogeneity is usually observed for gels synthesized at fairly dilute state and can be particularly important for gels formed by free-radical polymerization [9, 10]. This inhomogeneity is the consequence of cyclization and multiple cross-linking reactions taking place at the beginning of the gel synthesis.

For the non-ergodic systems the Siegert relation is not valid, thus the Pusey method is used to calculate the ensemble averaged autocorrelation function given as:

$$g_1^E(t, q) = \frac{Y-1}{Y} + \frac{(g_2^T(t, q) - \sigma^2)^{1/2}}{Y} \quad \text{Eq. 6}$$

Where $g_2^T(t, q)$ is the time averaged intensity correlation function, Y is the non-ergodic parameter, which is the ratio of the time averaged intensity and the ensemble averaged intensity (for an ergodic sample $Y = 1$). σ^2 is defined as

$$\sigma^2 = \frac{\langle I^2(0) \rangle_T}{\langle I(0) \rangle_T^2} - 1 \quad \text{Eq. 7}$$

This quantity is experimentally accessible from the initial amplitude of the autocorrelation function.

In order to circumvent this “error” of measurement coming from the dramatic dependence of I_s with the position, one need to measure this intensity over different positions, that way an ensemble averaging is possible and is relevant. The right measurement of the scattered intensity of gel needs the elaboration of a particular setup allowing translation or rotation of the samples, as presented in **Figure 5**.

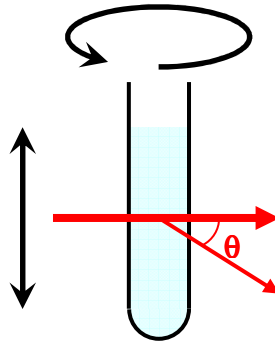


Figure 5: Schematic representation of the experimental setup: translational or rotational motion.

Our dynamic light scattering measurements were performed with an ALV CGS-3 goniometry system (ALV, Langen, Germany), equipped with a cuvette rotation/translation unit (CRTU) and a He-Ne laser (22 mW at $\lambda = 632.8$ nm). The time-averaged autocorrelation function of the scattered light intensity is measured by the system at different scattering vectors. In order to circumvent the non-ergodicity associated with the presence of frozen disorder in chemically cross-linked gels, the sample cell was vertically translated steadily

while time-averaging. Thus, $g_2(t)$ coincides with the ensemble-averaged autocorrelation function, up to a cut-off delay time fixed by the sample rotation speed. The averaging duration was more than 3600 seconds for each measurement, depending on the slowest relaxation modes found in the autocorrelation functions.

Let us consider the example of a pure PAAm hydrogel, chemically cross-linked and studied by this method of sample-translation during the measurements. The normalized autocorrelation function is plotted in **Figure 6** for four different angles of measurement (45° , 60° , 80° and 100°).

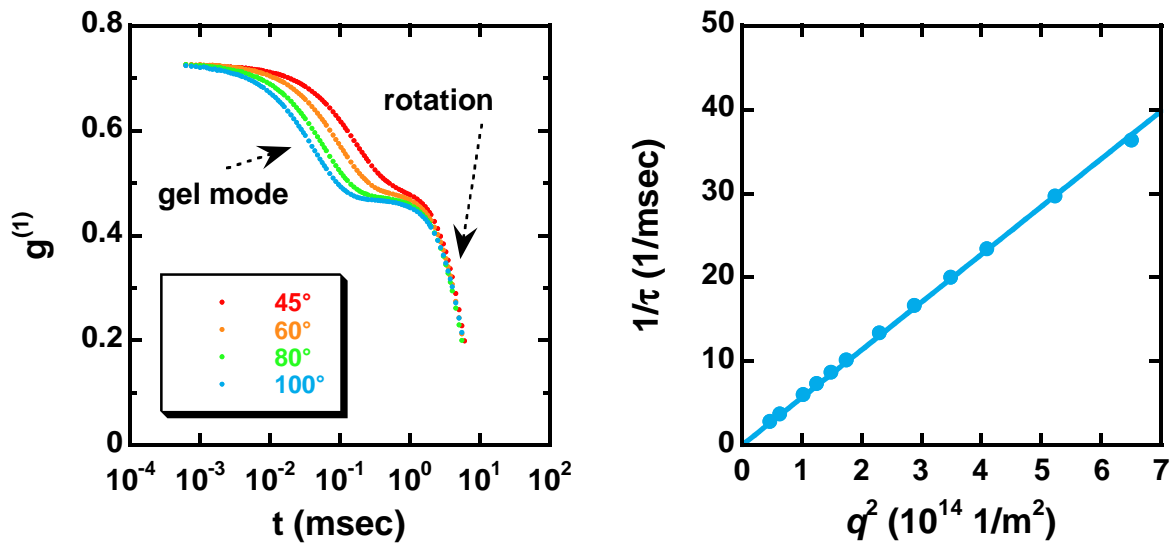


Figure 6: Left: representation of the field autocorrelation functions as a function of time for a PAAm hydrogel chemically cross-linked (1 mol%), measured at different angles.

Right: representation of the reciprocal fast characteristic time as a function of the modulus of the scattering vector q .

The representation of the field autocorrelation functions as a function of time for the chemically cross-linked PAAm hydrogel shows two decays. These two relaxations are present at different time-scales: one is fast, the other is slow. The fast mode presents a q^2 dependence, as represented in **Figure 6** (left), corresponding to the collective diffusion of the polymeric network. This collective diffusion is characterized by a diffusion coefficient D equal to $7.10^{-11} \text{ m}^2/\text{s}$, with a correlation length ξ of 3.5 nm. The other mode corresponds to a

slower dynamic, with no dependence with the magnitude of the scattering vector: q^0 . This second and slower mode is due to the displacement of the sample at a constant speed: the translation or rotation of the sample. This last mode has no physical meaning. It is interesting to notice that according to the translation velocity of the sample, different time ranges can be investigated. In the present case, a relative high translation velocity has been used during the measurement, but with a characteristic time of translation far above the characteristic time of diffusion.

As far as the study of hydrogels by light scattering is concerned, we can mention that several experimental setups exist. For instance, Shibayama and Oppermann use shorter acquisition times (between 30 and 60 seconds) which are not suitable for systems with slow dynamics [8, 11]. As a matter of fact, the maximal magnitude of characteristic times is limited by their experimental setups.

1.3. Gelation process

The DLS technique is a powerful tool for size evaluation but also for gel characterization in order to determine structural changes during the gelation process. It has ever been used together with SANS experiments on hybrid hydrogels in order to describe the morphology of the sol-gel process. Experimentally, the gelation threshold corresponds to an abrupt increase of the scattering intensity.

1.3.1. Gelation of polymeric hydrogels

Gelatin hydrogels are one of the most classical systems presenting a temperature dependent sol-gel transition. In 2007, a review concerning the gel point determination of gelatin hydrogels by DLS and rheological measurements has been published by Matsunaga and Shibayama [12]. From the DLS technique, the sol-gel transition of the gelatin system corresponds to a drastic increase in the scattering intensity which is the measurable phenomenon of the ergodic/non-ergodic transition of the system. The rheological measurements gave a precise evaluation of the macroscopic gel point transition. The combination of these two techniques led to the following conclusion: the “microscopic”

gelation temperature obtained by DLS is the same than the “macroscopic” gelation temperature obtained by rheological measurements.

Let us consider another example of a DLS study that has been realized by Karino *et al.* in 2006 [13]. The sol-gel transition of hydrophobically modified polyrotaxane (methylated polyrotaxane) was studied in terms of temperature dependence. The substitution of hydroxyl groups on polyrotaxane (consisting of poly(ethylene glycol) and α -cyclodextrin) by methyl groups was at the origin of an increase of water solubility, preventing the formation of a gel through hydrogen bonds. As presented on **Figure 7** (up), the degree of methylation has a direct consequence on the temperature of the structural reorganization observed in such systems.

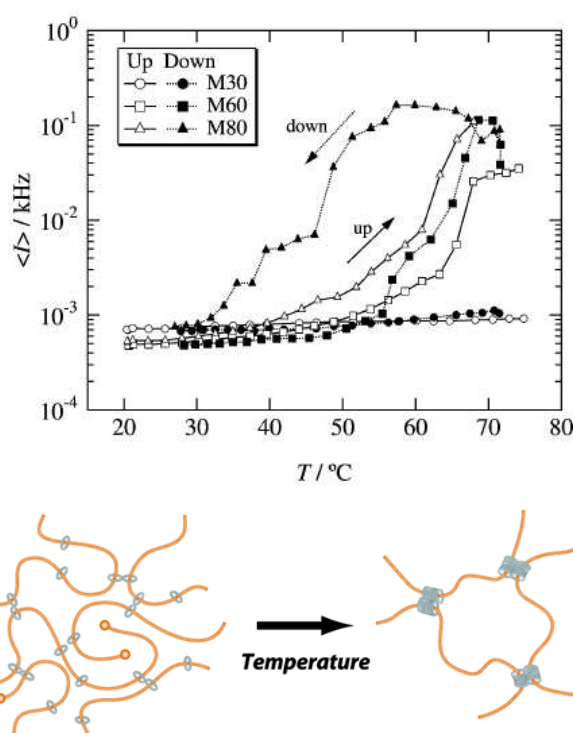


Figure 7: Up: light scattering intensity $\langle I \rangle$ as a function of temperature, open circles correspond to the heating process and closed circles to the cooling process, from [13].

Down: schematic models showing the temperature dependence of methylated polyrotaxane in solutions, from [13].

The combination of DLS results together with SANS experiments brought the detailed representation of a tunable sol-gel transition in methylated polyrotaxane as described in **Figure 7** (down).

1.3.2. Gelation of hybrid hydrogels

The study of the gelation process in polymeric network can be extended by adding the effect of the presence of inorganic nanoparticles, such as silica or clay. The same experimental setups are used in order to characterize the gelation of hybrid hydrogels.

One particular study that can be mentioned here is the one of the kinetics of gelation for various nanocomposite hydrogel systems prepared by free radical polymerization in the presence of inorganic particles. For instance, Suzuki *et al.* studied the gelation process and the microstructure of poly(*N*-isopropylacrylamide)/silica hybrid hydrogels [14]. Their system contains silica particles acting as multifunctional cross-linkers, various sizes of silica were studied but the effect of particle concentration was not discussed. Concerning the synthesis of PNIPAm hydrogels, the observation of an abrupt rise in the time-averaged scattering intensity after an induction period was interpreted in terms of growth from monomer to the polymer chains, leading to an entangled polymer network.

Haraguchi *et al.* and Okay *et al.* also studied the rheological aspects of the gelation process of PAAm or PNIPAm in the presence of clay particles [8, 11]. One particularity of their system comes from the inorganic part: clay particles are known to show gelation as a consequence of an increase of the ionic strength, without added polymer. For that reason, it is very difficult to characterize the gelation process of their nanocomposite system since the radical initiator used (persulfate) is a salt.

1.4. Dynamics of particles

The dynamics of particles have already been studied classically in suspensions but also in polymer solutions and in gels. The main motivations are the understanding of structure/properties relationships and the possible control of active components enclosed in

polymer gel matrices in pharmaceutical applications or biophysics. In 1990, Reina *et al.* were interested in the dynamics of polystyrene latex spheres in polyacrylamide solutions and gels, varying the cross-linking ratio and the size of the probes [15]. Let us consider with attention this example that describes all the different dynamics that can be observed.

In the case of non interacting polystyrene latex spheres introduced before the polymerization of acrylamide, in presence of MBA at different concentrations, several dynamics can be described, depending on the cross-linking ratio (corresponding to the molar amount of MBA in the polymer). Three domains have been pointed out by Reina *et al.*, with characteristic diffusion dynamics, determined by a double exponential fit:

- without chemical cross-linker, the probe particles can freely diffuse in the polymer solution;
- for a cross-linker concentration lower than 1.5 wt%, a pre-gel dynamics is observed: the autocorrelation function shows a slower decay compared to the one present in polymer solutions and a decrease of the dynamic amplitude is observed;
- above 1.5 wt% of cross-linker, a PAAm hydrogel is completely formed: the decays of the autocorrelation function are even slower and the decrease of the dynamic amplitude also.

The diffusion of the polystyrene latex spheres through the PAAm network is directly related to a pore size, ξ_{mesh} , initially fixed by the cross-linker concentration. The three domains previously described correspond to three geometrical situations as the cross-linker concentration increases:

- before the gel point (below 1.5 wt% of MBA), the particles are moving in large interconnected regions;
- at the critical concentration of cross-linker that is just enough to form an infinitely connected polymer cluster, the mesh size remains higher than the particles diameter ($\xi_{mesh} \gg d_{latex}$) and the particles are still able to diffuse;
- at higher cross-linker concentrations, the structure of the network can be heterogeneous with both large interconnected space and small pores highly cross-

linked: latex particles are trapped in the pores of size comparable to their diameter

$$(\xi_{mesh} \leq d_{latex}).$$

These three geometrical situations can be described in terms of particle and network dynamical behaviours, ξ_{mesh} being the relevant parameter determining the dynamics.

Another example of the study of dynamics of labelled polystyrene particles in a polymer network (PAAm) is the one of Oppermann *et al.* in 2008 [16]. This article also deals with the diffusion of labelled linear polymer chains in similar PAAm matrix, as represented in **Figure 8**. The studied PAAm matrices were semi-dilute uncross-linked polymer solutions and chemically cross-linked polymer gels.

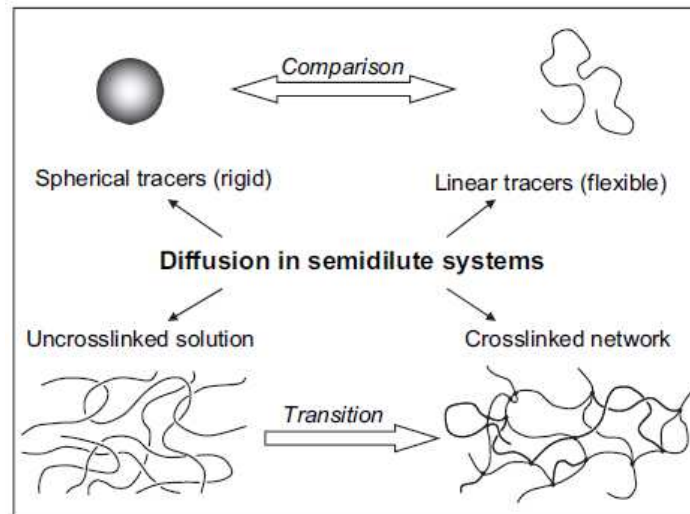


Figure 8: Schematic representation of Oppermann's intention of work, from [16].

With an increase of the cross-linking density of the polymer gel, a decrease in the amount of mobile particles is observed until a threshold of cross-linking density corresponding to a total trap of the latex particles is reached. Unsurprisingly, this cross-linking threshold depends on the particle diameter, decreasing when particles are bigger. Concerning the linear polymer chains, it appeared to be different, as almost no influence of the cross-linking density has been evidenced. The main advantage of Oppermann's system is the well defined cross-linking density, contrary to Reina's system where the heterogeneity of the network could not be neglected due to the choice of cross-linking copolymerization.

2. Dynamics of PAAm hybrid hydrogels studied by DLS

After this brief introduction to the light scattering techniques used in the hydrogel's domain, this first set of results concerns polyacrylamide hydrogels containing silica nanoparticles. We chose to start our study with low concentrated hydrogels of acrylamide in order to study the main parameters influencing the silica diffusion in such systems, without being perturbed by interaction between the polymer matrix and the particles. The study has been conducted on low concentrated hydrogels for experimental constraints related to experimental light scattering techniques.

As presented in Chapter 1, polyacrylamide does not show any interaction with silica nanoparticles. Acrylamide monomer is known to be hydrogen bonding donor, commonly involved in hydrogels studies [17]. We chose to use acrylamide in order to study the consequences of the presence of silica nanoparticles on the network formation in a way that prevents interactions between the monomer and silica. For that reason, the choice of acrylamide was evident.

This part of the chapter is a manuscript that has been published to *Macromolecules* in 2013: *Dynamics of Hybrid Polyacrylamide Hydrogels Containing Silica Nanoparticles Studied by Dynamic Light Scattering*, *Macromolecules*, 2013, **46** (11), pp 4567-4574.

2.1. Abstract and introduction

Abstract

Nanohybrid gels based on polyacrylamide (PAAm) and colloidal silica nanoparticles were synthesized by free radical polymerization. The influence of chemical cross-links and radical initiators on the dynamics of the network and the nanoparticles were studied by dynamic light scattering (DLS). In ensemble averaged autocorrelation functions we observed two decay modes in the hybrid gels, a gel mode and a Brownian diffusion mode of the silica nanoparticles particles at a concentration higher than 0.03 %. An increase in the chemical crosslinking ratio did not influence the gel mode while the silica nanoparticles diffusion

mode was slowed down. At lower silica concentrations, we observed (1) a higher scattered light intensity than for a silica suspension and for a gel without silica, (2) an increased plateau value and (3) no silica diffusion mode in the autocorrelation function. These results indicate that the hybrid gels were more heterogeneous. The gelation time decreased in the presence of silica at low concentration compared with the corresponding gel without silica, suggesting that the transfer of radicals from persulfate to silica surface occurs and that PAAm chains grow from the surface creating increased heterogeneity in the gels.

Introduction

Hydrogels are cross-linked polymer networks highly swollen by water that are used nowadays in many bio-applications such as contact lenses, drug delivery systems, superabsorbent, etc. Hydrogels can commonly be classified as solids, as no flowing under self-weight is observed, but diffusion mechanisms can also occur through hydrogels, exactly like in the case of liquids. The high water content of hydrogels is at the origin of their usual brittleness. The reinforcement of the poor mechanical properties of hydrogels is therefore a fundamental challenge for the numerous applications that can be considered. Over the past ten years, several reinforcement strategies have been developed all over the world, such as the elaboration of ideal networks [18, 19], the design of double networks [20, 21] and the combination of organic and inorganic components in nanocomposite hydrogels. This last strategy, that has been largely studied by Haraguchi [22-24], aims at mixing chemical and reversible interactions by introducing inorganic nanoparticles in the polymer network. Our group developed a system based on poly(*N*-alkylacrylamide) hydrogels with silica nanoparticles [25]. The mechanical properties of this hybrid system have been widely explored. Reinforcement due to strong but reversible adsorption of polymer chains onto the surface of silica nanoparticles has been demonstrated. The dynamic character of the polymer/silica interactions is believed to be responsible for internal energy dissipation upon deformation and leads to a simultaneous increase in elastic modulus and enhancement in fracture toughness through an increase in strain at break. These mechanisms work well both in un-notched samples (simple tensile test) and notched samples (crack propagation tests).

In these nanocomposite gels, prepared with and without chemical cross-linker such as *N,N'*-methylenebisacrylamide, inorganic particles behave as physical cross-linker. Different mechanisms for forming the unique network structure have been suggested. Haraguchi *et al.* proposed the formation of “clay-brush particles” [26]. As a matter of fact, the interactions between clay surfaces and a mixture of *N*-isopropylacrylamide monomer, potassium persulfate and a common catalyst (TEMED) lead to the growth of polymer brushes on the exfoliated clay platelets. With this specific grafting, occurring during the first steps of the polymerization, the obtained hybrid hydrogels are heterogeneous regarding the spatial organization of crosslinking points. Abdurrahmanoglu *et al.* proposed adsorption of *N*-alkylacrylamide monomers on the clay particle surfaces, leading to depletion-induced particle aggregates [27].

What are the dynamic behaviours of the polymer and the particles in nanohybrid systems? The dynamic behaviours of the chemically and/or physically cross-linked network and of the nanoparticles have been surprisingly poorly studied. The emerging questions are multiple and concern the dynamics of nanoparticles in hybrid hydrogels. Different kinds of interaction between the polymeric matrix and the nanoparticles can affect the dynamics and have to be precisely investigated. The characteristic relaxation times of the material have not been related to its molecular structure. Here, we study the dynamics of hybrid polyacrylamide hydrogels containing colloidal silica particles in order to study the effects of chemical cross-links, physical cross-links and radical polymerization separately. Different from poly(*N,N*-dimethylacrylamide) chains which are known to be able to form hydrogen-bonds with silica surfaces, polyacrylamide shows less interaction (since it is simultaneously hydrogen-bonding donor and acceptor). In fact, the hybrid polyacrylamide hydrogels do not show any reinforcement property when synthesized in the presence of silica nanoparticles [17]. Polyacrylamide/clay hydrogels have been studied by Okay and Oppermann [8]. Although they observed a large increase in elastic modulus of the gels with increase in the clay concentration, they did not discuss the nature of the polymer-clay interactions. Clay platelets are known to strongly interact with salts and especially with potassium persulfate which is used as the initiator of radical polymerization for poly(*N*-alkylacrylamide) systems

in most of the studies. This strong ionic interaction leads to the formation of three dimensional structures called “house-of-cards”.

Here we discuss the effects of:

1. chemical cross-links on the silica nanoparticle dynamics in the gels and
2. radical polymerization.

The originality of our work resides in the study of the dynamics of the polymer network combined to that of the silica nanoparticles. Relatively low silica concentrations were used in order to neglect interparticle interactions. Thus, the silica nanoparticles act as diffusion tracer probing the microenvironment in the PAAm hydrogel, giving information about the consequences of concentration parameters and crosslinking densities on the silica nanoparticles dynamics.

2.2. Synthesis and characterization methods

2.2.1. Synthesis of PAAm hybrid hydrogels

Acrylamide (AAm, 99%, Sigma Aldrich), *N,N'*-methylenebisacrylamide (MBA, Fluka) and potassium persulfate (KPS, Acros Organics) were used as received without further purification. The silica particles (Ludox-TM50 from Dupont) were obtained from Aldrich. They were characterized by dynamic light scattering using an ALV/CGS-3 compact goniometer (ALV, Langen, Germany). The measurements performed at different scattering angles (30°, 60°, 90°, 120° and 150°) in dilute conditions give an average hydrodynamic radius $R_H=17$ nm for the silica particles with a specific area $S_{spe} = (3/\rho_{Si}R_H) = 77$ m²/g, using $\rho_{Si} = 2.3 \cdot 10^6$ g/m³ for the density of pure silica. The silica suspension (52 wt%; pH = 8.5 – 9.5) was used as received.

Hybrid hydrogels were prepared by free-radical polymerization of AAm and MBA in an aqueous suspension of silica nanoparticles, using thermal dissociation of KPS as initiator, at 60°C. For all the syntheses the polymer concentration was set equal to 6 wt%. Aqueous solutions were prepared with the following concentrations: 10 wt% for AAm, 1 wt% for MBA, 1 wt% for KPS and 10 wt% for silica nanoparticles. The aqueous solutions were

introduced in a vessel in this order: AAm, MBA, KPS, silica nanoparticles and distilled water. After stirring, the obtained mixture was introduced in test tubes of 10 mm diameter through syringe filters of 0.8 μm . The sealed test tubes were placed in an oven at 60°C for 12 hours.

2.2.2. Dynamic light scattering measurements

Dynamic light scattering measurements were performed with an ALV CGS-3 goniometry system (ALV, Langen, Germany), equipped with a cuvette rotation/translation unit (CRTU) and a He-Ne laser (22 mW at $\lambda = 632.8$ nm). The system measures the time-averaged autocorrelation function of the scattered light intensity at a scattering vector q . In order to circumvent the non-ergodicity associated with the presence of frozen disorder in chemically cross-linked gels, the sample cell was vertically translated steadily while time-averaging. Thus, g_2 coincides with the ensemble-averaged autocorrelation function, up to a cut-off delay time fixed by the sample rotation speed. The averaging duration was more than 3600 seconds depending on the slowest relaxation modes found in the autocorrelation functions.

Gels samples for DLS measurements were prepared in test tubes (10 mm in diameter), prefiltered solutions were mixed in a test tube. Syringe filters of 0.8 μm were used.

Gelation of PAAm samples containing various amounts of silica nanoparticles was also studied by DLS. Gelation time was determined as the time where the system becomes non-ergodic, by measuring the scattered light intensity as a function of the elapsed time.

2.2.3. Microrheology by diffusing-wave spectroscopy

Microrheological measurements based on diffusing-wave spectroscopy (DWS) were performed using a laboratory-made setup. The coherent source was a Spectra Physics 2020 laser, operated at $\lambda = 488$ nm. The laser beam was expanded to approximately 1 cm at the sample. The diffused light was collected by an optical fibre placed in the transmission geometry.

Gels samples for DWS measurements were prepared in cuvettes for fluorescence spectroscopy (4 mm in path length). 1 wt% of commercial polystyrene microspheres (diameter: 500 nm) used as probes were dispersed in gels. The PVA-microsphere mixtures were stable, no aggregation was observed for all gels tested in this work for 6 months.

In order to obtain an ensemble-averaged autocorrelation function, a diffuser glass plate was placed in front of the optical fibre and rotated at a constant rate.

The procedure to obtain viscoelastic moduli, G' and G'' , from the DWS autocorrelation functions can be found elsewhere [28]. The field autocorrelation function and the scattered light intensity I_T were measured in the transmission geometry. The transport mean free path of the scattered light, l^* , which is the only unknown parameter, is obtained for each sample by comparing with the known value of l^* and I_T of water used as reference. The mean square displacement of the particles is then calculated from the expression given by Weitz and Pine [29], then G' and G'' are obtained using the generalized Stokes-Einstein equation.

2.3. Effect of chemical cross-linking

Figure 9 shows ensemble-averaged normalized field autocorrelation functions, $g^{(1)}(t)$, of PAAm gels with different chemical crosslinking ratios (without silica nanoparticle) measured at 90° .

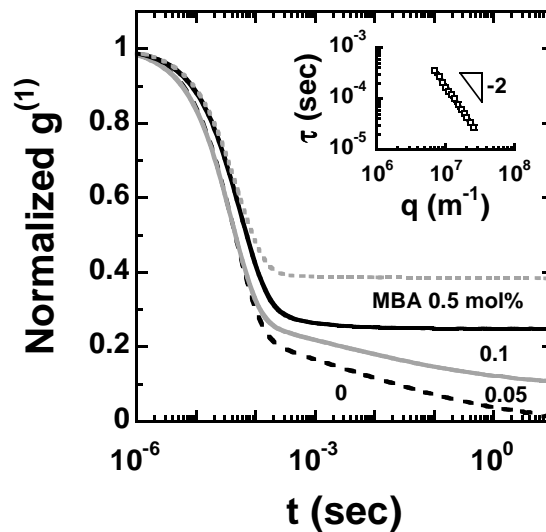


Figure 9: Normalized autocorrelation function of PAAm gels with different chemical cross-linking ratios. Inset: characteristic time of gel mode as a function of scattering vector q .

We observed one decorrelation around 10^{-4} sec followed by a plateau. This decorrelation is the so-called gel mode, or, collective dynamics of the gel network. The presence of the plateau corresponds to the presence of spatial heterogeneity which does not relax with time, indicating that the gels are non-ergodic. For the system without cross-linker (MBA) no clear plateau was found but a low amplitude slow mode, which corresponds to the dynamics of a concentrated PAAm polymer solution. The amplitude at the plateau increases with the increase in crosslinking ratio. The autocorrelation function of the cross-linked gels can be empirically well fitted with the following stretched exponential equation:

$$g^{(1)}(t) = A_{gel} \cdot \exp\left(\left(-\frac{t}{\tau_{gel}}\right)^\gamma\right) + g^{(1)}(\infty) \quad \text{Eq. 8}$$

where A_{gel} is the amplitude of the gel mode, τ_{gel} is its characteristic relaxation time, the exponent γ which takes into account the slight polydispersity, was found to be close to 1. $g^{(1)}(\infty)$ which is equal to $1 - A_{gel}$ indicates the amplitude of the plateau. For all the gels the characteristic time of the fast decay varies as $\tau_{gel} \sim q^{-2}$, as shown in the inset of **Figure 9** (the result for 0.1 mol% MBA), as usually observed for the gel mode. We did not observe a crosslinking ratio dependence of τ_{gel} .

Figure 10 shows ensemble-averaged normalized field autocorrelation functions of PAAm gels with different crosslinking ratios containing 1 wt% of silica nanoparticles. We observed two decorrelation modes followed by a plateau.

The autocorrelation function of these hybrid gels can be fitted similarly to the gels without nanoparticles by using the following equation with two stretched exponential decays:

$$g^{(1)}(t) = A_{gel} \cdot \exp\left(\left(-\frac{t}{\tau_{gel}}\right)^\gamma\right) + A_{Si} \cdot \exp\left(\left(-\frac{t}{\tau_{Si}}\right)^{\gamma_{Si}}\right) + g^{(1)}(\infty) \quad \text{Eq. 9}$$

Since τ_{Si} is at least two decades longer than τ_{gel} in these conditions, the two decorrelation modes can be discussed separately. The amplitude of the plateau $g^{(1)}(\infty)$ is almost the same as

that of the corresponding gel without silica nanoparticles in **Figure 9**. The faster decorrelation having a low amplitude is found around 10^{-4} sec similarly to the gels without silica nanoparticles. As shown in the inset of **Figure 10**, its characteristic time varies as $\tau_{gel} \sim q^{-2}$, indicating that this decorrelation corresponds to the gel mode. In the presence of silica nanoparticles, a slower mode appears, which is attributed to the dynamics of the nanoparticles in the gels. As we show later in this article, the amplitude of the two modes and the intensity from the polymer network and silica nanoparticles are correlated. Although the amplitude of the silica dynamics mode, A_{Si} , is much higher than that of the gel mode, A_{gel} , because silica nanoparticles scatter more light than the gel, we always observe the gel mode, in fact it is experimentally very difficult to neglect the component associated with the polymer concentration fluctuations of the gel without having multiple scattering from the particles.

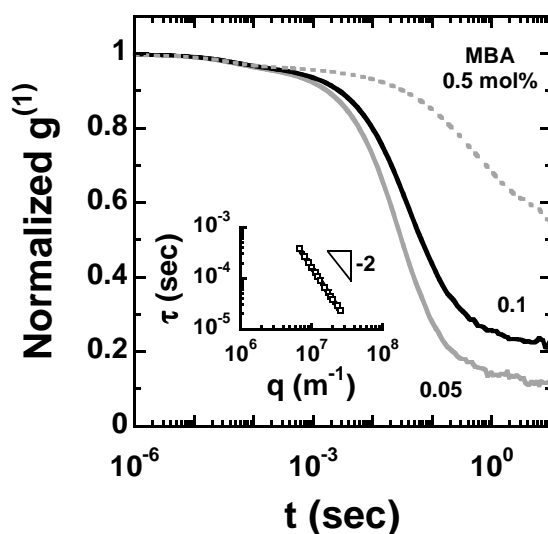


Figure 10: Normalized autocorrelation function of PAAm gels containing silica nanoparticles (at 1 wt%) with different chemical cross-linking ratios. Inset: characteristic time of gel mode as a function of scattering vector q .

Figure 11 shows the scattering vector dependence of the characteristic time of the silica dynamics. The characteristic time varies as $\tau_{Si} \sim q^{-2}$, indicating that the silica nanoparticles exhibit Brownian diffusion in PAAm gels. The value of τ_{Si} increases with the crosslinking ratio, suggesting that the diffusion is hindered by the chemical cross-links.

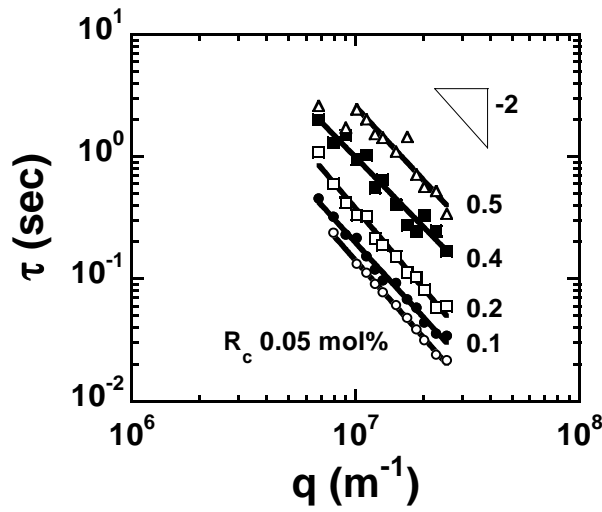


Figure 11: Characteristic times of silica nanoparticles diffusion mode of PAAm hybrid hydrogels at various chemical cross-linking ratios R as a function of scattering vector q .

In the literature one finds that the dynamic mode of bigger particles trapped in the gels scales as $\tau_{Si} \sim q^0$ [30, 31]. In other words, for trapped particles the characteristic length scale is no longer the observation scale $1/q$ but the size of the Brownian cage.

In **Figure 12**, we summarize the chemical crosslinking ratio dependence of the scattered light intensity of the hybrid gels (normalized by that of toluene), the collective diffusion coefficient of the gel mode, D_c , and the diffusion coefficient of silica nanoparticles, D_{Si} .

The scattered light intensity normalized by that of toluene used as reference was plotted as a function of the crosslinking ratio for PAAm gels with and without silica nanoparticles in **Figure 12 (a)** (measured at 90°). At the given silica nanoparticles concentration (1 %), silica nanoparticles scatter more light than the gel itself. The intensity from gels without silica increases slightly with the crosslinking ratio, indicating that the spatial inhomogeneity increases with increasing chemical cross-links. This result agrees with the increase in the amplitude of the plateau in the autocorrelation functions, $g^{(1)}(\infty)$. The intensity from the hybrid gel is independent of the crosslinking ratio, same as that of silica nanoparticles suspension without gel. This indicates that the spatial organization of the particles was not

changed by the hybridization, implying that no aggregation of nanoparticles occurs, neither polymer adsorption on the silica surface.

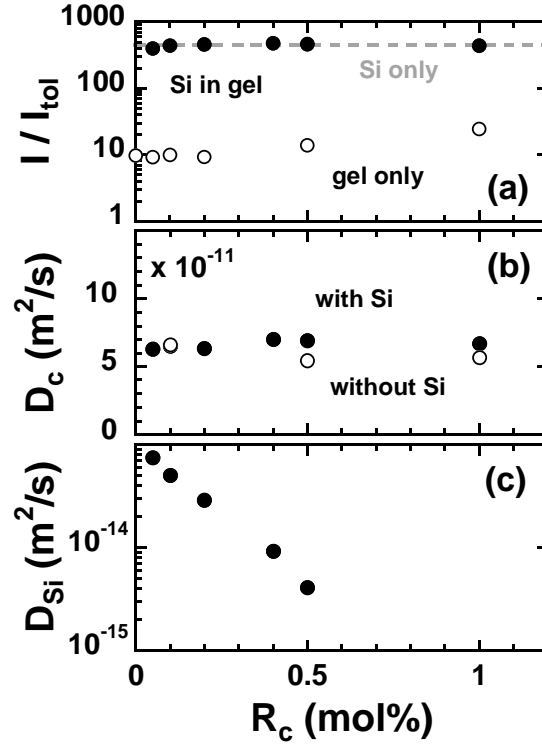


Figure 12: (a) Normalized scattering light intensity as a function of chemical crosslinking ratio of gels. The dashed line indicates the value for silica nanoparticle suspension at the same concentration without gel.

(b) Collective diffusion coefficient of PAAm chemical and hybrid gels.

(c) Diffusion coefficient of silica nanoparticles in PAAm hybrid gels.

As both decay modes found in the PAAm gels containing silica nanoparticles show q^{-2} dependence, the diffusion coefficient was calculated from the relation:

$$\tau = \frac{1}{D \cdot q^2} \quad \text{Eq. 3}$$

For the gel mode, the collective diffusion coefficient of the network, D_c , was determined. As shown in **Figure 12 (b)**, D_c does not depend on the crosslinking ratio or on the presence of silica nanoparticles, as observed in the literature [32]. We also observe a reasonable agreement with the absolute value of the diffusion coefficient found in the same reference.

Addition of 1 wt% of silica nanoparticle does not affect the value of D_c , confirming the observation in **Figure 12 (a)**: the presence of the nanoparticles does not modify the network structure or dynamics at this C_{Si} .

The diffusion coefficient for silica nanoparticles decreases exponentially with the crosslinking ratio as shown in **Figure 12 (c)**. For R_c less than 0.5 mol% in feed, we obtained the values of D_{Si} varying between $10^{-13} - 10^{-15} \text{ m}^2/\text{s}$. For $R_c = 1 \text{ mol\%}$ we did not observe the silica dynamics mode within the accessible time scale (less than about 10 seconds), due to very slow diffusion or total immobilization. Seiffert *et al.* studied tracer diffusion of polystyrene nanospheres in chemically photo-cross-linked PAAm hydrogels at different polymer concentrations and crosslinking ratios by fluorescence recovery after photobleaching (FRAP) [16]. For nanospheres having hydrodynamic radius of 17 nm, they found that D is about $2 - 3 \times 10^{-13} \text{ m}^2/\text{s}$ for R_c less than 0.05 mol%. The length scale they used to characterize the mesh size of the chemical gels was the mean distance between cross-links, ξ_x , defined as:

$$\xi_x = (\nu_{eff})^{-1/2} \quad \text{Eq. 10}$$

where ν_{eff} is the number concentration of efficient cross-links ($1/\text{m}^3$), related to the elastic modulus of the gel G' as:

$$G' = f \cdot \nu_{eff} \cdot RT \quad \text{Eq. 11}$$

where f is a structure factor equal to 1/2 for tetrafunctional cross-links, R is the gas constant and T the absolute temperature.

In order to evaluate correctly the efficiency of the crosslinking and mesh size, the shear elastic modulus of our PAAm gels was measured by diffusing-wave spectroscopy-based microrheology. The elastic and loss moduli of the PAAm gel as a function of angular frequency are plotted in **Figure 13**. The values of G' are plotted as a function of R_c in the feed.

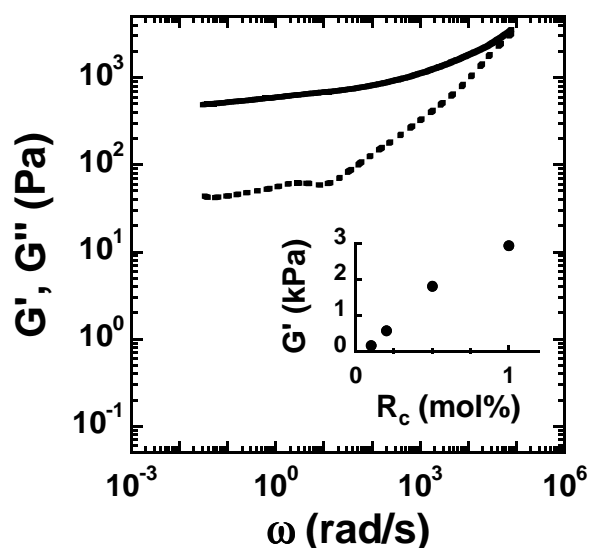


Figure 13: Storage and loss moduli of PAAM hydrogels ($R_c = 0.2$ mol%) measured by diffusing-wave spectroscopy: G' (solid line) and G'' (dashed line). Inset: storage modulus at 1 Hz as a function of R_c .

Using Eq. 11, an efficient crosslinking concentration can be calculated from G' and compared with the value calculated from the feed [33]. We found that the efficiency of the crosslinking reaction is about 15 % for the radical polymerization of AAm by MBA in these conditions. The efficiency is less than that of photo-cross-linked gels in the reference, suggesting that our gels have a less well defined, more loosely cross-linked network structure presumably more heterogeneous. This conclusion is confirmed also by the slight frequency dependence of G' and relatively high value of the loss modulus G'' . Orakdogan *et al.* obtained values of crosslinking efficiency lower than our results for 5 % PAAM concentration [34]. They attributed the low efficiency to cyclization and multiple crosslinking reactions leading to elastically inactive cross-links and an inhomogeneous crosslink distribution. For 5 % PAAM we did not obtain a reproducible gelation at the studied conditions.

The diffusion coefficient of the silica nanoparticles in PAAM gels in Figure 12 (c) was re-plotted against the effective crosslinking ratio in Figure 14.

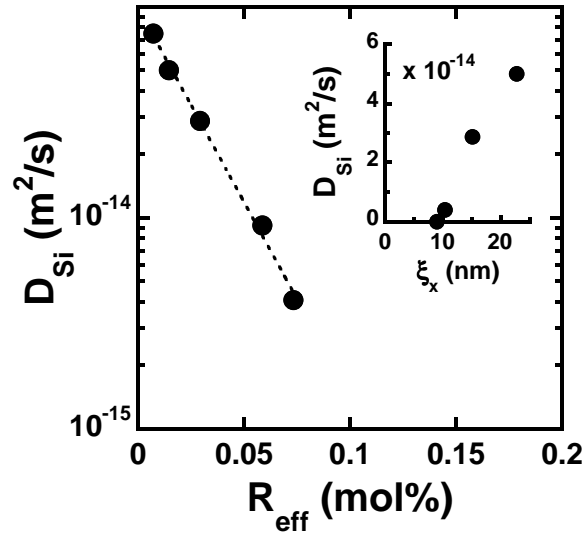


Figure 14: Diffusion coefficient of silica nanoparticles D_{Si} in PAAm gels as a function of the effective cross-linking ratio R_{eff} . Inset: D_{Si} as a function of the mean distance between cross-links.

D_{Si} increases exponentially with the crosslinking ratio, giving the relationship:

$$D_{Si} = D_0 \cdot \exp\left(-\frac{R_{eff}}{0.024}\right) \quad \text{Eq. 12}$$

where $D_0 = 1 \times 10^{-13} \text{ m}^2/\text{s}$ corresponds to the diffusion coefficient in an uncross-linked polymer solution. Note that it is rather difficult to measure correctly D_{Si} in uncross-linked polymer, because of the slow mode of the uncross-linked polymer which happened to superpose to the silica diffusion mode (**Figure 9**), and the separation of overlapping two modes is usually impossible.

This value is larger than that in the literature [32], presumably due to the difference in the molecular weight of the matrix polymer. At higher crosslinking density, where FRAP observed immobilization of the tracers, this DLS experiment provided a value without immobilization. This is presumably due to the fact that the length scale of observation accessible by DLS ($1/q$) is smaller than that of FRAP which requires the displacement over several microns, thus slow diffusion and immobilization can be separated.

The equation above is close to the universal scaling equation which describes the diffusion of various probes in polymer solutions that has been proposed by Phillies as a function of the

concentration and molecular weight of the matrix polymer and the tracer radius [35, 36]. Scaling with the crosslinking density of chemical gels, on the contrary, has rarely been studied. Langevin *et al.* proposed a scaling relation with the ratio of probe size to pore size [37], and Park *et al.* used the dynamic correlation length ξ_c as pore size [38] with:

$$\xi_c = \frac{k_B T}{6\pi\eta D_c} \quad \text{Eq. 13}$$

Instead of ξ_c , here we used ξ_x as characteristic length of the mesh size. The inset of the **Figure 14** shows the decrease in D_{Si} as a function of ξ_x . D_{Si} decreases to zero at $\xi_{xc} = 9$ nm. This value is very low compared with the radius of the silica nanoparticles ($R_h = 17$ nm), suggesting that an inhomogeneous crosslink distribution may result in a larger local mesh size for probe diffusion than the macroscopically determined average elastic mesh size ξ_x . Detailed studies using different probe sizes are required for further discussion.

2.4. Effect of silica nanoparticles concentration

Figure 15 shows the autocorrelation functions of hybrid gels containing silica nanoparticles of various concentrations. For all the gels shown in this figure except for the 0.02 wt%, which shows only a fast mode, we observed two decorrelation modes followed by a plateau. For 0.02 wt% the value of the plateau was much higher than for the other gels which had almost the same value as the gel without silica nanoparticles. This result suggests that the hybrid gel containing 0.02 wt% is more heterogeneous than the gels containing more silica nanoparticles.

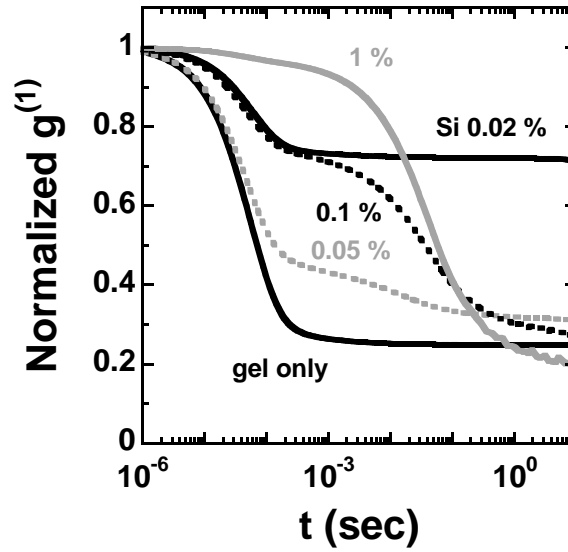


Figure 15: Normalized autocorrelation functions PAAm chemical gels containing silica nanoparticles at different concentrations.

The amplitude of the silica nanoparticles decorrelation mode is associated with the fluctuating part of the scattering intensity of the gel and nanoparticles: the ratio of the amplitudes A_{Si}/A_{gel} is proportional to the scattered light intensity of the nanoparticles. As shown in **Figure 16 (a)**, the ratio of the amplitude is proportional to the nanoparticles concentration at higher concentration, thus to the intensity. On the contrary, at lower concentrations, the ratio of the amplitudes deviates negatively from the linearity, we do not observe silica nanoparticle dynamics mode at lower concentration than 0.03 wt%. Two explanations are possible: (1) one part of the silica nanoparticles shows slower diffusion or is immobilized thus its characteristic time is not measured in the accessible time scale, and/or (2) the structure of the gel is different due to the presence of a small amount of silica nanoparticles, thus the network is more heterogeneous than with more nanoparticles. The latter possibility indicates that the silica nanoparticles diffusion is not a tracer diffusion.

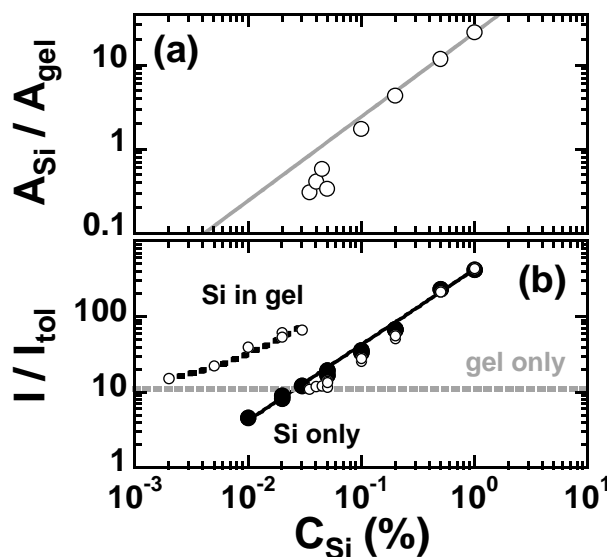


Figure 16: (a) Ratio of the amplitudes of silica diffusion mode to gel mode as a function of the silica concentration in PAAm gel. Solid line shows the linear fit of the data.

(b) Normalized scattering light intensity as a function of silica nanoparticles concentration in suspension (Si only), in PAAm hybrid gels (Si in gel). The dashed line indicates the value for PAAm gels without silica nanoparticles.

The normalized intensity of hybrid gels and silica nanoparticle suspensions as a function of silica nanoparticle concentration was shown in **Figure 16 (b)**. For silica nanoparticles in the suspension (filled circles), the intensity was proportional to the concentration within the studied concentration range. The black solid line shows the linear fit: $I/I_{tol} = B \cdot C_{Si}$ with B was found to be 420. In PAAm gels (open circles), the concentration dependence is more complicated: at concentrations higher than 0.1 wt%, the value of the intensity is the same as that in suspension. At lower concentration than 0.03 wt%, the intensity is significantly higher than that in suspension. The intensity decreases linearly with the concentration, approaching the value of gel without silica nanoparticle ($I_{gel}/I_{tol} = 11$, indicated by the gray dashed line). The black dashed curve shows the fitting curve: $I/I_{tol} = 2100 \cdot C_{Si} + I_{gel}/I_{tol}$. This result indicates that the structure, or spatial distribution of the silica nanoparticles and/or PAAm network, is modified by addition of a small amount of nanoparticles. The value of the coefficient B in the hybrid gel is 5 times as large as that of the corresponding suspension, suggesting that at such low Si concentration, the structure of the gel and/or silica nanoparticles is changed relative to the suspension in solution. We do not have clear explanation of this surprising result. We do

not believe that there is aggregation of the nanoparticles: the characteristic time of doublet formation is inversely proportional to the particle concentration [39], hence it is not probable to have aggregates at low concentration but not at higher concentrations. Furthermore, we did not observe any time evolution of the intensity during several days after polymerization/gelation, although the silica nanoparticles are diffusing in the gel network as shown previously in this article. We also observed exactly the same value of the intensity as for non-cross-linked system, while aggregates should be more sensitive to the network structure than the primary particles.

The effect of the concentration of silica nanoparticles on the dynamics of the network and on the diffusion of nanoparticles is studied. **Figure 17 (a)** shows the collective diffusion coefficient as a function of the silica nanoparticle concentration.

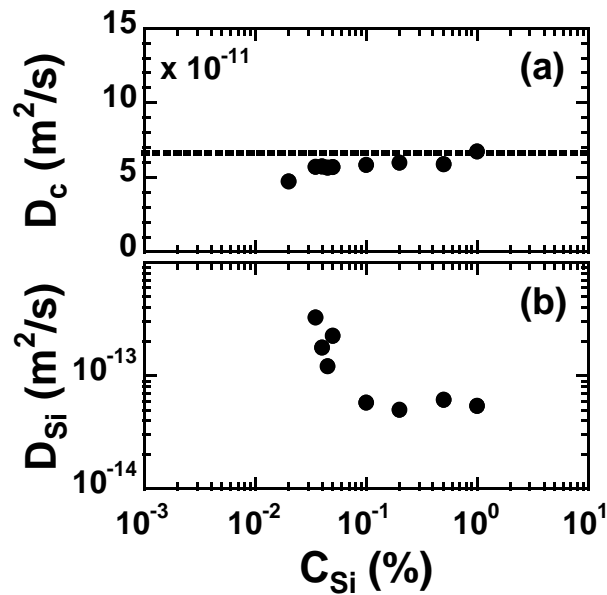


Figure 17: (a) Collective diffusion coefficient of PAAm hybrid gels.

(b) Diffusion coefficient of silica nanoparticles in PAAm hybrid gels as a function of silica nanoparticles concentration. The dashed line indicates the value for PAAm gels without silica nanoparticles.

We observed no effect of the nanoparticle concentration on the ensemble-averaged network dynamics. Since the silica nanoparticle concentration is low, the ensemble-averaged

dynamics of the network are not influenced by the change around the nanoparticles. The nanoparticle dynamics, however, are more sensitive to the micro-environmental change. **Figure 17 (b)** shows the diffusion coefficient of the silica nanoparticles as a function of the nanoparticle concentration. At concentrations higher than 0.1 %, the value of D_{Si} is constant, while between 0.03 and 0.05 %, D_{Si} increases with decrease in the concentration. The values of D_{Si} are higher than $1 \times 10^{-13} \text{ m}^2/\text{s}$, the value of the uncross-linked system, suggesting that the network concentration surrounding the nanoparticles is very different from the network with high amount of silica particles. These results indicate that the change in the intensity shown in **Figure 16 (b)** is localized in the vicinity of the particles.

In order to further characterize the effects of silica nanoparticle concentration on the radical polymerization, the gelation time of the PAAm hybrid gel was measured by DLS and plotted as a function of silica nanoparticles concentration in **Figure 18**.

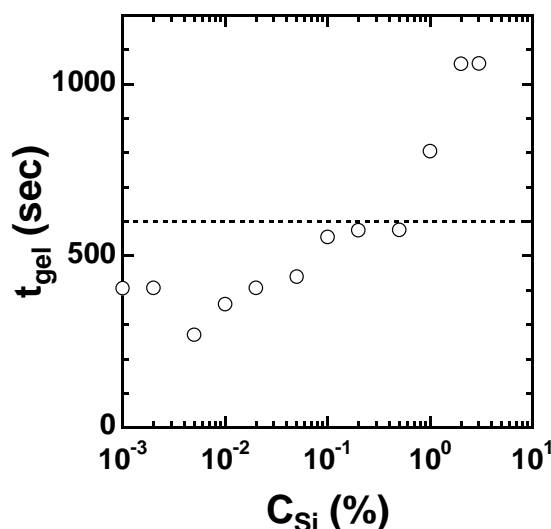


Figure 18: Gelation time of PAAm hybrid gels as a function of silica nanoparticles concentration.

Without silica nanoparticle the gelation time was measured to be 600 sec. In the presence of small amount of silica nanoparticles, the gelation time decreased to about 300 sec with increase in the silica nanoparticles concentration, and then it increased with C_{Si} higher than 0.01 %.

For various nanocomposite hydrogel systems prepared by radical polymerization in the presence of inorganic particles, kinetics of gelation have been studied. Haraguchi *et al.* and Okay *et al.* studied rheologically the gelation process of PAAm or PNIPAAm in the presence of clay particles [8, 26]. Clay particles can show gelation without added polymers when the ionic strength increases, it is very difficult to characterize the gelation of the nanocomposite since the radical initiator persulfate is salt. Suzuki *et al.* reported gelation kinetics of PNIPAAm in the presence of silica nanoparticles of different sizes studied by DLS [14]. Since PNIPAAm adsorbs strongly onto silica, they did not discuss the effect of nanoparticle concentration.

Caregnato *et al.* reported on the kinetics of radical polymerization in the presence of silica nanoparticles [40]. They showed that transfer of radicals from persulfate to silica surfaces can occur. There are three silica radical species which can initiate polymerization, each having different rate constants. Therefore, in our system we expect that the persulfate radicals can be transferred to the silica nanoparticle surfaces, so that grafting polymerization of PAAm starting from the silica nanoparticle surface can occur. From the results and discussion above, we can illustrate schematically the structure induced by radical transfer to the silica surface (Figure 19).

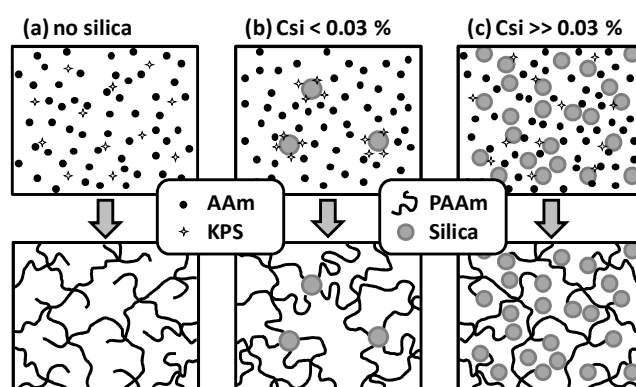


Figure 19: Schematic illustration of radical polymerization of PAAm gels initiated by $K_2S_2O_8$ in the presence of silica nanoparticles at different concentrations. (a) no silica nanoparticles. (b) at a lower nanoparticles concentration. (c) at a higher silica nanoparticle concentration.

At given AAm and KPS concentrations, when the silica nanoparticles concentration is high, most of the nanoparticles are not influenced by the persulfate radicals, and thus exhibit tracer diffusion in the gel after the polymerization. Decreasing the silica nanoparticles concentration results in an increase in the amount of persulfate radical per silica nanoparticle surface, thus most of nanoparticles have a layer of grafted polymer growing from the radicals transferred onto the surface. The silica nanoparticles can attract monomers in the vicinity of the reacting surface. This can create more heterogeneous structure. The critical change in the intensity between $C_{Si} = 0.003$ and 0.0035 (%) is presumably due to a certain cooperative radical polymerization. The radical polymerization localized at a small amount of silica particles surface induces localized consumption of monomers and growth of polymers coupled with gelation, creating a complex concentration gradient of the components. Further detailed investigation on the radical polymerization from the silica surface would be necessary.

2.5. Conclusions

The dynamics of hybrid polyacrylamide hydrogels containing silica nanoparticles have been studied by dynamic light scattering. The effects of two main physico-chemical parameters were observed and explained here. First, the concentration of the chemical cross-linker (MBA) was studied in several conditions. Without silica nanoparticles, an increase in cross-linker concentration led to an increase of the heterogeneity of the hydrogels, expressed in terms of a plateau value in the ensemble-averaged normalized field autocorrelation function, $g^{(1)}(t)$. In the presence of silica nanoparticles, we can observe the appearance of an additional slow mode corresponding to the dynamics of particles in the gels. This Brownian diffusion is hindered by an increase of the cross-linker concentration, as a direct consequence of the decrease of the network mesh size. We demonstrated here that there is no adsorption of polymer on the silica surfaces and that the presence of silica nanoparticles does not affect the network structure or dynamics.

Second, the effect of the silica concentration on the gel dynamics was studied. We reported the presence of two decorrelation modes followed by a plateau in a large range of silica concentrations. However, at a silica concentration lower than 0.03% , the silica dynamics was

not observed. At those low concentrations, only one fast mode is present and the plateau value of the autocorrelation function is very high, indicating that we are in presence of very heterogeneous networks. We believe that a transfer of radicals from the persulfate used to the surface of the silica nanoparticles is the origin of a PAAm chain growth from the silica surface: a grafting polymerization of AAm occurs, giving rise to the heterogeneous network structure schematically illustrated in **Figure 19**. At higher silica nanoparticles concentration, due to the more surface available this effect of the modified radical polymerization is averaged thus we observed no particular change. This radical transfer is expected to be valid for other nanocomposite hydrogels prepared by radical polymerization. In our experiments, decreasing the silica nanoparticles concentration revealed the effect on the dynamics.

Now that the silica dynamic inside PAAm hydrogels is well understood, the effect of the addition of an interacting monomer (DMA) will be studied in the following part.

3. Dynamics of PDMA hybrid hydrogels studied by DLS

This part of the chapter shows the study of the dynamics of poly(acrylamide-co-*N,N*-dimethylacrylamide) hydrogels containing silica nanoparticles by DLS. It is also a manuscript that has been accepted by *Macromolecules: Dynamics of Hybrid Poly(acrylamide-co-*N,N*-dimethylacrylamide) Hydrogels Containing Silica Nanoparticles Studied by Dynamic Light Scattering*, *Macromolecules*, 2013, **46** (13), pp 5329-5336.

3.1. Abstract and introduction

Abstract

Nanohybrid gels based on poly(acrylamide-co-*N,N*-dimethylacrylamide), P(AAm-co-DMA), and colloidal silica nanoparticles were synthesized by radical polymerization, and influence of hydrogen bonding between DMA and silica nanoparticles on the dynamics of the network and the nanoparticles were studied by dynamic light scattering. As previously reported, in the case of polyacrylamide homopolymer, PAAm, which have no hydrogen bonding with silica, we observed two decay modes in the hybrid gels, gel mode and Brownian diffusion mode of silica nanoparticles. When we increased the DMA weight fraction (or physical cross-link), we observed (1) higher scattered light intensity than silica suspension and gel without silica, (2) increased plateau value of the autocorrelation function, (3) slow down of the silica diffusion mode, and (4) no influence on the gel mode. These results, after a comparison with those of the mixtures of the linear PDMA and silica nanoparticles in solution showing an increase in the scattered light intensity and in the hydrodynamic radius, indicate that the P(AAm-co-DMA) hybrid gels have more heterogeneous structure due to the adsorption of the polymer on the silica nanoparticles, and that the silica nanoparticles, trapped in the network due to the adsorption of the polymer, show cage dynamics in the network. The local viscoelastic properties probed by the bound nanoparticles are discussed.

Introduction

Hydrogels are cross-linked polymers forming a three-dimensional network highly swollen by an aqueous medium. From a macroscopic point of view, if the lifetime of polymer cross-

links is long enough compared to the experimental time, hydrogels behave like solids; they have a defined geometry and they do not flow like liquids in the corresponding timescale. Simultaneously, these macromolecular reservoirs are similar to real solutions as diffusion mechanisms can occur through hydrogels, with diffusion coefficients depending on the mesh size of the network and on the level of interactions. Since the beginning of the 80's, hydrogels have had a continuous development, leading to many bio-applications such as drug delivery systems, superabsorbent or contact lenses, etc [41-44].

The high water content of hydrogels is at the origin of their dominating brittleness, limiting their applications: they break under few kPa of stress. The reinforcement of the poor mechanical properties of hydrogels is actually a fundamental challenge for a lot of research teams, motivated by the numerous future applications of hydrogels. Over the past ten years, several reinforcement strategies have been developed all over the world, such as the elaboration of ideal networks [18, 19], the design of double networks [20, 21], and the combination of organic and inorganic components in nanocomposite hydrogels. This last strategy has been largely studied by Haraguchi *et al.* [22-24] This strategy aims at mixing chemical and reversible interactions by introducing inorganic nanoparticles in the polymer network. The mechanical properties of a system based on poly(*N*-alkylacrylamide) hydrogels with silica nanoparticles have been widely studied [17, 25]. Reinforcement due to strong adsorption of polymer chains onto the surface of silica nanoparticles has been demonstrated, leading to a simultaneous enhancement of elasticity and strain at failure.

In these nanocomposite gels, prepared with and without chemical cross-linker (such as *N,N'*-methylenebisacrylamide), inorganic particles behave as physical multiple crosslinking points. Mechanisms for forming the unique network structure have been proposed. Haraguchi *et al.* proposed the formation of "clay-brush particles" [26]. As a matter of fact, the interactions between clay surfaces and a mixture of *N*-isopropylacrylamide monomer, potassium persulfate and a common catalyst (TEMED) lead to the growth of polymer brushes grafted on the exfoliated clay platelets. With this specific grafting, occurring at the first steps of the polymerization, the obtained hybrid hydrogels are heterogeneous regarding the spatial organization of crosslinking points. Abdurrahmanoglu *et al.* proposed adsorption

of N-alkylacrylamide monomers on the clay particle surfaces, leading to depletion-induced particle aggregates [27].

Recently, we studied the dynamic behaviours of these chemically and physically cross-linked networks and of the nanoparticles, that had been surprisingly less studied in the literature [45]. The nature and the quality of the interactions occurring between the polymeric matrix and the nanoparticles clearly affect the dynamics of the system. Working on the dynamics of hybrid polyacrylamide hydrogels containing colloidal silica particles, we explored the effects of chemical crosslink, physical crosslink and radical polymerization separately. Different from the poly(*N*-alkylacrylamides) which are known to be able to form hydrogen-bonds with silica, polyacrylamide shows less interaction since it is simultaneously hydrogen-bonding donor and acceptor: the hybrid polyacrylamide hydrogels do not show any reinforcement property when synthesized in presence of silica nanoparticles [17]. In our precedent study [45], the silica nanoparticles acted as diffusion tracer probing the microenvironment in the polyacrylamide hydrogel. We demonstrated that a transfer of radicals from the persulfate used to the surface of the silica nanoparticles was at the origin of a polyacrylamide chain growth from the silica surface: a grafting polymerization of acrylamide occurs, giving rise to heterogeneous network structures.

In the present study, we report a dynamic light scattering study of the dynamics silica nanoparticles in poly(AAm-co-DMA) hybrid gels. The physical interaction between DMA and silica nanoparticles is attenuated by changing the copolymerization composition. We show that the addition of the hydrogen bonding monomer DMA changes dramatically the dynamics of silica nanoparticles in the gels compared with the gels without specific interaction. The physical interaction traps the silica nanoparticles in the gel, showing a cage dynamic behaviour. We try to correlate this local dynamics with the separated mechanical experiments of poly(AAm-co-DMA) hybrid gels; previously it has ever been demonstrated [17, 25] that the first monomer (AAm) does not lead to any mechanical reinforcement, while the second one (DMA) clearly increases the initial stiffness and the strain at failure in presence of silica nanoparticles. This second study is also a commented version of another submitted article.

3.2. Synthesis and characterization methods

3.2.1. Synthesis of P(AAm-co-DMA) hybrid hydrogels

N,N-dimethylacrylamide (DMA, 99%, Sigma Aldrich), acrylamide (AAm, 99%, Sigma Aldrich), *N,N'*-methylenebisacrylamide (MBA, Fluka), potassium persulfate (KPS, Acros Organics), poly(*N,N*-dimethylacrylamide) (PDMA, Mw: 100000 g/mol, Scientific Polymer Products), urea (Sigma Aldrich) were used as received without further purification. The silica particles (Ludox-TM50) were purchased from Aldrich. They were characterized by dynamic light scattering using an ALV/CGS-3 compact goniometer (ALV, Langen, Germany) in dilute conditions giving an average hydrodynamic radius $R_h=17$ nm. A specific area $S_{spe} = (3/\rho_{si}R) = 100$ m²/g, using $\rho_{si} = 2.3 \cdot 10^6$ g/m³ for the density of pure silica. The silica suspension (52 wt%; pH=8.5 – 9.5) was used as received.

Hybrid hydrogels were prepared by free-radical co-polymerization of DMA and AAm monomers and MBA in an aqueous suspension of silica nanoparticles, using thermal dissociation of KPS as initiator, at 80°C. For all the syntheses the polymer concentration was set equal to 6 wt%. Aqueous solutions were initially prepared with the following concentrations: 10 wt% for AAm, 2.5 wt% for DMA, 1 wt% for MBA, 1 wt% for KPS and 10 wt% for silica nanoparticles. The aqueous solutions were introduced in a vessel in this order: AAm, DMA, MBA, KPS, silica nanoparticles and distilled water. After stirring, the obtained mixture was introduced in test tubes of 10 mm diameter through syringe filters of 0.8 µm. The sealed test tubes were placed in an oven at 80°C for 12 hours. The weight fraction of the DMA monomer to the total monomer content, ω_{DMA} was varied from 0 to 0.1. Since the total monomer concentration was kept to 6 wt%, the DMA concentration to the total gel weight is $6 \cdot \omega_{DMA}$ (wt%).

3.2.2. Dynamic light scattering measurements

Dynamic light scattering measurements were performed in the same manner as described in the previous study.

3.2.3. Hydrogels synthesis for mechanical measurements

Hydrogels were prepared at 25°C by free-radical polymerization of DMA and AAm in an aqueous suspension of silica nanoparticles using KPS and TEMED as redox initiators. For all syntheses, the (DMA)/(KPS) and (DMA)/(TEMED) molar ratio were fixed equal to 100. The crosslinking density was also kept constant, using a cross-linker/monomer molar ratio (MBA/DMA) equal to 0.1 mol%. The amount of silica nanoparticles was varied, keeping constant the matrix composition, *i.e.* the water /polymer ratio, corresponding to a concentration of 12.5 wt%.

Two aqueous solutions are prepared: KPS at 4.5 wt% and MBA at 1.2 wt%. First, MBA solution and DMA and/or AAm were dissolved at 25°C in an aqueous suspension of silica particles. The homogeneous suspension was purged with nitrogen during 15 minutes under magnetic stirring. At the same time, the aqueous solution of KPS was prepared and deoxygenated with nitrogen bubbling. KPS solution and TEMED were then rapidly added into the suspension under vigorous stirring. Finally, the mixture was transferred, under nitrogen atmosphere, into appropriate laboratory-made moulds. The samples were left for 24 hours in a closed vessel under nitrogen atmosphere before use.

3.2.4. Mechanical measurements

Mechanical tests were performed on a tensile Instron machine (model 5565) equipped with a 10 N load cell (with a relative uncertainty of 0.16 % in the range from 0 to 0.1 N) and a video extensometer (with a relative uncertainty of 0.11 % at full scale of 120 mm). The nominal strain was kept equal to 0.06 s⁻¹. Sample geometry was kept constant: the gauge length $L_0 \approx 20 - 25$ mm, the width $w = 5$ mm and the thickness $t = 2$ mm. In order to avoid any change in hydrogel composition, induced by swelling or drying during the experiment, samples were stored into paraffin oil until mechanical testing.

3.3. Effect of DMA/silica interactions on the dynamics

In order to clearly discuss the dynamics of P(AAm-co-DMA) hybrid gels, we characterized at first a reference network composed of cross-linked P(AAm-co-DMA) without silica

nanoparticles. In this work the chemical crosslinking ratio was fixed to 0.1 mol%, sufficient to obtain well defined plateau in the autocorrelation function, low enough to allow the particles to have certain dynamics. **Figure 20** shows a comparison of the normalized field autocorrelation functions of a PAAm hydrogel with a P(AAm-co-DMA) hydrogel (with a weight fraction of DMA to the total monomer content equal to $\omega_{DMA} = 0.05$) without silica nanoparticle. We found no difference between the two gels: for both hydrogels, a decorrelation corresponding to the gel mode characteristic of the collective diffusion of the cross-linked network, is followed by a plateau whose amplitude corresponds to the non-fluctuating concentration gradient of the gel. The addition of DMA monomer does not influence the dynamics of the gel presumably due to the physicochemical similarities of the two monomers and the small amount of added DMA. For all the gels studied in this work we found a q^2 dependence of the characteristic time of the gel mode (no data shown). The diffusion coefficient, D , is defined as $\tau = 1/(D \cdot q^2)$.

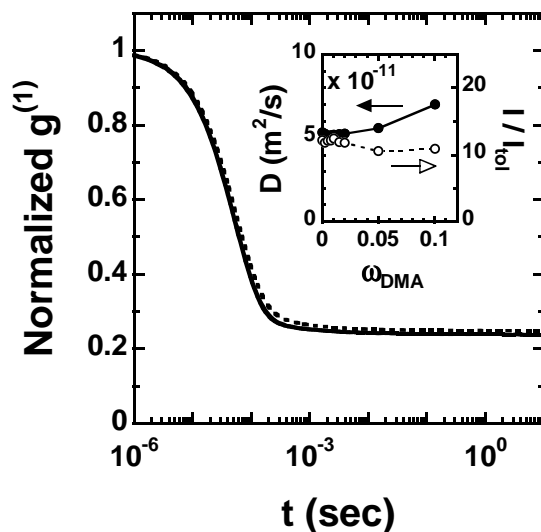


Figure 20: Normalized field autocorrelation functions for PAAm gel (solid line) and P(AAm-co-DMA) gel (dashed line). The weight fraction of DMA monomer was 0.05. Inset: collective diffusion coefficient and normalized intensity of P(AAm-co-DMA) chemical gels as a function of DMA weight fraction.

The effects of the silica nanoparticles added into the polymeric network on the dynamic properties of the polymeric network were studied. Here the reference hybrid hydrogel is

composed of a pure PAAm network chemically cross-linked by 0.1 mol% of MBA and containing 1 wt% of silica nanoparticles (grey line in **Figure 21**). This hybrid hydrogel shows a first decorrelation mode at about 10^{-4} sec (gel mode) and a second one at about 0.1 sec corresponding to the silica nanoparticles dynamics as previously reported [45]. The introduction of DMA to the acrylamide network leads to practically no effect on the gel mode even in the presence of the silica nanoparticles at given concentration, the characteristic time does not change with DMA concentration as shown in the inset of **Figure 21**. On the other hand, a pronounced change in the silica dynamics was observed: increasing the DMA content apparently results in (1) an increase in the characteristic time of the silica nanoparticles dynamics and (2) an increase in the amplitude of the plateau.

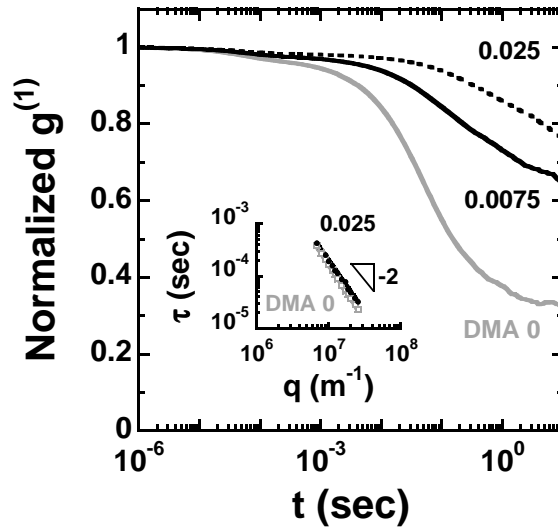


Figure 21: Normalized field autocorrelation functions of P(AAm-co-DMA) hybrid gels containing 1 % silica nanoparticles. Inset: q dependence of the gel mode characteristic time.

The characteristic times τ_{Si} of the silica nanoparticles dynamics are plotted as a function of the scattering vector q in **Figure 22**. We observed that τ_{Si} increased with increase in the DMA weight fraction showing a q^{-2} dependence at high q values. At low q values τ_{Si} is independent of q , $\tau = 0.5$ (sec) for $\omega_{\text{DMA}} = 0.0075$, and $\tau = 1.5$ (sec) for $\omega_{\text{DMA}} = 0.025$. This q independent dynamics can be interpreted as the dynamics of particles in a “cage”: the particles are bound to the polymer or trapped in the network and show a limited displacement in a cage. Thus, at the length scale of observation $1/q$ larger than the cage size δ , τ_{Si} is independent of q . And

at $1/q < \delta$, sub-diffusive movement inside the cage can be observed and τ_{Si} shows a q^{-2} dependence. The transition from the q^{-2} to the q^0 dependence occurs at $q_{\text{cage}} = 1/\delta = 1.3 \times 10^7 \text{ m}^{-1}$ for $\omega_{\text{DMA}} = 0.0075$ (thus $\delta = 77 \text{ nm}$) and at $q_{\text{cage}} = 1/\delta = 1.9 \times 10^7 \text{ m}^{-1}$ for $\omega_{\text{DMA}} = 0.025$ ($\delta = 52 \text{ nm}$). The cage size δ decreased with an increase in the DMA concentration, we will discuss the dependence later in this chapter.

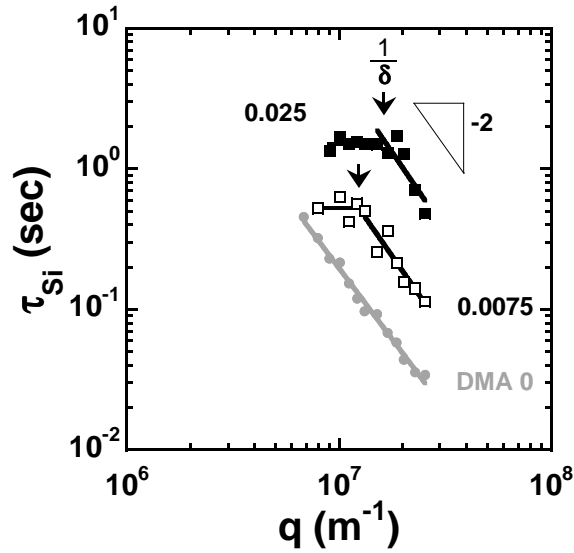


Figure 22: Characteristic times of gel mode and silica nanoparticle diffusive mode in P(AAm-co-DMA) hybrid gels having various DMA weight fraction.

For the system having caged particles, the asymptotic value at the plateau is related to the cage size δ [46]:

$$\begin{aligned} g^{(1)}(q, \infty) &= \exp(-q^2 \delta^2) \\ \ln g^{(1)}(q, \infty) &= -q^2 \delta^2 \end{aligned} \quad \text{Eq. 14}$$

Figure 23 shows logarithmic value of the normalized field autocorrelation function at the plateau as a function of q^2 . For the reference hybrid PAAm gel ($\omega_{\text{DMA}} = 0$), we observed that the plateau value is independent of q^2 . For the hybrid gels containing DMA, we observed the transition from the cage dynamics to diffusive movement: at lower q values, logarithmic of the plateau value of $g^{(1)}$ is proportional to q^2 , the slope should be equal to $-\delta^2$, while at higher q values, it is independent of q^2 . This result agrees with the observation of τ_{Si} : at low q , the silica nanoparticles show the cage dynamics.

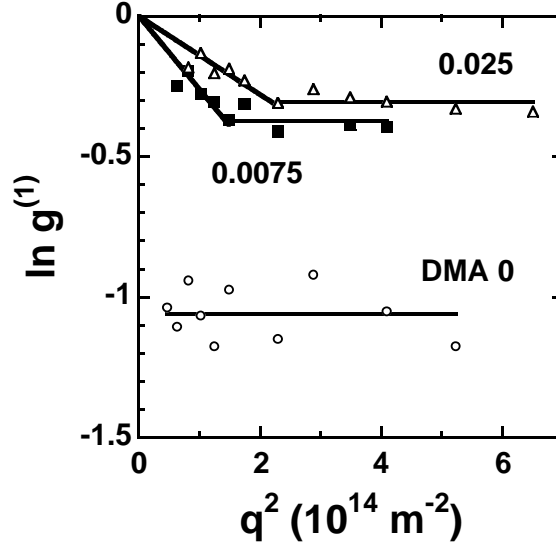


Figure 23: q^2 dependence of $\ln g^{(1)}$ at the plateau.

The two values of δ , one estimated from the transition point of q^0 to q^2 dependence, the other from the slope of the plateau value of $\ln g^{(1)}$ were compared. We found smaller value of δ for the second estimation (from the slope). For example, for $\omega_{\text{DMA}} = 0.0075$, we found $\delta = 77$ nm from the transition point and 51 nm from the slope.

This discrepancy can be interpreted as lower slope value due to high asymptotic value originating from the higher total scattered light intensity. The amplitude of each relaxation mode and that of the plateau value are related to the scattered light intensity of the corresponding mode. The plateau value is correlated also to the frozen-in component of the scattered light deriving from the static concentration gradient of the network. **Figure 24** shows the normalized scattered light intensity as a function of DMA weight fraction. At low DMA fractions (from 1×10^{-3} to 3×10^{-3}), the intensity is the same as that of silica nanoparticles in suspension ($I/I_{\text{tol}} = 450$), and much bigger than that of the gel without silica nanoparticle ($I/I_{\text{tol}} = 11$). At $\omega_{\text{DMA}} = 0.004$, the intensity suddenly increases up to about 900, showing no particular DMA fraction dependence at higher concentration. These results indicate that the structure of the network and/or silica dispersion in the gel were modified by DMA. Thus the plateau value of the network is higher than that estimated from the cage dynamics, giving lower value of the slope thus δ .

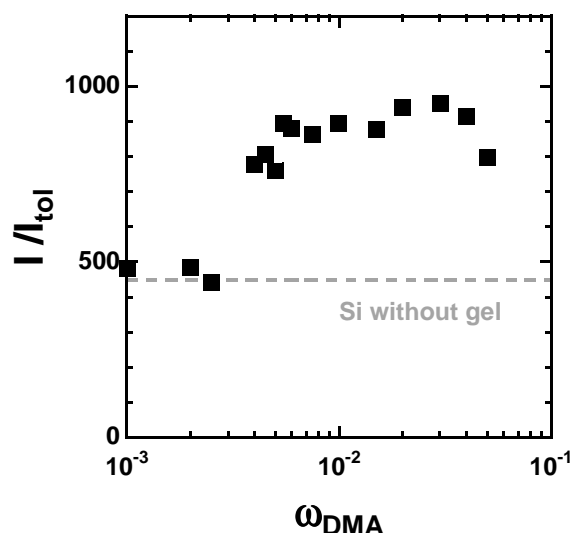


Figure 24: Normalized scattering light intensity as a function of DMA weight fraction in P(AAm-co-DMA) hybrid gels containing 1 wt% of silica nanoparticles. The gray dashed line indicates the value for silica nanoparticle suspension at the same concentration (without gel).

The effects of the DMA/silica physical interaction on the scattering intensity are further studied. In order to evaluate the stoichiometry of the interaction, the influence of the silica nanoparticle concentration on the scattered light intensity was studied. **Figure 25** shows the scattered light intensity of the hybrid gels normalized by that of the corresponding silica suspension as a function of the weight ratio of DMA to silica nanoparticles. We found that the intensity increases dramatically at a certain weight ratio, 0.12 (g/g), for all the studied silica nanoparticle concentrations. Using this value and that of the specific surface area (100 m²/g) [47], the amount of the DMA (incorporated in the P(AAm-co-DMA) copolymer) adsorbed onto the silica surface is estimated to be 1.2 mg/m². This value is close to the literature value of the linear PDMA polymer adsorption in solution (0.95 mg/m²) [47], suggesting that the adsorption of radically polymerized P(AAm-co-DMA) polymer starts from this weight ratio of 0.12.

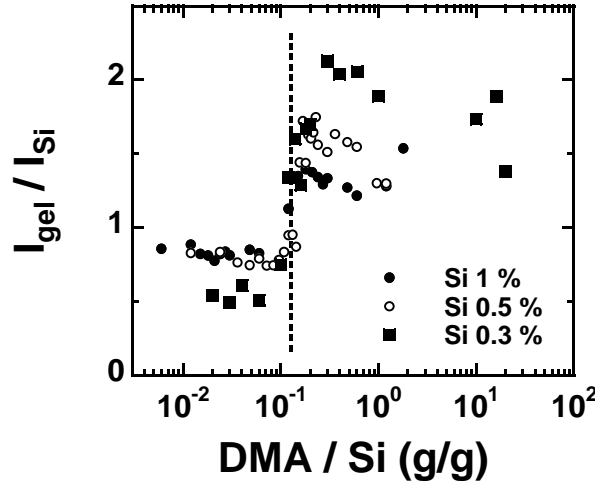


Figure 25: Scattered light intensity of P(AAm-co-DMA) hybrid gel normalized by that of the silica nanoparticles suspensions of the same concentration as a function of the weight ratio of DMA to silica nanoparticles.

The scattered light intensity from P(AAm-co-DMA) hybrid gels (**Figure 24**) was compared with that from the mixture of the linear PDMA polymer and the silica nanoparticles in solution. A commercially available PDMA polymer was used, and no radical polymerization in the presence of silica particles was performed. In **Figure 26 (a)**, the scattered light intensity normalized by that of toluene at 90° is plotted as a function of the PDMA concentration. The silica nanoparticles concentration is 1 wt% for both systems. We observed a gradual increase in the intensity from as low PDMA concentration as 0.02 wt%. The intensity levelled off at about $I/I_{\text{tol}} = 700$. At the same time the hydrodynamic radius of the silica nanoparticles was measured. The increase in the hydrodynamic radius, attributed to the adsorbed polymer layer, was calculated with the measured values of the diffusion coefficient and viscosity. By using the diffusion coefficient of the particles in water D_0 and in polymer solution D , and the viscosity of water η_0 and the polymer solution η , the hydrodynamic thickness of the adsorbed polymer layer, e , can be estimated from:

$$D_0 = \frac{k_B T}{6\pi\eta_0 R}, D = \frac{k_B T}{6\pi\eta_0 (R + e)}, \frac{R}{R + e} = \frac{D\eta}{D_0\eta_0} \quad \text{Eq. 15}$$

Figure 26 (b) shows the hydrodynamic adsorbed polymer layer thickness e as a function of the polymer concentration. The value of e increased gradually with the PDMA concentration

up to 10 nm. This value is comparable with that of poly(ethylene oxide) having the same molecular weight, which adsorbs also onto the silica surface by hydrogen bonding [48]. We found also that addition of urea in the solution decreased the adsorbed polymer thickness, indicating that the driving force of the DMA – silica interaction is hydrogen bonding.

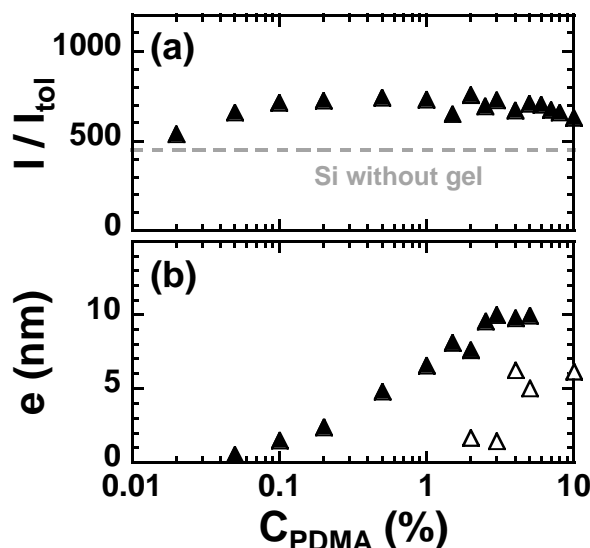


Figure 26: Hydrodynamic thickness of adsorbed PDMA polymer on silica nanoparticle surface in solution as a function of DMA weight fraction without (filled triangles) and with (open triangles) urea.

Comparing **Figure 24** and **Figure 26 (a)**, the critical increase in the intensity for the P(AAm-co-DMA) hybrid gel is presumably due to the radical copolymerization. The DMA fraction in the copolymer might be higher at the silica surface during the polymerization. We do not have any experimental proof of monomer adsorption.

From these experimental results we schematically illustrate the dynamics of the silica nanoparticles in hybrid gels with and without DMA (**Figure 27**). For 1 wt% of nanoparticles having a hydrodynamic radius of 17 nm, the average interparticle centre-to-centre distance is supposed to be 168 nm. Without DMA, or in chemically cross-linked PAAm gels, there is no interaction between the network and the silica nanoparticles, and the nanoparticles show diffusive motion in the network. Although the average hydrodynamic correlation length is

smaller than the particle radius, the network structure is very heterogeneous at the given polymer concentration and the low chemical crosslinking ratio, thus the particles can be diffusive [45]. With sufficient amount of DMA (DMA/Si > 0.12), the P(AAm-co-DMA) is partly adsorbed onto the silica surface by hydrogen bonding, hindering diffusive motion of the silica nanoparticles. Although we do not have any direct proof, from the comparison with the linear PDMA adsorption in solution (**Figure 26**), the adsorbed polymer layer thickness e in a P(AAm-co-DMA) gel is expected to be several nm. The maximum displacement of the nanoparticles with adsorbed polymer layer is the cage size δ . The silica nanoparticles bound to the network show sub-diffusive motion in the cage when observed at the length scale of observation $1/q < \delta$.

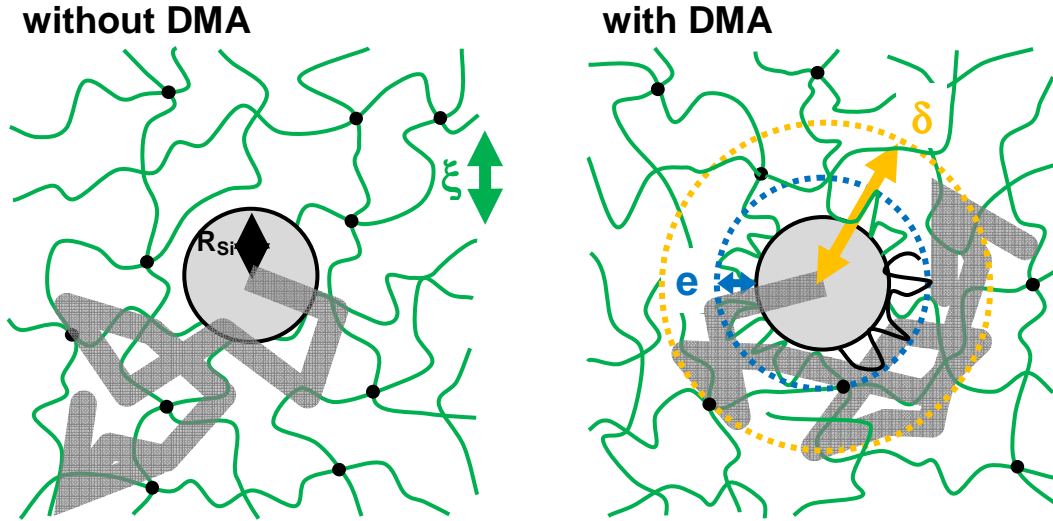


Figure 27: Schematic illustration of dynamics of silica nanoparticles in PAAm gel and P(AAm-co-DMA) gel.

In order to qualitatively discuss the effects of DMA concentration on the cage dynamics, the value of δ , estimated from the transition point of q , is used. The local shear modulus μ probed by the silica nanoparticles can be calculated from:

$$\mu = \frac{k_B T}{6\pi \cdot R \delta^2} \quad \text{Eq. 16}$$

and μ is plotted as a function of ω_{DMA} in **Figure 28**. The local shear modulus, which is in the order of Pa, increases monotonously with the DMA concentration. The shear modulus

measured by polystyrene particles much bigger than the mesh size (250 nm in radius) is about 200 Pa [45]. This result suggests that the silica nanoparticles having comparable size with the mesh of the network do not probe the viscoelasticity of the bulk network as do the bigger polystyrene particles. We believe that the local shear modulus probed by the silica particles corresponds to the elasticity of the adsorbed polymer chains connecting the silica particles to the network.

The increase in the local modulus with increase in the DMA fraction in the polymer network was further investigated. Since the local modulus measured here is entropic, it should be proportional to the density of elastic active chains:

$$G' = \frac{N}{V} k_B T \quad \text{Eq. 17}$$

where N is the number of elastically active chains in the considered volume V . If we only consider chemical cross-links, in the volume corresponding to the dynamic cage ($V = 4\pi\delta^3/3$), the value of N is almost 1 for all the data in **Figure 28**, suggesting that the increase in μ observed in **Figure 28** is not due to the increased number of elastically active chains. From the bulk modulus, we calculated the length of the elastically active chain between two chemical cross-links, ξ , to be 27 nm ($G' = k_B T / \xi^3$). With the values of the Kuhn length ($b = 0.6$ nm) and the exponent of Mark-Houwink relation ($\alpha = 0.75$) of polyacrylamide in water found in the literature, the number of monomers in an elastically active chain, n , was estimated to be 680 ($\xi = b \cdot n^{(\alpha+1)/3}$). For a random copolymerization of the given DMA amounts ω_{DMA} between 0.0075 and 0.025, 5 to 17 DMA units should be copolymerized in the chain. Since the chain adsorbs onto the silica surface by the DMA units, these DMA/silica interactions decrease the effective number of monomers n_{eff} of the elastically active chain as $n_{eff} \propto n / \omega_{DMA}$. The finite extensibility of the chain should scale with $n_{eff} / n_{eff}^{0.58} = n_{eff}^{0.42}$ and controls δ . Thus we expect that the extensibility of the adsorbed chain plays an important role on the measured local modulus: the more DMA in the copolymer, the less the adsorbed polymer chains can stretch, thus μ increases with ω_{DMA} .

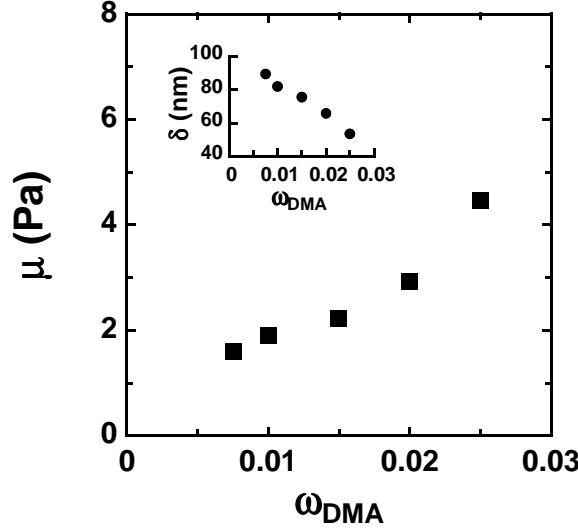


Figure 28: Local shear modulus μ probed by the silica nanoparticles as a function of weight fraction of DMA monomer in P(AAm-co-DMA) gels. Inset: cage size δ as a function of ω_{DMA} .

The local friction coefficient ν probed by the nanoparticles can be estimated from the characteristic time of the cage τ_{cage} and the cage size δ :

$$\nu = \mu \cdot \tau_{\text{cage}} = \frac{k_B T \cdot \tau_{\text{cage}}}{6\pi \cdot R \delta^2} \quad \text{Eq. 18}$$

This relation is essentially Stokes-Einstein relation, thus ν can also be estimated from the sub-diffusive motion in the q^{-2} dependent regime:

$$D = \frac{k_B T}{6\pi \cdot R \nu} = \frac{1}{\tau \cdot q^2} \quad \text{Eq. 19}$$

and thus:

$$\nu = \frac{k_B T \cdot \tau}{6\pi \cdot R q^{-2}} \quad \text{Eq. 20}$$

We found that the value of ν increased with the DMA concentration. The value is between 0.3 and 8 Pa·s at studied DMA concentration. Nisato *et al.* found about 2 Pa·s for chemically cross-linked PAAm gels, independent of the chemical crosslinking ratio [30]. Here increasing the DMA concentration results in an increase in the binding sites, slowing down the relaxation process of the surrounding polymer matrix.

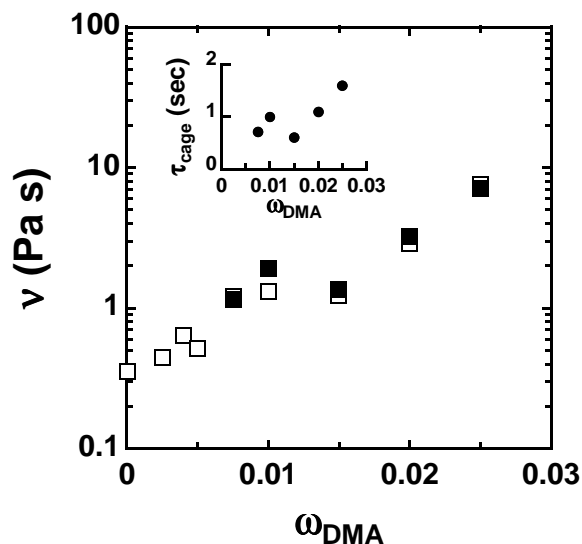


Figure 29: Local friction coefficient ν probed by the silica nanoparticles as a function of weight fraction of DMA monomer in P(AAm-co-DMA) gels. Closed squares: calculated from the cage size and characteristic time. Open squares: calculated from Stokes-Einstein relation in the cage. Inset: characteristic time of the cage τ_{cage} as a function of ω_{DMA} .

The diffusive mechanisms occurring in the hybrid network can be separated and analyzed in terms of a collective diffusion coefficient and a diffusion coefficient of the silica nanoparticles. The **Figure 30 (a)** shows the DMA weight fraction dependence of the collective diffusion coefficient. It is clear that the DMA has no effect on this collective diffusion coefficient at the given DMA and silica concentrations. Concerning the silica nanoparticles diffusion, increasing the DMA weight fraction strongly decreases their diffusion coefficient which is inversely proportional to ν , as shown on **Figure 30 (b)**. Note that a very small amount of DMA is sufficient to decrease considerably the diffusion coefficient. With our DLS setup it is practically impossible to detect the silica dynamics when $\omega_{\text{DMA}} > 0.03$.

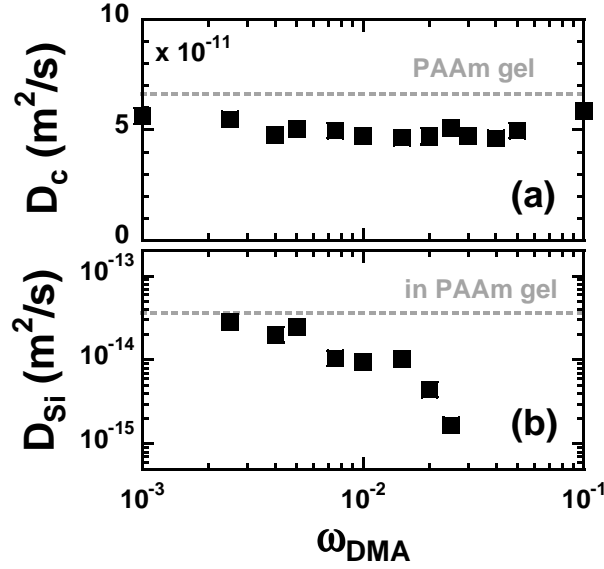


Figure 30: (a) Collective diffusion coefficient and (b) diffusion coefficient of silica nanoparticles (in the cage) as a function of DMA weight fraction in P(AAm-co-DMA) hybrid gels. The gray dashed line indicates the value for $\omega_{DMA} = 0$ (PAAm gel).

Before concluding this study, let us discuss the effect of copolymerization on the macroscopic mechanical behaviours. A comparison of the information obtained at a micro-structural level can be done with the macroscopic mechanical behaviour of hybrid hydrogels that have been studied in terms of Young's modulus as a function of the silica volume fraction. The results are presented in **Figure 31**. For hybrid hydrogels of pure PDMA matrix, an enhancement of the initial stiffness is obvious by increasing the silica content and can be explained thanks to the specific interactions between PDMA and the silica nanoparticles (black dots). This improvement has been studied and reported in details previously [17, 25], and contrary to most hybrid hydrogels, the mechanical properties are enhanced not only in terms of initial stiffness but also for the strain at failure. The reinforcement effect can be compared to the classical model of Guth, Gold and Simha developed in order to study the impact of filler content on the properties of rubbery matrix (grey line) [49, 50]. The conditions of use of this model are: an incompressible matrix and hard spherical particles without specific interaction with the matrix. This model can be used for low volume fractions of filler (typically lower than 0.2) and the Young's modulus of the reinforced material E is then:

$$E = E_0 (1 + 2.5\phi + 14.1\phi^2) \quad \text{Eq. 21}$$

with E_0 the Young's modulus of the unfilled matrix. As represented in **Figure 31**, the model of Guth and Gold is far below the experimental values of the initial modulus, revealing macroscopically the strong interactions taking place between the PDMA swollen matrix and the silica nanoparticles. The reinforcement is essentially visible at high silica contents (especially for silica volume fraction higher than 0.1), corresponding to weight ratio DMA/Si values from 0.2 to 0.5.

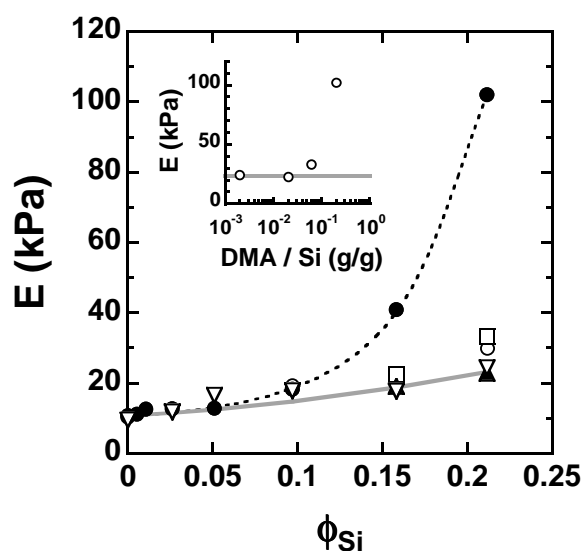


Figure 31: Modulus of P(AAm-co-DMA) hybrid gels as a function of volume fraction of silica nanoparticles. Filled circles: $\omega_{DMA} = 1$; open squares: $\omega_{DMA} = 0.3$; filled triangle: $\omega_{DMA} = 0.1$; open triangle: $\omega_{DMA} = 0.01$; open circles: $\omega_{DMA} = 1$ with 10 % of urea. The black dashed line is the guide for the eye. The gray solid line gives predicted values of the modulus calculated from the Guth-Gold model. Inset: Modulus of P(AAm-co-DMA) hybrid gels containing $\phi_{Si} = 0.21$ of silica nanoparticles as a function of volume fraction of the weight ratio of DMA to silica nanoparticles.

Introducing the non-hydrogen bonding monomer AAm into the PDMA network directly leads to a decrease of the mechanical properties compared to the pure PDMA system. The progressive loss of stiffness exactly follows the progressive incorporation of AAm monomer into the network: from $\omega_{DMA} = 1$ to 0.01 in the polymer matrix, the initial modulus decreases from 102 to 20 kPa at a fixed silica volume fraction of 0.21, as represented in **Figure 31**. In the inset, the modulus is plotted as a function of the weight ratio DMA/Si. It is shown that a

certain amount of DMA, more than $\text{DMA/Si} = 0.1$, is required for the mechanical reinforcement by the DMA adsorption. The result in **Figure 25** which indicates that $\text{DMA/Si} > 0.12$ is the condition for P(AAm-co-DMA) adsorption, qualitatively agrees with that of the inset in **Figure 31**.

The physical adsorption of the PDMA chains onto the silica surface can be annihilated in the presence of a hydrogen bonding competitor, such as urea. For that purpose, hybrid hydrogels were prepared following the same protocols as described in Part 2 but incorporating also urea in water with a fixed amount of urea for each gel (10 %). We observed that the initial modulus of the hydrogels with urea (open circles) is far below the reference hybrid hydrogels without urea (filled circles). Similarly to the result shown in **Figure 26 (b)**, the presence of urea reduces the hydrogen bonding between the PDMA and silica nanoparticles, decreases the polymer adsorption thus the mechanical reinforcement.

3.4. Conclusions

The dynamics of hybrid P(AAm-co-DMA) hydrogels with various weight ratios of AAm and DMA, containing silica nanoparticles have been studied by dynamic light scattering. We observed and explained the effects of the presence of silica nanoparticles, having interactions (hydrogen bonding) with DMA but not with AAm, on the dynamics of the network and of the nanoparticles in the polymeric network. When the amount of DMA is progressively increased in P(AAm-co-DMA) hybrid hydrogels, a trapping of the silica nanoparticles is observed due to the strong physical interactions with DMA, clearly demonstrated by the q -dependence of the characteristic time of the silica nanoparticles dynamics.

Microrheological properties of the hybrid gels probed by the silica nanoparticles with adsorbed polymer network were studied. The local shear modulus and the local friction coefficient increased with an increase in the amount of DMA monomer. These values are not comparable with those of the bulk network, suggesting that the nanoparticles motion is sensitive to the adsorbed polymer layer and the surrounding polymer structure, different from that of bulk which is also shown as increase in the total scattering intensity from the hybrid gels.

The physical adsorption of PDMA units onto the silica nanoparticles surface leads to an enhancement of the mechanical properties of the hydrogels: the initial stiffness and the strain at failure increased with the silica content. This improvement can be controlled and reversed by introducing a hydrogen bonding competitor, such as urea, leading to a dramatic decrease of the mechanical properties.

4. Conclusion on the DLS studies

In the first experimental part of this Chapter 6, DLS experiments performed on hybrid polyacrylamide hydrogels confirmed the possibility of light scattering to investigate the dynamics of such heterogeneous system. The study of the effects of chemical cross-linking density and of silica concentration led to an accurate picture of the architecture of such network, in terms of heterogeneity. As there is no specific interaction between acrylamide and silica nanoparticles, we show no adsorption of PAAm onto the silica surface and that the presence of silica nanoparticles does not affect the network structure and its dynamics.

Furthermore, the dynamics of the silica nanoparticles can be easily followed and appeared to be strongly impacted by the chemical cross-linking density. From the studies performed at low silica concentration, we brought to light the possibility of a transfer of radicals from the persulfate used to the surface of the silica nanoparticles, leading to a PAAm chain growth from the silica surface.

In the second part, we evidenced the interaction taking place between silica and PDMA by introducing progressively DMA in the polymer network. This result is in total agreement with the previous work of Petit *et al.* conducted by adsorption isotherms. The interaction existing between PDMA and the silica surface is in good agreement with the titration of extractable conducted on hybrid hydrogels. The trapping of the silica nanoparticles in the PDMA network has been observed even at low amounts of DMA.

An adsorbed polymer layer has been evidenced here by light scattering, with a thickness of several nanometres. This result can be related to the SANS experiments described in Chapter 3 where we did not observe a concentrated PDMA layer at the silica surface. As discussed in Chapter 3, the existence of a “concentrated” polymer layer revealed has been reported by Shibayama *et al.* but at a lower polymer concentration than ours [14]. This lower polymer concentration leads to a “higher” contrast of concentration between the corona and the bulk: 5 vol% of PNIPAm in the bulk and 17 vol% in the corona. The observation of this difference

in concentrations is easier than in our SANS experiments where the polymer concentration was 12 vol% in the bulk. The experimental accuracy of SANS may not be sufficient to detect such a difference in concentrations. However, in the case of light scattering experiments, the increase in size of silica nanoparticles, observed when PDMA is introduced in the polymer formulation, corresponds to an increase in hydrodynamic radius, easily detectable. Even if the polymer corona adsorbed on the silica surface is not concentrated, we revealed the existence of a diffuse corona directly coming from the strong interaction between silica and PDMA, as schematically represented in **Figure 27**.

The effects of the presence of silica nanoparticles on the PDMA hydrogels are now clear and unequivocal. As a matter of fact, from the DLS study, we demonstrated by a new mean the strong interaction existing between silica and PDMA and its consequences on the dynamics component of this system. This interaction leads to a trapping of the silica nanoparticles in the PDMA network.

Here, we obtained another proof of the interaction between silica nanoparticles and the PDMA network. The study has been conducted at low polymer concentration and lower silica content, for experimental constraints related to light scattering techniques.

References

1. Richter, J.B., Ueber die neuern Gegenstände der Chemie, 1802. **11**: p. 81.
2. Tyndall, J., Phil. Mag., 1869. **37**: p. 384.
3. Rayleigh, L., Phil. Mag., 1871. **41**: p. 447.
4. Rayleigh, L., Phil. Mag., 1881. **12**: p. 81.
5. Einstein, A., *Theorie der Opaleszenz von homogenen Flüssigkeiten und Flüssigkeitsgemischen in der Nähe des kritischen Zustandes*. Annalen der Physik, 1910. **338**(16): p. 1275-1298.
6. Mie, P., Ann. Phys. Lpz., 1908. **25**(3): p. 771.
7. Debye, P., *Light Scattering in Solutions*. Journal of Applied Physics, 1944. **15**: p. 338-342.
8. Okay, O. and W. Oppermann, *Polyacrylamide-Clay Nanocomposite Hydrogels: Rheological and Light Scattering Characterization*. Macromolecules, 2007. **40**: p. 3378-3387.
9. Funke, W., O. Okay, and B. Joos-Müller, *Microgels-Intramolecularly Crosslinked Macromolecules with a Globular Structure*. Advanced Polymer Science, 1998. **136**: p. 139-234.
10. Liu, R., X. Gao, and W. Oppermann, *Dynamic light scattering studies on random cross-linking of polystyrene in semi-dilute solution*. Polymer, 2006. **47**: p. 8488-8494.
11. Miyazaki, S., et al., *Gelation Mechanism of Poly(N-isopropylacrylamide)-Clay Nanocomposite Gels*. Macromolecules, 2007. **40**: p. 4287-4295.
12. Matsunaga, T. and M. Shibayama, *Gel point determination of gelatin hydrogels by dynamic light scattering and rheological measurements*. Physical Review E, 2007. **76**(3).
13. Karino, T., et al., *Sol-Gel Transition of Hydrophobically Modified Polyrotaxane*. Macromolecules, 2006. **39**(26): p. 9438-9440.
14. Suzuki, T., et al., *Dynamics and Microstructure Analysis of N-isopropylacrylamide/Silica Hybrid Gels*. Langmuir, 2009. **25**(15): p. 8824-8832.
15. Reina, J.C., R. Bansil, and C. Konak, *Dynamics of probe particles in polymer solutions and gels*. Polymer, 1990. **31**(6): p. 1038-1044.

16. Seiffert, S. and W. Oppermann, *Diffusion of Linear Macromolecules and Spherical Particles in Semidilute Polymer Solutions and Polymer Networks*. Polymer, 2008. **49**: p. 4115-4126.
17. Lin, W.C., et al., *Large Strain and Fracture Properties of Poly(dimethylacrylamide)/Silica Hybrid Hydrogels*. Macromolecules, 2010. **43**(5): p. 2554-2563.
18. Okumura, Y. and K. Ito, *The Polyrotaxane Gel: A Topological Gel by Figure-of-Eight Cross-links*. Advanced Mater., 2001. **13**(7): p. 485.
19. Sakai, T., et al., *Design and fabrication of a high-strength hydrogel with ideally homogeneous network structure from tetrahedron-like macromonomers*. Macromolecules, 2008. **41**(14): p. 5379-5384.
20. Gong, J.P., *Why are double network hydrogels so tough?* Soft Matter, 2010. **6**(12): p. 2583-2590.
21. Gong, J.P., et al., *Double-network hydrogels with extremely high mechanical strength*. Advanced Materials, 2003. **15**(14): p. 1155.
22. Haraguchi, K. and H.J. Li, *Mechanical properties and structure of polymer-clay nanocomposite gels with high clay content*. Macromolecules, 2006. **39**(5): p. 1898-1905.
23. Haraguchi, K. and H.J. Li, *The Effect of Water Content on the Ultimate Properties of Rubbery Nanocomposite Gels*. Journal of Polymer Science Part B-Polymer Physics, 2009. **47**(23): p. 2328-2340.
24. Haraguchi, K., T. Takehisa, and S. Fan, *Effects of clay content on the properties of nanocomposite hydrogels composed of poly(N-isopropylacrylamide) and clay*. Macromolecules, 2002. **35**(27): p. 10162-10171.
25. Carlsson, L., et al., *Nano-hybrid self-crosslinked PDMA/silica hydrogels*. Soft Matter, 2010. **6**(15): p. 3619-3631.
26. Haraguchi, K., et al., *Mechanism of Forming Organic/Inorganic Network Structures during In-situ Free-Radical Polymerization in PNIPA-Clay Nanocomposite Hydrogels*. Macromolecules, 2005. **38**(8): p. 3482-3490.
27. Abdurrahmanoglu, S. and O. Okay, *Rheological Behavior of Polymer-Clay Nanocomposite Hydrogels: Effect of Nanoscale Interactions*. Journal of Applied Polymer Science, 2010. **116**(4): p. 2328-2335.

28. Pinder, D.N., et al., *Micro-rheological investigation of dextran solutions using diffusing wave spectroscopy*. Food Hydrocolloids, 2006. **20**(2-3): p. 240-244.
29. Weitz, D.A. and D.J. Pine, *Dynamic Light Scattering: The Method and Some Applications*, ed. W. Brown. 1993, Oxford: Oxford University Press.
30. Nisato, G., et al., *Diffusing-wave-spectroscopy investigation of latex particle motion in polymer gels*. Physical Review E, 2000. **61**: p. 2879-2887.
31. Joosten, J.G.H., E.T.F. Geladé, and P.N. Pusey, *Dynamic light scattering by nonergodic media: Brownian particles trapped in polyacrylamide gels*. Physical Review A, 1990. **42**: p. 2161-2175.
32. Joosten, J.G.H., J.L. McCarthy, and P.N. Pusey, *Dynamic and Static Light Scattering by Aqueous Polyacrylamide Gels*. Macromolecules, 1991. **24**: p. 6690-6699.
33. Seiffert, S., K. Saalwächter, and W. Oppermann, *Hydrogel Formation by Photocrosslinking of Dimethylmaleimide Functionalized Polyacrylamide*. Polymer, 2007. **48**: p. 5599-5611.
34. Orakdogan, N. and O. Okay, *Inhomogeneity in Acrylamide-based Hydrogels*. Journal of Applied Polymer Science, 2007. **103**: p. 3228-3237.
35. Phillies, G.D.J., *Self and Tracer Diffusion of Polymers in Solution*. Soft Condensed Matter, 2004.
36. Phillies, G.D.J., *Optical Probe Diffusion in Polymer Solutions*. Soft Condensed Matter, 2007.
37. Langevin, D. and F. Rondelez, *Sedimentation of large colloidal particles through semidilute polymer solutions*. Polymer, 1978. **19**(8): p. 875-882.
38. Park, I.H., C.S. Johnson, and D.A. Gabriel, *Probe diffusion in polyacrylamide gels as observed by means of holographic relaxation methods: search for a universal equation*. Macromolecules, 1990. **23**(5): p. 1548-1553.
39. Gögelein, C., et al., *Polymer depletion-driven cluster aggregation and initial phase separation in charged nanosized colloids*. Journal of Chemical Physics, 2009. **130**.
40. Caregnato, P., et al., *Kinetic studies on the surface radical-initiated polymerization of vinyl acetate and 4-vinyl pyridine in the presence of silica nanoparticles*. Langmuir, 2005. **16**(21): p. 8001-8009.

41. Buchholz, F.L. and A.T. Graham, *Modern Superabsorbent Polymer Technology*. 1997: Wiley-VCH.
42. Peppas, N.A., *Hydrogels in Medicine and Pharmacy*. 1986: CRC Press, Boca Raton, FL.
43. Oppermann, W., B. Lindemann, and B. Vgerl, *Network Inhomogeneities in Polymer Gels*, in *Polymer Gels: Fundamentals and Applications*, H.B. Bohidar, P. Dubin, and Y. Osade, Editors. 2002.
44. Wichterle, O., *Soft Contact Lenses*. 1978, New York: Wiley.
45. Rose, S., et al., *Dynamics of Hybrid Polyacrylamide Hydrogels Containing Silica Nanoparticles Studied by Dynamic Light Scattering*. *Macromolecules*, 2013. **46**(11): p. 4567-4574.
46. Xue, J.Z., et al., *nonergodicity and Light Scattering from Polymer Gels*. *Physical Review A*, 1992. **46**: p. 6550-6563.
47. Petit, L., et al., *Responsive hybrid self-assemblies in aqueous media*. *Langmuir*, 2007. **23**(1): p. 147-158.
48. Van der Beek, G.P. and M.A. Cohen Stuart, *The hydrodynamic thickness of adsorbed polymer layers measured by dynamic light scattering: effects of polymer concentration and segmental binding strength*. *Journal de Physique de France*, 1988. **49**(8): p. 1449-1454.
49. Guth, E., *Theory of filler reinforcement*. *Journal of Applied Physics*, 1945. **16**: p. 20-25.
50. Guth, E. and R. Simha, *Explorations of the viscosity of suspensions and solutions 3 The viscosity of sphere suspensions (The calculation of wall influence and the exchange effect in viscosity as well as in rotating spheres)*. *Kolloid-Zeitschrift*, 1936. **74**(3): p. 266-275.

General conclusion

We developed hybrid hydrogels in order to overcome the intrinsic high brittleness of chemically cross-linked hydrogels. The strategy consisted of coupling a covalent polymer network with physical interactions taking place with silica nanoparticles. Indeed; adsorption mechanism can provide an efficient and transient anchorage of polymer chains onto the silica surface. The idea was to build a hybrid network composed of silica nanoparticles acting as physical cross-linker.

The polymer matrix has been first characterized in details, without silica nanoparticle. For that purpose, structural, thermodynamic and mechanic investigations have been performed. From these results, we chose to focus specifically our study on a slightly cross-linked PDMA matrix presenting a good swelling ability, a high deformability and a good reproducibility. Our hybrid reference system was composed of i) spherical silica nanoparticles (varying their concentration), ii) 0.1 mol% of chemical cross-linker and iii) a fixed polymer/water ratio. The samples were then characterized at their preparation state. We verified by Small Angle Neutron Scattering experiments that the cross-linking polymerization of DMA in presence of silica nanoparticles does not affect their initial dispersion, in spite of the physical interactions taking place between the two materials. However, contrast matching experiments did not evidence the presence of a dense polymer layer at the silica surface, probably due to the weak difference of polymer concentration between the matrix and the shell. The association between the PDMA network and the silica surfaces are responsible for a decrease of the swelling at equilibrium of hybrid hydrogels. A comparison with a theoretical model confirmed that the adsorbed layer is not dense. A layer of comparable density with the polymer matrix has been assumed for the following with adhesive properties.

After this structural study, we characterized in details the mechanical behaviour of hybrid networks. Preliminary tensile tests have shown that the attractive potential between PDMA and silica gives rise to a dramatic reinforcement of the mechanical behaviour, in terms of initial modulus and strain at failure. The silica nanoparticles can be considered as multifunctional physical cross-linkers, allowing the transient anchoring of surrounding chains. From an elastic unfilled gel matrix, the introduction of silica nanoparticles led to a viscoelastic behaviour. As a matter of fact, a strain rate dependence of the dissipation during

cycling and of a loss modulus amplitude has been evidenced and related to the presence of PDMA/silica interactions.

Our hybrid hydrogels can be depicted as double networks. The covalent polymer network drives the elasticity, recoverability and the long-time behaviour. The physical network formed by the reversible adsorption of polymer chains onto silica surface is at the origin of the strong stiffening effect at small strain, but appeared to be highly time-dependent. Thus, these hybrid gels are able to dissipate more than 10 times the amount of energy that the pure matrix can store while having a rapid recovery in strain (*i.e.*, typically in the time-scale of 1-10 seconds). Within this time-scale, the network is able to self-reorganize in order to recover an equivalent density of elastically-active chains, implying dynamic adsorption/desorption of polymer segments at the silica surface. We succeeded in modelling the behaviour of hybrid hydrogels by a simple generalized Maxwell model, leading to a comprehensive picture of their viscoelastic properties.

From the detailed mechanical characterization, we studied the versatility of our model systems, by changing some constitutive components. First, we focused on the PDMA matrix, showing that changing the chemical cross-linking of the network mainly leads to an amplitude variation of the general reinforcement. More interestingly, a study performed at the swelling equilibrium state revealed a loss of reinforcement and dissipation, suggesting that the number of physical connections created by adsorption/desorption are strongly reduced with the dilution. Then, the aggregation of the silica nanoparticles have been studied, leading to very high values of initial modulus but drastically lowering the possibilities of interactions with the PDMA matrix. Finally, two strategies have been successfully tested to switch the level of physical interactions: the use of acrylamide, known to weakly interact with silica nanoparticles and the introduction of urea, a hydrogen-bond competitor for DMA units. As a conclusion, the adaptability of our hybrid hydrogels appeared to be large and complex, leading to a wide range of properties.

A parallel study on hybrid hydrogels has been performed by light scattering methods to investigate the polymer/silica nanoparticles interactions in terms of dynamics. As a matter of

fact, the dynamics of the silica nanoparticles appeared to be strongly impacted by the chemical cross-linking density of the polymer networks and by their interactions. From a study performed at low silica concentration in a non-interacting polymer matrix, we evidenced transfer of radicals from the initiator used to the surface of the silica nanoparticles, leading to a polymer growth from the silica surface. A progressive introduction of DMA – the interacting monomer- in the non-interacting polymer matrix (PAAm) led to an increasing trapping of the silica nanoparticles in the hydrogel network, even at low amounts of DMA.

As a conclusion, the interaction existing between PDMA and silica nanoparticles is at the origin of a wide range of properties that we tried to characterize in this PhD work. Our project could be continued following various ideas. For instance, the impact of the inorganic fillers on the macroscopic behaviour could be investigated in other experimental conditions, changing the pH, the particles size and thus their surface. A systematic study of the pH effect on the silica surface – and thus on the polymer/silica interaction – would be of prime interest for the development of a wide range of hybrid materials with a broad spectrum of mechanical behaviour.

The polymer matrix could also be modified in several ways. First, the swelling state of hydrogels is a key parameter to tune the macroscopic properties. With a good knowledge of the swelling kinetics of hybrid hydrogels, it would be interesting to swell the hydrogels in order to study their properties at intermediate states. From a more fundamental point of view, the understanding of the mechanical behaviour at the swelling equilibrium is challenging as numerous studies of polymer interactions at the swelling equilibrium state could be lightened.

Inspired by our combination of covalent and physical networks, stimuli-responsive systems could also be designed mixing several types of interaction. Such combination of time-dependent bonds and permanent bonds may be relevant for other soft material systems where two populations of bonds co-exist.

Extended abstract in French

Résumé substantiel en français

Table des matières

Table des matières	300
Introduction	302
1. Hydrogels de PDMA, sans silice	303
1.1. Synthèses d'hydrogels de PDMA	303
1.2. Propriétés mécaniques : module élastique	303
1.3. Gonflement.....	304
1.4. Diffusion de neutrons aux petits angles	305
2. Hydrogels hybrides silice/PDMA	306
2.1. Synthèse d'hydrogels hybrides silice/PDMA.....	306
2.2. Structure des hydrogels hybrides silice/PDMA.....	306
2.3. Propriétés mécaniques : modules élastiques	307
2.4. Gonflement des hydrogels hybrides	308
3. Renforcement des propriétés mécaniques	308
3.1. Influence de la vitesse	308
3.2. Relaxation	311
3.3. Diffusion de neutrons aux petits angles sous déformation.....	311
3.4. Modélisation du comportement des hydrogels hybrides	312
4. Adaptabilité du système aux propriétés recherchées	314
4.1. Modification de la matrice polymère	314
4.1.1. Changement du taux de réticulation.....	314
4.1.2. Changement du taux de gonflement.....	315
4.2. Agrégation des nanoparticules de silice	315
4.3. Altération de l'interaction polymère/silice	316
4.3.1. Changement de monomère.....	316
4.3.2. Introduction d'un compétiteur de liaison hydrogène.....	316
5. Etude par diffusion de la lumière	317
5.1. Etude d'hydrogels hybrides PAAM/silice	317

5.2. Etude d'hydrogels hybrides P(DMA-co-AAm)/silice	318
6. Conclusions de l'étude	319
7. Références.....	320

Introduction

Les hydrogels présentent de nombreuses applications biotechnologiques, aussi bien dans des applications quotidiennes, pour les lentilles de contact par exemple, que dans des domaines de pointe, telle que la vectorisation de principes actifs. Cependant, le principal verrou au développement des hydrogels pour des applications techniques demeure leurs modestes performances mécaniques, en termes de module élastique et de taux de déformation. Pour palier à ce problème, différentes stratégies de renforcement ont été développées au cours des 20 dernières années, notamment les réseaux interpénétrés, les gels à points de réticulation coulissants et l'hybridation des hydrogels. L'introduction de nanoparticules au sein de matrices polymères permet d'améliorer les propriétés mécaniques des matériaux, l'exemple le plus connu étant celui des élastomères chargés. Ces améliorations ne sont possibles qu'à la condition qu'il existe de bonnes interactions entre la matrice polymère et les charges solides, assurant un bon état de dispersion de ces dernières.

Dans le domaine des hydrogels, des stratégies d'hybridation ont aussi été développées en particulier dans groupe de Haraguchi au Japon. Au laboratoire *Science et Ingénierie de la Matière Molle*, la possibilité d'utiliser les propriétés d'adsorption de polymères tels que le poly(N,N-diméthylacrylamide) (PDMA) avec des nanoparticules de silice a été démontrée, générant ainsi la formation d'assemblages hybrides réversibles, comme représenté **Figure 1**.

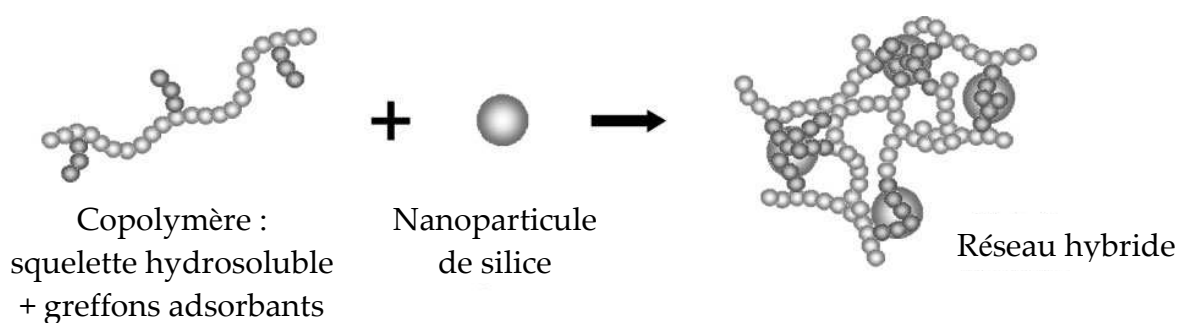


Figure 1 : Représentation schématique des réseaux hybrides à l'origine de notre étude : auto assemblage de nanoparticules de silice et de greffons de PDMA d'après Petit *et. al.* [1].

Ces travaux précurseurs sont à l'origine de ce travail de thèse dont l'objectif est d'étudier la structure et les propriétés mécaniques de gels covalents de PDMA renforcés par des nanoparticules de silice.

1. Hydrogels de PDMA, sans silice

1.1. Synthèses d'hydrogels de PDMA

Des gels de PDMA ont été synthétisés par polymérisation radicalaire conventionnelle de *N,N*-diméthylacrylamide (DMA) dans l'eau, en présence de réticulant *N, N'*-diméthylène-bisacrylamide (MBA), par amorçage redox, dans un environnement exempt d'oxygène. Le choix d'un taux d'hydratation commun à tous les matériaux (correspondant à un rapport massique polymère/eau égal à 0.14) a permis de comparer leurs propriétés en ne faisant varier que leur taux de réticulation chimique, d'un rapport molaire de 0.1 % par rapport au polymère jusqu'à un rapport molaire de 5%.

La nomenclature utilisée tout au long de l'étude est la suivante : SP désigne le rapport massique silice/polymère, variant de 0 à 5, PW représente le rapport massique polymère/eau, rendant compte du gonflement du gel, R symbolise le taux de réticulation chimique, exprimé en pourcentage molaire par rapport au polymère. Ainsi un gel de PDMA sans silice, ayant un gonflement initial de 8.5 et réticulé à 0.1 mo% sera désigné par :

« SP0_PW0.14_R0.1 ».

La synthèse de gels de PDMA s'est avérée être robuste mais la concurrence entre les réactions de polymérisation et de réticulation mène à la formation de défauts de structure caractérisables par des études mécaniques, thermodynamiques et structurales (diffusion de neutrons).

1.2. Propriétés mécaniques : module élastique

Des essais de traction simple réalisés à vitesse de déformation constante (0.06 s^{-1}) ont permis de caractériser les hydrogels de PDMA chimiquement réticulés, exclusivement en terme de module élastique dans un premier temps. Les gels sont testés dans leur condition de

préparation. L'augmentation du taux de réticulation est à l'origine d'une augmentation du module initial ainsi que d'une diminution de la déformation à rupture, comme représenté **Figure 2**. L'étude de ces résultats et leur comparaison au modèle de réseau fantôme ont permis de mettre en évidence la présence de défauts de structure et d'une réticulation chimique effective à seulement 42 %.

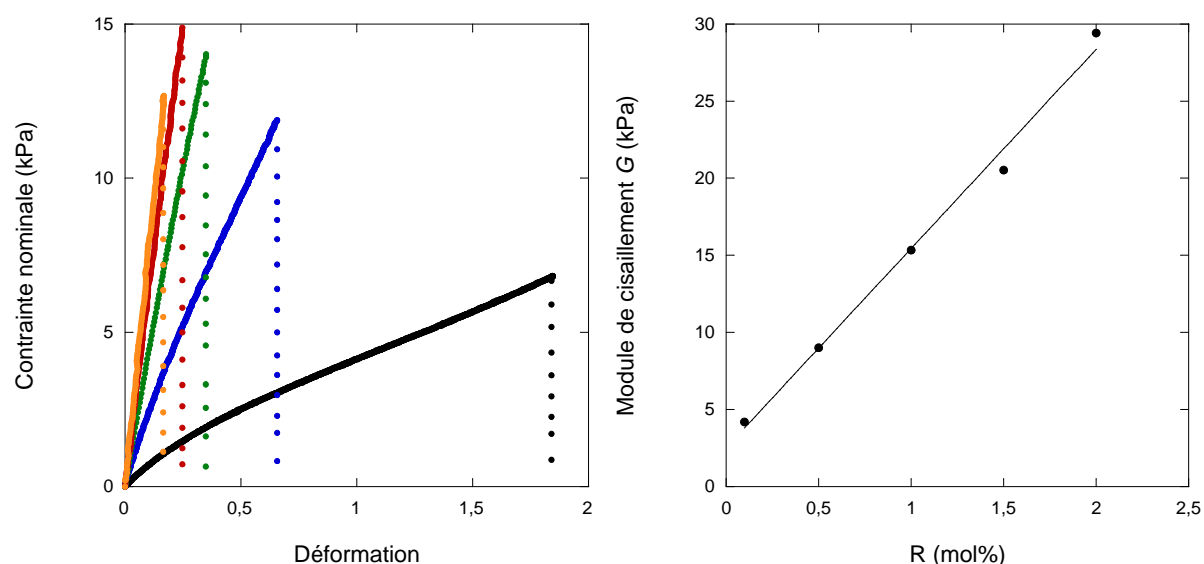


Figure 2: Gauche : courbes contrainte-déformation d'hydrogels SP0_PW0.14_Rz, avec R0.1 en noir, R0.5 en bleu, R1 en vert, R1.5 en rouge et R2 en orange.

Droite : variation du module de cisaillement G en fonction du taux de réticulation.

1.3. Gonflement

L'étude du gonflement des hydrogels par des solvants permet d'appréhender leur structure : un fort taux de réticulation est associé à de faibles propriétés de gonflement. La comparaison des résultats de gonflement d'hydrogels de PDMA chimiquement réticulés à des modèles thermodynamiques nous informe aussi sur les interactions existant entre la matrice polymère et le solvant. Dans le cas de l'étude du gonflement dans l'eau, les gels de PDMA sont proches de leurs conditions θ . L'augmentation du taux de réticulation se traduit par la diminution des valeurs de gonflement d'équilibre : alors qu'un gel contenant 0.1 mol% de MBA atteint un gonflement à l'équilibre de 40.5, un gel réticulé à 2 mol% présente un gonflement à l'équilibre de 12.8.

1.4. Diffusion de neutrons aux petits angles

La diffusion de neutrons aux petits angles (DNPA) est une technique de choix pour la caractérisation de la structure des hydrogels. Par l'utilisation de D₂O, au lieu de H₂O, lors de la synthèse des gels de PDMA, il a été possible de mesurer les longueurs de corrélations ξ et Ξ , respectivement associées aux fluctuations thermiques et statiques. La longueur de corrélation ξ s'est révélée être inversement proportionnelle à la concentration en gel, comme attendu dans le cas de solutions semi diluées de polymères dans les conditions non perturbées. Quant à la longueur de corrélation Ξ , elle apparaît être comparable à celle des fluctuations thermiques lorsque les gels sont étudiés à leur gonflement de synthèse. En revanche, le gonflement des gels jusqu'à l'équilibre permet de magnifier la longueur de corrélation associée aux inhomogénéités statiques.

En conclusion de cette étude mécanique, thermodynamique et structurale, les principales caractéristiques des gels de PDMA chimiquement réticulés peuvent être résumées par le **Tableau 1** et la **Figure 3**.

Taux de réti-culation (mol%)	Fraction volumique ϕ_0	Nombre d'unités monomère entre points de réti-culation	Gonflement d'équilibre Q_e	Module élastique E (kPa)	Défor-mation à rupture ϵ_r	ξ (Å)	Ξ (Å)
R 0.1	0.128	1200	40.5	12.6	1.84	5.8	14.1
R 0.5	0.128	240	22.9	27	0.66	7.0	10.4
R 1	0.128	120	15.2	46	0.34	8.8	13.3
R 1.5	0.128	80	14.5	61.6	0.25	-	-
R 2	0.128	60	12.8	88.3	0.24	-	-

Tableau 1 : Caractéristiques des hydrogels de PDMA préparés à un gonflement initial $Q_0 = 8.5$.

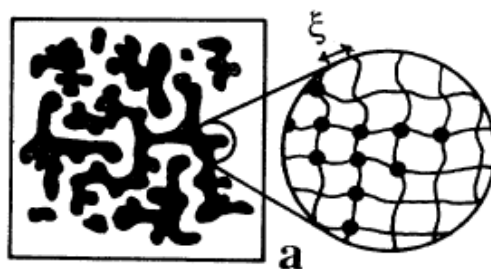


Figure 3 : Représentation schématique de la structure des gels : les régions plus fortement réticulées sont marquées en noir, présentant une taille caractéristique Ξ distribués dans un milieu peu concentré, d'après [2]. Les chaînes ne sont pas représentées, sauf dans le grossissement. Dans chaque domaine, la longueur de corrélation polymère-polymère ξ , correspondant à la taille de blob, est inchangée.

2. Hydrogels hybrides silice/PDMA

A partir de l'étude détaillée des propriétés de gels de PDMA chimiquement réticulés, l'impact de l'introduction de nanoparticules de silice sur les propriétés de ces réseaux a ensuite été étudié.

2.1. Synthèse d'hydrogels hybrides silice/PDMA

Les nanoparticules de silice utilisées dans cette étude proviennent de suspensions aqueuses commerciales concentrées à 50 % en masse. Des caractérisations par diffusion de la lumière, DNPA et microscopie électronique à balayage ont permis d'estimer le rayon des particules à environ 14 nm. La synthèse des hydrogels hybrides contenant de la silice est analogue à celle précédemment décrite : la suspension de silice est ajoutée au mélange réactionnel, sans purification.

2.2. Structure des hydrogels hybrides silice/PDMA

L'impact de la présence de nanoparticules de silice sur la structure des hydrogels a été caractérisé par DNPA. Différents ratios H_2O/D_2O ont été spécifiquement déterminés selon le principe de variation de contraste permettant d'ajuster sélectivement le contraste neutronique du solvant à celui d'un des composants, dans le but de l'écranter. Ainsi nous

avons vérifié que l'introduction de particules de silice dans la matrice de polymère hydraté ne modifie pas son état de dispersion : aucune aggrégation de particule n'a été observée.

2.3. Propriétés mécaniques : modules élastiques

La comparaison des tractions simples des hydrogels avec et sans nanoparticules de silice témoigne de l'interaction existant entre la silice et le PDMA, comme représenté **Figure 4** (gauche). En effet, l'augmentation de module initial générée par la présence de la silice a été comparée au modèle de Guth et Gold, comme représenté **Figure 4** (droite). Ce modèle a été développé dans le cas de particules sphériques non déformables introduites dans une matrice polymère et ne présentant pas d'interaction spécifique avec cette dernière. Dans le cas de nos hydrogels hybrides, l'augmentation remarquable du module initial observée aux fortes teneurs en silice provient de l'interaction privilégiée entre la silice et le PDMA. De manière plus singulière, la présence de nanoparticules de silice permet d'augmenter significativement la déformation à rupture des hydrogels.

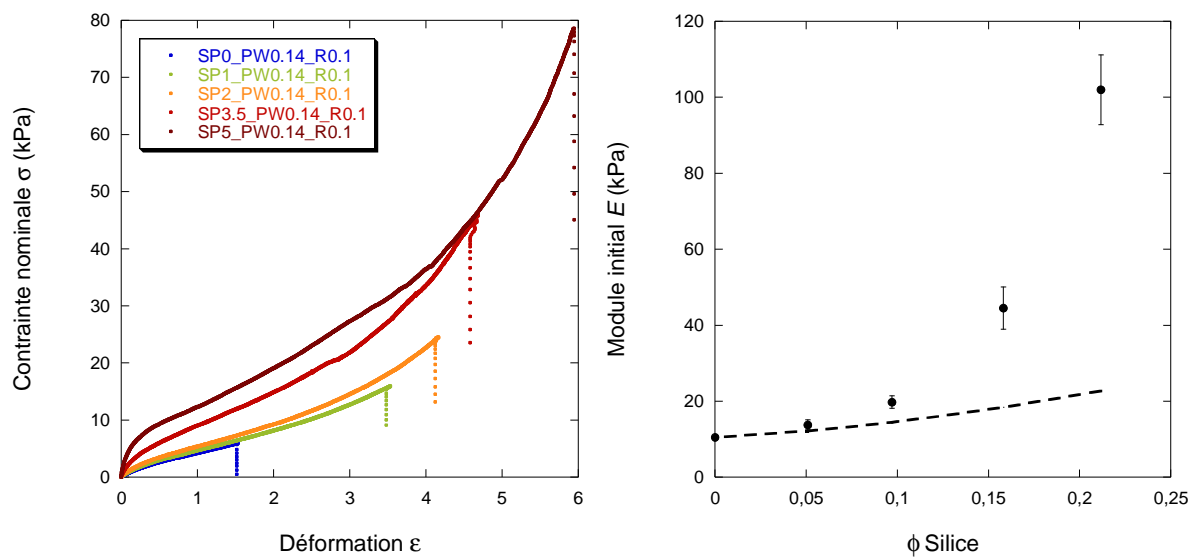


Figure 4 : Gauche : Allure des tractions simples d'hydrogels hybrides, obtenues à 0.06 s^{-1} .

Droite : Comparaison du module initial expérimental E (en cercles pleins) au modèle de Guth et Gold (en pointillés), obtenu à un taux de déformation de 0.06 s^{-1} , pour des hydrogels hybrides $\text{SP}_x\text{-PW0.14-R0.1}$, avec $x = 0 ; 1 ; 2 ; 3.5$ et 5 .

2.4. Gonflement des hydrogels hybrides

La présence de nanoparticules de silice au sein des hydrogels de PDMA provoque une diminution du gonflement à l'équilibre dans LiNO_3 (0.5 mol/L), comme représenté **Figure 5**. La comparaison de ces valeurs au modèle théorique de Lequeux (en pointillés) ne permet pas de caractériser la présence d'une couche de polymère « sous-gonflée » en surface des nanoparticules de silice. En revanche, les valeurs expérimentales correspondent au cas d'un polymère en interaction avec les particules, prédit par ce modèle [3].

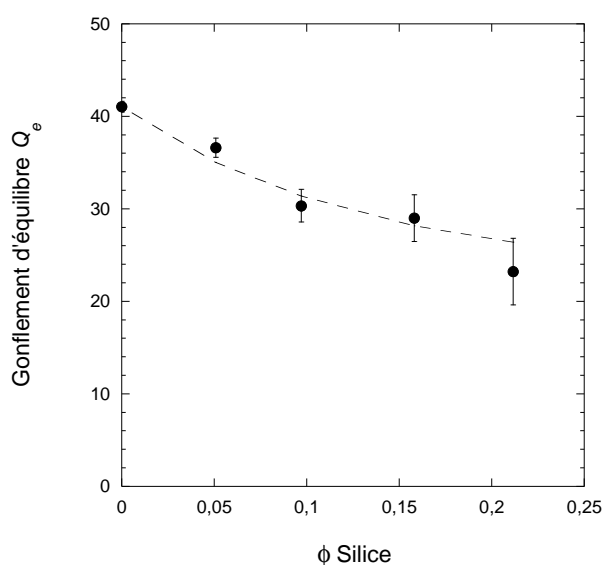


Figure 5 : Variation du gonflement d'équilibre Q_e en fonction de la fraction volumique en silice ϕ_{Si} .
Les résultats expérimentaux (cercles pleins) sont comparés au modèle de Lequeux dans le cas d'une bonne interaction, sans couche de polymère « sous-gonflée » adsorbée, [3].

3. Renforcement des propriétés mécaniques

3.1. Influence de la vitesse

En se concentrant sur les interactions polymère/silice, les propriétés mécaniques des hydrogels hybrides ont été étudiées sur une large gamme d'échelle de temps, comme représenté **Figure 6** : trois vitesses de déformation ont été utilisées : $3 \cdot 10^{-4} \text{ s}^{-1}$, $0,06 \text{ s}^{-1}$ et $0,6 \text{ s}^{-1}$. A vitesse de déformation intermédiaire ($0,06 \text{ s}^{-1}$), il a été montré que les propriétés mécaniques des hydrogels sont largement améliorées, grâce à une adsorption des chaînes de

PDMA à la surface des nanoparticules de silice. Cependant, ce processus implique des mécanismes dynamiques d'adsorption/désorption de segments de chaînes : le renforcement est ainsi fortement lié à l'échelle de temps sondée. A grande vitesse de déformation, l'interaction silice/PDMA semble « gelée » : le temps d'observation alloué n'est pas suffisant pour que le mécanisme d'adsorption/désorption ait lieu. En revanche, à très faible taux de déformation, le réseau physique est totalement relaxé et la signature mécanique du gel hybride est celle du réseau purement covalent : à cette échelle de temps, la contribution des nanoparticules de silice est invisible. Cet effet de vitesse concerne aussi la dissipation mise en évidence par cycles de traction, comme représenté **Figure 6** (droite). En effet, alors que la matrice de PDMA ne présente aucune dissipation, l'introduction de nanoparticules de silice apporte une composante dissipative au système.

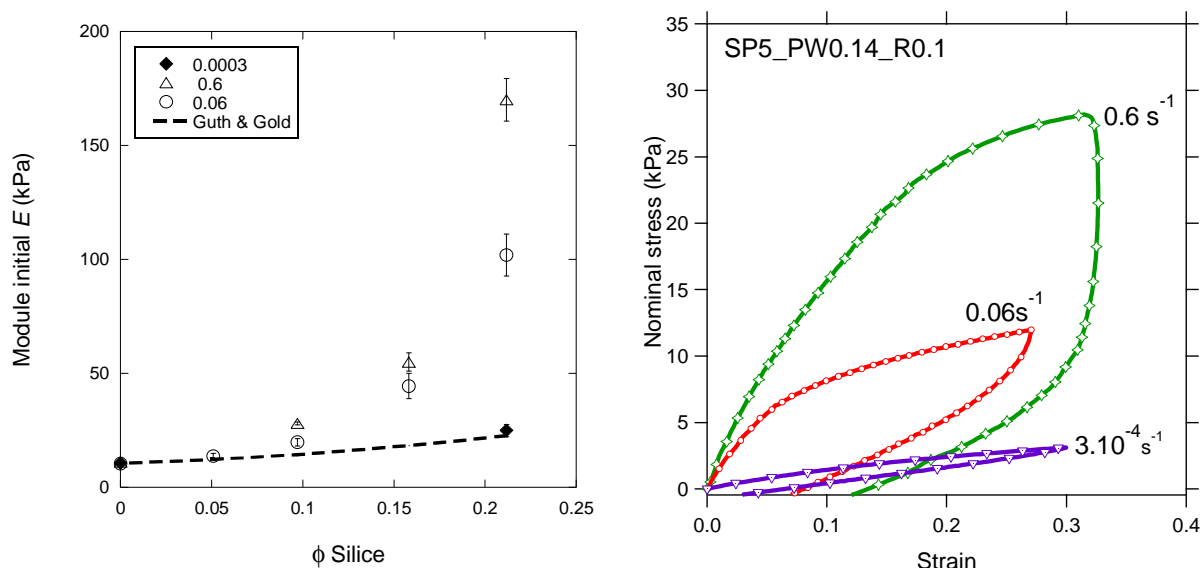


Figure 6 : Gauche : comparaison des valeurs expérimentales de module initial E à trois taux de déformation : 3.10^{-4} s^{-1} (losanges pleins), 0.06 s^{-1} (cercles) et 0.6 s^{-1} (triangles). Le modèle de Guth et Gold est représenté pour comparaison.

Droite : comportement en traction cyclique (jusqu'à 30 % de déformation) en fonction du taux de déformation appliqué, pour SP5_PW0.14_R0.1.

Les cycles de traction témoignent d'un autre effet de la vitesse de déformation : la comparaison des modules initiaux des cycles successifs permet de déterminer un taux de recouvrance, défini comme étant le rapport du module initial des second et premier cycles.

Alors que le taux de recouvrance à vitesse moyenne (0.06 s^{-1}) est égal à 1 quelle que soit la teneur en nanoparticules de silice, témoignant de la réparation du réseau hybride, les essais conduits à grande vitesse de déformation (0.6 s^{-1}) montrent un fort endommagement du système, la valeur du module élastique du SP5_PW0.14_R0.1 chutant de 70 %. Une preuve expérimentale du phénomène d'adsorption/désorption du PDMA à la surface des nanoparticules de silice est la recouvrance totale du module initial à grande vitesse de déformation lorsque 10 secondes d'attente sont introduites entre deux cycles consécutifs, comme présenté **Figure 7**. Dans cet intervalle de temps, les processus de réarrangement et d'échanges permettent aux chaînes du réseau de PDMA de reformer une densité de chaînes élastiquement actives équivalente en s'adsorbant à la surface des particules.

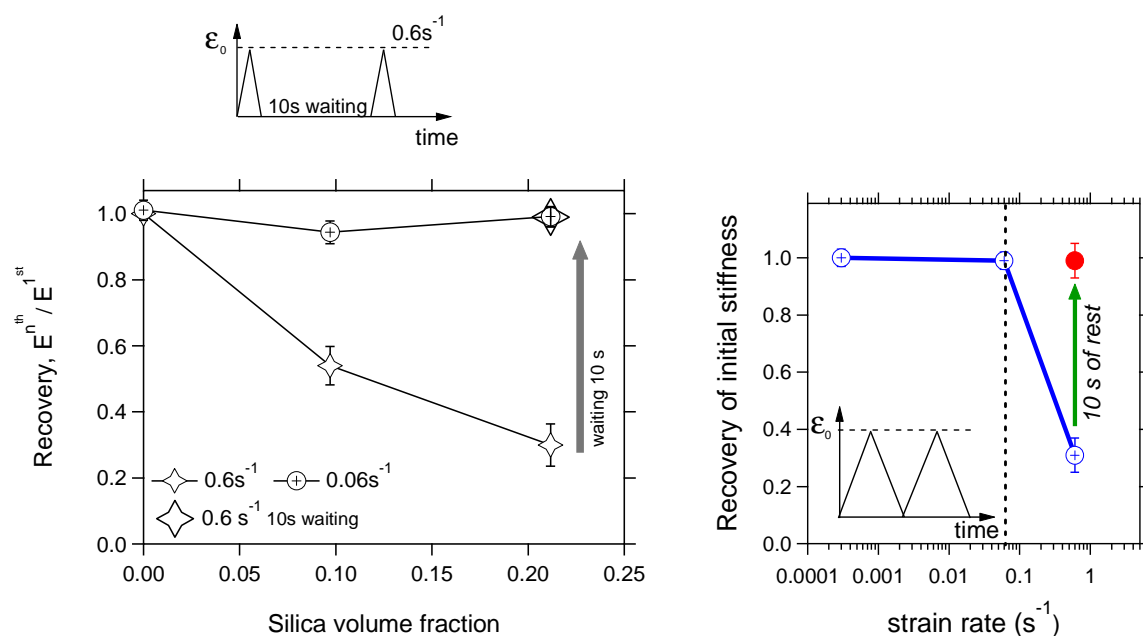


Figure 7 : Gauche : recouvrance du module initial en fonction de la fraction volumique en silice à différents taux de déformation : 0.06 s^{-1} (cercles) et 0.6 s^{-1} (étoiles).

Droite : recouvrance du module initial en fonction du taux de déformation, pour le système SP5_PW0.14_R0.1, effet de 10 secondes de pause.

De même, la résistance à la fracture est améliorée par la présence des nanoparticules de silice au sein du réseau chimiquement réticulé de PDMA.

3.2. Relaxation

L'étude de la relaxation des contraintes des hydrogels hybrides a permis de confirmer le caractère transitoire du réseau physique formé par les chaînes de PDMA adsorbées à la surface des nanoparticules de silice. Quel que soit le taux de déformation imposé (de 2 % à 200 %), l'observation de la réponse des hydrogels aux temps courts met en évidence un temps caractéristique de 14 secondes, comme représenté **Figure 8** dans le cas du SP5_PW0.14_R0.1.

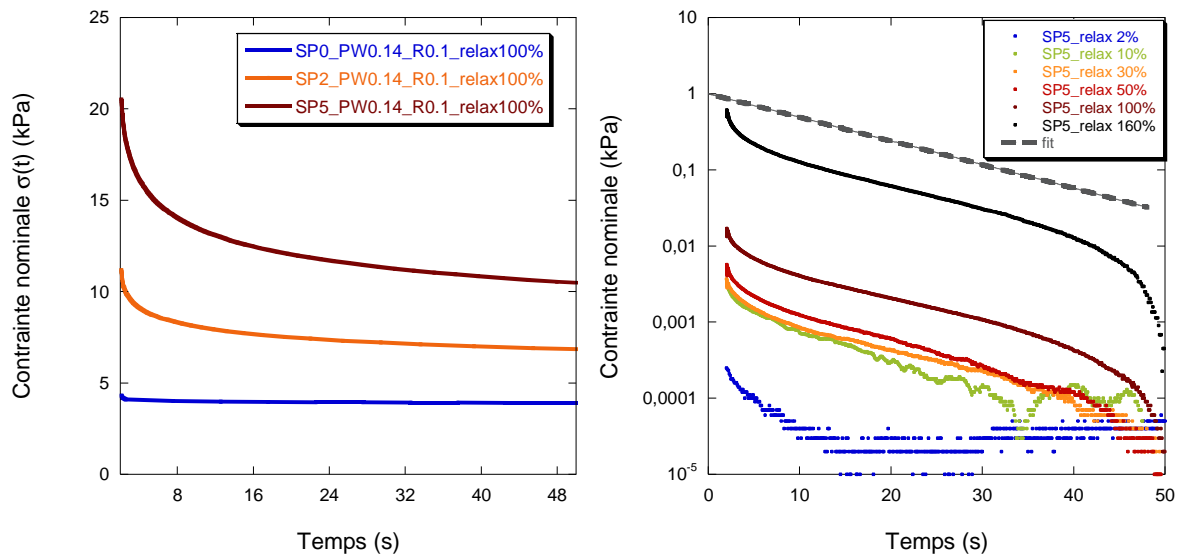


Figure 8 : Gauche : Essais de relaxation représentés sur 50 secondes avec 100 % de déformation, pour SPx_PW0.14_R0.1, x = 0 ; 2 ; 5.

Droite : Représentation logarithmique de la contrainte nominale sur 50 secondes, pour les gels SP5_PW0.14_R0.1 à différentes déformations initiales imposées.

3.3. Diffusion de neutrons aux petits angles sous déformation

Des mesures de DNPA ont été réalisées sous déformation, grâce à un détecteur anisotrope et à un montage spécialement développé pour l'étude d'hydrogels. La visualisation de l'évolution de l'anisotropie de la répartition des nanoparticules de silice au sein des hydrogels étirés permet de confirmer l'effet crucial du temps sur la recouvrance et la réparation des hydrogels hybrides PDMA/silice. Ainsi, le maintien pendant une heure d'un SP5_PW0.14_R0.1 à une déformation de 100 % se traduit visuellement par la présence de

quatre lobes sur la figure de diffusion 2D, témoins de l'anisotropie du système étiré. Dès lors que l'hydrogel hybride est déchargé, l'anneau isotrope est retrouvé, signe de la recouvrance de la répartition homogène des nanoparticules de silice, comme représenté **Figure 9**. Cette recouvrance n'est possible qu'en dessous du contact particule/particule typiquement atteint au-delà de 100 % de déformation dans le cas de SP5_PW0.14_R0.1. En revanche, une déformation de 200 % ne permet pas le retour à l'isotropie : les quatre lobes persistent et une déformation rémanente est observée, due au contact irréversible des nanoparticules de silice.

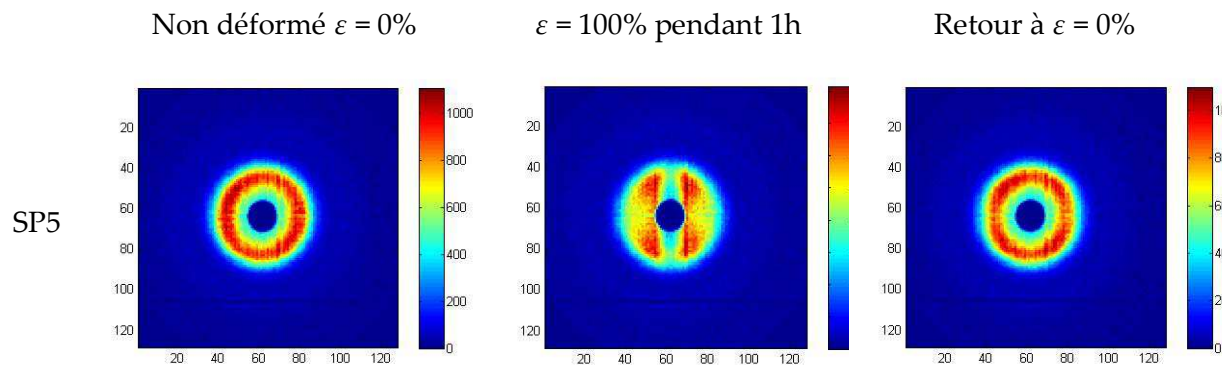


Figure 9 : Images de DNPA bidimensionnelle du SP5_PW0.14_R0.1 : non étiré (à gauche), étiré à 100 % de déformation (au centre) puis déchargé à 0 % de déformation (à droite).

3.4. Modélisation du comportement des hydrogels hybrides

Au vu du comportement macroscopique étudié, un modèle viscoélastique visant à décrire le caractère de double réseau de notre système a été développé, basé sur le modèle généralisé de Maxwell : combinaison de ressorts et d'amortisseurs.

L'utilisation et la détermination d'un nombre limité de paramètres, choisis en connaissance du comportement mécanique, ont permis de modéliser la réponse mécanique de l'hydrogel hybride SP5_PW0.14_R0.1, comme représenté **Figure 10**. Bien que cette modélisation reste assez simple dans sa conception, elle rend bien compte des différentes contributions au caractère viscoélastique de notre système.

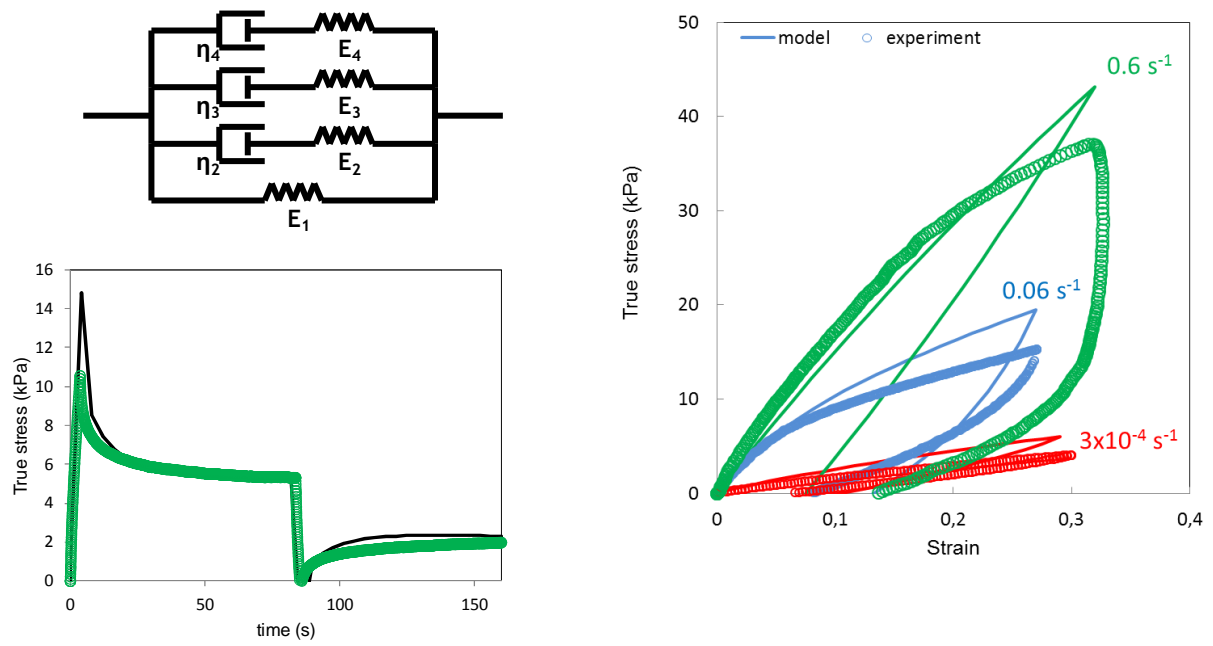


Figure 10 : Gauche : Représentation schématique du modèle utilisé et comparaison du modèle à un essai expérimental de dip-test sur un échantillon SP5_PW0.14_R0.1.

Droite : comparaison du modèle aux tests de traction cyclique sur SP5_PW0.14_R0.1 à trois taux de déformation.

4. Adaptabilité du système aux propriétés recherchées

4.1. Modification de la matrice polymère

4.1.1. Changement du taux de réticulation

L'amplitude du renforcement des propriétés mécaniques peut être magnifiée ou diminuée par des changements du taux de réticulation : en l'absence de réticulant et avec un taux de réticulation 10 fois plus élevé, comme présenté **Figure 11**.

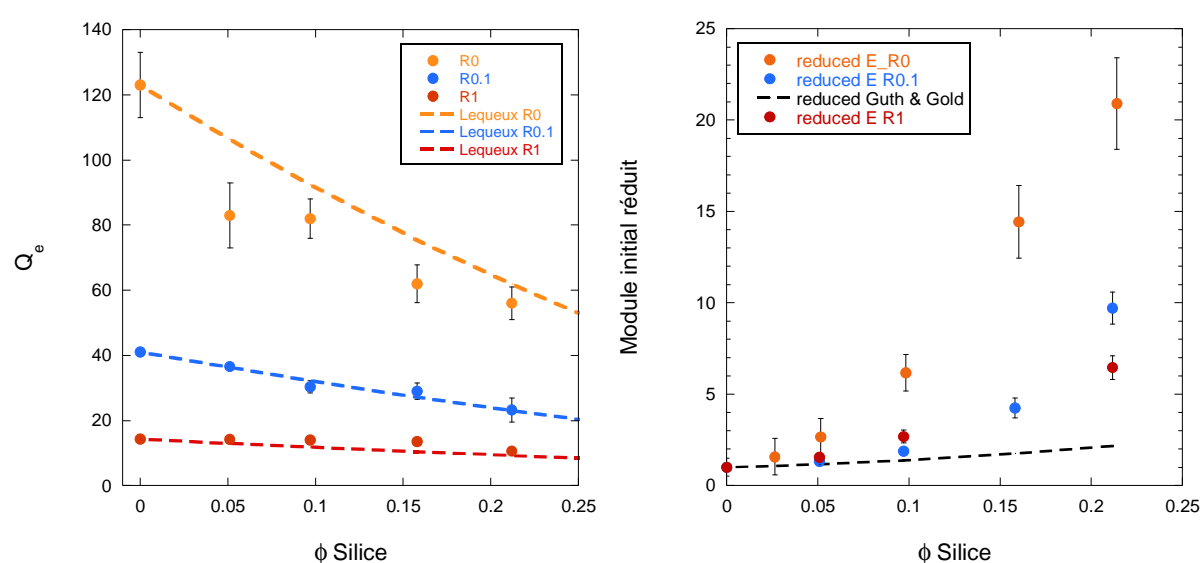


Figure 11 : Gauche : Variation du gonflement d'équilibre en fonction de la fraction volumique en silice pour différents taux de réticulation chimique : 0 mol% (en orange), 0.1 mol% (en bleu) et 1 mol% (en rouge). Les résultats expérimentaux sont comparés au modèle de Lequeux, en l'absence de couche adsorbée.

Droite : Variation du module initial réduit en fonction de la fraction volumique en silice pour différents taux de réticulation chimique : 0 mol% (en orange), 0.1 mol% (en bleu) et 1 mol% (en rouge). Les résultats expérimentaux sont comparés au modèle de Guth et Gold.

4.1.2. Changement du taux de gonflement

Le comportement des hydrogels hybrides a été étudié à l'équilibre de gonflement dans l'eau. Une forte atténuation du renforcement mécanique a été observée, bien que les interactions restent actives, comme présenté **Figure 12**.

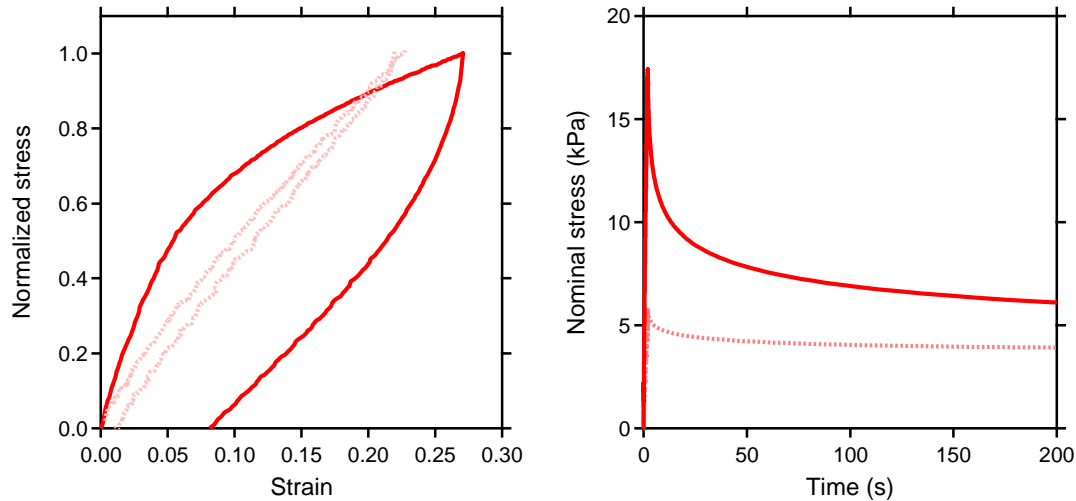


Figure 12 : Gauche : Comparaison de l'allure des cycles de traction, à 0.06 s^{-1} , au gonflement de synthèse (en rouge) et au gonflement d'équilibre (en rose).

Droite : Comparaison de l'allure des essais de relaxation au gonflement de synthèse (en rouge) et au gonflement d'équilibre (en rose).

4.2. Agrégation des nanoparticules de silice

L'état de dispersion des nanoparticules de silice peut être facilement modifié par un changement de pH. En effet, en se plaçant à pH 5, les particules de silice forment un réseau percolant inorganique. Dans ces conditions, les hydrogels hybrides formés sont fortement affectés par la présence des deux réseaux, avec une superposition de leurs propriétés plutôt qu'un couplage. Dans ce cas, le réseau inorganique dur et fragile est rapidement et irréversiblement détérioré aux faibles déformations (**Figure 13**) alors que le réseau organique permet de maintenir des propriétés d'élongation intéressantes.

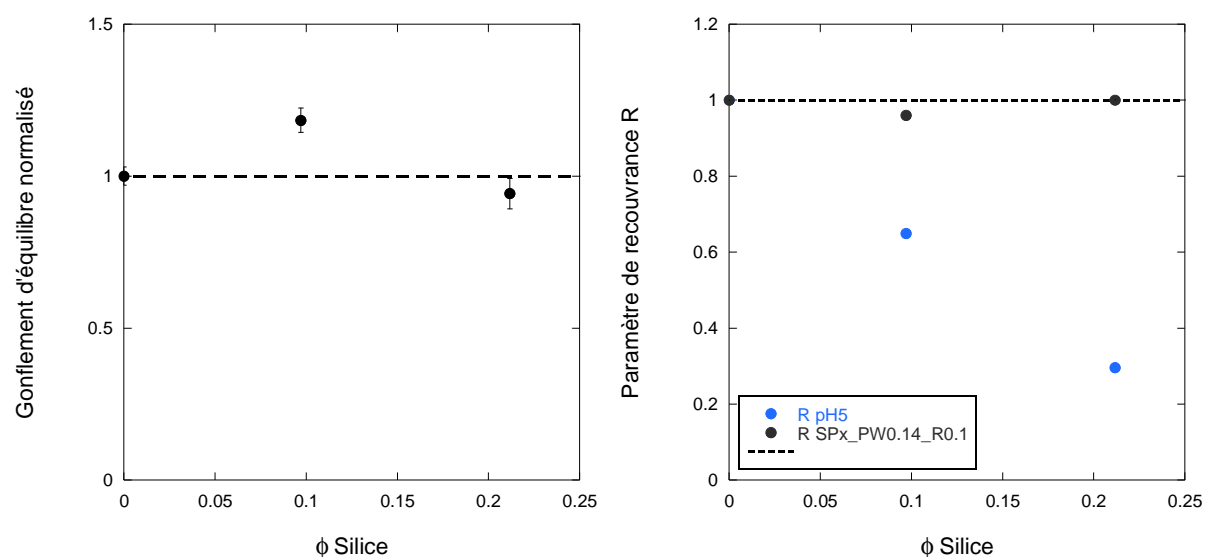


Figure 13 : Gauche : Variation du gonflement d'équilibre des hydrogels synthétisés à pH 5.

Droite : Comparaison du paramètre de recouvrance en fonction de la fraction volumique en silice pour les gels hybrides de référence (en noir) et les gels synthétisés à pH 5 (en bleu).

4.3. Altération de l'interaction polymère/silice

4.3.1. Changement de monomère

L'utilisation de l'acrylamide (AAm), monomère ne présentant pas d'interaction spécifique avec les nanoparticules de silice, a été étudiée. L'augmentation progressive de la teneur en acrylamide dans la composition des gels de copolymères P(DMA-co-AAm) mène à la diminution progressive du renforcement des propriétés mécaniques des hydrogels, comme représenté **Figure 14** (gauche).

4.3.2. Introduction d'un compétiteur de liaison hydrogène

L'urée est utilisée en tant que compétiteur de liaison hydrogène dans de nombreux systèmes associatifs. L'introduction d'urée dans nos hydrogels hybrides a pour conséquence une diminution drastique du renforcement mécanique, comme observé **Figure 14** (droite).

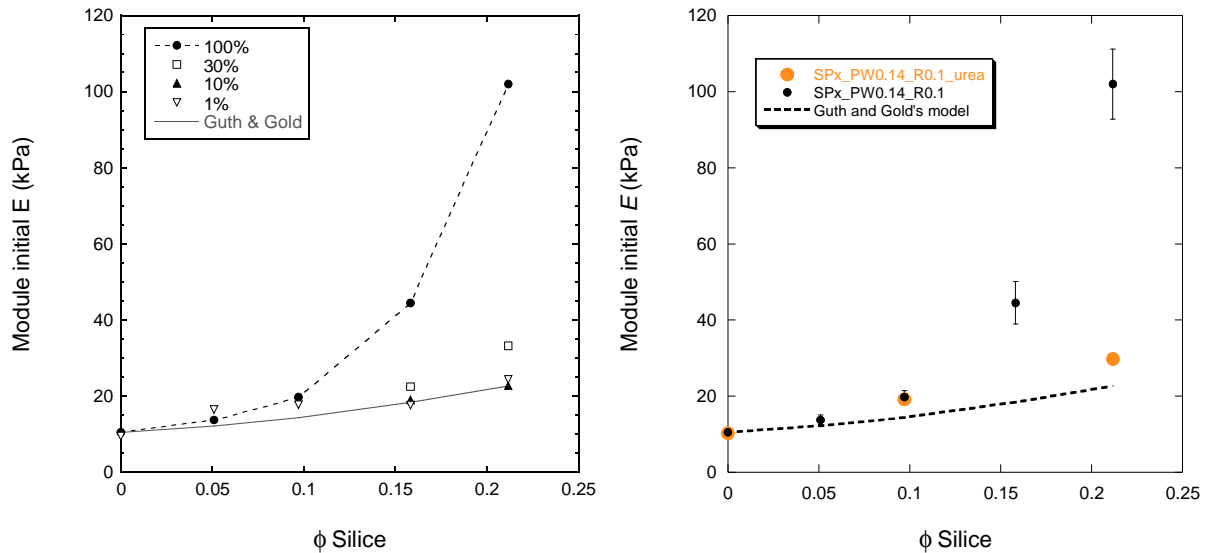


Figure 14 : Gauche : Evolution du module initial E (kPa) pour différentes composition de copolymère P(DMA-co-AAm). Les pourcentages correspondent aux pourcentages massiques de DMA contenu dans la matrice polymère.

Droite : Comparaison des modules initiaux obtenus pour les hydrogels hybrides de références et des hydrogels hybrides contenant de l'urée. Les résultats sont comparés au modèle de Guth et Gold.

5. Etude par diffusion de la lumière

5.1. Etude d'hydrogels hybrides PAAm/silice

Les méthodes de diffusion de la lumière sont particulièrement adaptées à la caractérisation précise des interactions existant entre la matrice polymère et les nanoparticules de silice. Dans un premier temps, nous nous sommes intéressés à l'étude de la dynamique de réseaux hybrides composés d'un polymère ne présentant pas d'interaction avec la silice (le PAAm). L'impact de la concentration en nanoparticules de silice ainsi que l'effet du taux de réticulation chimique du réseau de PAAm sur la dynamique du système ont été étudiés, comme représenté **Figure 15**. Ainsi le coefficient de diffusion des nanoparticules de silice au sein du réseau de PAAm diminue à mesure que le taux de réticulation chimique est augmenté.

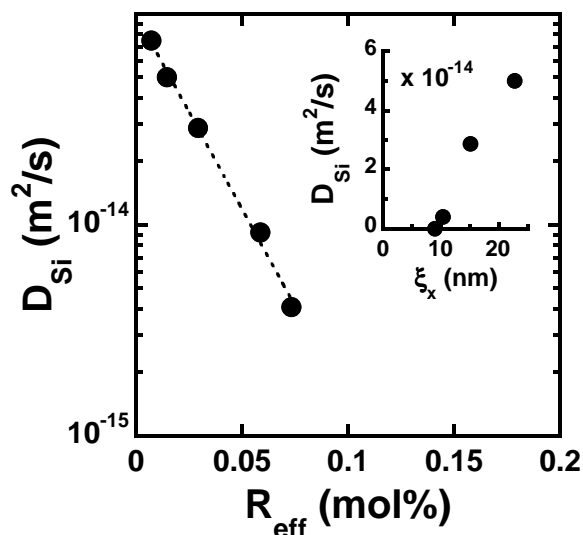


Figure 15 : Coefficient de diffusion des nanoparticules de silice D_{Si} dans les gels de PAAm en fonction du taux de réticulation effectif R_{eff} . Insert : D_{Si} en fonction de la distance moyenne entre points de réticulation.

De plus, cette étude a mis en évidence des réactions de transferts lors de la polymérisation en présence de nanoparticules de silice. En présence de faibles taux de nanoparticules de silice, une croissance de chaînes à partir de la surface de silice est possible.

5.2. Etude d'hydrogels hybrides P(DMA-co-AAm)/silice

Nous avons étudié l'impact de l'introduction progressive d'un monomère ayant des interactions avec la silice, le DMA, sur la dynamique du système. Lorsque le gel n'est composé que d'acrylamide, les nanoparticules de silice présentent une dynamique Brownienne, uniquement affectée par la concentration en polymère ainsi que par le taux de réticulation. A mesure que du DMA est introduit, on assiste à un « emprisonnement » progressif des nanoparticules de silice en raison de leur interaction importante avec ce monomère. Cette situation est illustrée **Figure 16**.

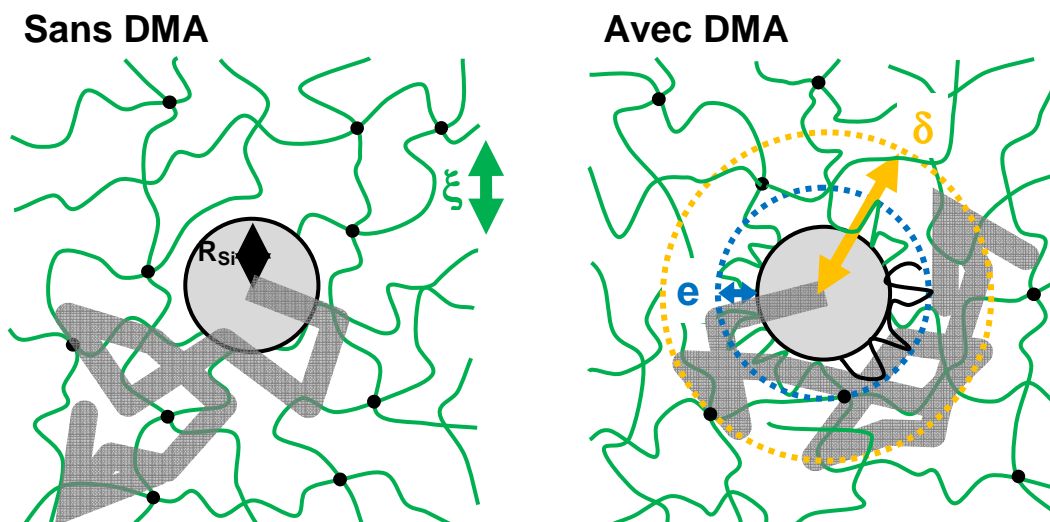


Figure 16 : Illustration schématique de l'impact du DMA sur la dynamique des nanoparticules de silice au sein d'un hydrogel, à gauche en l'absence de DMA, à droite en présence de DMA.

6. Conclusions de l'étude

En conclusion de cette étude, nous nous sommes intéressés au renforcement des propriétés des hydrogels, connus pour leur grande fragilité. Pour cela nous avons développé des hydrogels hybrides composés d'une matrice de polymère hydrosoluble présentant des interactions attractives avec des nanoparticules de silice. Le but était de coupler un réseau polymère chimiquement réticulé à des associations physiques à la surface de nanoparticules de silice.

Les conséquences de ces interactions ont été étudiées en termes de structure (par différentes techniques de diffusion), de caractéristiques thermodynamiques et de propriétés mécaniques. D'un point de vue structural, les hydrogels hybrides obtenus présentent une distribution homogène de nanoparticules de silice, grâce à l'association existant avec la matrice polymère. Cette association se traduit en termes de diminution des propriétés de gonflement des hydrogels, la matrice hybride étant ainsi plus contrainte. Enfin, les propriétés mécaniques des hydrogels ont été largement améliorées et apparaissent être dépendantes de

la vitesse de sollicitation. Les hydrogels PDMA/silice peuvent être considérés comme des doubles réseaux, formés d'une matrice polymère chimiquement réticulée et d'un réseau de nanoparticules de silice dispersées s'associant de façon réversible avec le PDMA. Il en ressort un système robuste, facilement adaptable aux propriétés recherchées et basé sur des interactions dynamiques promettant d'intéressantes applications stimulables.

7. Références

1. Petit, L., et al., *Responsive hybrid self-assemblies in aqueous media*. Langmuir, 2007. **23**(1): p. 147-158.
2. Mendes, E., et al., *Experimental evidence for inhomogeneous swelling and deformation in statistical gels*. Phys. Rev. Lett., 1991. **66**: p. 1595-1598.
3. Berriot, J., et al., *Reinforcement of model filled elastomers: experimental and theoretical approach of swelling properties*. Polymer, 2002. **43**(23): p. 6131-6138.

Annex 1: Rheological behaviour

The linear viscoelastic regime has been determined for covalent PDMA cross-linked hydrogels and for hybrid hydrogels, at a strain sweep of 1 Hz, as presented in **Figure 1**. The measurement was repeated.

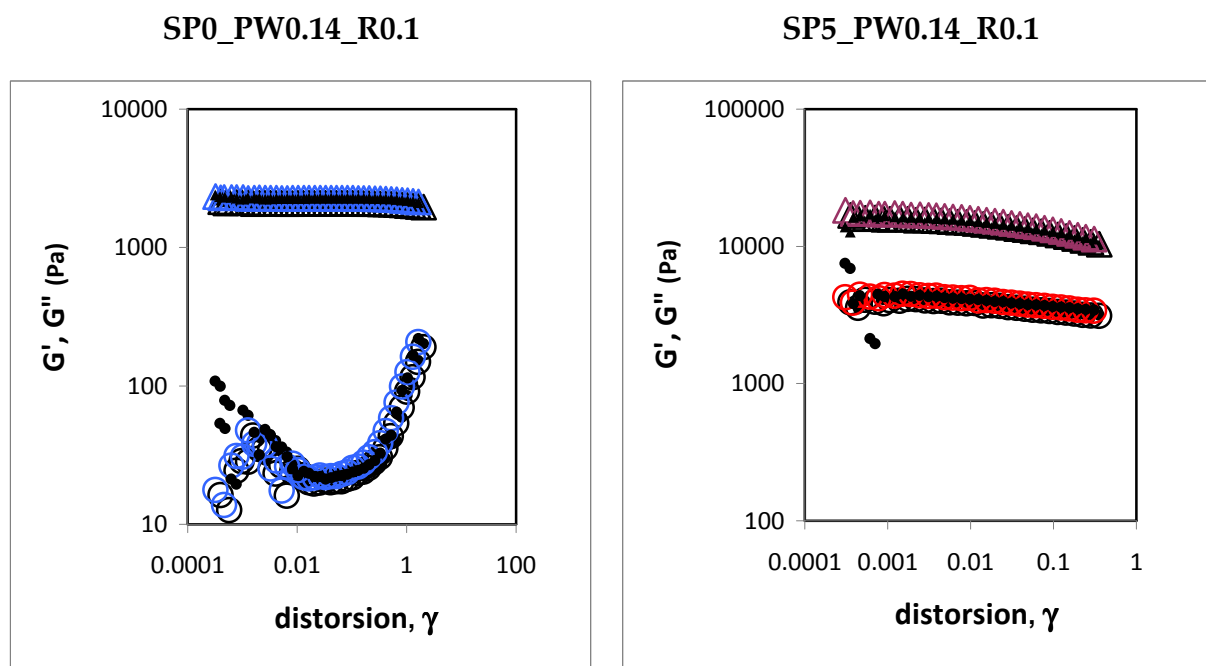


Figure 1: Representation of G' and G'' at 1 Hz strain sweep, for SP0_PW0.14_R0.1 (in blue) and SP5_PW0.14_R0.1 (in red). The two successive measurements are superimposed.

Annex 2: Fracture energy

Lake and Thomas developed a theory of fracture energy in the 60's for elastomers [1]. In the case of a crack propagation through an elastomer, the threshold fracture of an elastic network is related to the energy necessary to stretch to fracture each elastic strand crossing the plane of fracture. When the covalent bound breaks, the energy of the N monomers stretched is completely and irreversibly released:

$$G_{LT} = \Sigma N_c E_R \quad \text{Eq. 1}$$

with Σ the surface density of chains crossing the plane of fracture, N_c the number of monomers between two cross-linking points and E_R the fracture energy of one carbon-carbon bound.

In the case of a statistic cross-linking with a functionality of 4 per crosslink, the surface density of chains crossing the plane of fracture becomes:

$$\Sigma = \frac{\tau d_c}{2} \quad \text{Eq. 2}$$

where τ is the number of cross-linking points per volume unit and d_c the distance between two cross-linking points.

Using this last equation, the fracture energy of Lake and Thomas is:

$$G_{LT} = \frac{\rho N_A b}{2 M_0 N_c^{1/2}} N_c E_R = \frac{\rho b}{2 M_0} N_c^{1/2} E_{Rm} \quad \text{Eq. 3}$$

with ρ the volume concentration of polymer, N_A the Avogadro number, b the monomer length, M_0 the monomer molar mass and E_{Rm} the molar fracture energy of carbon-carbon bound.

[1] - Lake, G.J. and A.G. Thomas, *The Strength of Highly Elastic Materials*. Proceedings of the Royal Society London, 1967. 300(1460): p. 108-119

Résumé

Nous étudions les relations structure/propriétés d'hydrogels contenant des nanoparticules inorganiques. Les interactions spécifiques existant entre le poly(*N,N*-diméthylacrylamide) et des nanoparticules de silice sont à l'origine d'un fort renforcement mécanique des hydrogels, tant en termes de raideur que de résistance à la fracture. L'impact de l'introduction de nanoparticules de silice a été étudié d'un point de vue structural, thermodynamique et mécanique. Une étude détaillée des propriétés mécaniques des hydrogels hybrides à différentes échelles de temps a révélé une forte dépendance à la vitesse de sollicitation. Une modélisation du caractère viscoélastique de tels réseaux hybrides a été proposée et confrontée aux résultats expérimentaux, visant à décrire le comportement de ces doubles réseaux. Par ailleurs, une étude par techniques de diffusion de la lumière a été menée afin de caractériser la dynamique des nanoparticules de silice au sein des réseaux de polymère gonflés. Il a été démontré que le renforcement général des propriétés des hydrogels par les nanoparticules de silice est contrôlé par la dynamique de l'association PDMA/silice.

Mots clés : hydrogels hybrides, nanoparticules de silice, interactions spécifiques, renforcement mécanique, diffusion de la lumière, diffusion de neutrons.

Abstract

We are investigating the consequences of the introduction of inorganic nanoparticles in a polymer hydrogel. The specific interactions existing between poly(*N,N*-dimethylacrylamide) and silica nanoparticles are at the origin of a strong mechanical reinforcement in terms of stiffness and strain at failure. Indeed, the impact of silica nanoparticles onto the general characteristics of hydrogels has been investigated in terms of structural, thermodynamical and mechanical properties. The study of the mechanical properties of hybrid hydrogels has been conducted in details with a special focus on PDMA/silica interactions at different strains and probing the time-scale effects. A strong time-dependence has been evidenced and a brief modelling of the hybrid structure has been proposed, taking into account the viscoelastic nature of the system. The behaviour of these hybrid hydrogels can be described as double networks. The PDMA/silica specific interaction has also been studied by light scattering experiments, evidencing several dynamics. We show that the general reinforcement can be controlled by the dynamics of the PDMA/silica association.

Keywords: hybrid hydrogels, silica nanoparticles, specific interactions, mechanical reinforcement, light scattering, neutron scattering.